

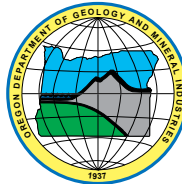
STATE OF OREGON
DEPARTMENT OF GEOLOGY AND MINERAL INDUSTRIES
VICKI S. McCONNELL, STATE GEOLOGIST

SPECIAL PAPER 44

**COASTAL FLOOD INSURANCE STUDY,
COOS COUNTY, OREGON**



By Jonathan C. Allan¹, Peter Ruggiero², and Jed T. Roberts³



2012

¹Oregon Department of Geology and Mineral Industries, Coastal Field Office, P.O. Box 1033, Newport, OR 97365

²Department of Geosciences, Oregon State University, 104 Wilkinson Building, Corvallis, OR 97331

³Oregon Department of Geology and Mineral Industries, 800 NE Oregon Street, #28, Suite 965, Portland, OR 97232

Cover image: Moderate wave runup adjacent to the Coquille jetties generated by a storm on February 9, 2009. Photo by Jonathan Allan, DOGAMI.

NOTICE

The Oregon Department of Geology and Mineral Industries is publishing this report because the subject matter is consistent with the mission of the Department. The publication is not intended to be used for site specific planning. It may be used as a general guide for emergency response planning. The views and conclusions contained in this document are those of the authors and should not be interpreted as necessarily representing the official policies, either expressed or implied, of the U.S. government.

Oregon Department of Geology and Mineral Industries Special Paper 44
Published in conformance with ORS 516.030

For copies of this publication or other information about Oregon's geology and natural resources, contact:

Nature of the Northwest Information Center
800 NE Oregon Street #28, Suite 965
Portland, Oregon 97232
(971) 673-2331
<http://www.NatureNW.org>

For additional information:
Administrative Offices
800 NE Oregon Street #28, Suite 965
Portland, OR 97232
Telephone (971) 673-1555
Fax (971) 673-1562
<http://www.oregongeology.com>
<http://egov.oregon.gov/DOGAMI/>

TABLE OF CONTENTS

1.0 INTRODUCTION	1
2.0 COASTAL GEOLOGY AND GEOMORPHOLOGY OF COOS COUNTY	4
2.1 Local geology	4
2.2 Tsunami hazards associated with the Cascadia subduction zone and from distant earthquake sources.....	5
2.3 Coastal geomorphology	7
2.4 Coastal erosion and flood history	12
2.4.1 Bandon shoreline	12
2.4.2 Bastendorff/Lighthouse Beach.....	17
3.0 BEACH AND BLUFF MORPHOLOGY ASSESSMENTS.....	19
3.1 Survey methodology.....	19
3.2 Beach characterization.....	24
3.3 Recent coastal changes along the Bandon and Bastendorff beaches	29
3.4 Bathymetry	29
4.0 TIDES	32
4.1 Tides along the Coos County coast.....	32
4.2 Still water level (SWL)	35
5.0 PACIFIC NORTHWEST WAVE CLIMATE.....	37
5.1 Development of a synthesized wave climate for input into SWAN	39
5.2 Initial total water level calculations	44
5.3 SWAN model development and parameter settings	47
5.4 Summary of SWAN results	52
6.0 WAVE RUNUP AND OVERTOPPING	54
6.1 Runup models for beaches	55
6.1.1 Stockdon runup model.....	55
6.1.2 Direct integration method — beaches	55
6.1.3 Comparison of Stockdon and DIM runup calculations	56
6.2 Barrier runup calculations	58
6.2.1 Introduction	58
6.2.2 Specific procedure for calculation of “barrier” runup	59
6.2.3 Barrier runup reduction factors	61
6.3 Coos County wave runup and total water level calculations	62
6.4 Overtopping calculations	65
6.4.1 Mean overtopping rate at the “barrier” crest	66
6.4.2 Overtopping limits and flood hazard zones landward of the “barrier” crest	67
6.4.3 Initial testing of the landward limit of wave overtopping	68
6.4.4 Wave overtopping and hazard zone limits calculated for Coos County	70
7.0 COASTAL EROSION	72
7.1 Geometric model of foredune erosion	72
8.0 FLOOD MAPPING	83
8.1 Detailed coastal VE flood zone mapping	83
8.1.1 Bluff-backed beaches	83
8.1.2 Dune-backed beaches	83
8.2 Coastal V-zone mapping along Coos County shoreline	86
8.2.1 Dune-backed beaches	86
8.2.2 V-zone mapping at creek mouths	91
8.2.3 V-zone mapping along coastal bluffs.....	93
9.0 REFERENCES	94
APPENDIX A. GROUND SURVEY ACCURACY ASSESSMENT PROTOCOLS	
DETERMINED BY WATERSHED SCIENCES, INC.	97
A.1 Base station protocols	97
A.2 RTK protocols	97
A.3 Monument and RTK results	98
APPENDIX B. BANDON BEACH PROFILES	100
APPENDIX C. COOS-BASTENDORFF/LIGHTHOUSE BEACH PROFILES	111
APPENDIX D. SPLASH OVERTOPPING NOTES DERIVED BY W. G. McDUGAL	117

LIST OF TABLES

Table 3-1.	Survey benchmarks used to calibrate GPS surveys of the beach at Bandon and Bastendorff Beach, Coos County.....	21
Table 3-2.	Comparison of horizontal and vertical coordinates derived by the NGS, WS, OPUS, and DOGAMI.....	22
Table 3-3.	Identified beach morphological parameters from the most eroded winter profile (MLWP) at Bandon	27
Table 3-4.	Identified beach morphological parameters from the most eroded winter profile (MLWP) at Bastendorff Beach.....	27
Table 5-1.	Summary variables derived from the synthesized wave climate, showing the range of wave statistics associated with the 267 extreme total water level storm events.....	45
Table 6-1.	"Barrier" runup reduction factors used for calculating runup on beaches backed by bluffs along the Bandon shore	61
Table 6-2.	"Barrier" runup reduction factors used for calculating runup on beaches backed by bluffs along the Lighthouse Beach shore	61
Table 6-3.	100-year (1%) and 500-year (0.2%) total water levels calculated for the Bandon profile sites.....	63
Table 6-4.	100-year (1%) and 500-year (0.2%) total water levels calculated for the Coos profile sites.....	63
Table 6-5.	Splashdown and hazard zone limits calculated for Coos County detailed coastal sites.....	70
Table 7-1.	Maximum potential dune erosion (DE_{max}) values determined for Bandon using the geometric model.....	74
Table 7-2.	Maximum potential dune erosion (DE_{max}) values determined for Bastendorff and Lighthouse Beach using the geometric model	74
Table 7-3.	Simple statistics determined from an analysis of the time scale of profile response (T_s) values along the Coos County shore.....	75
Table 7-4.	Simple statistics determined from an analysis of storm duration values determined for the Coos County shore	78
Table 7-5.	Summary parameters used to determine the storm recession reduction factor	79
Table 7-6.	Calculated duration limited recession (R_m) for the Bandon shore and along Bastendorff Beach	79
Table 8.1.	Overtopping calculations for surveyed transects located on dune-backed beaches.....	85
Table A.1.	Base stations and measurement statistics from the OLC South Coast Project.....	99

LIST OF FIGURES

Figure 1-1.	Location map of Coos County coastline	1
Figure 1-2.	Three representative examples of the steps that may be taken to derive coastal flood hazard maps	3
Figure 2-1.	Aerial view looking north along Bastendorff Beach and the North Coos Spit.....	4
Figure 2-2.	Bluff-backed beaches at Fivemile Point north of the Bandon Dune Golf Course	5
Figure 2-3.	Geomorphic classification of the southern Coos County shoreline.....	8
Figure 2-4.	Geomorphic classification of the northern Coos County shoreline.....	9
Figure 2-5.	Bluff-backed beaches characterize much of the shoreline at Bandon	10
Figure 2-6.	Dune/bluff-backed beaches near Johnson Creek in Bandon during a small storm in February 2009.....	11
Figure 2-7.	Steep cliffs characterize much of the coastal geomorphology at Cape Arago State Park	11
Figure 2-8.	Survey line drawings prepared by the Corps of Engineers prior to and during construction of the Coquille jetties adjacent to Bandon	13
Figure 2-9.	High wave runup and overtopping during a major storm (December 22, 2000) near the south Coquille jetty at Bandon.....	14
Figure 2-10.	Wave overtopping during a major storm (December 22, 2000) surrounds the restroom and covers the parking lot adjacent to the south Coquille jetty at Bandon	14
Figure 2-11.	1939 aerial photograph of the Bandon "triangle" adjacent to the Coquille jetties showing evidence of blowouts.....	15
Figure 2-12.	History of coastal flooding events in the south jetty area of Bandon (January 1955 to April 1994)	16
Figure 2-13.	Historical shoreline changes at Bastendorff Beach adjacent to the Coos Bay jetties	17
Figure 2-14.	Historical shoreline changes at Bastendorff Beach adjacent to the Coos Bay jetties	18
Figure 2-15.	Photo of Bastendorff Beach on April 9, 2010, showing the well-vegetated foredune and backshore	18
Figure 3-1.	Location map of beach profiles measured at Bandon and at Bastendorff Beach in Coos County	19
Figure 3-2.	The Trimble 5700 base station antenna located over a known reference point at Cape Lookout State Park, northern Oregon coast.....	21

continued on next page

Figure 3-3.	A 180-epoch calibration check is performed on a survey monument (OLC5PGW1) established by WS near the Coast Guard observation tower at the mouth of Coos Bay.....	22
Figure 3-4.	Surveying the morphology of the beach at Bandon using a Trimble 5800 "rover" GPS	23
Figure 3-5.	Residuals of GPS survey points relative to zero (transect) line	24
Figure 3-6.	Plot showing the location of the dune crest, the landward extent of the primary frontal dune, and the beach/dune junctures (bottom) identified from lidar data on the North Coos Spit.....	25
Figure 3-7.	Example plots of the combined beach profile data for the Bandon 3 and 5 sites	26
Figure 3-8.	Alongshore changes in beach slopes beach/dune juncture elevations, and dune/bluff crest/tops along the Bandon shore.....	27
Figure 3-9.	The Coos 2 profile site indicating the generally low backshore elevations that suggest that the beach probably prograded rapidly seaward following jetty construction, while the high contemporary foredune indicates that the shoreline has stabilized.....	28
Figure 3-10.	Collected bathymetry transects measured offshore the coast of the north Umpqua Spit near Winchester Bay, Oregon	31
Figure 3-11.	Example cross-shore transect measured off the Umpqua Spit showing the presence of two prominent sand bars, characterized by significant relief	31
Figure 4-1.	Daily tidal elevations measured at Charleston on the southern Oregon coast. Data from the National Ocean Service.....	32
Figure 4-2.	Seasonal cycles in monthly-mean water levels based on data from the Charleston tide gauge	33
Figure 4-3.	The trends of "winter" and "summer" mean-sea levels measured by the Charleston tide gauge	34
Figure 4-4.	Extreme-value analyses of the still water level determined for the Charleston tide gauge.....	36
Figure 5-1.	Location map showing NDBC and CDIP wave buoys and model boundary	38
Figure 5-2.	Available wave data sets timeline	39
Figure 5-3.	Example of the development of transformation parameters between NOAA buoy 46002 (Oregon) and 46015 (Port Orford) for period bin 10 s to 12 s	40
Figure 5-4.	Raw probability density functions for buoy 46002 and the Port Orford buoy.....	41
Figure 5-5.	Synthesized wave climate developed for Coos County.....	42
Figure 5-6.	Synthesized wave climate developed for Coos County.....	43
Figure 5-7.	Seasonal variability in the deepwater wave climate offshore from the southern Oregon coast.....	43
Figure 5-8.	Predominant wave directions for the summer months (April-September) and the winter (October to March)	44
Figure 5-9.	Time series of the combined wave height and period record along with the measured tide and computed TLW values for a beach slope ($\tan \beta$) of 0.03 and 0.08.....	46
Figure 5-10.	Coos County study area bathymetry	47
Figure 5-11.	Focus area bathymetry offshore from Bastendorff and Lighthouse Beach, adjacent to Coos Bay	48
Figure 5-12.	Focus area bathymetry offshore from Bandon	48
Figure 5-13.	Coos County computational grid.....	49
Figure 5-14.	Charleston Region Computational grid for the Charleston region	49
Figure 5-15.	Computational grid – Coquille region	50
Figure 5-16.	Grid depths	50
Figure 5-17.	Example SWAN run (Case 53)	52
Figure 5-18.	Example results of SWAN run showing alongshore varying wave height and period at the 20-m contour	53
Figure 6-1.	Conceptual model showing the components of wave runup associated with incident waves (modified from Hedges and Mase, 2004).....	54
Figure 6-2.	Total water level calculations using the Stockdon and DIM runup equations using slope values of 0.016 (DIM) and 0.079 (Stockdon)	57
Figure 6-3.	Total water level calculations using the Stockdon (2006) and DIM runup equations using slope values of 0.019 (DIM) and 0.033 (Stockdon).....	57
Figure 6-4.	Wave runup on a beach backed by a structure or bluff (modified from NHC, 2005).....	58
Figure 6-5.	Determination of an average slope based on an iterative approach	60
Figure 6-6.	Locations of the Bandon beach profiles and intersection points with the 20-m contour	62

continued on next page

Figure 6-8.	Example peak over threshold (POT) extreme value results for the 1% and 0.2% total water levels at Coos Profile 4, located at Bastendorff Beach (dune-backed beach).....	64
Figure 6-7.	Locations of the Coos beach profiles and intersection points with the 20-m contour.....	64
Figure 6-9.	Nomenclature of overtopping parameters available for mapping base flood elevations (BFEs) and flood hazard zones.....	65
Figure 6-10.	Calculations of bore height decay from wave overtopping at Cape Lookout State Park at the peak of the March 2-3, 1999 storm based on a range of alpha (α) values.....	69
Figure 7-1.	Foredune erosion model and geometric model used to assess the maximum potential beach erosion in response to an extreme storm	73
Figure 7-2.	Plot of T_s for the Bandon and Bastendorff Beach shorelines	75
Figure 7-3.	The Bandon 21 profile site showing the locations of h_b , used to define the cross-shore width (W_b) of the surf zone	76
Figure 7-4.	Example plot of the approach used to define storm duration along the Coos County shoreline.....	77
Figure 7-5.	Plot of T_d for the Bandon and Bastendorff/Lighthouse beach shorelines	78
Figure 7-6.	Application of the duration-reduced erosion estimate to the most eroded winter profile at Bandon 16.....	80
Figure 7-7.	Application of the duration-reduced erosion estimate to the most eroded winter profile at Bandon 4 where overtopping occurs.....	81
Figure 7-8.	Garrison Lake, Port Orford, example profile where a barrier beach is overtopped and eroded	82
Figure 7-9.	Overtopping of the barrier beach adjacent to Garrison Lake during a major storm on February 16, 1999	82
Figure 8-1.	Example of a bluff-backed beach (Bandon 11) where the calculated total water level and defined velocity (VE) zone extends into the bluff.....	83
Figure 8-2.	Example of along-shore zone breaks and their relationship to geomorphic barriers and surveyed transects	84
Figure 8-3.	Example of zone breaks for dune-backed beaches.....	85
Figure 8-4.	Example beach profiles for the north Coos Spit derived from 1998, 2002, and 2008 lidar data	87
Figure 8-5.	Storm-induced dune response determined for dune-backed beaches in Coos County for the period 1998–2008.....	88
Figure 8-6.	Plot showing the locations of the primary frontal dune, 6-m contour, projected storm induced erosion, and final V-zone (red line) at profile sites 1368, 1369, and 1371	88
Figure 8-7.	Example profile from Coos Spit with multiple dune features	89
Figure 8-8.	Plot showing the locations of the primary frontal dune, 6-m contour, projected storm-induced erosion, and final V-zone at profile sites 1419, 1421, 1422, and 1423	91
Figure 8-9.	Example of V-zone mapping undertaken where a creek arrives at the coast and is subject to varying outlet locations	92
Figure 8-10.	V-zone mapping along coastal bluffs located on the south side of Cape Arago, Coos County.....	93

LIST OF ACRONYMS AND SYMBOLS

"A" zone	FEMA; Areas subject to inundation by the 1-percent-annual-chance flood event generally determined using approximate methodologies	NGDC	National Geophysical Data Center
AMM	annual maximum method	NGS	National Geodetic Survey
BFE	base flood elevations	NHC	Northwest Hydraulics Consultants
CDIP	Coastal Data Information Program, Scripps Institution of Oceanography	NOAA	National Oceanic and Atmospheric Administration
CORS	continuously operating GPS reference stations	NOS	National Ocean Service
DEM	digital elevation model	NSRS	National Spatial Reference System
DFIRM	digital flood insurance rate map	NTP4	NOS tide prediction program
DGPS	differential GPS	OLC	Oregon Lidar Consortium
DIM	Direct Integration Method	OPRD	Oregon State Parks and Recreation Department
DSAS	Digital Shoreline Analysis System	OPUS	online positioning user service, maintained by the NGS
DWL _{2%}	2% dynamic water level	OSU	Oregon State University
E_j	beach-dune juncture	PDF	probability density functions
E_{jMLWP}	beach-dune junction elevation at the most eroded winter profile	PDOP	position dilution of precision
ENSO	El Niño Southern Oscillation	PFD	primary frontal dune
EV-I	Gumbel extreme value distribution	PNW	Pacific Northwest
EV-II	Frechet class of extreme value distributions	POT	peak-over-threshold
EV-III	Weibull class of extreme value distributions	R	total vertical wave runup
FEMA	Federal Emergency Management Agency	RMSE	Root mean squared error
FIS	Flood Information Studies	RTK	Real-time kinematic
GCPs	ground control points	RTK-DGPS	Real-Time Kinematic Differential Global Positioning System
GEV	generalized extreme value	SWAN	Simulating WAves Nearshore
GPD	Generalized Pareto Distribution	SWL	still water level
GPS	Global Positioning System	$\tan \beta$	beach slope
JONSWAP	Joint North Sea Wave Project spectra, an empirical relationship that defines the distribution of energy with frequency within the ocean	TAW	Technical Advisory Committee for Water Retaining Structures
MATLAB	computer programming software	TIN	triangulated irregular network
MHHW	mean higher high water	T_{WL}	total water level
MHW	mean high water	USACE	USACE
MLLW	mean lower low water	USGS	U.S. Geological Survey
MLWP	most likely winter profile	"V" zone	FEMA; Areas along coasts subject to inundation by the 1-percent-annual-chance flood event with additional hazards associated with storm-induced waves.
MPED	maximum potential erosion distance	"VE" zone	FEMA; Areas subject to inundation by the 1-percent-annual-chance flood event with additional hazards due to storm-induced velocity wave action
M_w	earthquake magnitude	VERTCON	National Geodetic Survey online vertical conversion tool
MSL	mean sea level	WAAS	Wide Area Augmentation System
MWL	mean water level	WIS	Wave Information Studies
NAD 83	North America Datum 1983	WS	Watershed Sciences, Inc.
NASA	National Aeronautics and Space Administration	ΔBL	beach-level change
NAVD88	North American Vertical Datum of 1988		
NDBC	National Data Buoy Center		

1.0 INTRODUCTION

The objective of the Coos County coastal flood map project is to develop a digital flood insurance rate map (DFIRM) and flood insurance study (FIS) report for Coos County, Oregon (Figure 1-1). A parallel effort is underway as of September 2008 to convert Coos County to a Federal Emergency Management Agency (FEMA) countywide format in the North

American Vertical Datum of 1988 (NAVD88); however, the scope of that project is strictly digital conversion and no new studies and/or updated floodplain boundaries are being incorporated. For this effort, the Oregon Department of Geology and Mineral Industries (DOGAMI) will be using available light detection and ranging (lidar) data to redelin-

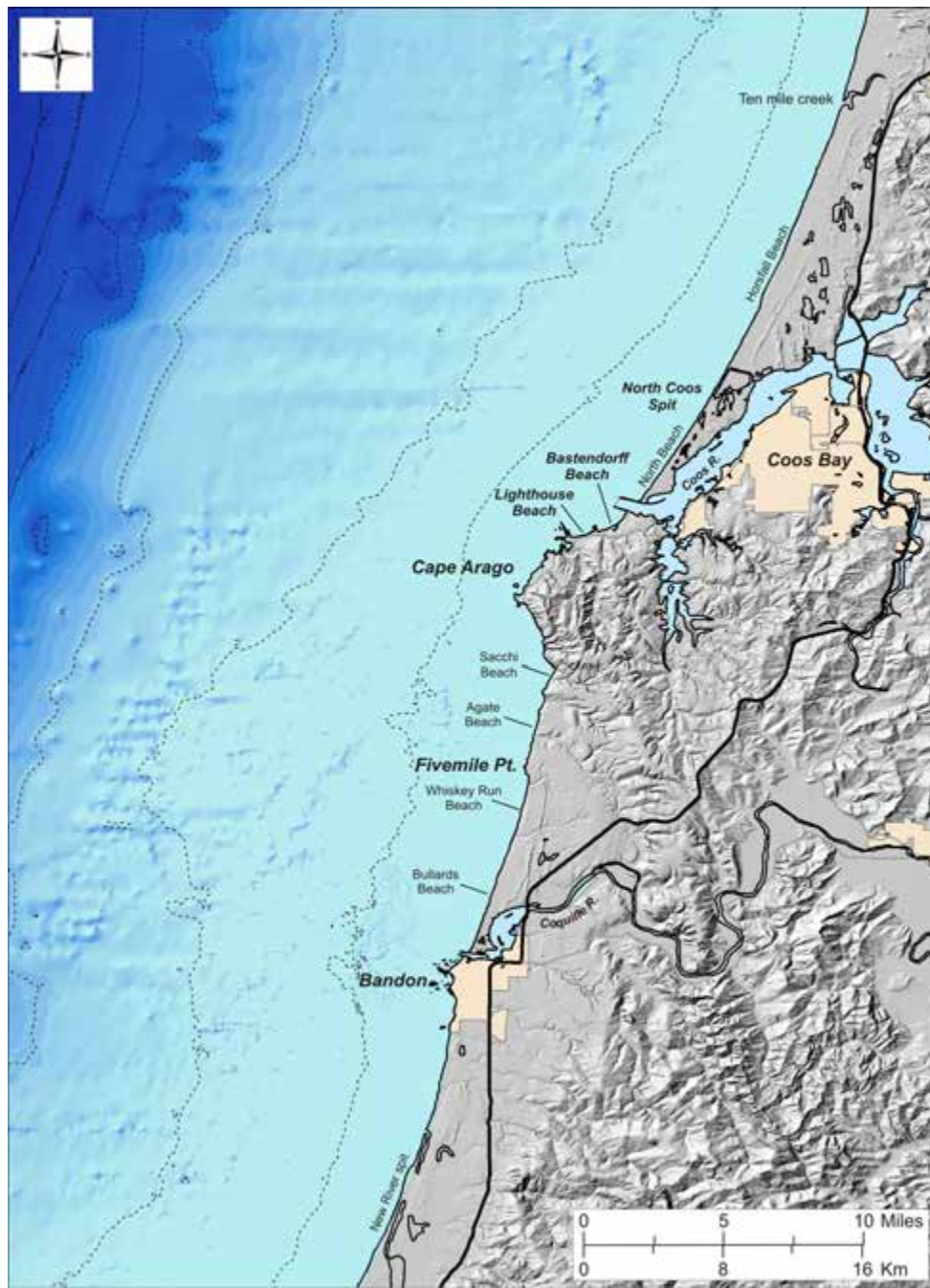


Figure 1-1. Location map of Coos County coastline. Note: Tan shading denotes city urban growth boundaries.

eate hazards within Coos County, produce revised DFIRMs and a revised FIS report, and produce other mapping products usable at the local, state, and federal level for mitigation planning, risk analysis, and disaster response.

As part of the redelineation, DOGAMI has been contracted to perform detailed coastal flood hazard studies for two limited stretches of beach along the Coos County shoreline of the Pacific Ocean. These analyses are to include assessments of the 1% annual probability, or 100-year, extreme storm wave event and the associated calculated wave setup, runup, and total water level (i.e., the wave runup superimposed on the tidal level) to help determine the degree of coastal flood risk along those shores. Additional modeling of the 0.2%, or 500-year, event will also be undertaken.

These detailed analyses will be limited to two key areas (Figure 1-1):

- Bandon shoreline, which extends from the Coquille Jetty south to the southern extent of the Bandon urban growth boundary (approximately 0.5 miles south of Johnson Creek), and
- Bastendorff and Lighthouse Beach, located to the south of the Coos Bay jetties, and a small portion of Sunset Bay State Park.

Aside from those two areas, DOGAMI will develop revised velocity ("V") zones for the remainder of the county shoreline. Presently, the bulk of the coastline is characterized as an Approximate ("A") zone. However, after consulting with FEMA and state government representatives, the decision was made to revise the A-zones to reflect the geomorphology of the coast and to redefine these zones as velocity ("V") zones.

The development of coastal flood maps is complicated due to its dependence on a myriad of data sources required to perform wave transformation, runup, and overtopping calculations. These challenges are further compounded by an equally wide range of potential settings in which the data and methods can be applied, which range from dune-to-bluff-backed beaches, sites that may be backed by coastal engineering structures such as sea walls, riprap revetments, or wooden bulkheads, to gravel and hard-rock shorelines. Figure 1-2 broadly summarizes the steps described in the ensuing sections in order to help understand conceptually the process that leads ultimately to the completed coastal flood hazard zones.

This report first examines the coastal geology and geomorphology of the Coos County shoreline, including a discussion of the erosion history of the coast. The results presented in this section will ultimately form the basis for defining the flood zones along the Coos County coast. Section 3, "Beach and Bluff Morphology Assessments," presents the results of real-time kinematic differential Global Positioning System (RTK-DGPS) surveys of the two detailed study sites located at Bandon and along Bastendorff and Lighthouse Beach near Coos Bay, undertaken at the peak of the 2008-2009 winter. These surveys are compared with historical data derived from light detection and ranging (lidar) data, which are used to help define the most eroded winter profile used in the runup calculations described in Section 6, "Wave Runup and Overtopping." Section 3 also documents various parameters associated with the measured beach profile data, including beach-dune junction elevation, beach slope, and dune/bluff crest-top elevations.

An examination of the tide data measured by the Charleston tide gauge, located in Coos Bay, is presented in Section 4, "Tides," and includes an analysis of the 1% and 0.2% still water levels (SWL). Section 5, "Pacific Northwest Wave Climate," describes the steps undertaken to develop a synthesized wave climate, critical for developing the input wave statistics used in calculating the wave runup. Section 5 also examines the procedures used to refract the waves from deep-water waves to the 20-m bathymetry contour using the SWAN (Simulating WAves Nearshore) wave model. Analyses of the wave runup, including the calculation of the 1% and 0.2% total water levels (T_{WL}) as well as any overtopping calculations is presented and discussed in Section 6. Section 7, "Coastal Erosion," discusses the steps used to determine the degree of erosion that might occur on the dune-backed beaches, including the approach used to define the duration reduced erosion factor, important for further establishing the initial conditions on which the runup and overtopping calculations are ultimately performed. No such analyses are performed for the coastal bluffs since these are considered to be essentially non-erodible. Finally, Section 8, "Flood Mapping" synthesizes all of the information and describes the steps taken to draft new flood maps along the Coos County shoreline.

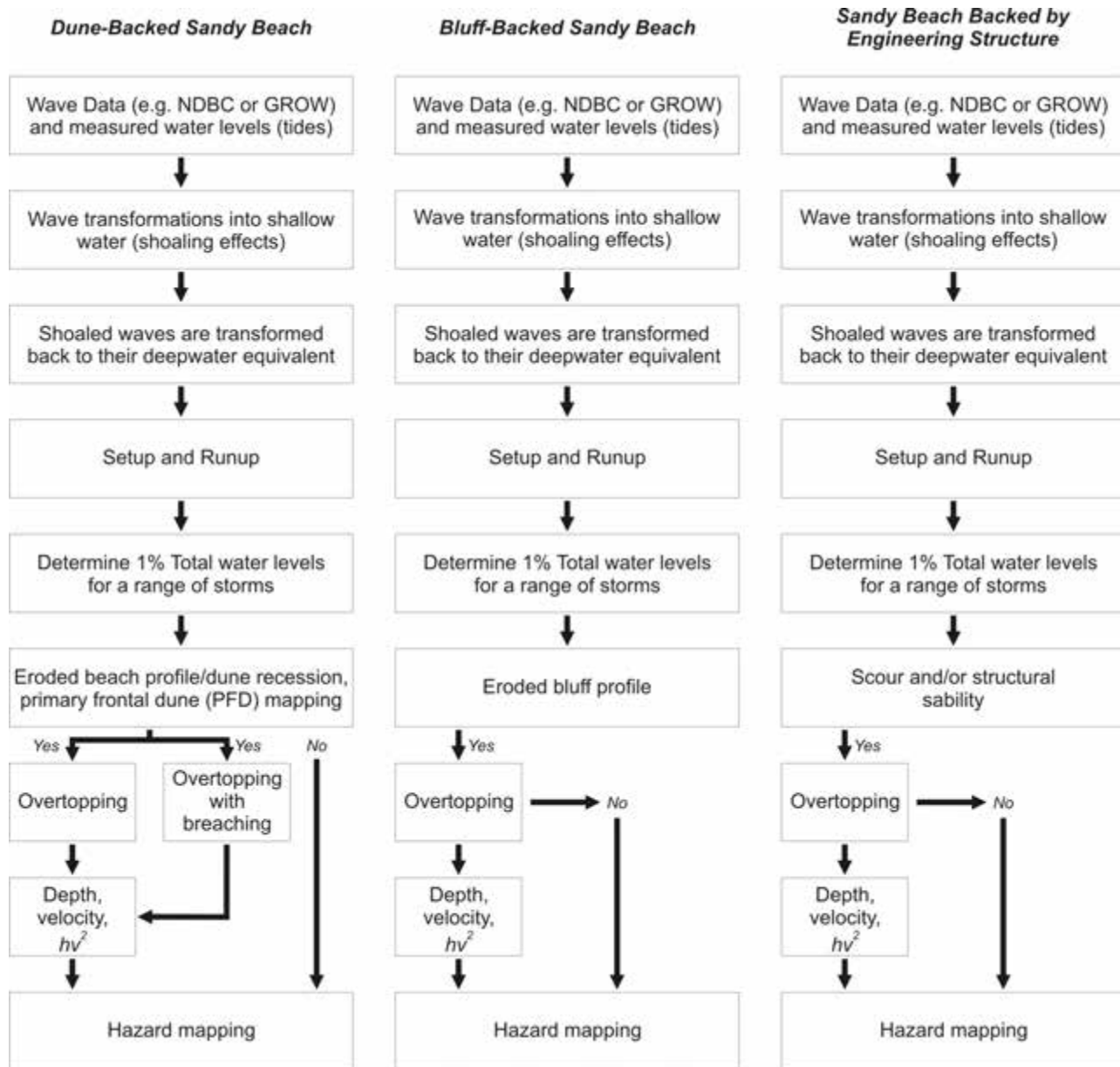


Figure 1-2. Three representative examples of the steps that may be taken to derive coastal flood hazard maps. NDBC is National Data Buoy Center, and GROW is Global Reanalysis of Ocean Waves.

2.0 COASTAL GEOLOGY AND GEOMORPHOLOGY OF COOS COUNTY

Coos County is located on the southwest Oregon coast, between latitudes 43°36'39.33"N (North Coos spit) and 42°57'15.67"N (central portion of New River spit), and longitudes 124°29'3.29"W and 123°42'3.04"W. The terrain varies from low-elevation sandy beaches and dunes on the coast itself to elevations over 1,100 m (3,609 ft) inland. Along the flank of the Coast Range mountains are a series of marine terraces (Baldwin and others, 1973). The southern part of the county (south of Cape Arago) is drained by the Coquille River, which reaches the coast at Bandon, while the northern part of the county is drained by the Coos River (Figure 1-1).

2.1 Local geology

The geology of the region is characterized by a wide variety of lithologic units. Along the coast the predominant units consist of Quaternary alluvium and Quaternary sand that make up the bulk of the shore between Fivemile Point (to the north of the Bandon dunes golf course), and south along the New River Spit (Baldwin and others, 1973; Peterson and others, 2007). The sediments that compose the Bandon and

New River Spit beaches are derived from erosion of alluvial terraces at the southern end of the littoral cell at Blacklock Point in northern Curry County (generally yielding gravel to coarse sand), and from the Coquille River (predominantly fine sand). North of Cape Arago the shoreline is also composed of Quaternary sand that makes up the North Coos Spit and Horsfall Beach (Figure 2-1).

At Bandon the older rocks along the coastline are characterized by a complex mix of bedded graywacke, sheared mélange of the Jurassic Otter Point Formation of varying thickness, and marine and alluvial terrace sediments (Marra, 2002). The ocean-facing bluffs, 12–26 m (40–85 ft) high in the vicinity of Bandon, formed from erosion into the Jurassic Otter Point Formation, are described by Marra as a thick assemblage of resistant sandstone, siltstone, conglomerate, and volcanic rocks with random blocks of blueschist (e.g., the north end of Bandon). Between Fivemile Point and Cape Arago, the beaches are backed by a sequence of high marine terraces formed from erosion into various siltstone and sandstone units of the Coaledo and Elkton Formations (Figure 2-2). Midway along this stretch of coast, Cape Arago formed from wave erosion into the Coaledo Forma-



Figure 2-1. Aerial view looking north along Bastendorff Beach and the North Coos Spit. Photo taken by Jonathan Allan, DOGAMI, in August 2009.

tion, which is characterized by tilted, cross-bedded sandstone rocks. More resistant sandstone beds form steep cliffs around the headland or project into the sea as long parallel ribs (Baldwin and others, 1973). Less resistant rocks have been eroded to form small bays (re-entrants), such as Sunset Bay.

2.2 Tsunami hazards associated with the Cascadia subduction zone and from distant earthquake sources

Considerable geologic evidence from estuaries and coastal lakes along the Cascadia subduction zone provides evidence for episodic occurrences of abrupt coastal subsidence immediately followed by significant ocean flooding associated with major tsunamis that swept across the ocean beaches and also traveled well inland through the bays and estuaries. Coastal paleoseismic records document the impacts of as many as 13 major subduction zone earthquakes and associated tsunamis over the past ~7,000 years (Kelsey and others, 2005; Witter and others, 2003; Witter and others, 2010), while recent studies of turbidite records within sediment cores collected in deep water at the heads of Cascadia submarine canyons provide evidence for at

least 41 distinct tsunami events over the past ~10,000 years (Goldfinger, 2009; Goldfinger and others, 2003; Goldfinger and others, 2009). The length of time between these events varies from as short as a century to as long as 1,200 years, with the average recurrence interval for major Cascadia earthquakes (magnitude $> [M_w] 9$) estimated to be ~530 years (Witter and others, 2010).

The most recent Cascadia subduction zone earthquake occurred on January 26, 1700 (Atwater and others, 2005; Satake and others, 1996) and is estimated to have been magnitude (M_w) 9 or greater from the size of the tsunami documented along the coast of Japan. From correlations between tsunami deposits identified at multiple sites along the length of the Pacific Northwest (PNW) coast this event probably ruptured the full length (~1,200 km) of the subduction zone.

There is now increasing recognition that great earthquakes do not necessarily result in a complete rupture of the Cascadia subduction zone (i.e., rupture along the full 1,200-km fault zone); the paleorecord indicates that partial ruptures of the plate boundary have occurred due to smaller earthquakes with magnitudes (M_w) < 9 (Kelsey and others, 2005; Witter and others, 2003). These partial segment ruptures appear to occur more frequently on the



Figure 2-2. Bluff-backed beaches at Fivemile Point north of the Bandon Dune Golf Course. Note the well-vegetated bluff face, indicating that the dunes have been stable for some time. Photo taken by Jonathan Allan, DOGAMI, in August 2009.

southern Oregon coast, as determined from paleotsunami studies (stratigraphic coring, radiocarbon dating, and marine diatom analyses) undertaken at several locations on the southern Oregon coast, including Bradley Lake located just south of Bandon, the Sixes River, and the Coquille estuary. According to Kelsey and others (2005), initial estimates of the recurrence intervals of Bradley Lake tsunami incursion is typically shorter (~380–400 years) than average recurrence intervals inferred for great earthquakes (~530 years). Furthermore, Kelsey and others have documented from those records that local tsunamis from Cascadia earthquakes recur in clusters (~250–400 years) followed by gaps of 700–1,300 years, with the highest tsunamis associated with earthquakes occurring at the beginning and end of a cluster.

Recent analyses of turbidite records (Goldfinger, 2009; Goldfinger and others, 2009) suggest that of the 41 events in the geologic past:

- 20 events were probably associated with a rupture of the full Cascadia subduction zone, characterized by a magnitude (M_w) ~9 or greater earthquake;
- 2 or 3 events reflected a partial rupture (~75%) of the length of the subduction zone, characterized by an estimated earthquake magnitude (M_w) of ~8.5–8.8 earthquake;
- 10 or 11 events were associated with a partial rupture (~50%), characterized by an estimated earthquake magnitude (M_w) of ~8.3–8.5 earthquake; and
- 8 events reflected a partial rupture (~25%), with an estimated earthquake magnitude (M_w) of ~7.6–8.4.

These last 19 shorter ruptures are concentrated in the southern part of the margin and have estimated recurrence intervals of ~240–320 years. Goldfinger (2009) estimated that time-independent probabilities for segmented ruptures range from 7–9% in 50 years for a full margin rupture to ~18% in 50 years for a partial southern segment rupture.

Aside from local tsunamis associated with the Cascadia Subduction Zone, the Oregon coast is also susceptible to tsunamis generated by distant events, particularly along the coast of Japan, along the Aleutian Island chain, and from the Gulf of Alaska. The most recent distant tsunami event occurred on March 11, 2011, when a magnitude (M_w) 9.0 earthquake occurred 129 km (80 miles) offshore from the coast of Sendai, northeast Honshu, Japan (Allan and others, 2012). This earthquake triggered a catastrophic tsunami that within minutes inundated the northeast coast of Japan, sweeping far inland; most recent reports indicate 15,854 dead and another 3,155 missing. Measurements derived from a tide gauge on the impacted shore (Ayukawa, Ishino-

maki, Miyagi Prefecture) recorded a tsunami amplitude of 7.6 m before the gauge was destroyed by the initial tsunami wave (Yamamoto, 2011), while post-tsunami surveys indicate that tsunami water levels within the inundation zone reached as high as 19.5 m (Mori and others, 2011). The tsunami also propagated eastward across the Pacific Ocean, impacting coastal communities in Hawaii and along the west coast of the continental United States—Washington, Oregon, and California.

Damage in Oregon, Washington, and northern California from the tsunami was almost entirely confined to harbors, including Depoe Bay, Coos Bay, and Brookings in Oregon, and Crescent City in California. Damage was moderated by the arrival of the tsunami's highest waves during a relatively low tide (Allan and others, 2012). At Crescent City, an open-coast breakwater, the to-and-fro surge of the water associated with the tsunami waves overturned and sank 15 vessels and damaged 47, while several boats were swept offshore. Flood damage also occurred during the early hours of March 12 at an RV park near the mouth of Elk Creek when a 1.05-m tsunami wave arrived, coinciding with high tide. The total damage to the harbor and from this flooding has been placed at \$12.5 million. At Brookings, on the southern Oregon coast, 12 fishing vessels had put to sea at about 6 am, prior to the arrival of the tsunami waves. However, the *Hilda*, a 220-ton fishing boat and the largest in the harbor, broke loose under the forces of the wave-induced currents, washing around the harbor and smashing into and sinking several other boats. Much of the commercial part of the harbor and about one-third of the sports basin were destroyed; total damage has been estimated at about \$10 million.

Prior to the Tōhoku tsunami, the previous most significant distant tsunami occurred on March 27, 1964, when a magnitude (M_w) 9.2 earthquake occurred near Prince William Sound in Alaska and generated a catastrophic local tsunami; the effects of the tsunami was also felt around the Pacific Basin. The tsunami caused significant damage to infrastructure in the Oregon coastal communities of Seaside and Cannon Beach and killed four people camping along Beverly Beach in Lincoln County. However, on the south coast of Oregon the wave did comparatively little damage. For example, the tsunami at Bandon raised the tide by an estimated 4 feet above the normal tide and caused considerable surging upstream in the Coquille River (CH2M HILL, 1995).

In 2009 the Oregon Department of Geology and Mineral Industries initiated a multi-year study to accelerate remapping of the Oregon coast for tsunami inundation using state-

of-the-art computer modeling and laser-based terrain mapping (lidar). The outcome of this effort will be the creation of new and more accurate tsunami evacuation maps for the entire length of the coast. DOGAMI, in collaboration with researchers at the Oregon Health and Science University (OHSU; Zhang and Baptista), Oregon State University (Goldfinger) and the Geological Survey of Canada (Wang), have developed a new approach to produce a suite of next-generation tsunami hazard maps for Oregon (Priest and others, 2009; Witter and others, 2010). Modeling tsunami inundation on the southern Oregon coast was initiated late in 2009 and consists of a range of scenarios, including 15 Cascadia events and two distant earthquake source events (e.g., 1964 Prince William Sound earthquake magnitude [M_w] 9.2 earthquake [Witter, 2008]). Results from this effort are scheduled to be completed for the entire southern Oregon coast by the summer of 2010.

Associated with great Cascadia earthquakes is a nearly instantaneous lowering (subsidence) of the coast by ~ 0.4 m to as much as 3 m (Witter and others, 2003). This process equates to raising sea level by the same amount along the coast, which almost certainly would have initially resulted in extensive erosion of the coast as the beaches and shorelines adjusted to a new equilibrium condition that over time would have likely caused the erosion response to decrease asymptotically (Komar and others, 1991). Komar and others have argued that the extensive development of sea stacks offshore from Bandon is evidence for massive erosion following the AD 1700 earthquake and that the Bandon shoreline has not experienced measurable erosion in more than a century because much of the coast is now being uplifted (estimated to be ~ 0.6 to 1.1 m) due to the Cascadia subduction zone having become locked, such that strain is now building toward the next major earthquake. With the release of energy from the next major earthquake and consequent land subsidence, cliff erosion along the Bandon shore would certainly begin again.

2.3 Coastal geomorphology

On the basis of geology and geomorphology the Coos County shoreline can be broadly divided into six morphological beach types (Figure 2-3 and Figure 2-4). These include:

1. Barrier beaches: The New River Spit reflects an active barrier beach system and is composed of both mixed sand and gravel and fine sandy beaches. These beaches are subject to periodic overtopping, dune blowouts, and breaching of the barrier. Dunes have developed

along much of this stretch of the barrier shore and have become stabilized by the introduction of European beach grass in the 1930s. Analyses of 2008 lidar data indicate that dune crest elevations along the New River Spit range from a height of 11.9 m (39 ft) near the southern end of the spit to lows of less than 3 m (10 ft) near the mouth of the river; the average dune crest height is 8.1 m (27 ft, $\sigma = 1.9$ m [6 ft]). The average beach slope ($\tan \beta$) along the spit is 0.079 ($\sigma = 0.033$), indicating that the beach foreshore is steep—characteristics of mixed sand and gravel beaches. However, a significant feature of the New River Spit is the existence of a marked and regular alongshore variation in its grain sizes and resulting beach slopes, which is due to the mixing of gravels (coarse sand to pebbles) derived from the erosion of Blackrock Point to the south and finer sands from the Coquille River to the north (Komar and others, 1991).

2. **Dune-backed beaches:** Dune-backed beaches characterize three small sections of shore in the vicinity of Bandon: Bullards Beach located to the north of the north Coquille jetty and south of the Bandon Dunes golf course, Bastendorff Beach near Coos Bay, and along the North Coos Spit and Horsfall beach (Figure 2-1–Figure 2-4). Dune crest elevations are highest along the North Coos Spit and Horsfall Beach, where they reach 14.1 m (46 ft), and are on average lowest at Bastendorff Beach, where they average 6.8 m (22 ft) high. The average beach slope ($\tan \beta$) for all dune-backed beaches is 0.067 ($\sigma = 0.021$), indicating that the beach foreshore is moderately steep, while the lowest beach slopes can be found at Bastendorff Beach (Figure 2-1).
3. **Bluff-backed beaches:** Bluff-backed beaches dominate the shoreline adjacent to Bandon, and from the Bandon Dunes golf course north to Cape Arago (Figure 2-2–Figure 2-4). The bluffs that back the beaches vary in height from 9.7 m (32 ft) to as much as 53 m (174 ft). Beach slopes ($\tan \beta$) seaward of the bluffs are consistently lower when compared with the dune-backed beaches, averaging about 0.032 ($\sigma = 0.006$). Along the Bandon shoreline, the bluffs have an average slope of 26° and are well vegetated today (Figure 2-5) as well as in historical photographs of this area dating back for more than a century, indicating that they have not been subject to significant wave erosion processes along the toe of the bluffs during the twentieth century.

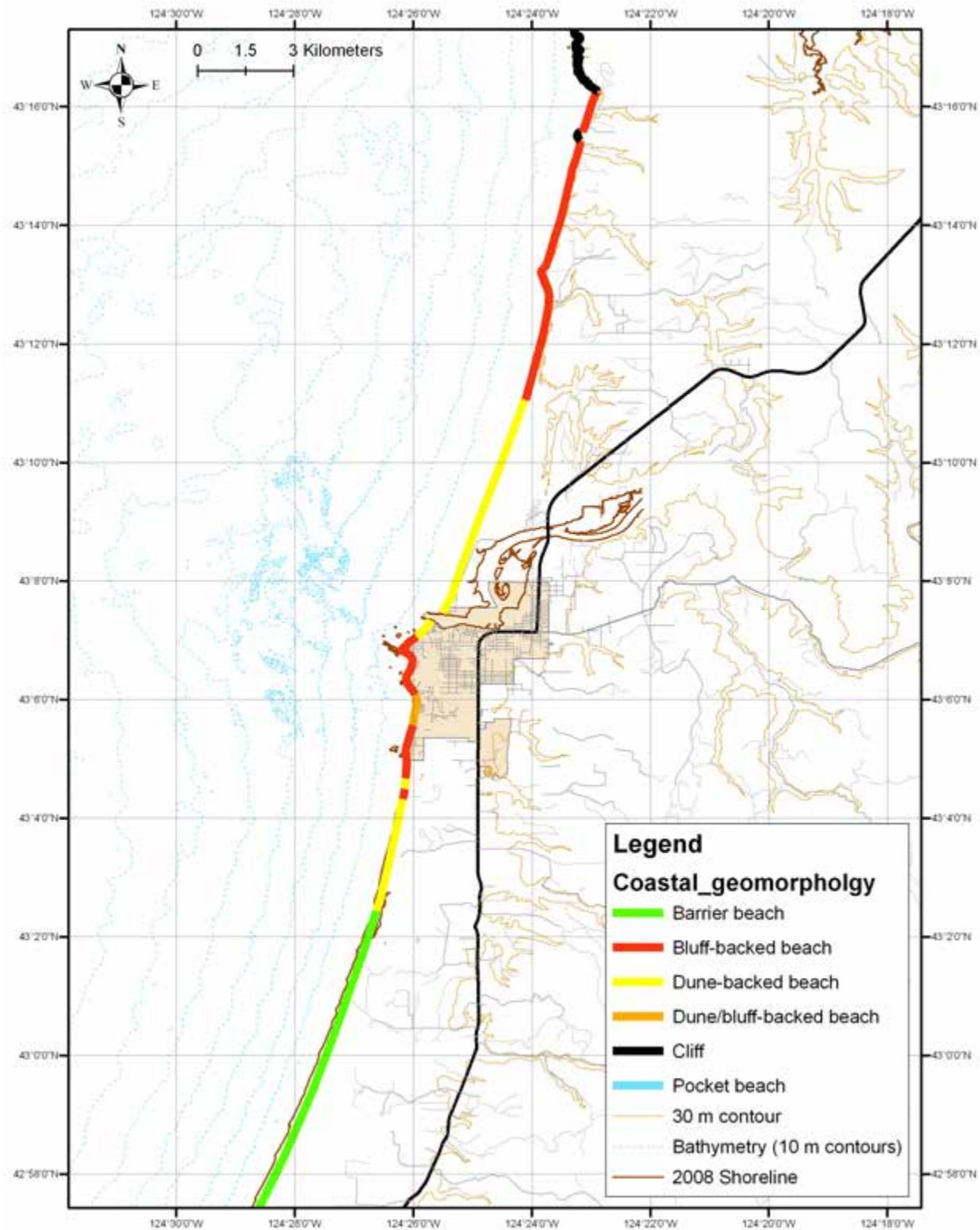


Figure 2-3. Geomorphic classification of the southern Coos County shoreline (New River spit to Cape Arago).

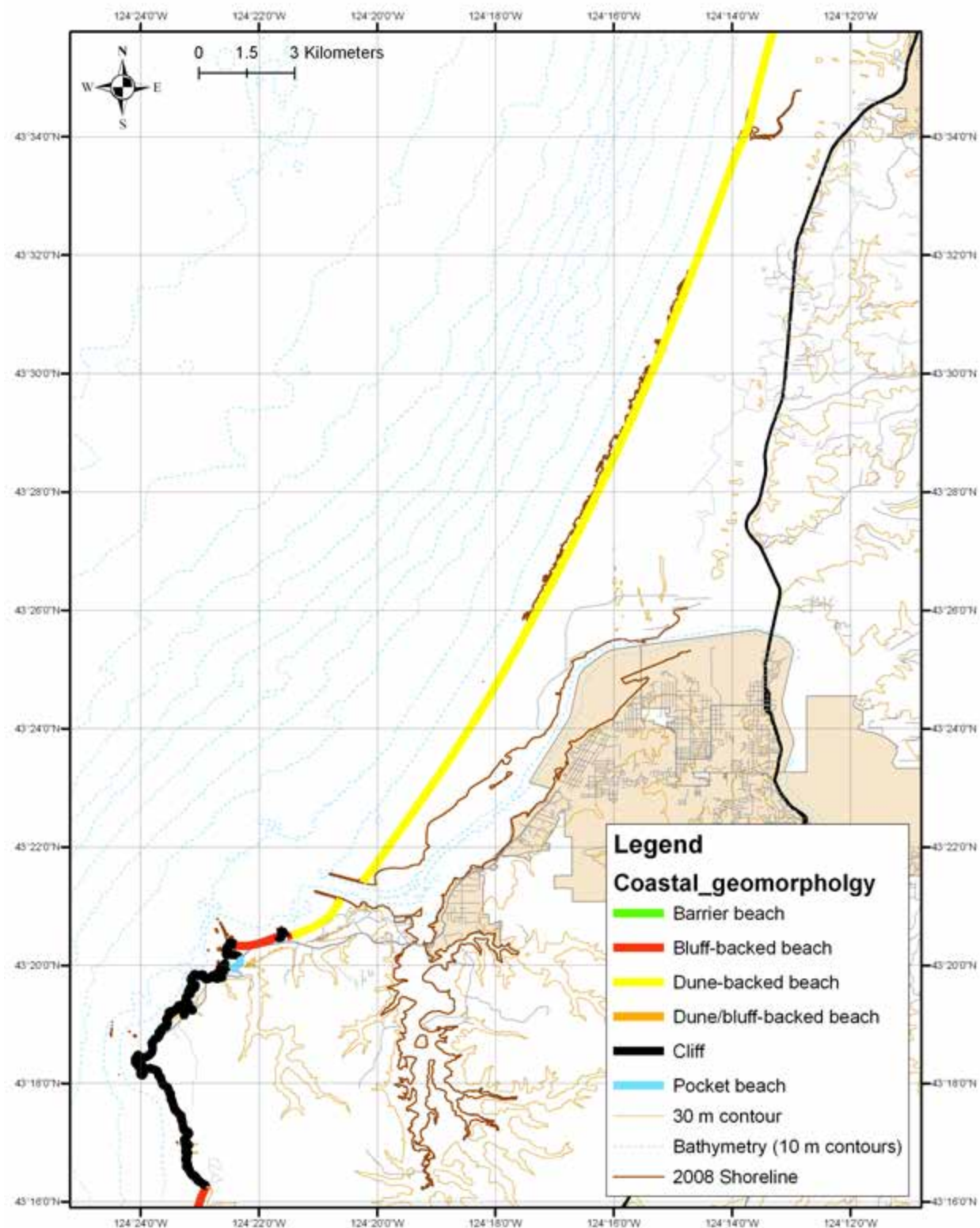


Figure 2-4. Geomorphic classification of the northern Coos County shoreline (Cape Arago to North Coos Spit).

- 4. Dune/bluff-backed beaches:** These beaches characterize a small section of shore to the north and south of Johnson Creek in Bandon (Figure 2-6). At that site the dunes are relatively small (dune crest = 7–11.9 m) and could be periodically washed away during major storms. The beaches are characterized by very low beach slopes; average beach foreshore slope is 0.028 ($\sigma = 0.006$). European beach grass has become established on the developing dunes. Backing the beach and dune are vegetated (stable) coastal bluffs that span the bulk of the Bandon shore (e.g., Figure 2-5).
- 5. Cliffs:** Midway along the Coos County coastline is a sequence of high coastal cliffs that mark the seaward edge of the Cape Arago headland (Figure 2-7). These cliffs have been formed by gradual wave erosion into the sandstone of the Coaledo Formation and are subject to periodic rockfalls and landsliding. The Cape Arago cliffs have an average elevation of 26.5 m (87 ft) but can exceed 80 m (262 ft). Seaward of the cliffs there is a combination of rock reefs, shore platforms, and boulder beaches.
- 6. Pocket beaches:** Sunset Bay forms a small crescentic pocket beach at the northwestern end of Cape Arago, bounded by resistant sandstone cliffs on both sides of the bay. The beach is protected from the large ocean waves that typically form out of the west and southwest Pacific during the winter. As a result, Sunset Bay is exposed only to waves that refract around the Cape Arago headland and waves that arrive from the northwest. The arcuate shoreline of the beach within the embayment is characterized by a composite morphology that consists of a gently sloping fine sand beach below the mean tide level, and a steeper sand beach above mean tide level. The average beach foreshore slope is 0.075 ($\sigma = 0.027$). The crest of the beach includes a low dune with an average crest elevation of 5 m (16 ft).



Figure 2-5. Bluff-backed beaches characterize much of the shoreline at Bandon. Note the well-vegetated bluff face. Bluff stability, as shown by the presence of thick vegetation that extends to the beach, indicates that the bluff toe is rarely impacted by high wave runup elevations generated during storms. This observation is supported by historical photos (late 1800s/early 1900s) of the Bandon shore, which indicate that the bluffs have changed little over this time interval. Photo taken by Jonathan Allan, DOGAMI, in May 2007.



Figure 2-6. Dune/bluff-backed beaches near Johnson Creek in Bandon during a small storm in February 2009. Photo taken by Jonathan Allan, DOGAMI.



Figure 2-7. Steep cliffs characterize much of the coastal geomorphology at Cape Arago State Park. Photo taken by Jonathan Allan, DOGAMI, in March 2009.

2.4 Coastal erosion and flood history

The Coos County shoreline is the product of a variety of processes that have helped shape the morphology of the beaches and shorelines over the past several thousand years. These include the effects from great earthquakes associated with the Cascadia subduction zone that produced giant tsunamis that inundated significant areas of the coast as well as lowered the coastal land elevations, thereby initiating a new sequence of shoreline evolution. More recent effects due to humans include the construction of jetties at the mouths of the Coquille and Coos estuaries, and the introduction of non-native dune grasses that have stabilized significant stretches of the coast, thereby enhancing the growth of dunes and dramatically changing the character of the coast. This section briefly reviews these processes for the Coos County shoreline.

2.4.1 Bandon shoreline

Beach morphodynamics along the Bandon shoreline today is a function of the response of the coast to the most recent AD 1700 Cascadia subduction zone earthquake, with the coast now being emergent due to tectonic uplift, and human effects associated with the construction of the Coquille jetties. The primary sediment sources for the Bandon beaches are fine sand that is carried down the Coquille River and gravel (sand to pebbles) supplied by the erosion of Blacklock Point, located to the north of Cape Blanco in northern Curry County. Sand has also been lost from this stretch of shore due to aeolian processes that have carried the finer sand inland, where the sand has accumulated and formed dunes, a loss that is particularly significant south of Bradley Lake near Bandon, where a field of dunes has formed. Sand dunes have also accumulated at the back of the beach along the length of the New River Spit, a ridge of foredunes that separates the ocean beach from the channel of the river.

To the south, erosion of Blacklock Point north of Cape Arago is actively contributing coarser beach sediments to the beach system. Analyses of changes in the position of the bluff-top using historical aerial photos indicate that the bluffs along Blacklock Point are eroding at rates of ~0.09 m per year (Komar and others, 2001). These coarser sediments move along the shore in a predominantly northward direction, where they have mix with the finer sand contributed by the Coquille River to produce a longshore variation in beach sediment grain sizes along this shore (see Figure 3 of Komar and others [2001]). Pebbles dominate the beach sediments along the southern portion of the New River Spit, while the sand content decreases away from the Coquille

River southward toward the southern end of the New River Spit; this southward decrease of sand in the beach reflects both the increasing distance away from the Coquille River (the source of the sand) and the loss of the sand inland to form dunes. The general patterns of sediment movement identified by Komar and others (2001) do not reflect a prevailing net longshore sediment transport in any particular direction, as within the “pocket beach” littoral cells of the Oregon coast the net transport is effectively zero (Komar, 1997). Nevertheless, sand and gravel derived from the mixing of these two sediment sources has enabled the New River Spit to prograde as the mouth of the river has slowly migrated to the north in recent decades and as the elevations of the foredunes has increased with time, aided by the introduction of European dune grass. Over approximately 1.5 km near the tip of the Spit nearest the present-day position of the river’s mouth, the beach is characterized by intermittent clumps of low dunes, separated by zones where winter storm waves actively wash over the spit. With increasing distance southward, the dunes become progressively higher and more effective at preventing overwash during storms.

In the north along the Bandon bluffs, the beach and shoreline are considered to be stable and appear geomorphically to be unchanged from photographs taken in the early 1900s. As can be seen in Figure 2-5, the bluffs are covered by dense vegetation, mainly impenetrable brush (salal and gorse), and have not been subject to wave-induced toe erosion during the 140 years of settlement of Bandon (Komar and others, 1991).

The Bandon jetties were constructed in the late 1800s at the mouth of the Coquille River, and this locally resulted in significant changes in the shorelines. Construction of the jetties was initiated in December 1883. The response of the shoreline is documented in Figure 2-8, derived from periodic surveys undertaken by the U.S. Army Corps of Engineers (Komar and others, 1976). As can be seen in Figure 2-8, the shoreline response in 1884 indicates that rapid accretion took place south of the jetty. This accretion occurred in the form of a sand spit that grew northward where it became attached to the south jetty. East of the spit, the northward advance of the spit effectively trapped a low area within the accreted land, forming a lagoon shown in the 1891 survey that still exists (Figure 2-8). Aside from the buildup of sand south of the south Coquille jetty, aggradation also occurred north of the north jetty. From this evidence and from similar studies undertaken elsewhere on the coast, this type of response demonstrates the existence of a seasonally reversing longshore sediment transport, northward during the winter and southward in the summer, but with long-term

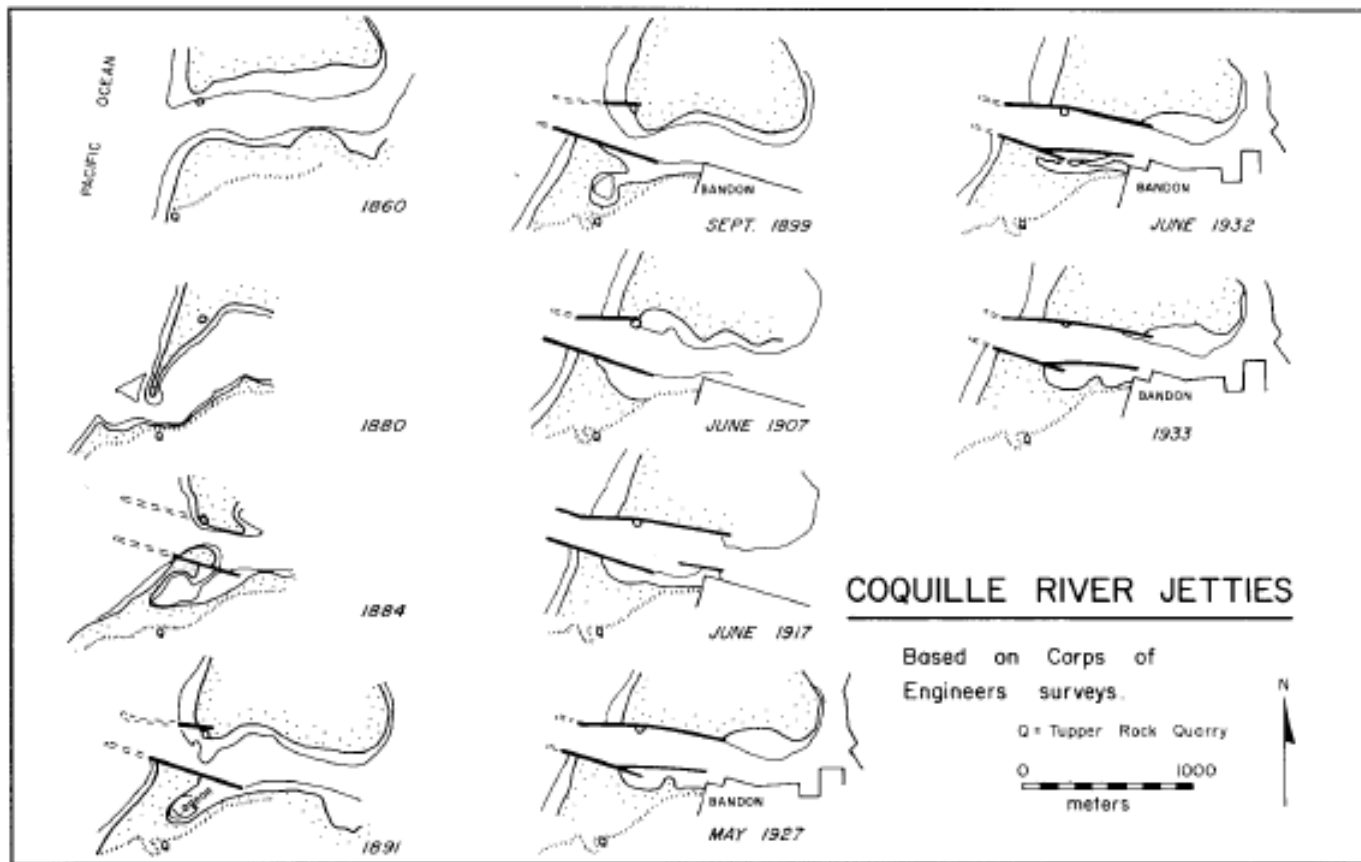


Figure 2-8. Survey line drawings prepared by the U.S. Army Corps of Engineers prior to and during construction of the Coquille jetties adjacent to Bandon (Komar and others, 1991).

net transport being effectively zero (Komar and others, 1976).

The shoreline adjacent to the Coquille jetties has been broadly stable for some decades, although the dunes and low-lying land characteristic of this area remain susceptible to both dune erosion and flooding from extreme ocean waves coupled with high tides (Figure 2-9 and Figure 2-10). Figure 2-9 and Figure 2-10 highlight the effects of a major wave event that occurred on December 22, 2000, which resulted in waves overtopping the parking lot adjacent to the south Coquille jetty in the Bandon "triangle." As can be seen from the photos, wave runup inundated this section of the shore, including the public rest room, carrying logs and

other forms of debris. Prior to this event, Komar and others (1991) noted that the primary foredune in 1991 was characterized by a steep seaward face, evidence that the dune had been subject to recent wave undercutting; this feature of the foredune remains the case today as described in Section 3.3, "Recent coastal changes along the Bandon and Bastendorff beaches." However, although there has been a history of erosion with some overwash of accreted lands immediately adjacent to the south jetty, there has not been a major erosion event in recent decades. Komar and others (1991) did observe drift logs buried at the base of the foredune, suggesting that the dune had been breached in the past but then reformed by aeolian processes.



Figure 2-9. High wave runup and overtopping during a major storm (December 22, 2000) near the south Coquille jetty at Bandon carried logs onto the main parking lot, adjacent to a public restroom. Photo courtesy of J. Marra, pers. commun., May 2010.



Figure 2-10. Wave overtopping during a major storm (December 22, 2000) surrounds the restroom and covers the parking lot adjacent to the south Coquille jetty at Bandon. Photo courtesy of J. Marra, pers. commun., May 2010.

Figure 2-11 is an historical 1939 aerial photo of the “triangle” adjacent to the jetties. The photo has been rubber-sheeted¹ using Esri ArcGIS® software so that it can be compared with more recent orthorectified images of the area. Included in the figure is a dashed cyan line that denotes blowouts in the foredune that are likely to have been caused

by a major storm(s), possibly an event in January 1939 (Figure 2-11). Evidence for the blowouts includes a large number of logs and significant amounts of flotsam carried well inland from the coast. The January 1939 storm resulted in extensive erosion elsewhere on the Oregon coast and is thought to be one of the most significant events to affect the coast in historical times (P. Komar, Emeritus Professor, Oregon State University, pers. commun., December 2009). According to Komar, the 1939 aerial photographs were flown by the U.S. Army Corps of Engineers to document the effects of the storm and constitute the first coastwide suite

¹ The process by which an historical aerial photograph can be distorted to allow it to be seamlessly joined to an adjacent geographic layer of matching imagery, such as an orthorectified aerial photograph. The rubbersheeting process uses common ground control points (GCPs) evident in both photographs to perform the distortion.

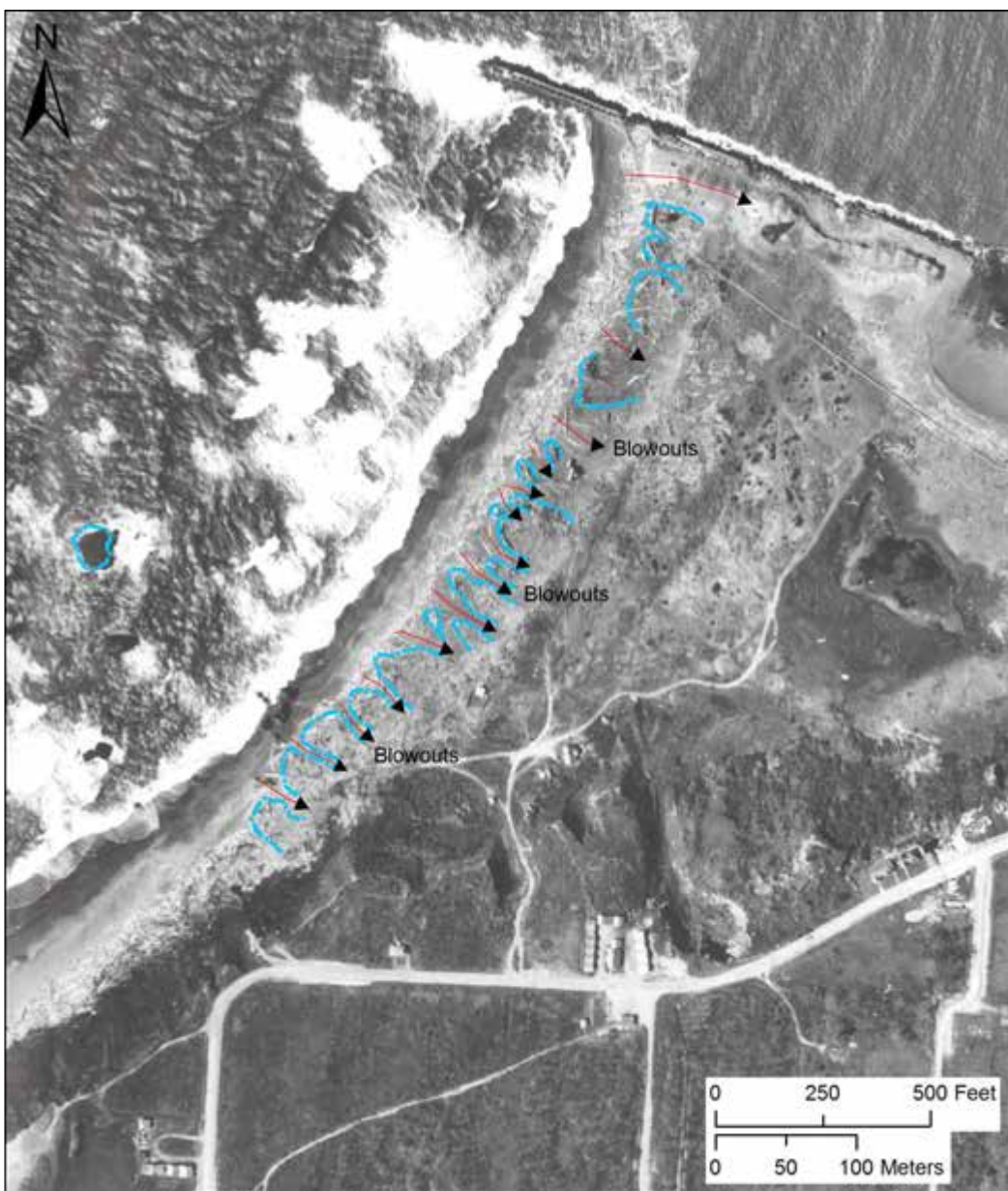


Figure 2-11. 1939 aerial photograph of the Bandon “triangle” adjacent to the Coquille jetties showing evidence of blowouts in the developing foredune that likely occurred during a major storm in January 1939.

of aerial photographs of the Oregon coast. A comparison of the shoreline mapped in 1939 with the 2009 shoreline indicates little difference in the general position, reaffirming the fact that there has been little net change in the position of the shoreline over the past 70 years.

As part of the original flood information study undertaken in Bandon, CH2M HILL (1995) compiled a history of flood events between 1960 and 1993. These are summarized in Figure 2-12.

As an example, one local resident described a storm between 1945 and 1977, which generated ocean flooding

History of Coastal Flooding Events at South Jetty Area of Bandon, Oregon (January 1955 – April 1994)			
Date	Comments	Observed Tide Level (ft, NGVD)*	Estimated Return Period of Tide Level (yrs)
2/9/60	Beach erosion at foot of South Jetty with drift logs 1-2 dia. and stumps 3-4 dia. (est. from photos) washed est. 200' into parking lot.	NHT	—
11/20/60	62 mph southwest winds at Bandon with high tides and surf. No reported flooding, but flood damage at Newport and Tillamook.	NHT	—
10/12/62	Columbus Day wind storm "hurricane-like" winds caused much damage but no reported flooding.	5.45	2
1/18/64	Stormy SW wind. Seafoam 2-3 ft. deep drifted into parking lot at S. Jetty.	NHT	—
12/1/67-12/2/67	Very high tides and "ferocious" winds wash logs into S. Jetty parking lot and jetty access road. 10.1 ft tide (no datum reported) associated with flooding.	NHT	—
1/17/73	S. Jetty Road and top of S. Jetty littered with stumps 2-3 ft. dia and 1 ft. (est) logs. Sand deposited on S. Jetty Road.	6.05	10
11/9/75	Worst windstorm since 1-12/62. 145 mph gusts at C. Blanco. 100 mph W-NW gusts Bandon Airport. No flooding mentioned.	MD	—
10/28/77	Highest waves in years. "Water surged 9.5 feet (?) instead of normal 1 foot in Bandon Harbor." Drift logs 1-2 ft dia washed into S. Jetty parking lot approximately 200 ft.	4.63	< 1
12/13/77	Foam and sheets of water surge over foot of S. Jetty.	NHT	—
2/7/78	3 ft. dia drift logs and wand on S. Jetty Road from high tide and breaking waves.	6.25	18
11/22/79	2-3 ft. diameter stumps and sand washed onto S. Jetty Road. High waves reported.	NHT	—
11/13/81-11/14/81	Est. 100 mph gusts at Bandon. Much wind damage. No reported flooding.	5.91	7
1/28/83 - 1/29/83 (dates approx.)	Waves wash across S. Jetty Road opposite Bandon lighthouse into freshwater pond. Coos County in process of placing rock along road shoulder to prevent further damage.	6.90	141
11/22/88	High tides and waves scattered foam over S. Jetty parking lot.	5.24	1.1
1/29/90	62-98 mph wind gusts. Driftwood tossed into S. jetty parking lot. "[Significant] waves measured at 26 feet" at wave buoy 5 miles off Bandon's Bar.	NHT	—
10/22 and 10/24/90	Tree trunks piled high on the beach near S. Jetty parking lot. "Waves [significant] measured 12 feet from seabed wave gauge just off the jetty."	NHT	—
1/30/92-1/31/92	"Huge piles" of driftwood washed up on beach at the S. Jetty.	NHT	—
12/10/92-12/11/92	"Heavy surge" cuts through the bank behind Bandon Boatworks Restaurant with new channel cut to Redmon Pond. Small driftwood logs (4" dia) deposited next to 2 houses immediately south of parking lot.	5.28	1.2
12/9/93-12/10/93	Ocean waves and river erode backshore shoreline vicinity of Redmon Pond	N/A	—

*Tide elevations based on observed tides at Crescent City, which is the primary reference station for tides at Bandon. Elevations shown are for recorded monthly maximums. NHT = not highest monthly tide observed at Crescent City. MD = Missing data for month. N/A = Not available as of late 1994 from NOAA.

Figure 2-12. History of coastal flooding events in the south jetty area of Bandon (January 1955 to April 1994) (modified from CH2M HILL, 1995, Table 1-1).

near the Bandon triangle that reached an estimated 5.6 m (NAVD88)² elevation at the shore. It is interesting to note that two of the most extreme storms to impact the Oregon coast in recent decades (March 2-3, 1999 and December 2-3, 2007) did not result in any significant damage along the Bandon shore. This was due to the fact that the storm tracks were located farther north such that the bulk of their energy was directed at the northern Oregon coast (e.g., Tillamook County and Clatsop County).

2.4.2 Bastendorff/Lighthouse Beach

Beach morphodynamics along Bastendorff Beach are not too dissimilar from those observed along the Bandon shore. Prior to construction of the Coos Bay jetties, the entrance to Coos Bay reflected a rocky stretch of coast along its south bank, while an extensive barrier spit was located to the north that protected the Coos Bay estuary from the direct effects of ocean waves. Jetty construction was initiated on the north spit, and by the beginning of the twentieth cen-

tury the shoreline had prograded seaward by about 1 km (~3,000 ft), while the shoreline had straightened significantly as sand piled up against the north jetty. With the construction of the south jetty early in the twentieth century, a similar response was observed in the south (Figure 2-13). Sand accreted against the jetty and against the rocky shore, and the shoreline began to prograde seaward. As can be seen in Figure 2-13, the shoreline rapidly prograded seaward up until the 1960s. Since 1967, however, the shoreline has essentially remained much the same, suggesting that the beach has reached a quasi-equilibrium state with the sediment transport processes. With shoreline progradation having all but ceased by 1967, the back shore portion of the beach rapidly became stabilized due to the introduction of non-native beach grasses, particularly European beach grass, and from growth of shore pines immediately landward of the primary dune (Figure 2-14 and Figure 2-15). This type of response is characteristic of the entire length of Bastendorff Beach. Farther south, at Lighthouse Beach, the shoreline in 1967 and again in 2008 is essentially unchanged from its position in the 1920s. This indicates that the effects of jetty construction did not extend south of Bastendorff Beach and furthermore that the shoreline has been broadly stable over the past 80–90 years.

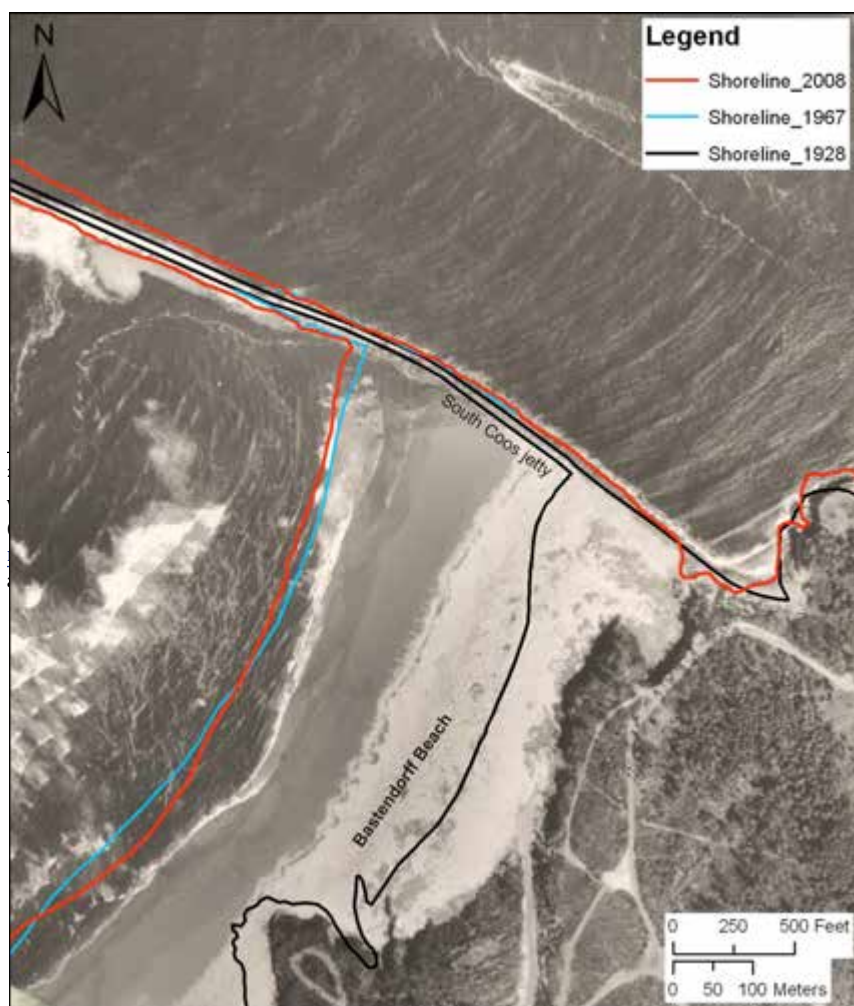


Figure 2-13. Historical shoreline changes at Bastendorff Beach adjacent to the Coos Bay jetties. The photo is of the beach in 1939.

Figure 2-14. Historical shoreline changes at Bastendorff Beach adjacent to the Coos Bay jetties. The photo is of the beach in 1967 and shows the degree to which the back-shore has become stabilized due to introduction of European beach grass and from growth of shore pines.

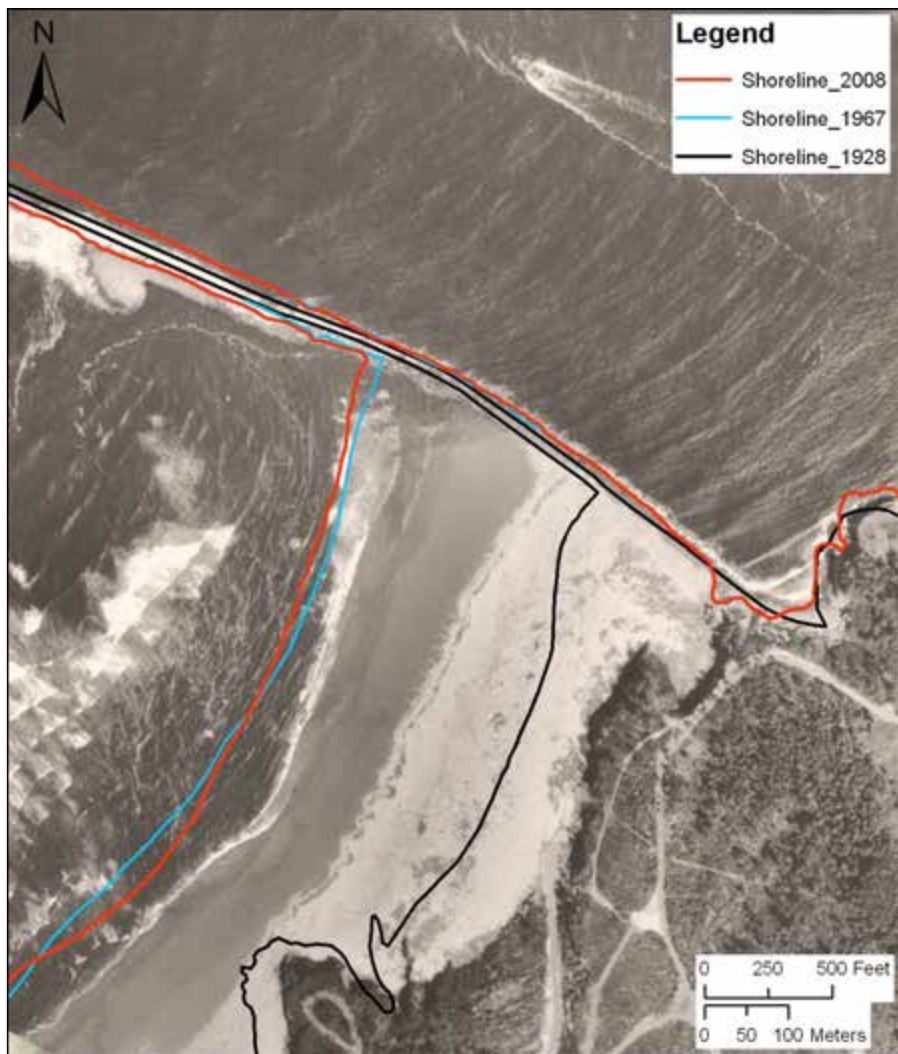


Figure 2-15. Photo of Bastendorff Beach on April 9, 2010, showing the well-vegetated foredune and back-shore. Photo taken by Jonathan Allan, DOGAMI.



3.0 BEACH AND BLUFF MORPHOLOGY ASSESSMENTS

Field surveys were undertaken during the 2008-2009 winter along the two “limited detailed” beach study sites (Bandon, and Bastendorff and Lighthouse Beach) in Coos County. The purpose of these surveys was to provide measurements of the beach in its most eroded state (i.e., most eroded winter profile) in order to define the morphology, elevation, and slope of the beach face for use in subsequent wave runup and overtopping computations. Surveying at Bandon was carried out over a period of three days on February 8-10, 2009, and on March 8-10, 2009, at Bastendorff and Lighthouse Beach, respectively. In both cases, the surveys were completed late in the winter season when Oregon beaches are typically in their most eroded state (Aguilar-Tunon and Komar, 1978; Allan and Hart, 2008; Allan and Komar, 2002b; Komar, 1997). A total of 21 transects were established along the Bandon shoreline, while 11 transects

were established between Sunset Beach State Park and Bastendorff Beach, adjacent to the mouth of Coos Bay (Figure 3-1).

3.1 Survey methodology

Beach profiles that are oriented perpendicular to the shoreline can be surveyed using a variety of approaches, including a simple graduated rod and chain, surveying level and staff, Total Station theodolite and reflective prism, light detection and ranging (lidar) airborne altimetry, and RTK-DGPS technology. Traditional techniques such as leveling instruments and Total Stations are capable of providing accurate representations of the morphology of a beach but are demanding in terms of time and effort. At the other end of the spectrum, high-resolution topographic surveys of the

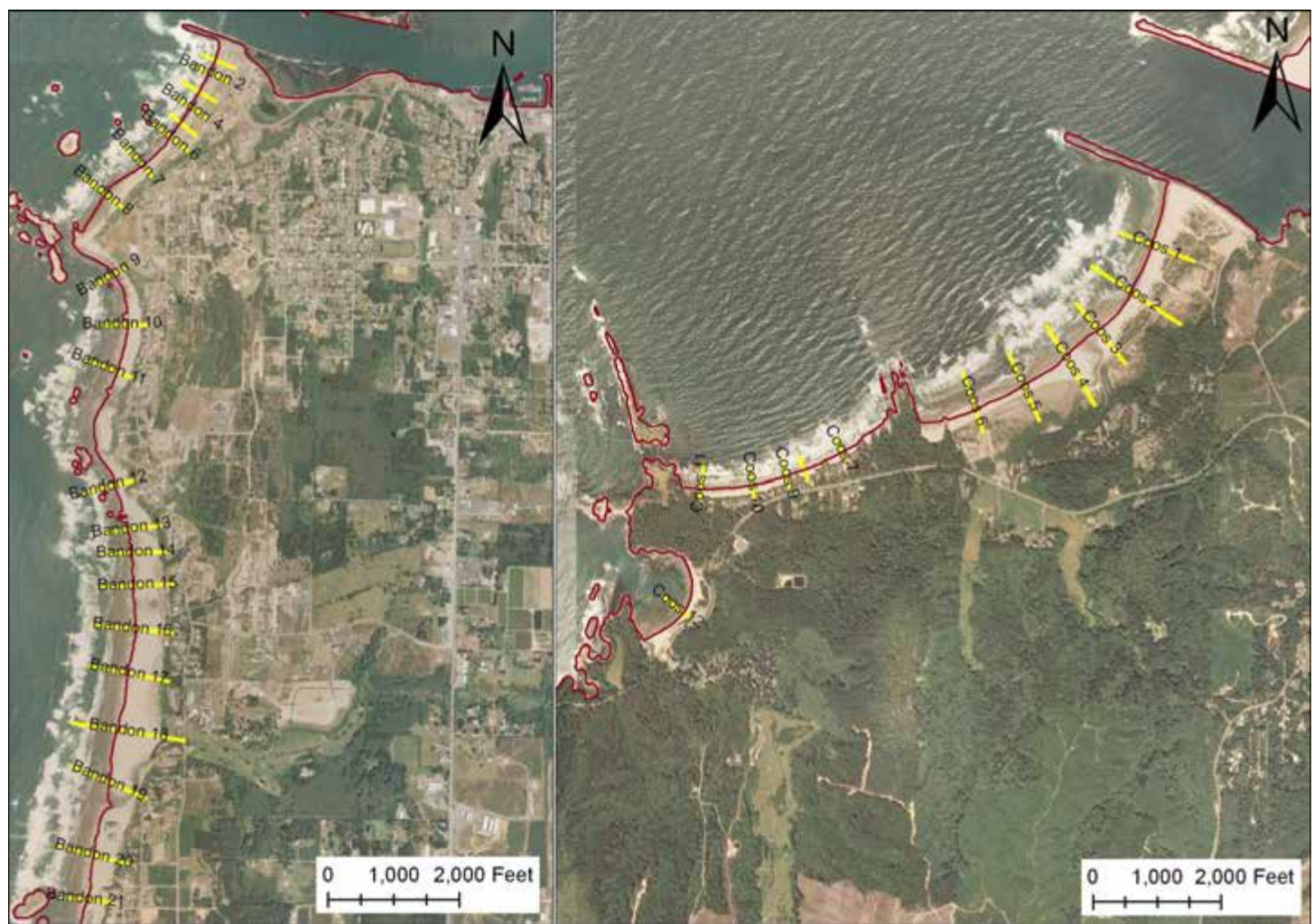


Figure 3-1. Location map of beach profiles (yellow lines) measured (*left*) at Bandon and (*right*) at Bastendorff Beach in Coos County. The red line denotes the position of the mean higher high water (MHHW) shoreline in 2008..

beach derived from lidar are ideal for capturing the three-dimensional state of the beach over an extended length of coast within a matter of hours; other forms of lidar technology are now being used to measure nearshore bathymetry out to moderate depths but are dependent on water clarity. However, lidar technology remains expensive and is impractical along small segments of shore and, more importantly, the high cost effectively limits the temporal resolution of surveys and hence the ability of the end-user to understand short-term changes in the beach morphology (Bernstein and others, 2003).

Within this range of technologies, the application of RTK-DGPS for surveying the morphology of both the subaerial and subaqueous portions of the beach has effectively become the accepted standard (Bernstein and others, 2003; Morton and others, 1993; Ruggiero and others, 2005; Ruggiero and Voigt, 2000) and is the surveying technique used in this study. The Global Positioning System (GPS) is a worldwide radio-navigation system formed from a constellation of 30 satellites and their ground stations, originally developed by the U.S. Department of Defense. In its simplest form, GPS can be thought of as triangulation with the GPS satellites acting as reference points, enabling users to calculate their position to within several meters (e.g., by using inexpensive off-the-shelf handheld units), while survey-grade GPS units are capable of providing positional and elevation measurements that are accurate to a centimeter. At least four satellites are needed mathematically to determine an exact position, although more satellites are generally available. The process is complicated because all GPS receivers are subject to error, which can significantly degrade the accuracy of the derived position. These errors include the GPS satellite orbit and clock drift plus signal delays caused by the atmosphere and ionosphere and multipath effects (where the signals bounce off features and create a poor signal). For example, handheld autonomous receivers have positional accuracies that are typically less than about 10 m (<~30 ft), but can be improved to less than 5 m (<~15 ft) using the Wide Area Augmentation System (WAAS). This latter system is essentially a form of differential correction that accounts for the above errors, which is then broadcast through one of two geostationary satellites to WAAS-enabled GPS receivers.

Greater survey accuracies are achieved with differential GPS (DGPS) using two or more GPS receivers to simultaneously track the same satellites—enabling comparisons to be made between two sets of observations. One receiver is typically located over a known reference point, and the position of an unknown point is determined relative to that reference point. With more sophisticated 24-channel

dual-frequency RTK-DGPS receivers, positional accuracies can be improved to the subcentimeter level when operating in static mode and to within a few centimeters when in RTK mode (i.e., as the rover GPS is moved about). In this study we used a Trimble® 24-channel dual-frequency 5700/5800 GPS, which consists of a GPS base station (5700 unit), Zephyr Geodetic™ antenna, HPB450 radio modem, and 5800 “rover” GPS (Figure 3-4). Trimble reports that the 5700/5800 GPS system has horizontal errors of approximately $\pm 1 \text{ cm} + 1 \text{ ppm}$ (parts per million \times the baseline length) and $\pm 2 \text{ cm}$ in the vertical (Trimble, 2005).

To convert a space-based positioning system to a ground-based local grid coordinate system, a precise mathematical transformation is necessary. While some of these adjustments are accomplished by specifying the map projection, datum, and geoid model prior to commencing a field survey, an additional transformation is necessary whereby the GPS measurements are tied to known ground control points. This latter step is called a GPS site calibration, such that the GPS measurements are calibrated to ground control points with known vertical and horizontal coordinates using a rigorous least-squares adjustment procedure. The calibration is initially undertaken in the field using the Trimble® TSC2™ GPS controller and then re-evaluated in the office using Trimble Geomatics Office™ software.

Survey control (Table 3-1) along the Bandon shore was provided by occupying two National Geodetic Survey (NGS) monuments and one Watershed Sciences, Inc. (WS) benchmark.³ At Bastendorff Beach, survey control was provided by one NGS and two WS benchmarks. For both surveys, additional control and field checking was provided using the Online Positioning User Service (OPUS) maintained by the NGS (<http://www.ngs.noaa.gov/OPUS/>). OPUS provides a simplified way to access high-accuracy National Spatial Reference System (NSRS) coordinates using a network of continuously operating GPS reference stations (CORS, <http://www.ngs.noaa.gov/CORS/>). In order to use OPUS, static GPS measurements are typically made using a fixed height tripod for periods of 2 hours or greater. OPUS returns a solution report with positional accuracy confidence intervals for adjusted coordinates and elevations for

³ As part of calibrating the light detection and ranging (lidar) surveys of the southern Oregon coast, Watershed Sciences, Inc. established numerous survey monuments on the south coast. Coordinates assigned to these monuments were derived using the Online Positioning User Service (OPUS) maintained by the NGS (<http://www.ngs.noaa.gov/OPUS/>). In many cases, the same benchmarks were observed multiple times and the horizontal and vertical coordinates were continually updated. Given the high level of accuracy assigned to the Watershed Sciences monuments, we used their coordinates and elevations in place of NGS reported values to perform GPS site calibrations at both Bandon and Coos Bay. More detailed information about the survey procedures used by Watershed Sciences can be found in Appendix A.

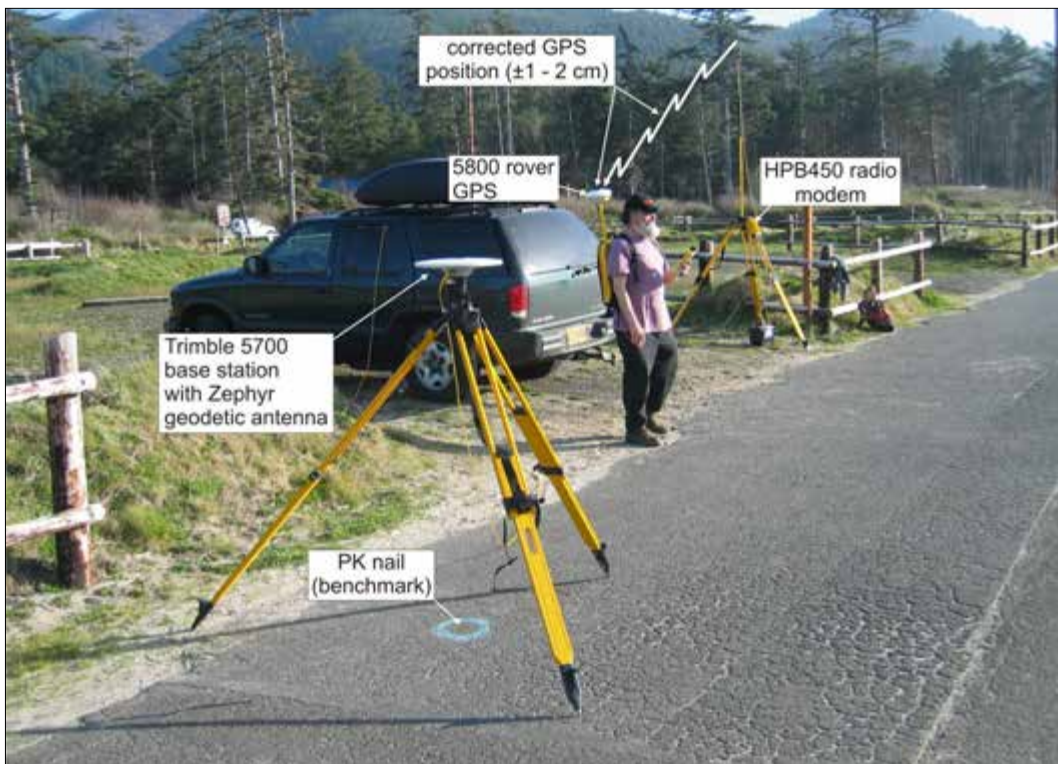


Figure 3-2. The Trimble® 5700 base station antenna located over a known reference point at Cape Lookout State Park, northern Oregon coast. Corrected GPS position and elevation information is then transmitted by an HPB450 base radio modem to the 5800 GPS rover unit.

Table 3-1. Survey benchmarks used to calibrate GPS surveys of the beach at Bandon and Bastendorff Beach, Coos County, Oregon.

Study Area	Benchmark Name	Northing (m)	Easting (m)	Elevation (m)
Bandon	OA0424* - NGS/OPUS	168317.314	1179842.918	25.095
	DH7020 - WS/OPUS	165128.177	1181992.590	34.681
	OA0754 - WS/OPUS	166508.606	1181403.971	25.899
	OLCJN8 - WS/OPUS	172882.656	1184660.963	6.866
Bastendorff Beach	DH7197 - NGS	193386.414	1190052.313	4.470
	OLC5PGW1 - WS/OPUS	194194.631	1189042.650	24.004
	OLCPWH17 - WS/OPUS	194670.870	1209846.912	4.952
	GPSBASE 1* - OPUS	194008.043	1188400.312	6.320
	GPSBASE 2* - OPUS	194008.028	1188400.297	6.365
	sunset pk - DOGAMI/OPUS	192345.181	1186013.440	5.349
	arago pk - DOGAMI/OPUS	189485.789	1183657.742	37.734

Asterisk signifies the location of the GPS base station during each respective survey. NGS denotes National Geodetic Survey monument, WS denotes Watershed Sciences, Inc. monument, NGS/OPUS signifies OPUS (Online Positioning User Service) derivation solution. DOGAMI denotes Oregon Department of Geology and Mineral Industries.

the observed point. In all cases we used the Oregon State Plane coordinate system, southern zone (meters), while the vertical datum is relative to the North American Vertical Datum of 1988 (NAVD88).

For the Bandon survey, the 5700 GPS base station was located on NGS monument OA0424 (Table 3-1), using a 2.0-m fixed-height tripod. Survey control was provided by undertaking 180 GPS epoch measurements (~ 3 minutes of measurement per calibration site) using three calibration sites (Table 3-1), enabling us to perform a GPS site calibration that brought the survey into a local coordinate system (Figure 3-3). This step is critical in order to eliminate various survey errors that may be compounded by factors such as poor satellite geometry, multipath, and poor atmospheric conditions, combining to increase the total error to several centimeters. Table 3-2 shows the relative errors identified when compared against the reported values determined by the NGS and Watershed Sciences. To further validate

the accuracy of the GPS base station, an OPUS solution was derived from nearly 6 hours of GPS measurements on benchmark OA0424. Table 3-2 indicates that horizontal errors at the GPS base station (OA0424) were less than 2 cm, while the vertical error was 1 mm. Similarly, errors observed at the other control sites were found to be low (Table 3-2).

At Bastendorff and Lighthouse Beach, the 5700 GPS base station was located over a temporary benchmark established in the dune. Survey control was provided by undertaking 180 GPS epoch measurements using seven calibration sites (Table 3-1), including an NGS tidal reference benchmark (DH7197). OPUS solutions were derived from two 5-6 hour static GPS occupations for comparative purposes and for survey control. Extended occupations (> 2 hours) were also undertaken on the arago pk and sunset pk benchmarks and processed using OPUS to derive coordinates for these two temporary monuments. After all these data were pro-

Table 3-2. Comparison of horizontal and vertical coordinates derived by the NGS, WS, OPUS, and DOGAMI.

Study Area	Name	Northing (m)	Easting (m)	Elevation (m)
Bandon				
	OA0424*	-0.009	0.017	-0.002
	DH7020#	-0.007	-0.005	0.001
	OA0754#	0.007	0.006	0.001
	OLCJN8°	0.000	-0.002	0.000
Bastendorff Beach				
	DH7197*	-0.074	0.010	0.011
	OLC5PGW1°	0.010	-0.015	-0.013
	OLCPWH17°	-0.004	0.006	0.000
	GPSBASE 1%	-0.009	-0.012	0.018
	GPSBASE 2%	0.003	0.010	-0.018
	sunset pk%	0.016	0.001	-0.002
	arago pk%	-0.003	0.023	0.004

* Denotes comparison between Trimble® Geomatics Office solution (i.e., DOGAMI) and NGS OPUS solution.

Denotes comparison between multiple WS occupations and NGS benchmark datasheets.

° Denotes comparison between WS datasheet and DOGAMI GPS survey.

% Denotes comparison between DOGAMI and NGS OPUS solution.

Grey shading indicates horizontal and vertical coordinates that were NOT used to calibrate the field survey.

NGS is National Geodetic Survey, WS is Watershed Sciences, Inc., OPUS is NGS Online Positioning User Service, and DOGAMI is Oregon Department of Geology and Mineral Industries.



Figure 3-3. A 180-epoch calibration check is performed on a survey monument (OLC5PGW1) established by WS near the Coast Guard observation tower at the mouth of Coos Bay. This procedure is important for bringing the survey into a local coordinate system and for reducing errors associated with the GPS survey.

cessed, a site calibration was performed.⁴ From analyses of the statistics it was found that the best solution involved using the horizontal and vertical coordinates from several of the sites (OLC5PGW1, OLCPWH17, GPSBASE 1, GPSBASE 2, sunset pk, and arago pk), while only vertical control was used from the tidal benchmark DH7197. Processing these data yielded coordinates that were directly comparable to the OPUS solutions derived for GPSBASE 1 and GPSBASE 2 (Table 3-2). Table 3-2 indicates that horizontal and vertical errors at the various monuments were less than 2 cm, while the vertical error ranged from 5 mm to 1.8 cm.

After the local site calibration was completed, cross-shore beach profiles were surveyed with the 5800 GPS rover unit mounted on a backpack, worn by an operator (Figure 3-4). This was undertaken during periods of low tide, enabling more of the beach to be surveyed. The approach was to walk from the landward edge of the primary dune or bluff edge, down the beach face, and out into the ocean to approximately wading depth. A straight line perpendicular to the shore was achieved by navigating along a predetermined line displayed on a handheld Trimble® TSC2™ computer controller connected to the 5800 rover. The computer shows the position of the operator relative to the survey line and indicates the deviation of the GPS operator from the line. The horizontal variability during the survey is generally minor, typically less than about ± 0.25 m either side of the line (Figure 3-5), which results in negligible vertical uncertainties due to the relatively uniform nature of beaches characteristic of much of the Oregon coast (Ruggiero and others, 2005). On the basis of previous research at numerous sites along the Oregon coast, this method of surveying can reliably detect elevation changes on the order of 4–5 cm, that is, well below normal seasonal changes in beach elevation, which typically varies by 1 to 2 m (3 to 6 ft) (Allan and Hart, 2007, 2008; Ruggiero and others, 2005).



Figure 3-4. Surveying the morphology of the beach at Bandon using a Trimble® 5800 “rover” GPS.

Analysis of the beach survey data involved a number of stages. The data were first imported into MATLAB⁵ using a customized script. A least-squares linear regression was then fit to the profile data. The purpose of this script is to examine the reduced data and eliminate those residuals (e.g., Figure 3-5) that exceed a ± 0.5 -m horizontal threshold on either side of the predetermined profile line. The data are then exported into a Microsoft[®] Excel[®] database for archiving purposes. A second MATLAB script takes the Excel profile database and plots the survey data (relative to the earlier surveys) and outputs the generated figure as a Portable Network Graphics (PNG) file. Appendix B shows the reduced beach profile data for the Bandon shore, while Appendix C covers those profiles measured at Bastendorff Beach adjacent to the mouth of Coos Bay.

To supplement the GPS beach and bluff data, high-resolution lidar data measured by WS in 2008 for DOGAMI were also analyzed and integrated into the beach profile dataset. This was especially the case for backshore areas where it was not possible to easily survey with the GPS gear. In addition, lidar data flown by the U.S. Geological Survey (USGS), National Aeronautics and Space Administration (NASA),

and National Oceanic and Atmospheric Administration (NOAA) in 1998 and 2002 were also used to extend the time series of the beach and bluff profile data. In particular, the 1998 lidar data measured at the end of the major 1997–1998 El Niño was analyzed, providing additional measurements of the beach in an eroded state that can be compared with more recent winter surveys of the beach. The 1998 and 2002 lidar data were downloaded from the NOAA Coastal Service Center⁶ and gridded using a triangulated irregular network (TIN) approach. The distance and elevation data were then extracted from the gridded lidar data.

3.2 Beach characterization

Analyses of the beach profile data were undertaken using additional scripts developed in MATLAB. The profile analysis script requires the user to interactively locate the positions of the seaward edge and crest of the primary frontal dune backing the beach, and then evaluate the beach-dune juncture (E_j) elevations for the 1998, 2002, 2008, and 2009 profiles, and beach slopes ($\tan \beta$) at each transect site. Beach slope was determined by fitting a linear regression through

⁵ Computer programming languages.

⁶ <http://www.csc.noaa.gov/digitalcoast/data/coastallidar/index.html>

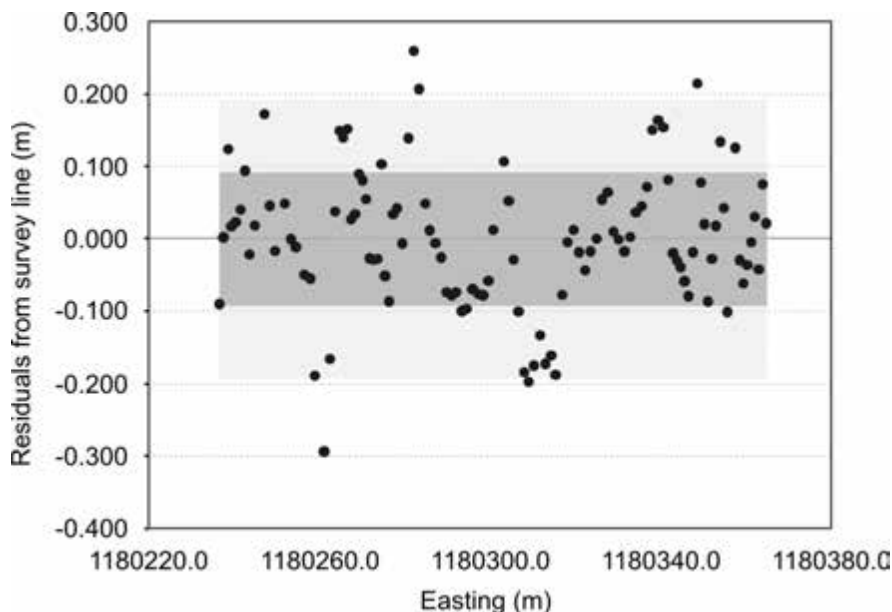


Figure 3-5. Residuals of GPS survey points relative to zero (transect) line. Example reflects the Bandon 3 profile line. Dark grey shading indicates 68.3% of measurements are located ± 0.096 m (1σ) from the transect line, while 95.5% (2σ) of the measurements are located within ± 0.192 m of the profile line (grey shading).

the measured GPS data. In all cases, the slope of the beach face was determined to be the region of the beach located between mean sea level (1.09 m, MLLW [mean lower low water]) and the highest observed tide (3.26 m, MLLW), an approach that is consistent with methodologies adopted by previous workers (Ruggiero and others, 2005; Stockdon and others, 2006). Determination of the location of the beach-dune juncture (E_j) was accomplished interactively using the MATLAB script and from local knowledge of the area. In general, the beach-dune juncture (E_j) reflects a major break in slope between the active part of the beach face and the toe location of the primary dune. For most sites along the Oregon coast, the beach-dune juncture (E_j) typically occurs at elevations between about 4 and 6 m (NAVD88). Figure 3-6 provides an example of identified beach-dune junctures (E_j) determined for one site on the North Coos Spit. In this example, it is apparent that the beach has undergone significant erosion during the past decade, having eroded landward by 25.2 m (82.7 ft) since 1998 as measured at the

6-m contour elevation. Analysis of the profile data indicates that the beach-dune juncture (E_j) has varied in elevation, a function of repeated phases of both erosion and accretion events. As of summer 2008, a prominent erosion scarp had formed and the beach-dune juncture reflected the toe of the scarp, located at an elevation of 5.7 m⁷ (18.7 ft). Figure 3-6 also identifies the crest of the primary dune as well as the landward boundary of the primary frontal dune. These latter data are used later to develop V zones in those areas where no detailed coastal study was undertaken.

To estimate beach erosion and profile changes for a specific storm, it is essential to first determine the conditions of the morphology of the beach prior to the actual event of interest (NHC, 2005). This initial beach profile is referred to as the most likely winter profile (MLWP) condition for that particular coastal setting. The MLWP was assessed from an

⁷ All elevations are relative to the North American Vertical Datum of 1988 (NAVD88) unless otherwise stated.

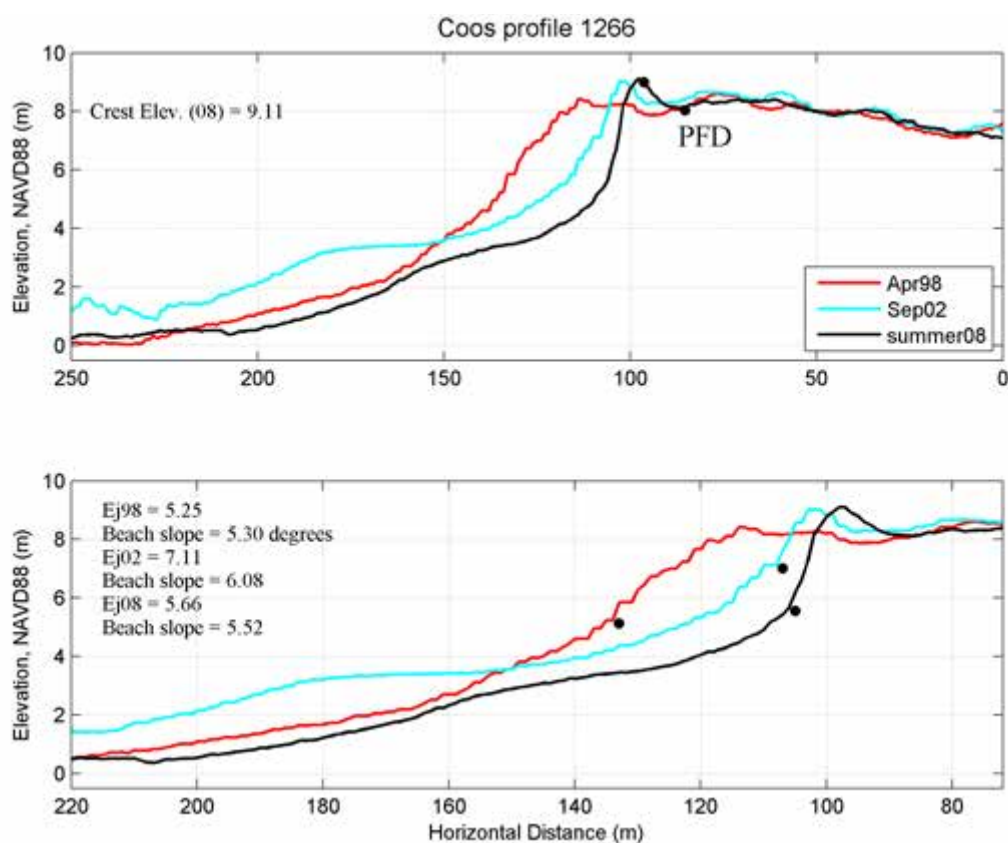


Figure 3-6. Plots showing (top) the location of the dune crest and the landward extent of the primary frontal dune (PFD), and (bottom) the beach-dune junctures identified from lidar data on the North Coos Spit. Example plot provides a dramatic example of recent erosion along the spit.

examination of the combined profile data. Figure 3-7 provides an example for the Bandon 3 and 5 profile sites. In both cases the April 1998 lidar data best characterize the MLWP, but for different sections of the beach. In the case of the Bandon 3 site (Figure 3-7, top), the April 1998 data show an eroded profile between the zero datum and the 4-m (13 ft) elevation contour. However, because the 1998 data do not capture the morphology of the beach below mean lower low water (MLLW), while the upper part of the dune face has eroded landward since 1998, we have incorporated the February 2009 GPS survey for these sections of the beach. In the case of the Bandon 5 site the MLWP is established for the upper beach face (Figure 3-7, bottom), while the GPS survey documented the lower beach elevations below mean higher high water (MHHW). Like the Bandon 3 profile, here we combine data from the April 1998 lidar with the GPS survey data. Landward of the dune crest, information on

the backshore topography was derived by incorporating the actual measured GPS data, as those data provided the best representation of the actual ground surface. Where GPS survey data were not available, we used topographic data derived from the 2008 lidar flown for DOGAMI.

Tables 3-3 and 3-4 summarize the morphological parameters identified for each transect site at Bandon and at Bastendorff Beach, including a geomorphic classification of the site. Figure 3-8 provides a plot of the alongshore changes in beach slopes ($\tan \beta$), beach-dune juncture (E_j) elevations, and where applicable the dune crest and/or bluff top. In general, sediment grain sizes are coarsest nearer the south Coquille jetty and become finer to the south. Grain size analyses by Peterson and others (1994) indicated that mean grain sizes (M_z) ranged from coarse sand ($M_z = 0.68 \text{ mm} \pm 0.36 \text{ mm}$) nearest to the Coquille River and decreased in size toward the south, where the sediments are classi-

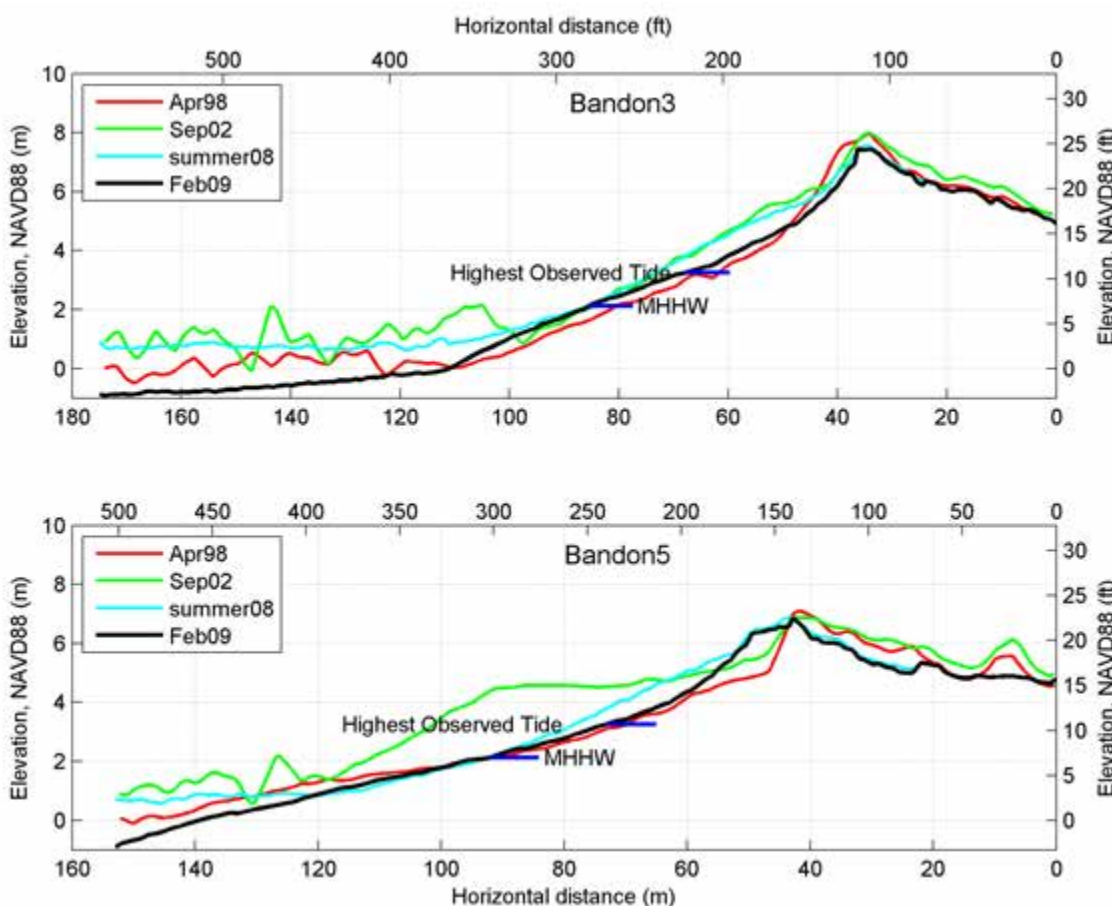
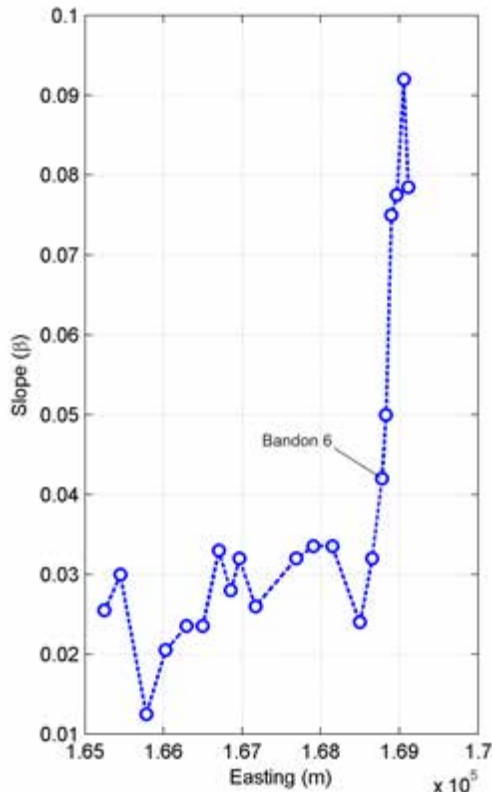


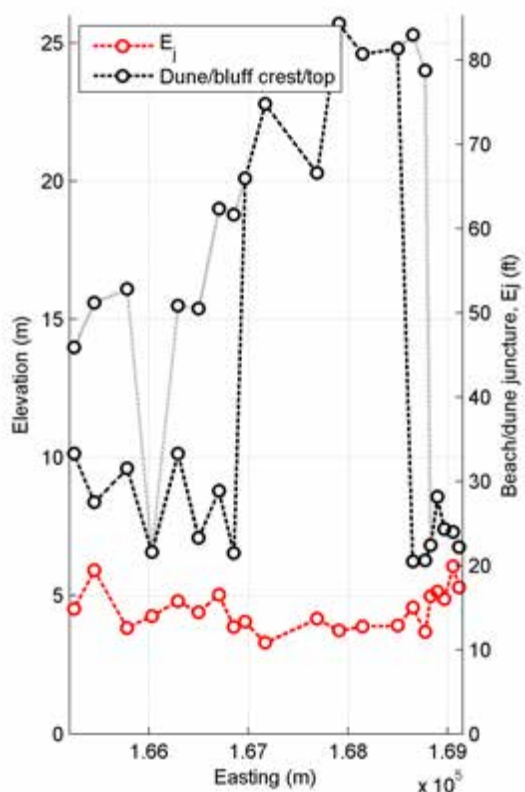
Figure 3-7. Example plots of the combined beach profile data for (top) Bandon 3 and (bottom) Bandon 5 sites. Wiggly lines that characterize the April 1998 and September 2002 lidar data on the lower beach face at Bandon 3 are wave bores associated with broken waves. Progradation of the beach face in 2002 at Bandon 5 indicates the development of a berm as sand eroded from the beach during the previous winter is returned to the beach face. Note: MHHW denotes the mean higher high water level as measured by the Charleston tide gauge (2.095 m).

Table 3-3. Identified beach morphological parameters from the most likely winter profile (MLWP) at Bandon.

Profile No.	Dune Crest/ Bluff Top (m)	Beach-Dune Junction, E_j _{MLWP} (m)	Beach Slope (tan β)	Site Description
1	6.76	5.30	0.079	dune backed
2	7.31	6.07	0.092	dune backed
3	7.42	4.89	0.078	dune backed
4	8.59	5.14	0.075	dune backed
5	6.84	4.99	0.050	dune backed
6	6.28 / 24.0	3.66	0.042	dune/bluff backed
7	6.24 / 25.3	4.58	0.032	dune/bluff backed
8	24.8	4.15	0.024	bluff backed
9	24.6	3.89	0.034	bluff backed
10	25.7	3.74	0.034	bluff backed
11	20.3	4.17	0.032	bluff backed
12	22.8	3.30	0.026	bluff backed
13	20.1	4.81	0.032	bluff backed
14	6.54 / 18.8	3.88	0.028	dune/bluff backed
15	8.80 / 19.0	4.79	0.033	dune/bluff backed
16	7.10 / 15.4	4.40	0.024	dune/bluff backed
17	10.2 / 15.5	4.82	0.024	dune/bluff backed
18	6.59	4.27	0.021	dune/bluff backed
19	9.61 / 16.1	3.84	0.013	dune/bluff backed
20	10.57 / 15.6	5.93	0.030	dune/bluff backed
21	10.14 / 14.0	4.53	0.026	dune/bluff backed

**Table 3-4.** Identified beach morphological parameters from the most likely winter profile (MLWP) at Bastendorff Beach.

Profile No.	Dune Crest/ Bluff Top (m)	Beach-Dune Junction, E_j _{MLWP} (m)	Beach Slope (tan β)	Site Description
1	6.88	5.56	0.038	dune backed
2	7.27	5.28	0.036	dune backed
3	6.63	5.10	0.026	dune backed
4	5.76	4.13	0.023	dune backed
5	6.21	4.83	0.039	dune backed
6	7.30	4.73	0.037	dune backed
7	18.3	5.80	0.101	bluff backed
8	18.5	5.02	0.078	bluff backed
9	18.1	5.10	0.087	bluff backed
10	16.5	6.66	0.072	bluff backed
11	19.1	3.83	0.060	bluff backed
12	5.43	4.91	0.068	dune backed

**Figure 3-8.** Alongshore changes in (left) beach slopes (tan β), and (right) beach-dune juncture (E_j) elevations and dune/bluff crest/tops along the Bandon shore. Grey line denotes those beaches that are backed by both a foredune and a bluff.

fied as medium sand ($M_z = 0.28 \text{ mm} \pm 0.06 \text{ mm}$) south of Coquille Point. This longshore variation is reflected by the parallel changes in beach slopes (a function of the sediment grain size) along this stretch of shore, with steeper slopes in the north adjacent to the south Coquille jetty and gentler slopes predominating south of the Bandon 6 profile site (Figure 3-8, left). As can be seen in Table 3-3 and in Figure 2-3, much of the shoreline at Bandon is protected by moderately high bluffs, which range in height from 14 to 24 m (46–79 ft). The bluffs are highest in the central to northern portion of the shore and decrease in elevation to the south, where a small section of the shore (between the Bandon 21 and Bandon 14 profile sites) exhibits a developing dune system that fronts a coastal bluff (Figure 2-6). In the north, between the Bandon 6 and Bandon 1 profile sites (Figure 3-1), the beach is backed by a low dune. This section of beach is the product of jetty construction at the mouth of the Coquille River (Section 2.4.1), which has enabled sand

to become trapped and over time, vegetated by European beach grass.

At Bastendorff Beach, sediment grain size is significantly finer compared with the sediments along the Bandon shore. Analyses by Peterson and others (1994) indicate that the mean grain sizes are approximately 0.19 mm ($\pm 0.05 \text{ mm}$). Accordingly, the beach slopes tend to be relatively low sloping, while the foreshore is backed by a generally low foredune, with elevations that range from 5.8 to 7.3 m NAVD88 (19–24 ft) (Table 3-4). As can be seen in Figure 3-9, the low backshore elevations located between the 0 and 130 m horizontal distance (0–427 ft) reinforce the fact that the shoreline likely advanced rapidly following jetty construction, while the higher, more seaward foredune present today suggests that progradation of the shore has slowed, allowing the dune to begin to aggrade vertically. This is entirely consistent with the post-jetty shoreline responses described previously in Section 2.4.2. South of Bastendorff

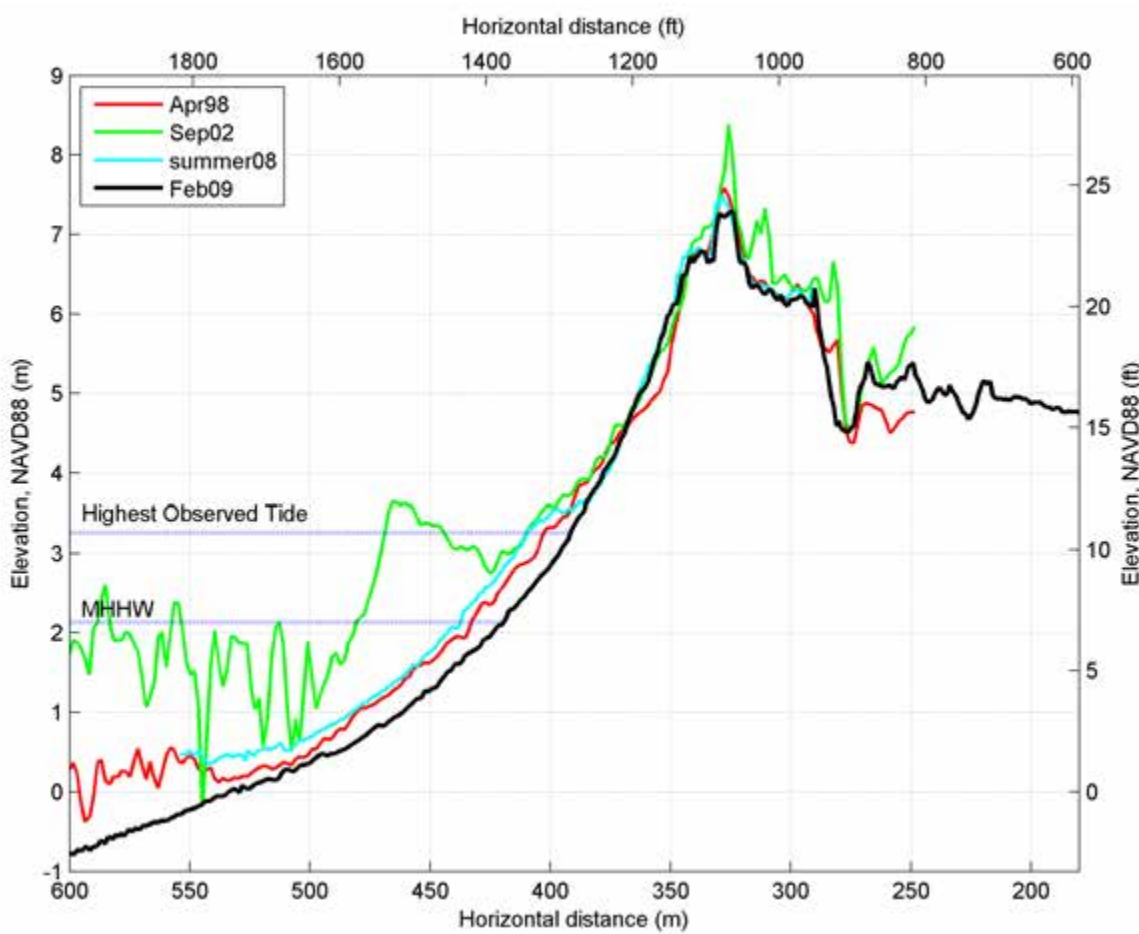


Figure 3-9. The Coos 2 profile site indicating the generally low backshore elevations that suggest that the beach probably prograded rapidly seaward following jetty construction, while the high contemporary foredune indicates that the shoreline has stabilized.

Beach at Lighthouse Beach, the slopes of the beach are significantly steeper (Table 3-4), becoming broadly similar to beach slopes adjacent to the Coquille jetties. Along this section of shore the beach is backed by a prominent bluff with crest elevations that range from 16 to 19 m (52.5–62 ft) that effectively preclude wave overtopping along this stretch of shore.

3.3 Recent coastal changes along the Bandon and Bastendorff beaches

This section briefly reviews beach profile changes over the past decade that have been documented by lidar and recent GPS surveys of the shore. In general, beach profile changes along the Bandon “triangle” adjacent to the Coquille jetties (Bandon 1, 2, 5, and 6 sites) indicate that the shore was in its most eroded state following the major 1997–1998 El Niño. However, since then the beach has regained much of the sand that was lost in the late 1990s. In contrast, two of the transects (Bandon 3 and 4) that cross a small dune along the “triangle” contain less sand than was present in the late 1990s, making those sites more susceptible to future erosion and potentially overtopping and inundation.

Profile changes along the Bandon bluffs from Bandon 7 to 13 indicate little overall change during the past decade. However, between the Bandon 14 and 18 profile sites, the beach and foredune has gained sand, enabling the foredune to both aggrade vertically and prograde seaward. This section of shore is therefore generally in a much healthier state compared to its condition in the late 1990s. At the Bandon 19 profile site, the beach has eroded landward mostly due to the migration of Johnson Creek to the south, allowing the beach foreshore to remain in a saturated state and thereby contributing to the erosion of this stretch of shore. Finally, the Bandon 20 and 21 profile sites have also gained significant amounts of new sand, which has enabled the foredune to aggrade vertically. The foredune protects backshore properties located landward of this section of coast.

Along Bastendorff Beach, no change has occurred in the morphology of the beach over the past decade at Coos 1 and 2 profile sites. However, south of these sites, erosion of the beach increases. For example, the Coos 5 and 6 profiles sites indicate that the beachface has eroded landward some 10–20 m (33–66 ft) during the past decade. In contrast, the Coos 7–11 profile sites have shown little to no change in the position of the bluff face. Finally, at Sunset Bay State Park the Coos 12 profile site indicates that the beach face has experienced some minor erosion over the past decade; the upper portion of the beachface has eroded landward by about 5 m (16 ft).

3.4 Bathymetry

Information on the local bathymetry offshore from the Coos County coast is particularly important for the purposes of undertaking numerical wave modeling in order to transform waves into the nearshore, and for determining various morphological features such as the slope of the nearshore. In the absence of undertaking our own nearshore bathymetric surveys, we have used data compiled by the National Geophysical Data Center (NGDC), an office of the National Oceanic and Atmospheric Administration (NOAA), for the purposes of developing an integrated bathymetric-topographic digital elevation model (DEM) for tsunami inundation modeling. The synthesized bathymetric-topographic DEM (Port Orford⁸) is a 1/3 arc-second (approximately 10 m [~33 ft]) DEM of the southern Oregon coast that spans all of Coos County (Carignan and others, 2009) and includes offshore rocks, small islands, and reefs that affect wave shoaling. The DEM was generated from a diverse suite of digital datasets that span the region. A summary of the data sources and methods used to synthesize the data to develop the Port Orford DEM is described by Carignan and others (2009). In general, the best available data were obtained by the NGDC and shifted to common horizontal and vertical datums: North America Datum 1983 (NAD 83) and mean high water (MHW). According to Carignan and others (2009), the final DEM is estimated to have an accuracy of up to 10 m (~33 ft), while some portions of the grid are more accurate (e.g., the coastal strip where high-resolution lidar data were available). The bathymetric portion of the dataset is estimated to have an accuracy of between 0.1 m (0.33 ft) and 5% of the water depth, again depending on the type of survey data that were used to calibrate the final grid development.

Finally, despite all these best efforts it is important to note that a limitation of the DEMs being developed by NGDC is the virtual absence of suitable bathymetric data in the nearshore (effectively landward of the 10 m (33 ft) bathymetry contour), as few boats are able to venture into this highly turbulent portion of the surf zone. The exception to this is where surveys have been undertaken by the U.S. Army Corps of Engineers (USACE) in the entrance channels to those estuaries where navigable water depths need to be maintained. Thus, there is some uncertainty about estimating nearshore slopes for the surf zone due to the absence of sufficient data for this region; the user must make some assumptions on the basis of the best available data present

⁸ <http://www.ngdc.noaa.gov/dem/showdem.jsp?dem=Port%20Orford&state=OR&cell=1/3%20arc-second&vdat=MHW>

outside the surf zone and information at the shoreface. This is a recognized problem with all coastal flood analyses. We recommend future efforts to explore the benefits of collecting data in nearshore bathymetric surveys that make use of a personal water craft to enhance wave runup and modeling components. For example, Ruggiero and others (2005) described a coastal profiling system that was developed for nearshore bathymetric surveys across the surf zone as part of the Southwest Washington Coastal Erosion Study (SWCES). This system consists of a highly maneuverable

personal watercraft that is equipped with a survey-grade GPS receiver and antenna, an echo sounder, and an on board computer. Repeatability tests suggest subdecimeter accuracy on the order of 0.15 m (0.5 ft) (Ozkan-Haller and others, 2009). Figure 3-10 and Figure 3-11 show examples of the types of products that could be adopted in future coastal flood mapping efforts. These data would greatly assist the coastal flood mapping specialist and facilitate the modeling of ocean waves into the surf zone.

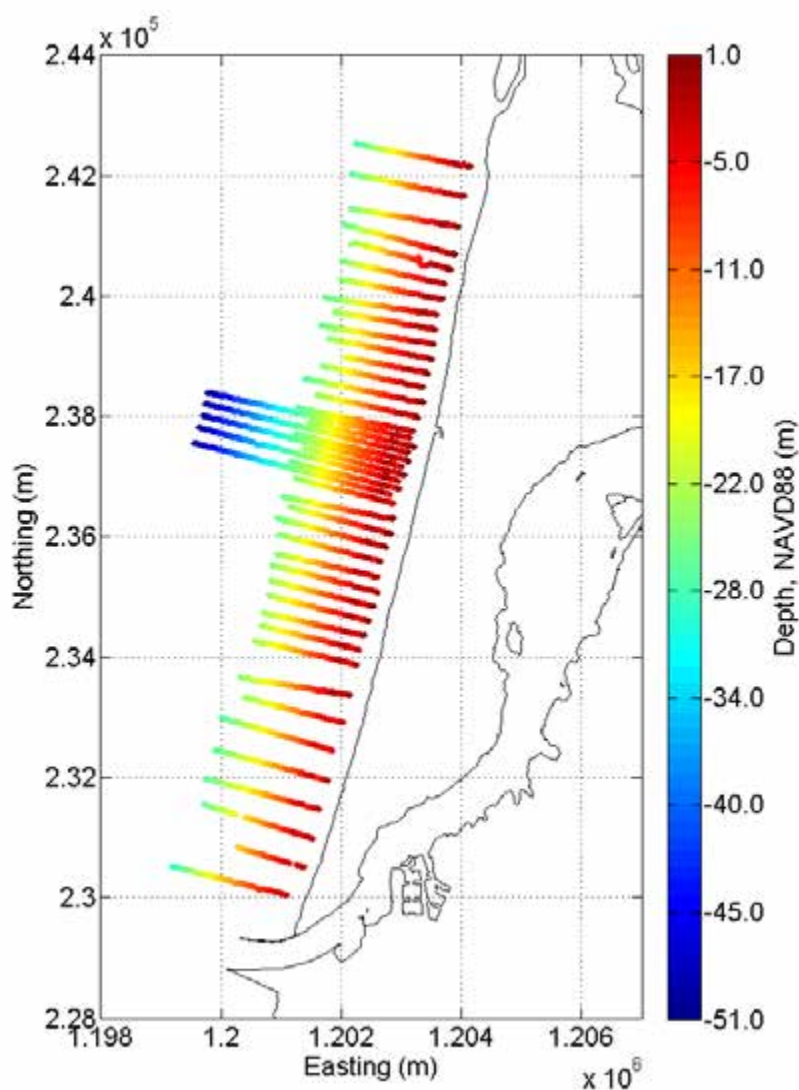


Figure 3-10. Collected bathymetry transects measured offshore the coast of the north Umpqua Spit near Winchester Bay, Oregon (after Ozkan-Haller and others, 2009).

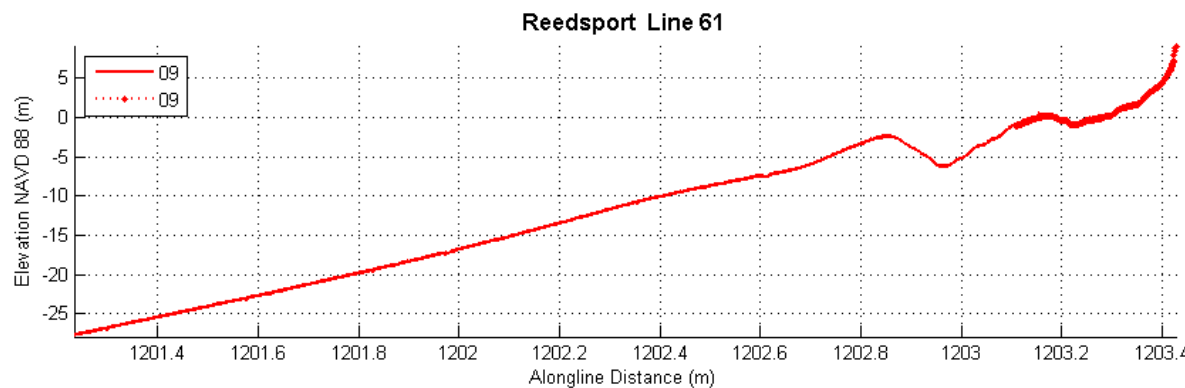


Figure 3-11. Example cross-shore transect measured off the Umpqua Spit near Winchester Bay, Oregon, showing the presence of two prominent sand bars, characterized by significant relief (Ozkan-Haller and others, 2009).

4.0 TIDES

4.1 Tides along the Coos County coast

Measurements of tides on the Oregon coast are available from various tide gauges⁹ operated by the National Ocean Service (NOS). Hourly tidal records are available from the following long-term (30+ years) coastal sites: the Columbia River (Astoria, #9439040); South Beach (Newport, #9435380); Port Orford (#9431647); and Charleston (#9432780), located midway along the Coos County shoreline. Long-term tidal records are also available from the Crescent City tide gauge (#9419750), located in northern California, and have been used in previous FEMA Flood Insurance Studies (FIS) carried out in Coos County (e.g., CH2M HILL, 1995). For the purposes of this study, we have based our still water level (SWL) and wave runup calculations on the Charleston tide gauge due to its central proximity along the Coos County coast and, importantly, because of its relatively long record (38 years¹⁰). All hourly tide data

were purchased from NOS and were processed using various scripts developed in MATLAB. In addition to the measured tides, hourly tide predictions were calculated for all years using the NOS tide prediction program, NTP4¹¹.

Tides along the Oregon coast are classified as moderate, with a maximum range of up to 4.3 m (14 ft) and an average range of about 1.8 m (6 ft) (Komar, 1997). There are two highs and two lows each day, with successive highs (or lows) usually having markedly different levels (Figure 4-1). Tidal elevations are given in reference to the mean of the lower low water levels (MLLW) and can be easily adjusted to the NAVD88 vertical datum. As a result, most tidal elevations are positive numbers with only the most extreme lower lows having negative values. Figure 4-1 shows the tidal elevation statistics derived from the Charleston tide gauge (#9432780), with a mean range of 1.73 m (5.69 ft) and a diurnal range of 2.32 m (7.62 ft). The highest tide measured at Charleston reached 3.41 m (11.18 ft), recorded in January 1983 during the peak of the strong 1982-1983 El Niño.

⁹ http://www.co-ops.nos.noaa.gov/station_retrieve.shtml?type=Tide%20Data&state=Oregon&id1=943

¹⁰ The Charleston gauge became operational in April 1970.

¹¹ <http://tidesandcurrents.noaa.gov/faq2.html#65>

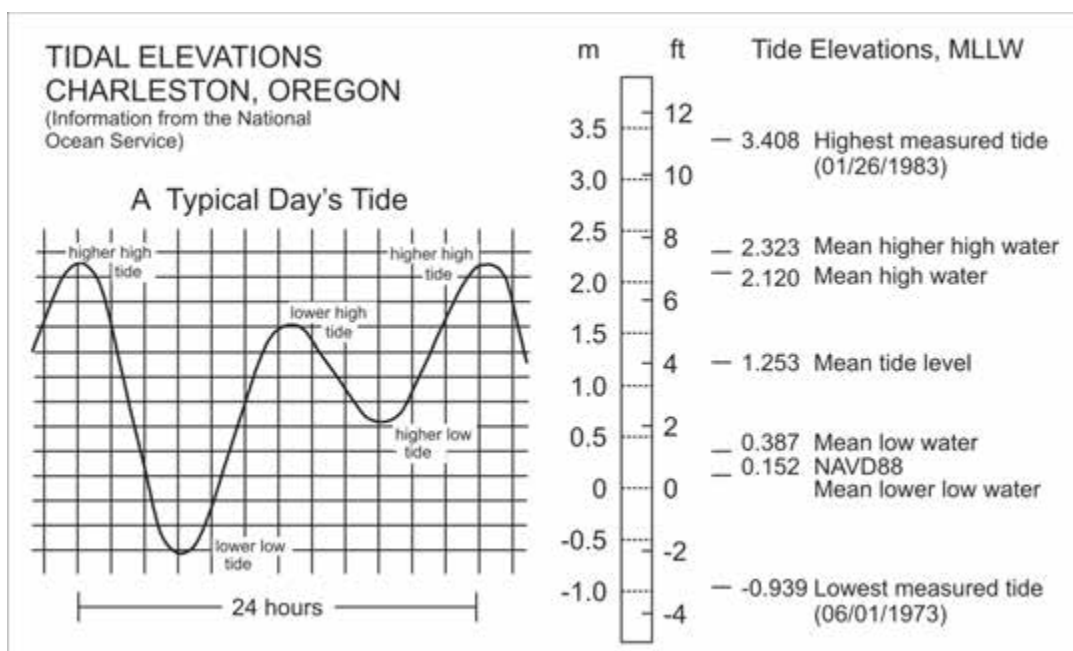


Figure 4-1. Daily tidal elevations measured at Charleston on the southern Oregon coast. Data from the National Ocean Service (http://www.co-ops.nos.noaa.gov/data_menu.shtml?stn=9432780%20Charleston,%20OR&type=Bench%20Mark%20Sheets).

The actual level of the measured tide can be considerably higher than the predicted level provided in standard Tide Tables and is a function of a variety of atmospheric and oceanographic forces, which ultimately combine to raise the mean elevation of the sea. These latter processes also vary over a wide range of time scales and may have quite different effects on the coastal environment. For example, along the Pacific Northwest coast strong onshore winds coupled with the extremely low atmospheric pressures associated with a major storm can cause the water surface to be locally raised along the shore as a storm surge by as much as 1.5 m (4.9 ft) (Allan and Komar, 2002b). However, during the summer months these processes can be essentially ignored due to the absence of major storms systems.

On the Oregon coast, tides tend to be enhanced during the winter months due to warmer water temperatures and the presence of northward flowing ocean currents that raise water levels along the shore. These conditions persist throughout the winter rather than lasting for only a couple of days as is the case for a storm surge. This effect can be

seen in the monthly averaged water levels derived from the Charleston tide gauge (Figure 4-2), where the averaging process has removed the water-level variations of the tides, yielding a mean water level for the entire month. Combining 38 years of data, the results in Figure 4-2 show that on average monthly-mean water levels during the winter are nearly 20 cm (0.7 ft) higher than in the summer. Water levels are most extreme during El Niño events, due to an intensification of the processes (mostly, enhanced ocean sea surface temperatures offshore from the Oregon coast). This occurred particularly during the unusually strong 1982-1983 and 1997-1998 El Niños. As seen in Figure 4-2, water levels during those climate events were approximately 25 cm (0.8 ft) higher than the seasonal peak and as much as 50 cm (1.6 ft) higher than during the preceding summer. These higher water levels enabled wave swash processes to reach much higher elevations on the beach during the winter months, with storm surges potentially raising the water levels still further.

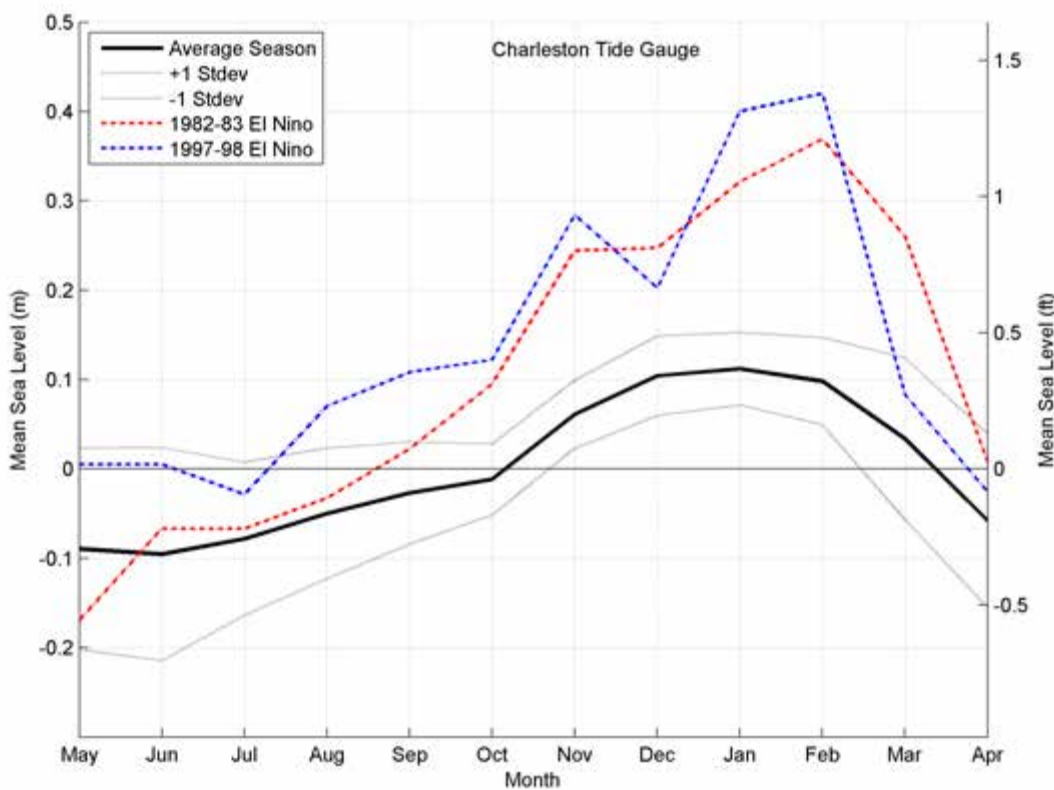


Figure 4-2. Seasonal cycles in monthly-mean water levels based on data from the Charleston, Oregon, tide gauge. Monthly data are based on hourly measurements collected over 38 years (1970-2007). Water levels for the 1982-1983 and 1997-1998 El Niño events are also shown.

Aside from seasonal to interannual effects of climate events on ocean water levels, also of interest are long-term trends along the Coos County coastline associated with relative sea level changes due to climate change. Figure 4-3 presents results from an analysis of long-term annual changes based on a separate analysis of the summer and winter tide levels for the Charleston gauge. For our purposes “winter” is defined as the combined average tide level measured over a 3-month period around the peak of the seasonal maximum in winter water levels, typically the months of December through February. Similarly, “summer” water levels reflect the combined average tide level measured over a 3-month period around the seasonal minimum, typically the months between May through August when water levels also tend to be less variable (Komar and others, 2011). As shown in Figure 4-2, winter tidal elevations in Figure 4-3 are systematically displaced upward by about 20 cm (0.7 ft) above summer tidal elevations, with the difference between the regression lines reflecting the seasonal change in ocean

water levels from summer to winter. Figure 4-3 also emphasizes the extremes associated with major El Niño events, with the peaks between the 1983 and 1997 major events having been systematically shifted upward over the years due to relative sea level changes along this particular section of the coast. In contrast, the summer regression line is characterized by significantly less scatter in the residuals as it effectively excludes the influence of storms and El Niño events that are dominant during the winter. Using this approach, it can be seen that the Coos Bay coastline is slowly being transgressed at a rate of $\sim 1.12 \pm 0.95 \text{ mm}\cdot\text{yr}^{-1}$, a slightly lower value than that reported by NOS ($\sim 1.29 \pm 1.15 \text{ mm}\cdot\text{yr}^{-1}$). Finally, it is important to appreciate that the trends shown in Figure 4-3 reflect relative sea level changes due to the fact that the PNW coast of Oregon and Washington is locally influenced by changes in the elevation of the land due to regional tectonics as well as by the global rise in sea level, with the net change being important to both coastal erosion and flood hazards.

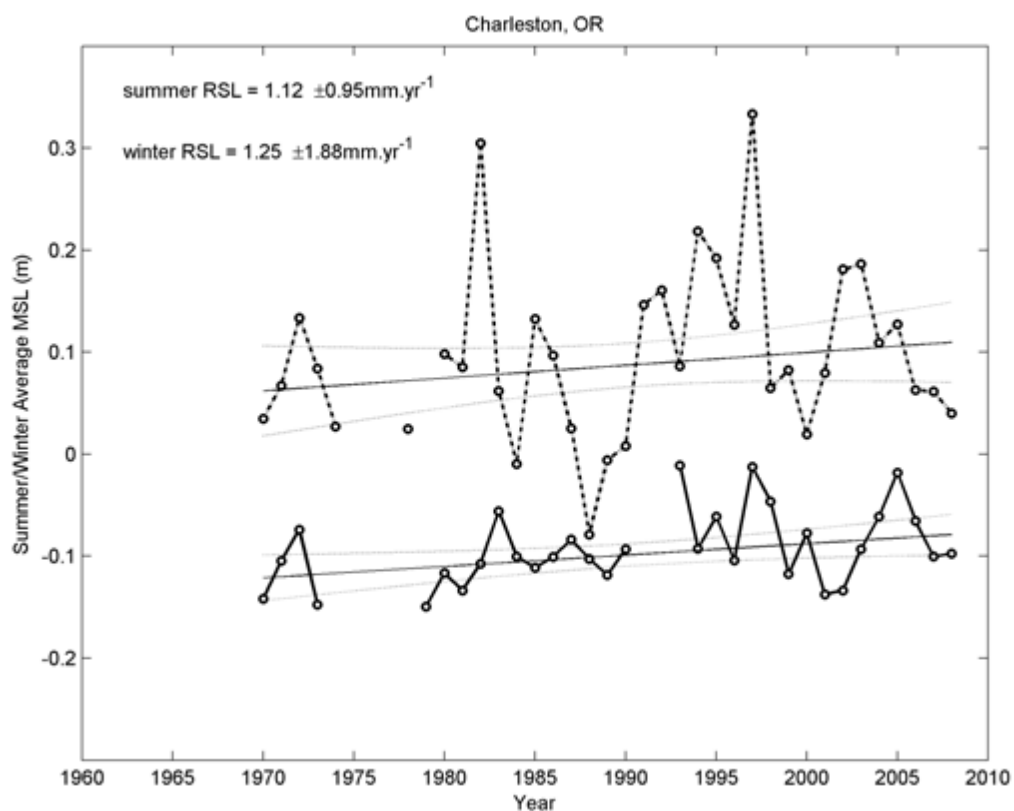


Figure 4-3. The trends of “winter” and “summer” mean-sea levels measured by the Charleston, Oregon, tide gauge. Results for the summer regression are statistically significant, while the estimated winter rate is not significant at the 95% confidence level.

4.2 Still water level (SWL)

The still water level (SWL) is the sum of the predicted astronomical tide listed in tide tables, plus the effects of processes such as an El Niño event or storm surge that can elevate the measured tide above the predicted tide (NHC, 2005). Of importance to erosion and flooding hazards are the extremes of the measured tides. In conventional analyses of extreme values, the general assumption is that the data being analyzed (e.g., the annual maxima) represent independent and identically distributed (stationary) sequences of random variables. The generalized extreme value (GEV) family of distributions is the cornerstone of extreme value theory, in which the cumulative distribution function is given as

$$G(z, \mu, \sigma, \xi) = \exp \left\{ - \left[1 + \xi \left(\frac{z - \mu}{\sigma} \right) \right]^{-1/\xi} \right\} \quad (\text{eq. 4-1})$$

defined on $\{z: 1 + (\xi(z - \mu)/\sigma) > 0\}$, where the parameters satisfy $-\infty < \mu < \infty$, $\sigma > 0$, $-\infty < \xi < \infty$ (Coles, 2001). The model has three parameters; μ is a location parameter, σ is a scale parameter, and ξ is a shape parameter. The EV-II (Frechet) and EV-III (Weibull) classes of extreme value distributions correspond respectively to the cases of $\xi > 0$ and $\xi < 0$. When $\xi = 0$, Equation 4.1 collapses to the Gumbel or EV-I type extreme value distribution. By inferring the shape parameter ξ (estimated here, along with the other parameters, by maximizing the log-likelihood function), the data themselves determine the most appropriate type of tail behavior, and it is not necessary to make an a priori assumption about which individual extreme family to adopt as in a classical Weibull-type extreme wave height analysis (Coles, 2001).

The GEV is often applied to annual maxima data in an approach referred to as the annual maximum method (AMM). However, one of the primary shortcomings of fitting an extreme-value distribution with annual maximum data is that useful information about the extremes is inherently discarded, particularly when data are sampled on either a daily or hourly basis (as in the case of the measured

tides and deep-water significant wave heights measured by Charleston tide gauge and NDBC wave buoys). Two well-known approaches exist for characterizing extremes by utilizing data other than simply annual (block) maxima. The first is based on the behavior of the r -largest-order statistics within a block, for low r , and the second is based on exceedances above a high threshold value. For the purposes of this study, we use the peak-over-threshold (POT) approach for determining the extreme SWL and wave heights.

In the POT method, a high threshold, u , is chosen in which the statistical properties of all exceedances over u and the amounts by which the threshold is exceeded are analyzed. It is assumed that the number of exceedances in a given year follows a Poisson distribution with annual mean vT , where v is the event rate and $T = 1$ year, and that the threshold excesses $y > 0$ are modeled using the Generalized Pareto Distribution (GPD) given by

$$H(y, \sigma, \xi) = 1 - \left(1 + \frac{\xi y}{\sigma} \right)^{-1/\xi} \quad (\text{eq. 4.2})$$

where ξ is the shape parameter of the GEV distribution and σ is a scale parameter related to GEV parameters by $\sigma = \sigma + \xi(u - \mu)$. The event rate can also be expressed in a form compatible with the GEV distribution provided that

$$v = \left(1 + \frac{\xi(u - \mu)}{\sigma} \right)^{-1/\xi}.$$

Estimates of extreme quantiles of the distributions are obtained by inverting the distributions in Equation 4.3. For GPD-Poisson analyses the N -year return level, y_N , is given as

$$y_N = \mu + \frac{\sigma}{\xi} \left[(N n_y \zeta_u)^\xi - 1 \right] \quad (\text{eq. 4.3})$$

where n_y is the number of observations per year and ζ_u is the probability of an individual observation exceeding the threshold, u .

Figure 4-4 presents results of the GEV analyses for the Charleston tide gauge. In constructing this plot, we used a threshold of 2.81 m (9.2 ft). Included in the figure are the calculated 1- through 100-year SWLs. As can be seen in Figure 4-4, the 1% SWL calculated for the Charleston gauge is 3.41 m (11.2 ft, relative to MLLW). When adjusted to the NAVD88 vertical datum, this value becomes 3.26 m (10.7 ft, NAVD88); note the adjustment from NAVD88 to MLLW is

0.152 m (0.5 ft). The 500-year SWL is estimated to be 3.33 m (10.9 ft) relative to the NAVD88 vertical datum. As observed previously, the highest tide measured at the Charleston gauge reached 3.26 m (10.7 ft, relative to NAVD88). Of interest, the SWL identified in the original flood mapping calculations at Bandon from Crescent City tide gauge data (and compared with the Charleston tide gauge data) indicated a SWL of 3.22 m (10.6 ft), close to the current estimate.

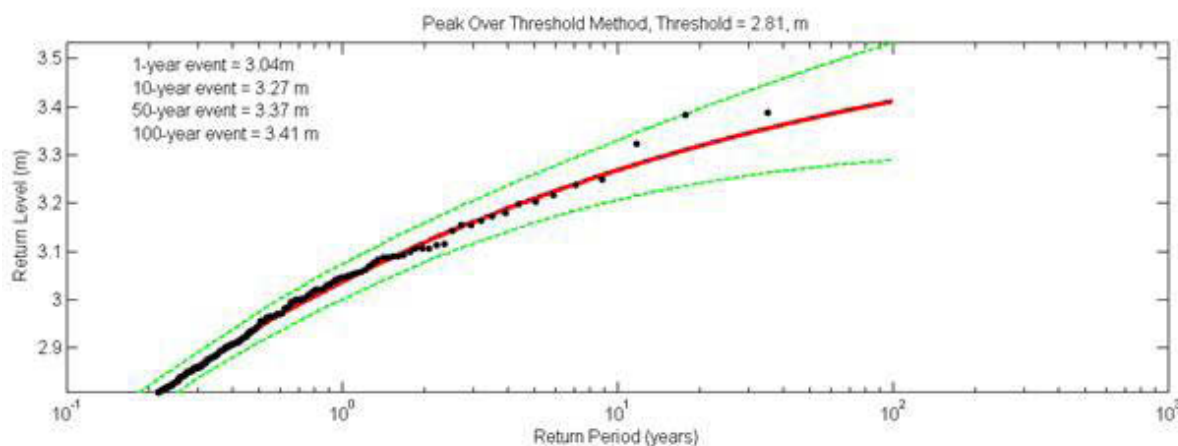


Figure 4-4. Extreme-value analyses of the still water level (SWL) determined for the Charleston, Oregon, tide gauge. Black dots denote actual tide data used to fit the model distribution (red line) and the associated confidence band (green lines).

5.0 PACIFIC NORTHWEST WAVE CLIMATE

The wave climate offshore the Oregon coast is one of the most extreme in the world, with winter storm waves regularly reaching heights in excess of several meters. This is because the storm systems emanating from the North Pacific travel over fetches that are typically a few thousand miles in length and are also characterized by strong winds, the two factors that account for the development of large wave heights and long wave periods (Tillotson and Komar, 1997). These storm systems originate near Japan or off the Kamchatka Peninsula in Russia and typically travel in a southeasterly direction across the North Pacific toward the Gulf of Alaska, eventually crossing the coasts of Oregon and Washington or along the shores of British Columbia in Canada.

Wave statistics (heights and periods) have been measured in the North Pacific using wave buoys and sensor arrays since the mid 1970s. These data have been collected by the National Oceanic and Atmospheric Administration (NOAA), which operates the National Data Buoy Center (NDBC), and by the Coastal Data Information Program (CDIP) of Scripps Institution of Oceanography. The buoys cover the region between the Gulf of Alaska and Southern California and are located in both deep and in intermediate to shallow water over the continental shelf. The NDBC operates some 30 stations along the West Coast of North America, while CDIP has at various times carried out wave measurements at 80 stations. Presently, there is one CDIP buoy operating offshore from Coos Bay (46229), and two NDBC buoys (Oregon [46002] and Port Orford [46015]) located offshore from the southern Oregon coast. Wave measurements by NDBC are obtained hourly (CDIP provides measurements every 30 minutes) and are transmitted via satellite to the laboratory for analysis of the wave energy spectra (dominant energy band by direction), significant wave heights (H_s , the

average of highest one third of the waves in record), and peak spectral wave periods (T_p , the peak period associated with dominant energy spectra). These data can be obtained directly from the NDBC through their website¹².

Analyses of the wave climate offshore from Coos County were undertaken under subcontract by Peter Ruggiero, Department of Geosciences, Oregon State University (OSU), and included numerical analyses of the 1%, or 100-year, extreme storm wave event and the associated calculated wave setup¹³, runup¹⁴, and total water level (i.e., the wave runup superimposed on the tidal level) to help determine the degree of coastal flood risk along the coast of Coos County.

OSU performed a series of analyses including wave transformations, empirical wave runup modeling, and total water level modeling. For the purposes of this study, OSU used the SWAN (Simulating Waves Nearshore) wave model to transform deep-water waves (for a range of 1% scenarios) to the nearshore (typically the 20 m (65.6 ft) contour). The deep-water equivalent of these refracted nearshore waves was determined using the linear shoaling relation in order to calculate wave runup levels, which were then combined with the tidal component in order to estimate the flood risk along the Bandon shore and at Bastendorff Beach. The general area over which the SWAN grid was set up is shown in Figure 5-1.

¹² <http://seaboard.ndbc.noaa.gov/Maps/Northwest.shtml>

¹³ Wave setup is the elevation of the still-water level due to breaking waves.

¹⁴ Wave runup is the rush of water up the beach face or a structure due to the process of wave breaking. The amount of runup is the vertical height above the still water level that the rush of water reaches.



Figure 5-1. Location map showing NDBC and CDIP wave buoys and model boundary.

In general, our analyses proceeded in the following order:

1. Develop long time series of wave conditions (approximately 27 years long) at approximately the shelf edge offshore of the study area;
2. Compute initial wave runup time series for two representative beach slopes within the study region, 0.03 and 0.08;
3. Combine the two runup time series with the measured water level time series at the Charleston tide gage to generate two representative total water level, T_{WL} , time series;
4. Develop two sets of input wave conditions (~135 conditions each, about 5 per year) that were associated with T_{WL} elevations above a determined threshold value (4.9 m [16.1 ft] for beach slope = 0.03 and 6.5 m [21.3 ft] for beach slope = 0.08);
5. Run the SWAN model with two sets of input conditions, using constant offshore boundary conditions, to compute bathymetric induced wave transformations to the 20 m (65.6 ft) contour;
6. Using the deep-water equivalent wave conditions and the appropriate measured tides from Charleston, compute T_{WL} for 21 beach profiles in Bandon and 12 profiles near Bastendorff Beach;
7. Using a Poisson-generalized Pareto distribution, compute 100-year and 500-year T_{WL} elevations with a peak-over-threshold (POT) approach;
8. Compare extreme T_{WL} s with topographic elevations of various beach backing features to determine the potential extent of coastal flooding during extreme events.

The following sections describe the procedures used in each of the aforementioned steps in our analyses.

5.1 Development of a synthesized wave climate for input into SWAN

Our primary goal was to use existing measured and hindcast wave time series to generate as long a time series of the deep-water wave climate as possible at the offshore boundary of the SWAN model, approximately the edge of the continental shelf break. To this end, we downloaded all available National Data Buoy Center (NDBC¹⁵) and Coastal Data Information Program (CDIP¹⁶) hourly wave buoy data in the region for several wave buoys (data availability shown in Figure 5-2). In addition to hourly measured wave buoy data, we obtained wave hindcast information on the deep-water wave climate determined through the Wave

Information Studies (WIS) project¹⁷ (Baird, 2005). For the purposes of this study, we used wave hindcast data determined for station 074, which is located adjacent to NDBC buoy 46002, the primary wave buoy used in this study due to its high-quality long record of data (1975–present). However, because this buoy is located in 3,525 m of water and is over 450 km from the location of the shelf edge buoys (Port Orford 46015 and Umpqua Offshore 46229), we needed to develop a methodology to transform these “off-shelf” waves to the “shelf-edge” offshore boundary condition of the SWAN model. This was necessary as the wave climate observed at buoy 46002 has significant differences compared to the climate observed at either the Port Orford or Umpqua offshore buoys.

¹⁵ <http://www.ndbc.noaa.gov/>

¹⁶ <http://cdip.ucsd.edu/>

¹⁷ <http://wis.usace.army.mil/wis.shtml>

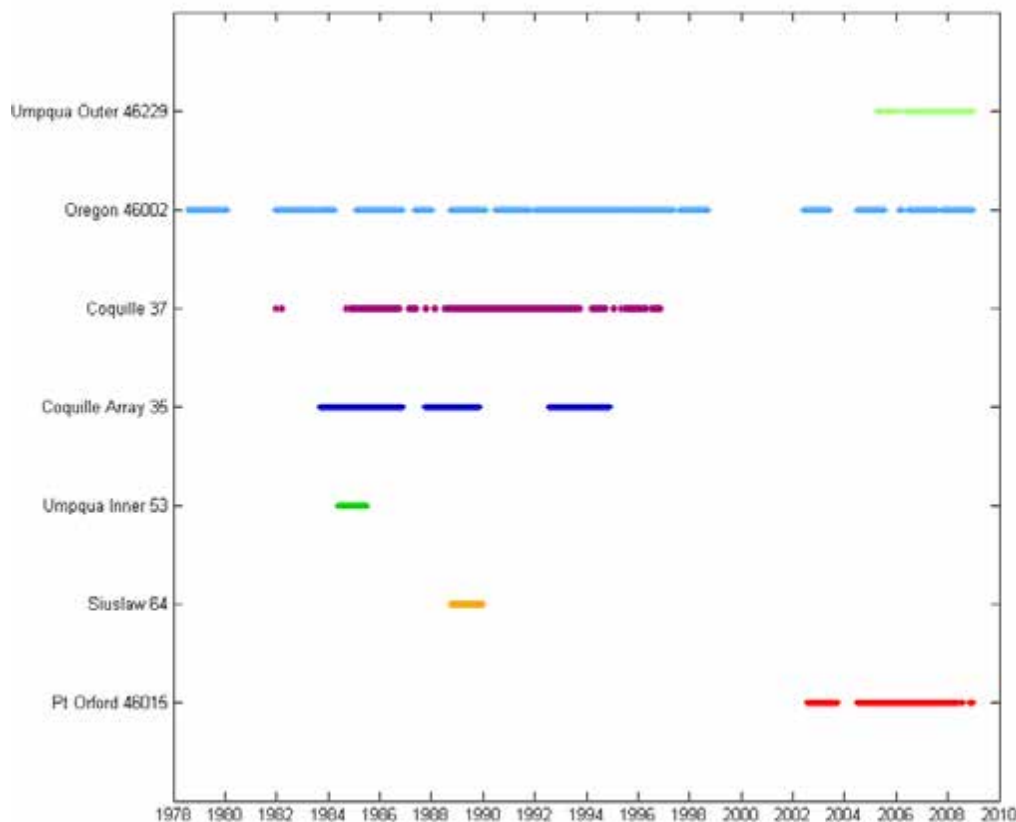


Figure 5-2. Available wave data sets timeline for wave buoys in the study region.

To transform the buoy 46002 waves to the shelf edge, we created wave period bins (0–6, 6–8, 8–10, 10–12, 12–14, 14–16, 16–21, and 21–30 seconds¹⁸) to evaluate if there has been a wave-period-dependent difference in wave heights observed at Oregon 46002 compared with the Port Orford wave buoy (or Umpqua Offshore). For our comparisons, the time stamps associated with waves measured at 46002 were adjusted on the basis of group celerity (for the appropriate wave period bin) and travel time it takes the wave

¹⁸ The NDBC wave buoys only relatively coarsely resolve long-period waves. Between 21 s and 30 s only a wave period of 25 s is populated in the data set. There are no 30-s waves in the time series. Of the waves with periods between 16 s and 20 s, over 80 percent are at approximately 16 s. Only a relatively few waves in the record have recorded periods of 17 s, 18 s, and 19 s, respectively. This coarse resolution in the raw data determined our choice of period bin widths.

energy to propagate to the Port Orford wave gage location. For example, for waves in the period bin 10 to 12 s the group celerity is about 8.3 m/s, and therefore it takes 15 hours for the energy to propagate from buoy 46002 to the Port Orford gage.

After correcting for the time of wave energy propagation, the differences in wave heights between the two buoys, for each wave period bin, were examined in two ways as illustrated in Figure 5-3:

1. A best fit linear regression through the wave height differences was computed for each wave period bin; and,
2. A constant offset was computed for the wave height differences for each period bin.

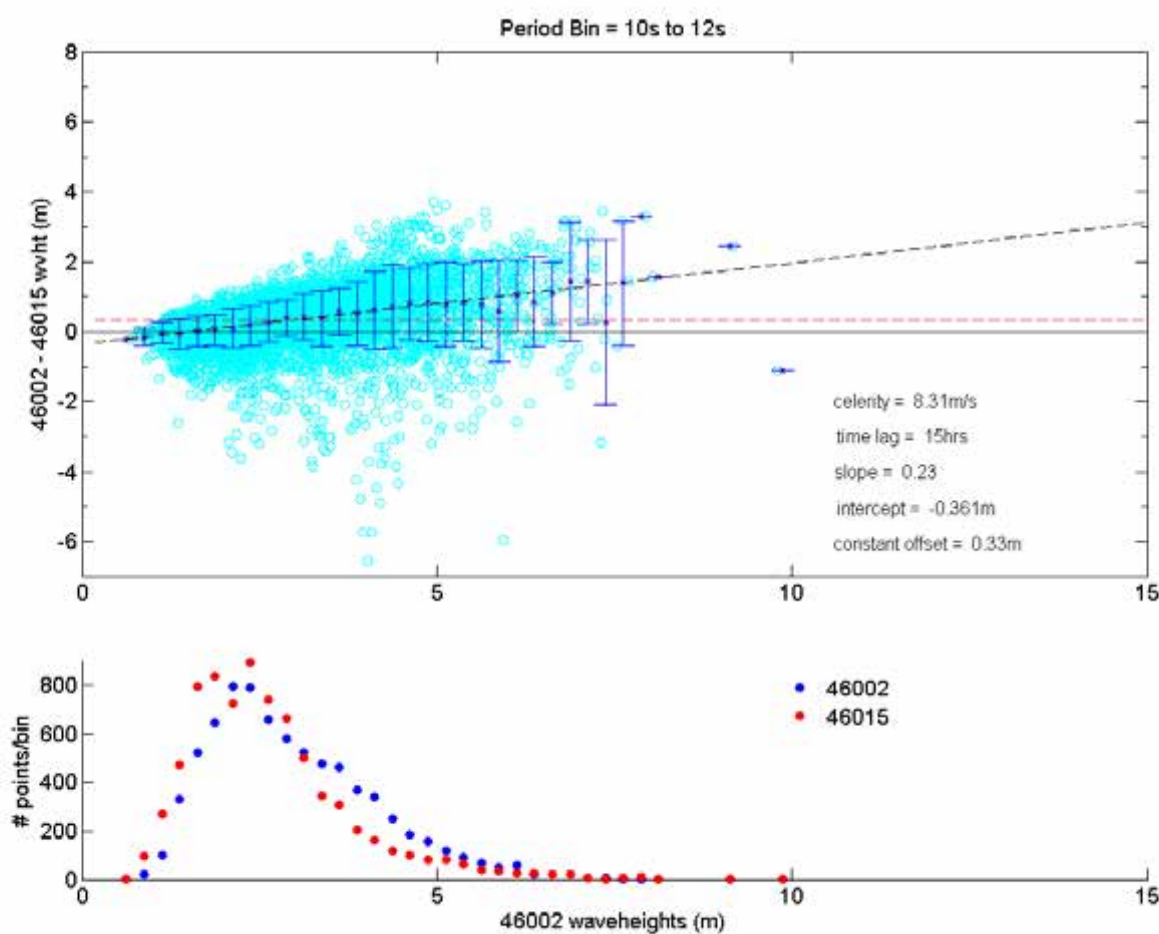


Figure 5-3. (top) Example of the development of transformation parameters between NOAA buoy 46002 (Oregon) and 46015 (Port Orford) for period bin 10–12 s. The dashed black line is the linear regression, and the dashed red line is the constant offset. Blue circles indicate the difference in the wave heights between the Oregon and Port Orford buoys for the same time period, with the Oregon data having been adjusted for the wave group speed. (bottom) Distribution plot of the number of waves processed in the example period bin.

Upon examination of the empirical probability density functions (PDF) of both buoys' raw time series (using only approximately the last 5 years of buoy 46002 data, the time of overlap with the shelf buoys) and after applying both transformation methods (Figure 5-4), it was determined that the constant offset method did a superior job of matching the PDF, particularly at high wave heights. Therefore, a constant offset adjustment dependent on the wave period was applied to the wave heights of Oregon 46002. Because the WIS hindcast data used in this study were also located well beyond the boundary of the SWAN model (basically at the location of 46002), the same series of steps comparing WIS wave heights to those from the Port Orford buoy was carried out, with a new set of constant offsets having been calculated and applied. Data from the Port Orford and Umpqua Offshore buoys were also compared in this same

manner, and it was determined that their wave height differences in the alongshore extent (i.e., offshore from Coos County) are negligible. Therefore we assume that a constant offshore wave height boundary condition¹⁹ is appropriate for the SWAN model.

After applying the wave height offsets to the Oregon 46002 buoy, gaps in this time series were filled in first with data from the Port Orford buoy and subsequently with data from the Umpqua buoy. Where there were still gaps following this procedure we then filled in the time series with the corrected WIS data. Because wave transformations (particularly refraction) computed by SWAN are significantly

¹⁹ Because the Umpqua Offshore buoy (46229) did not become directional until 2008, it was not possible to perform a detailed analysis on the differences in the directional wave climate that may be characteristic of the study area, varying in the alongshore direction along the shelf edge.

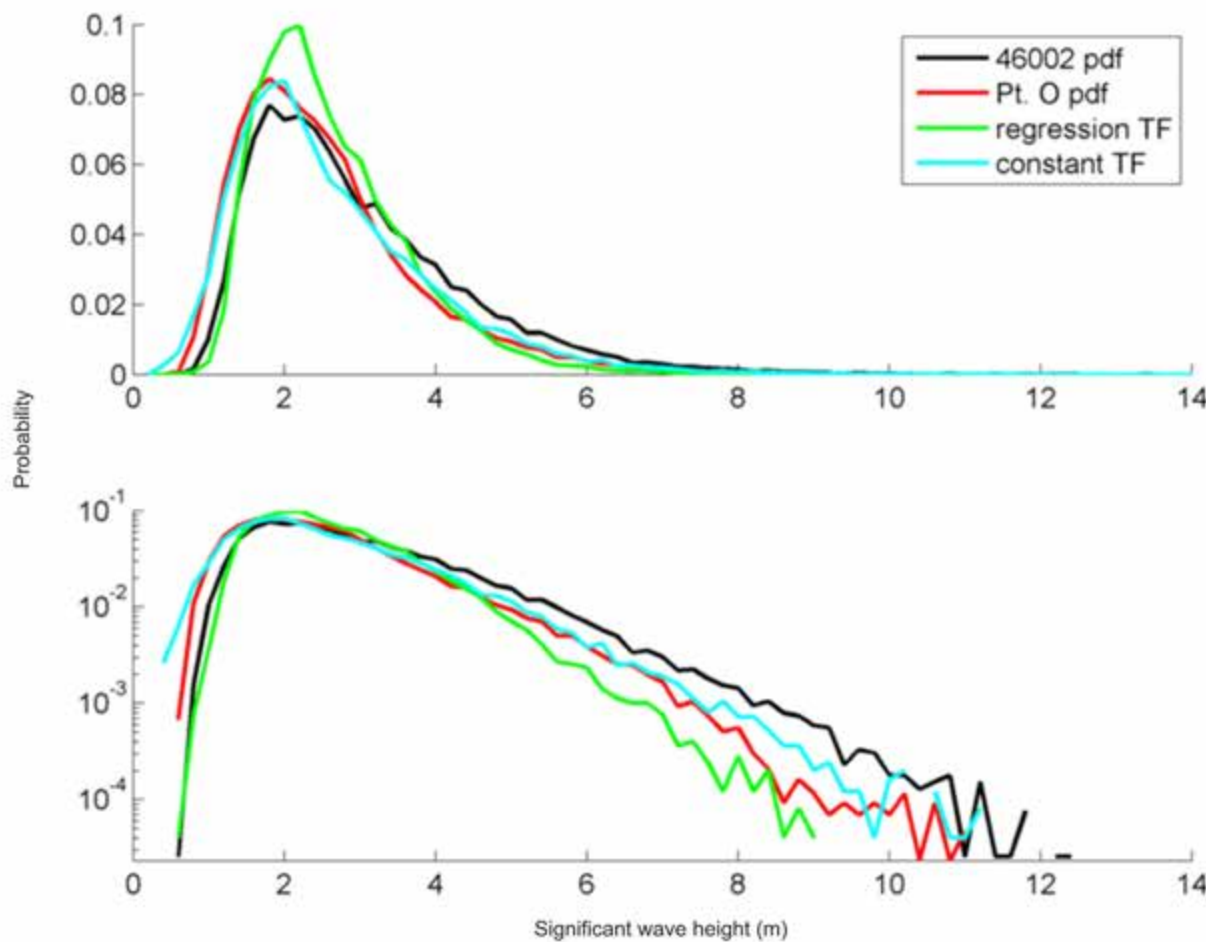


Figure 5-4. Raw probability density functions (PDF) for buoy 46002 (black line) and the Port Orford (Pt O) buoy (red line). The probability density function of the transformed wave time series using the linear regression approach (green line) and the constant offset approach (blue line) are also shown.

dependent on wave direction, when this information was missing in the buoy records it was replaced with WIS data for the same date in the time series (but the wave height and period data remained buoy observations where applicable). For conditions in the time series that had no estimate of wave direction from either the buoys or the WIS data a value of 270 degrees (i.e., westerly waves) was assumed. This is reasonable, as the majority of the waves originate from the west.

The final synthesized wave time series developed for Coos County extends from late 1979 through to the end of 2008 and consists of approximately 27.5 years of good data (measurements including at least wave height and periods) out of a possible 29.2 years (Figure 5-5 through Figure 5-8). As can be seen from Figure 5-5A, the wave climate offshore from the Oregon coast is episodically characterized by large wave events ($> 8 \text{ m}$ (26 ft)²⁰, with some storms having gen-

erated deep-water extreme waves on the order of 15 m (49 ft). The average wave height offshore from Coos County is 2.6 m (8.5 ft), while the average peak spectral wave period is 11.1 seconds, although periods of 20–25 seconds are not uncommon (Figure 5-5B). The PNW wave climate is characterized by a distinct seasonal cycle that can be seen in Figure 5-5 by the variability in the wave heights and peak periods²¹ between summer and winter. Monthly mean significant wave heights are typically highest in December and January (Figure 5-7), although large wave events ($> 12 \text{ m}$ [39.4 ft]) have occurred in all of the winter months except March. The highest significant wave height observed in the wave climate record is 15.5 m (50.9 ft), substantially exceeding the 1% wave height used in the original Bandon study, which was 7.5 m (24.6 ft) and was derived from WIS hindcasts for the period 1956–1975. In general, the small-

²⁰ The original CH2M HILL study for Bandon estimated the 100-year storm wave offshore from Bandon at 7.5 m (24.6 ft).

²¹ The groupings evident in the peak periods (Figure 5-5B) are directly from the data and are a product of the data processing methods used by the NDBC to establish the wave frequencies and hence periods. It is for this reason that we chose coarse wave period bins for long-period waves (i.e., greater than 16 s).

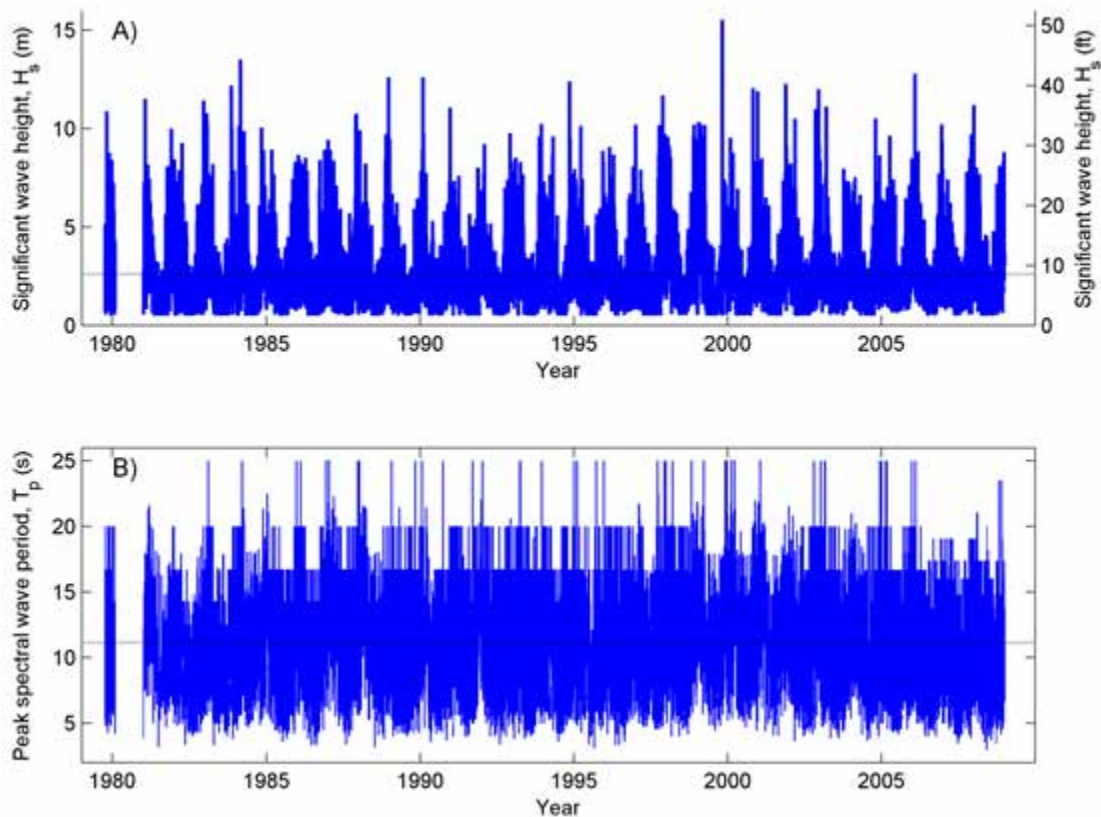


Figure 5-5. Synthesized wave climate developed for Coos County. (A) Significant wave height with mean wave height denoted (dashed line). (B) Peak spectral wave period with mean period denoted (dashed line).

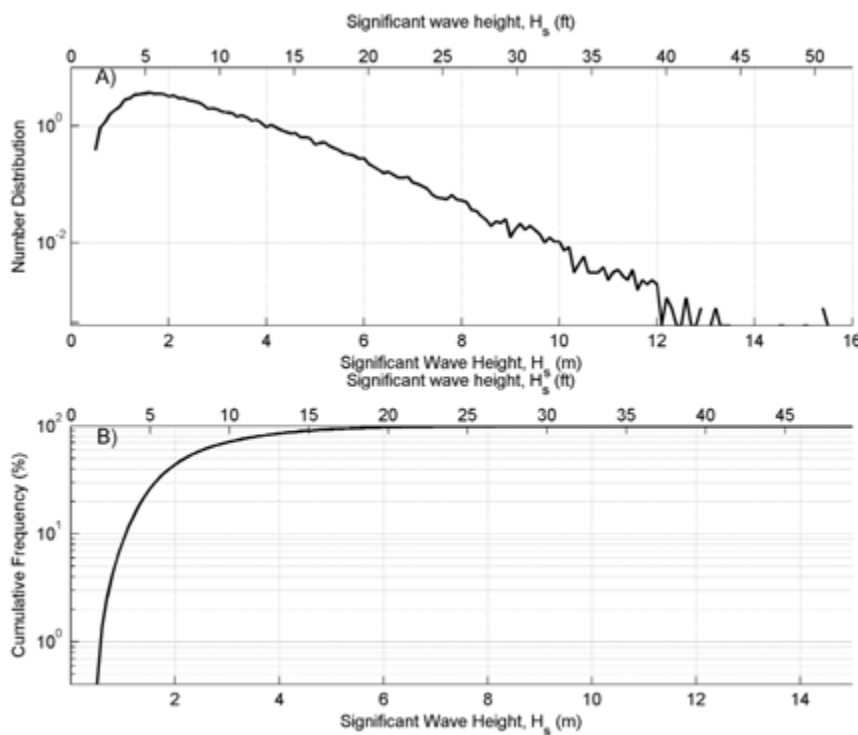


Figure 5-6. Synthesized wave climate developed for Coos County. (A) Probability distribution of wave heights plotted on a semi-log scale. (B) Significant wave height cumulative frequency curve plotted on a semi-log scale.

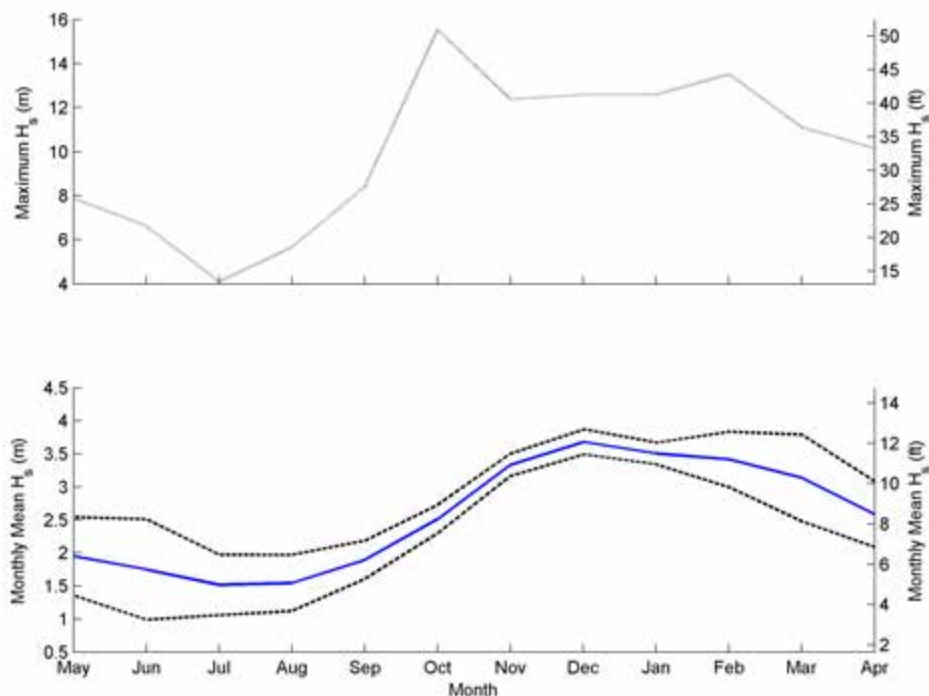


Figure 5-7. Seasonal variability in the deep-water wave climate offshore from the southern Oregon coast. (top) The maximum monthly significant wave height. (bottom) The monthly average wave height (blue line) and standard deviation (dashed line).

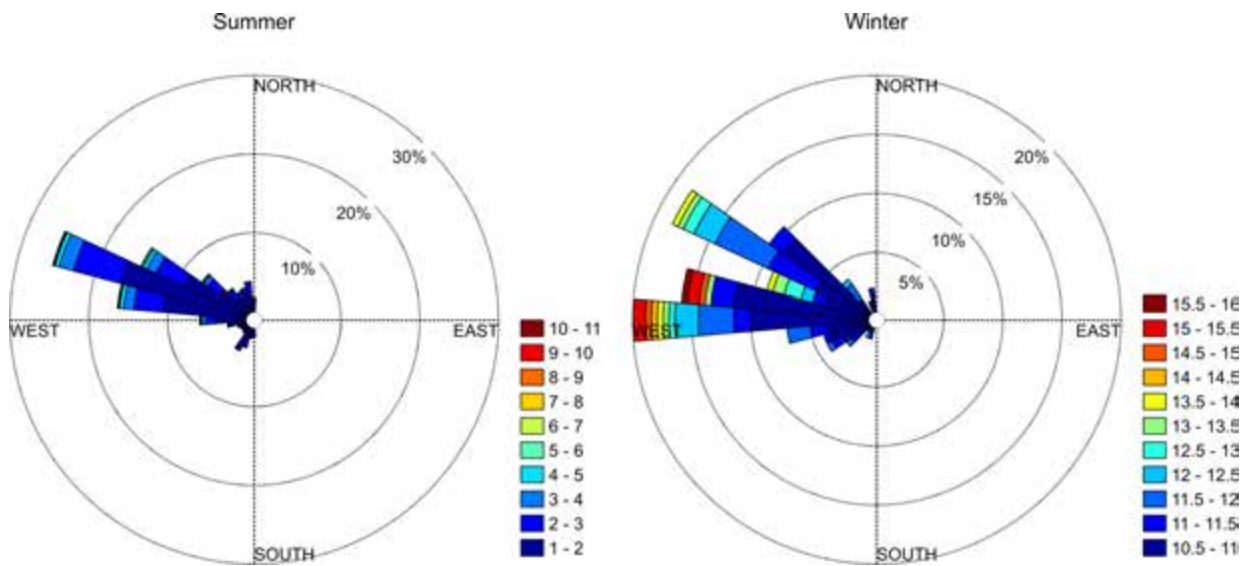


Figure 5-8. Predominant wave directions for the summer months (April-September) and the winter (October to March). Colored scale indicates the significant wave height in meters. For the winter months, waves <10 m are ignored, with the focus being on the larger waves.

est waves occur during late spring and in summer, with wave heights typically averaging ~1.5 m during the peak of summer (July-August). These findings are consistent with other studies that have examined the PNW wave climate (Allan and Komar, 2006; Ruggiero and others, 2010b; Tilletson and Komar, 1997). Figure 5-6A shows a probability density function determined for the complete time series, while Figure 5-6B is a cumulative frequency curve. The latter indicates that 50% of the time waves are typically less than 2.2 m (7.2 ft) and 90% of the time waves are less than 4.5 m (14.8 ft). Wave heights exceed 7.4 m (24.3 ft) for 1% of the time. However, it is these latter events that typically produce the most significant erosion and flooding events along the Oregon coast.

Finally, Figure 5-8 provides a wave rose of the significant wave height versus direction developed for the southern Oregon coast. In general, the summer is characterized by waves arriving from the northwest, while winter waves typically arrive from the west or southwest (Komar, 1997). This pattern is shown in Figure 5-8, which is based on separate analyses of summer and winter directional data developed from the synthesized time series (composed of both WIS station data (074) and data from the inshore buoys). To better highlight the predominant wave directions for the winter months, wave heights less than 10 m (33 ft) have been eliminated from the analysis. As can be seen in Figure 5-8, summer months are characterized by waves arriving from mainly the west-northwest (~25%) to northwest (~21%), with few waves out of the southwest. The bulk of these reflect waves with amplitudes that are predominantly

less than 3 m (9.8 ft). In contrast, the winter months are dominated by much larger wave heights out of the west (~25–35%), and to a lesser extent the northwest (~18%).

5.2 Initial total water level calculations

Having established a synthesized wave climate time series for the southern Oregon coast, the data were then used to calculate initial wave runup heights on the beaches included in this study, which in turn were combined with the measured tide data to generate a total water level (T_{WL}) time series. The purpose of these initial total water level calculations is to identify specific storm events that would eventually be used in SWAN wave modeling to transform the waves to shallow water. Assessments of the total water level (T_{WL}) achieved on the beaches is therefore simply:

$$T_{WL} = \text{measured tide} + \text{wave runup} \quad (\text{eq. 5.1})$$

where the tide is derived from water levels measured by the Charleston, Oregon, tide gauge from the NOS, and R is the total vertical wave runup which includes both the wave setup (a super elevation of the water level due to wave breaking) and swash oscillations around the wave setup (combined incident and dynamic wave runup components) (NHC, 2005). Here we employ an extreme wave runup statistic $R_{2\%}$ (Holman, 1986), the two percent exceedance value of wave runup maxima, because it is the highest swash events in a wave runup distribution that are initially responsible for erosion and overtopping, and because empirical formu-

lae have been developed for the calculation of this statistic. In this application we have based runup calculations on the formula derived by Stockdon and others (2006), who combined data from 10 nearshore field experiments to obtain an expression for $R_{2\%}$ (a more detailed discussion of the final wave runup calculations is described in Section 6.1.1, "Stockdon runup model"):

$$R_{2\%} = 1.1 \left(0.35 \tan \beta (H_o L_o)^{1/2} + \frac{[H_o L_o (0.563 \tan \beta^2 + 0.004)]^{1/2}}{2} \right) \quad (\text{eq. 5.2})$$

where $\tan \beta$ is the foreshore beach slope, H_o is the deep-water significant wave height, L_o is the deep-water wave length, given by Airy (linear) wave theory as $(g/2\pi T)^2$ where g is the acceleration of gravity and T is the peak spectral wave period. This formulation to calculate the runup levels is directly incorporated into Equation 5.1, applicable to a wide range of morphologic conditions.

Figure 5-9(A-D) shows the complete wave height, period, tide, and T_{WL} time series developed based on a foreshore beach slope of 0.03, typical of much of the southern Bandon shore and along Bastendorff Beach. For SWAN input conditions presented in the following section, we chose all T_{WLs} that exceeded a threshold value of 4.9 m (16.1 ft) NAVD88, or approximately five major events per year. Using this approach, we were able to identify a total of 134 discrete events. These input event conditions are identified as black dots in Figure 5-9. To account for higher wave runups associated with the steeper beaches characteristic of the Lighthouse Beach (Coos 7-11) and Bandon profiles (Bandon 1-4), we performed the same analysis using a foreshore beach slope of 0.08, and chose all T_{WLs} that exceeded a threshold value of 6.5 m (21.3 ft) NAVD88. This latter

approach yielded 133 events (Figure 5-9E and 5-9F). Beach slopes of 0.03 and 0.08 were chosen as they represent the range of beach slopes measured along the two study areas.

The wave conditions associated with these 267 extreme total water level events were then used as input into our SWAN wave model. These conditions are summarized in two ASCII text files with six fields including MATLAB serial time, significant wave height, peak period, dominant wave direction, measured tide and T_{WL} . Table 5-1 provides a summary of the wave climate statistics determined using this approach. As can be seen from the table, mean storm wave heights averaged ~7.5 m (24.6 ft), while the maximum waves that occurred within this set of 267 events reached 13.9 m (45.6 ft). Periods typically averaged ~17.9 seconds, with some wave events characterized by very long peak periods (up to 25 seconds). The waves predominantly arrived from the west, with some storms producing waves from south-southwest and north-northwest. These events coincided with a range of tidal elevations that varied from 1.5 to 3.2 m (4.9 to 10.5 ft).

Table 5-1. Summary variables derived from the synthesized wave climate, showing the range of wave statistics associated with the 267 extreme total water level storm events.

	Significant Wave Height (m)	Peak Spectral Wave Period (s)	Wave Direction (degrees)	Tide (m)
Slope = 0.03				
Mean	7.41	17.6	279.9	2.44
Maximum	13.10	25.1	353.1	3.23
Minimum	3.63	11.1	190.8	1.53
Slope = 0.08				
Mean	7.62	18.1	281.2	2.31
Maximum	13.94	25.1	353.1	3.07
Minimum	3.63	14.3	190.8	1.53

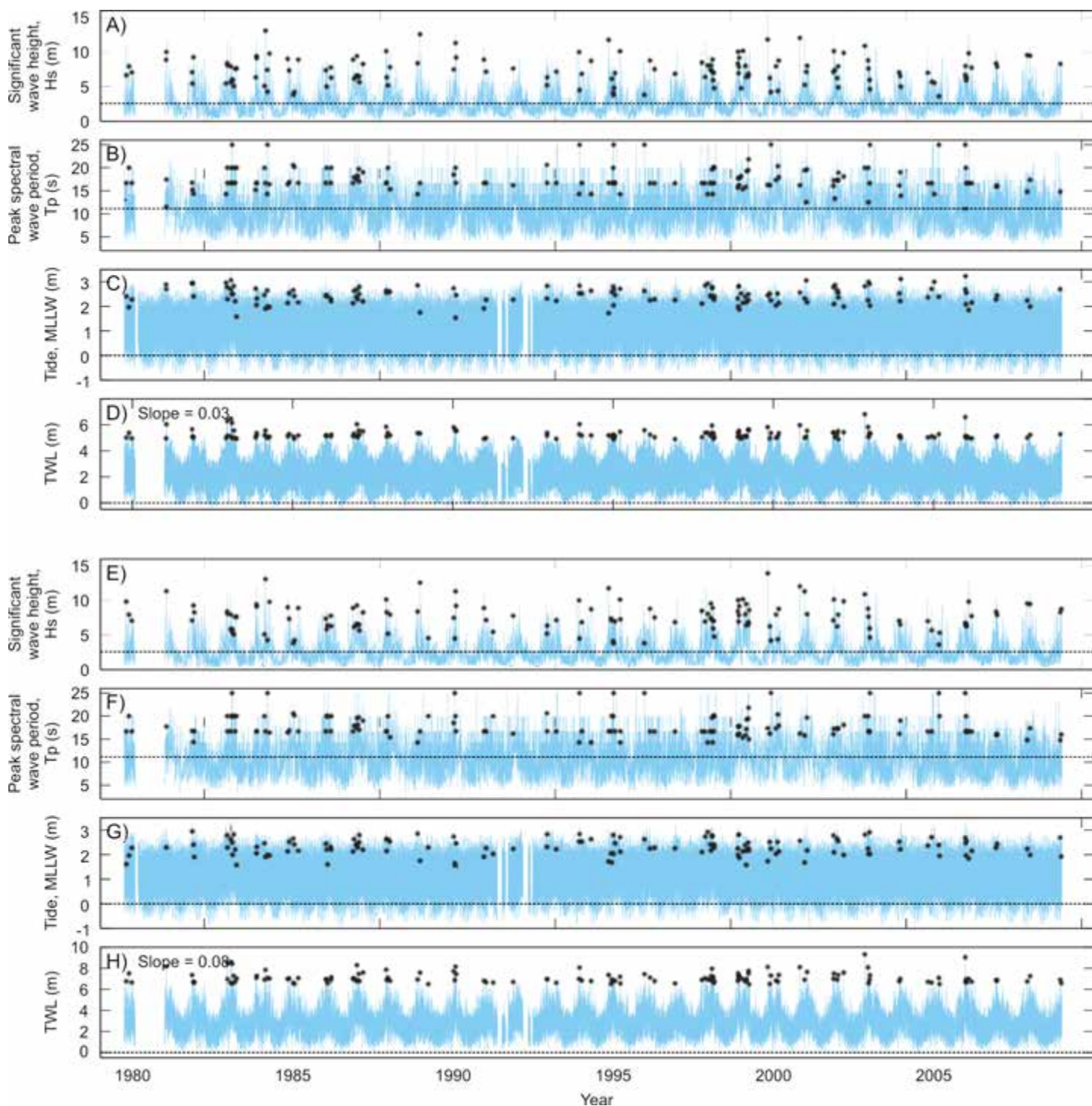


Figure 5-9. Time series of the combined wave height and period record along with the measured tide and computed total water level (T_{TW}) values for a beach slope ($\tan \beta$) of (D) 0.03 and (H) 0.08. The black dots represent the specific events above a threshold that were used as SWAN input conditions. MLLW is mean lower low water.

5.3 SWAN model development and parameter settings

We utilized the historical bathymetry assembled by the NGDC (described in section 3.4) and created an unstructured model grid that covers a large portion of the southern Oregon coastline (Figure 5-10 through Figure 5-16).

SWAN (Simulating Waves Nearshore) version number 40.72ABCD, a third generation wave model developed at the Technical University of Delft, Netherlands (Booij and others, 1999; Ris and others, 1999), was used in this study. The model solves the spectral action balance equation using finite differences for a spectral or parametric input (as in our case) specified along the boundaries. The model grid is

unstructured to allow for increased spacing in the areas of interest. For the Coos County study, the grid spacing varied from about 930 m offshore to 27 m in shallow-water areas of interest.²² The SWAN runs were executed in stationary mode and all model settings varying from the default values are discussed below.

²² The offshore boundary of the Coos County SWAN grid was determined to be in deep water for all but less than 10% of the input conditions that have wave periods of 25 seconds. For these conditions, over only a small section of the grid, at Coquille Banks, is the offshore boundary condition in transitional waters. The minor impact on wave transformations due to this small section of the grid being in transitional waters was deemed to be negligible relative to the increase in computation time required by extending the grid farther offshore.

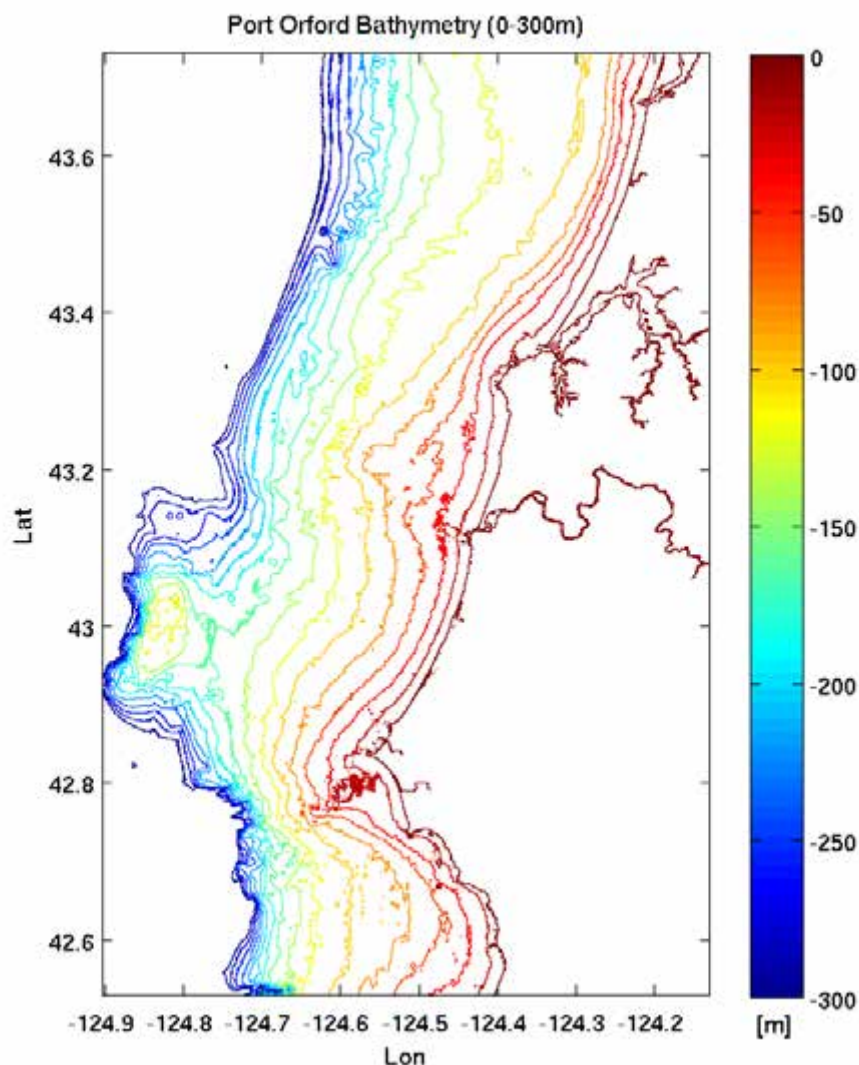


Figure 5-10. Coos County, Oregon, study area bathymetry developed using the Port Orford 1/3 arc-second (~10 m) DEM downloaded from the NOAA National Geophysical Data Center.

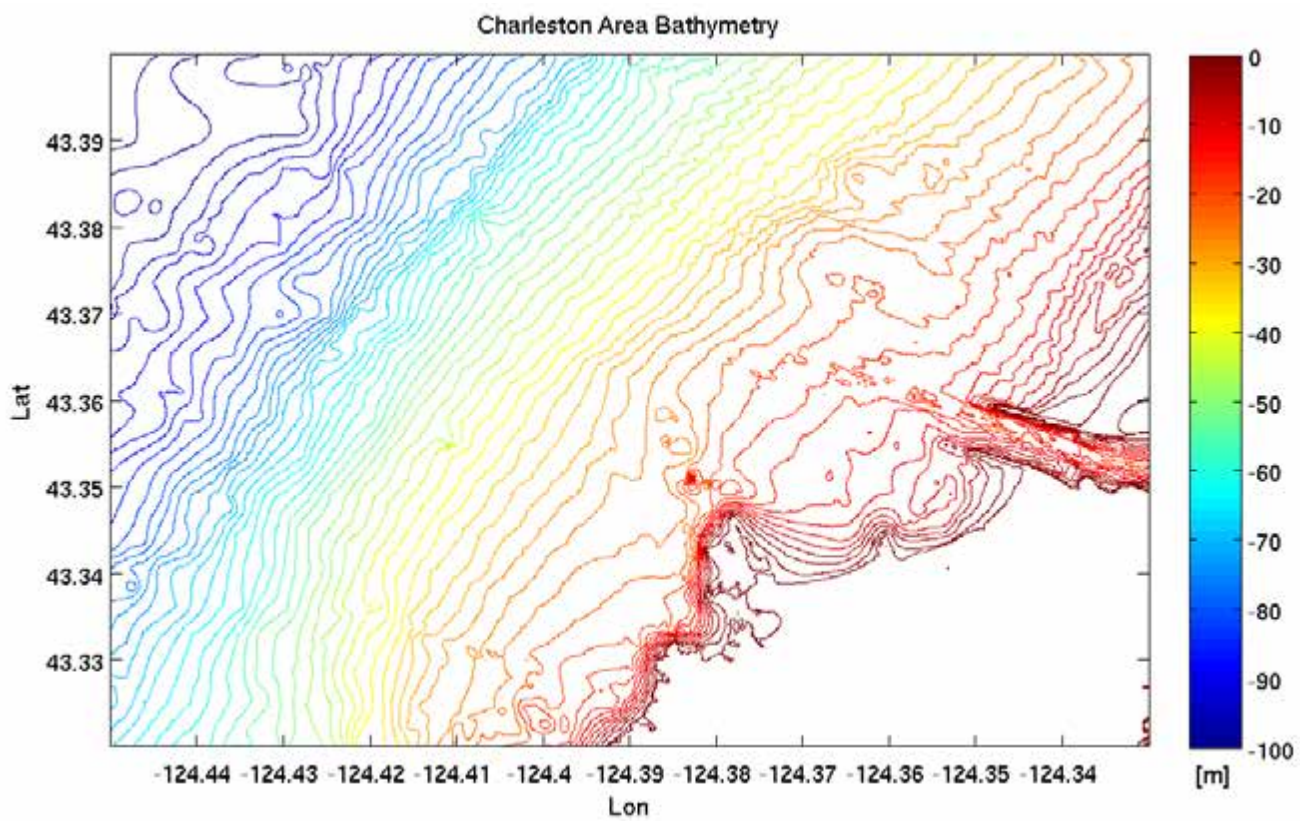


Figure 5-11. Focus area bathymetry offshore from Bastendorff and Lighthouse Beach, adjacent to Coos Bay, Oregon.

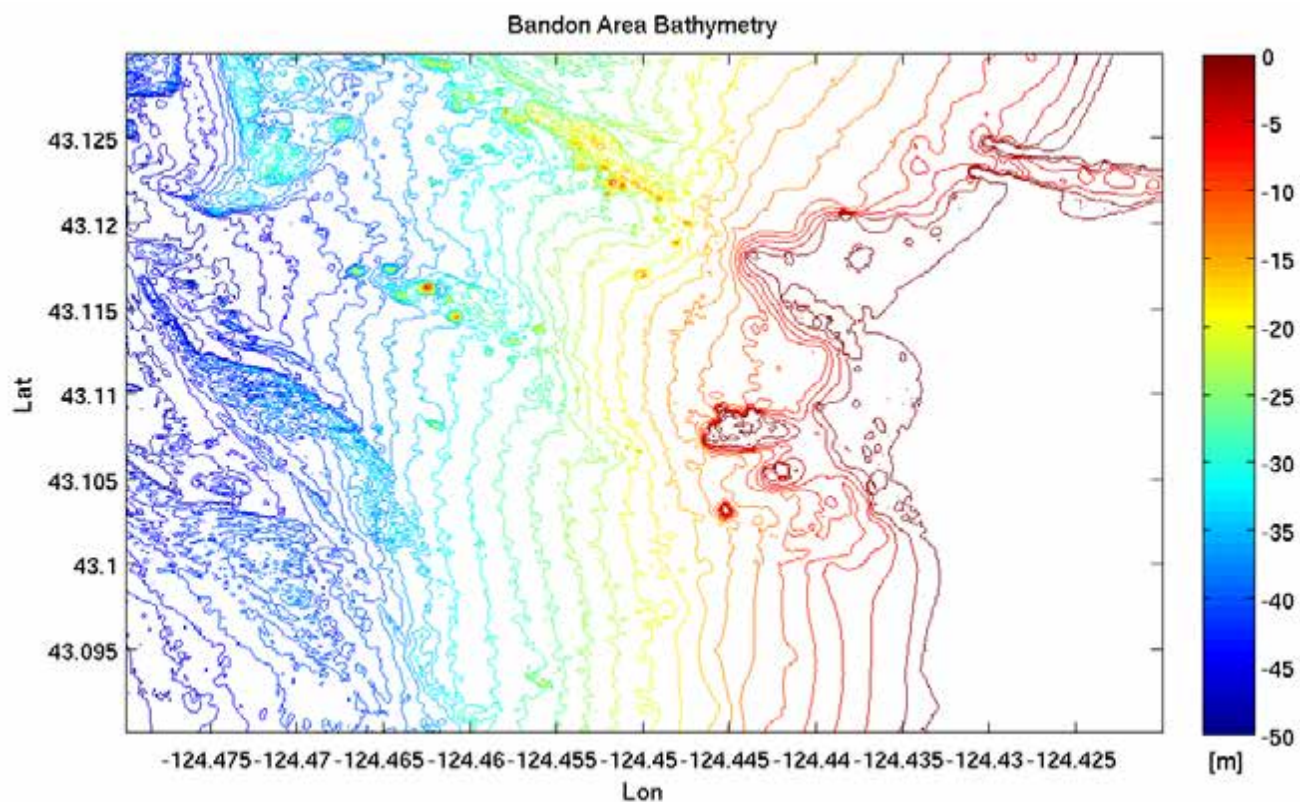


Figure 5-12. Focus area bathymetry offshore from Bandon, Oregon.

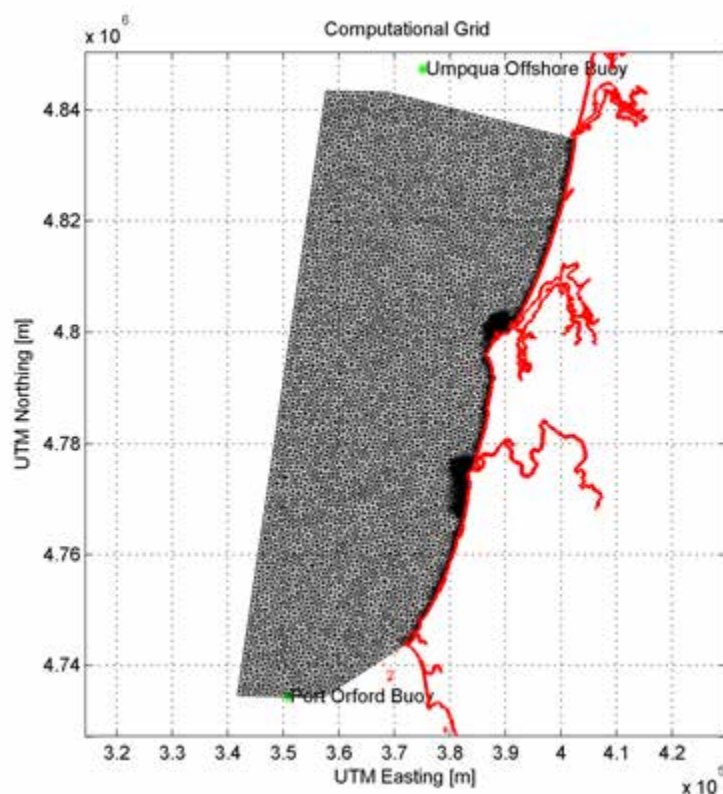


Figure 5-13. Computational grid for Coos County, Oregon.

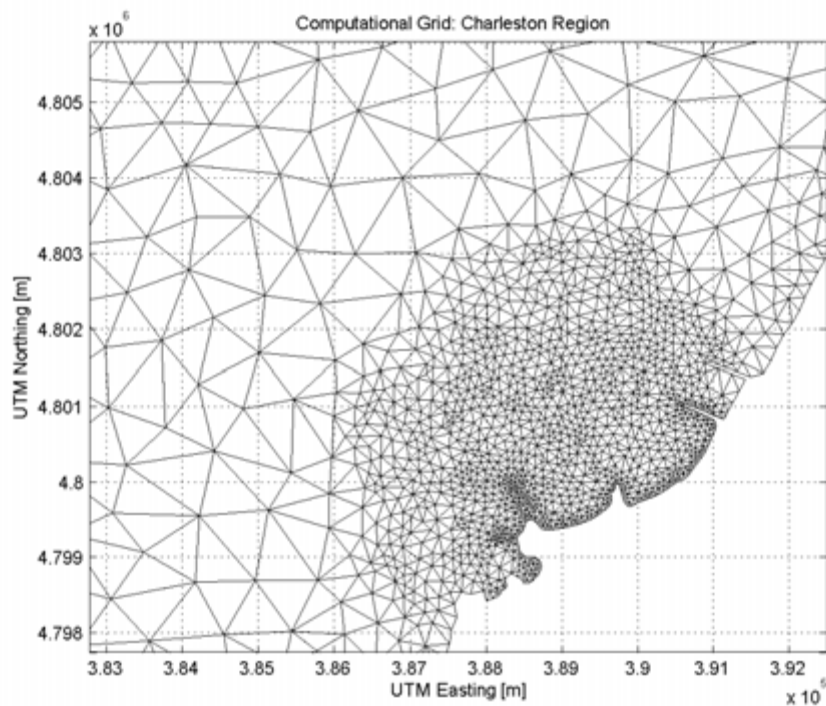


Figure 5-14. Computational grid for the Charleston, Oregon, region.

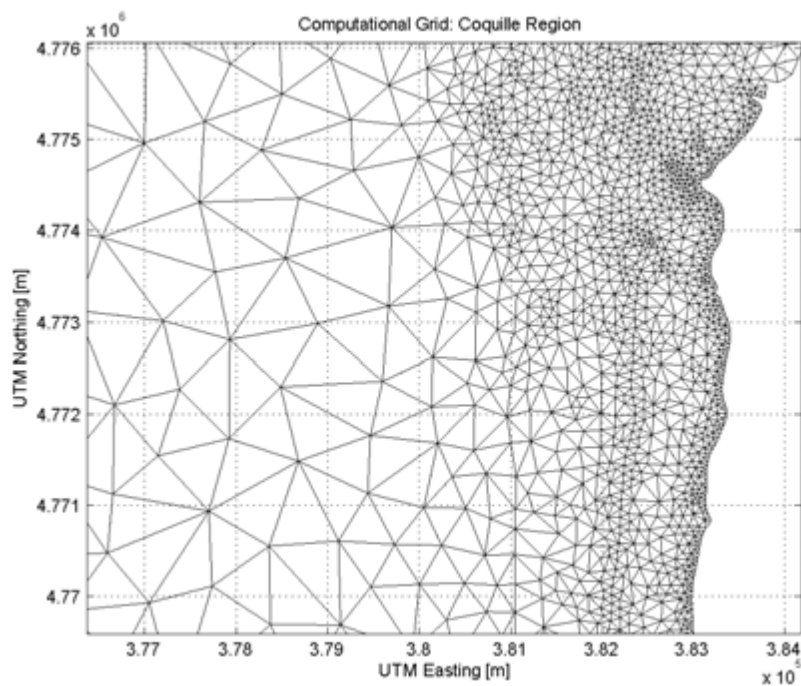


Figure 5-15. Computational grid — Coquille region.

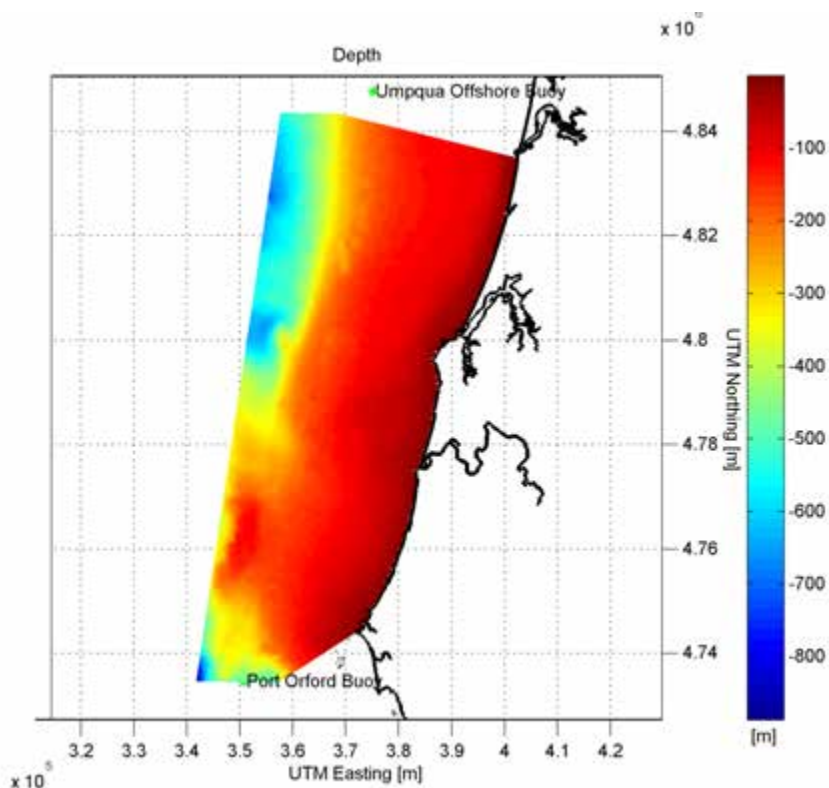


Figure 5-16. Grid depths.

The north, south, and west boundaries of the model were specified using grid coordinates and forced using a parameterized JONSWAP (Joint North Sea Wave Project) spectrum. The functions for spectral peakedness parameters γ and nn in the JONSWAP directional spectra are given as:

$$\gamma = \begin{cases} 3.3 & \text{if } T_p < 11s \\ 0.5 T_p - 1.5 & \text{if } T_p \geq 11s \end{cases}$$

$$nn = \begin{cases} 4 & \text{if } T_p < 11s \\ 2.5 T_p - 20 & \text{if } T_p \geq 11s \end{cases}$$

(eq. 5.3)

Thus, the directional distribution is generated by multiplying the standard JONSWAP frequency spectrum by $\cos^{nn}(\theta - \theta_{peak})$ (Smith and others, 2001). Wind wave spectra are broad (low γ and nn values), while swell typically have narrow distributions (high γ and nn values). Values used in the SWAN wave modeling were based on input peak periods, which ranged from $4.055 \leq \gamma \leq 11.03$ and $7.775 \leq nn \leq 42.65$. To ensure that the wave directional spread is sufficiently resolved by the model, we specified directional bins giving a 4-degree directional resolution. Our frequency bins have a Δf of $0.11*f$, which is variable as the distribution of the frequency bins is logarithmic. Our SWAN simulations did not include any additional wave growth across the shelf due to winds, nor did they include quadruplet wave-wave interactions. Triad interactions, diffraction, and wave setup were also not activated in the model setup. We used the Janssen frictional dissipation option. No model calibration or verification was performed in this study.

The decision not to model the impact that winds have on wave growth was based on the fact that we do not have any nearshore wave data for which to perform a model calibra-

tion. To develop our combined wave time series, we performed a "statistical" wave transformation between buoy 46002 and the buoys at the edge of the continental shelf and found that in general the wave heights during storm events decreased even with hundreds of kilometers of additional fetch. Without understanding the details of this phenomenon (e.g., white capping versus wind wave growth) and with no data for calibration, we felt that attempting to model wind growth would add to the uncertainty of our input wave conditions. We also have previous experience with SWAN wave modeling in the region (U.S. Pacific Northwest) in which sensitivity runs including wind were performed with only minor impact on results (Ruggiero and others, 2010a). Because wind growth was not incorporated in the runs, quadruplet wave-wave interactions do not occur in the simulations. Wave setup was not included in the simulations because we extracted the transformed wave parameters at the 20-m depth contour and used the Stockdon and others (2006) empirical model to compute wave runup (which incorporates setup) along the coast.

In total, three sets of SWAN runs were made for each of the two sets of extreme T_{WL} conditions, to test the influence of white capping and wave breaking on the model results.

- Set 1: Dissipation due to white capping is set to ON and dissipation due to wave breaking is set to ON;
- Set 2: Dissipation due to white capping is set to ON and wave breaking is set to OFF; and
- Set 3: Dissipation due to white capping is set to OFF and wave breaking is set to ON.

There were virtually negligible differences between the three sets of runs, but in general Set 2 produced slightly higher wave heights than either Set 1 or Set 3. Only Set 2 SWAN runs will be discussed in the remainder of this report.

5.4 Summary of SWAN results

Significant alongshore variability is apparent in many of the conditions examined with SWAN (Figure 5-17). To calculate the wave runup along the Bandon shore and along Bastendorff and Lighthouse Beach, we extracted the wave characteristics along the 20-m contour throughout the model (Figure 5-18). Because both the Stockdon and others

(2006) model and the Direct Integration Method (DIM [NHC, 2005]) rely on information on the deep-water equivalent wave height and peak periods as inputs, we then computed the linear wave theory shoaling coefficient and back shoaled our transformed waves to deep-water waves. These transformed deep-water equivalent waves were then used to calculate the wave runup and generate the T_{WL} conditions used in the subsequent extreme value analysis.

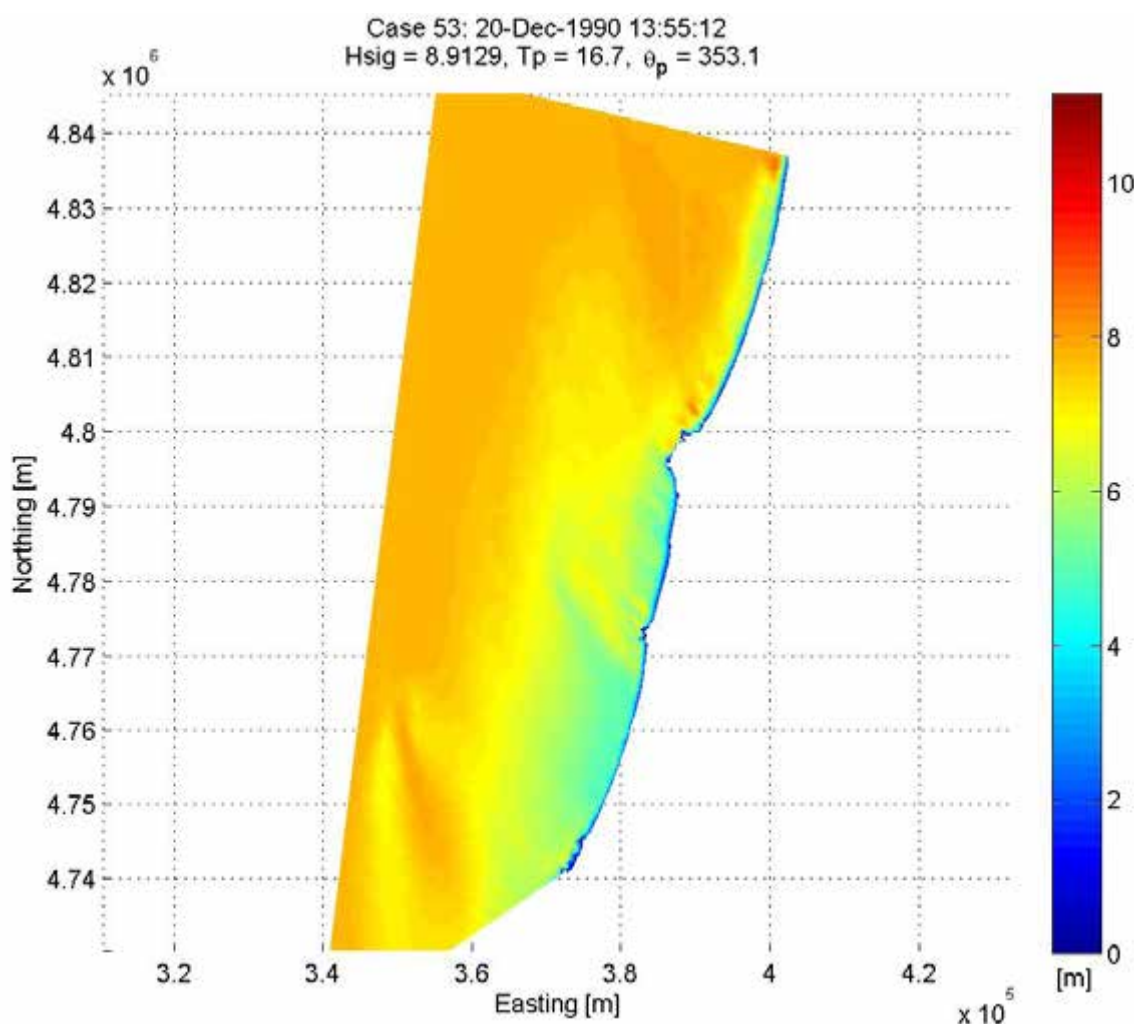


Figure 5-17. Example SWAN run (Case 53).

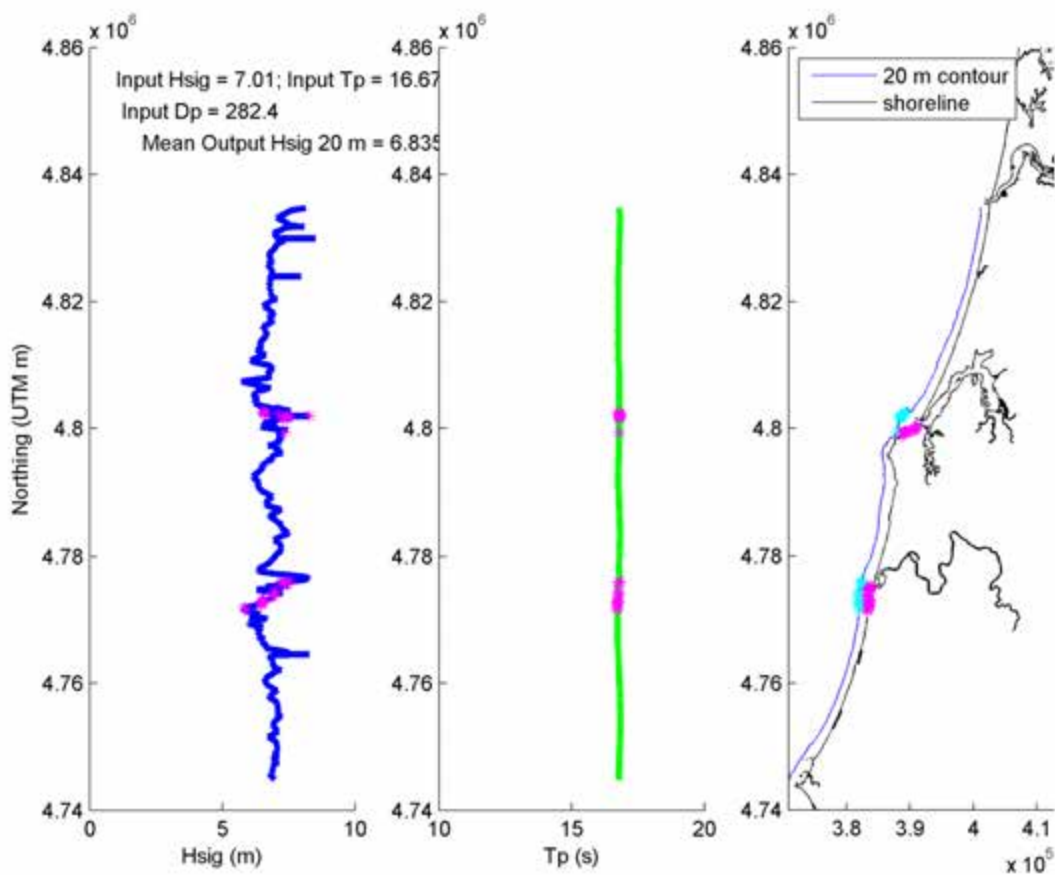


Figure 5-18. Example results of SWAN run (case 81, beta=0.03) showing alongshore varying wave height and period at the 20-m contour. Purple stars denote the locations (Northing) of the beach profiles, while the blue stars indicates where the transects cross the 20-m depth contour.

6.0 WAVE RUNUP AND OVERTOPPING

Wave runup is the culmination of the wave-breaking process whereby the swash of the wave above the still water level is able to run up the beach face, where it may encounter a dune, structure, or bluff, potentially resulting in the erosion, or overtopping, and flooding of adjacent land (Figure 6-1). Runup, R , or wave swash is generally defined as the time-varying location of the intersection between the ocean and the beach, and as summarized above is a function of several key parameters. These include the deep-water wave height (H_o or H_s), peak spectral wave period (T_p), wave length (L_o) (specifically the wave steepness, H_o/L_o), and, through the breaker parameter (or Iribarren number), $\zeta_o = \beta/\sqrt{H_o/L_o}$, which accounts for the slope (β) of a beach or an engineering structure and the steepness of the wave.

The total runup, R , produced by waves includes three main components:

- wave setup, $\langle \eta \rangle$;
- a dynamic component, $\hat{\eta}$; and,
- incident wave runup, R_{inc}

$$R = \langle \eta \rangle + \hat{\eta} + R_{inc} \quad (\text{eq. 6.1})$$

Along the Pacific Northwest Coast (PNW) of Oregon and Washington, the dynamic component²³ of runup, $\hat{\eta}$, has been demonstrated to be a major component of the total wave runup due to infragravity energy becoming trapped in the surf zone, allowing the swash to reach to much higher elevations at the shore.

Several models have been proposed for calculating wave runup on beaches (Hedges and Mase, 2004; NHC, 2005; Ruggiero and others, 2001; Stockdon and others, 2006). Here we explore two approaches available for runup calculations along Coos County, Oregon. These include the runup model developed by Stockdon and others (2006) and the Direct Integration Method (DIM) described by NHC (2005).

²³ The dynamic component of runup reflects a component of wave setup that oscillates with the wave group period, which may be amplified in the nearshore (Dean and Walton, 2009).

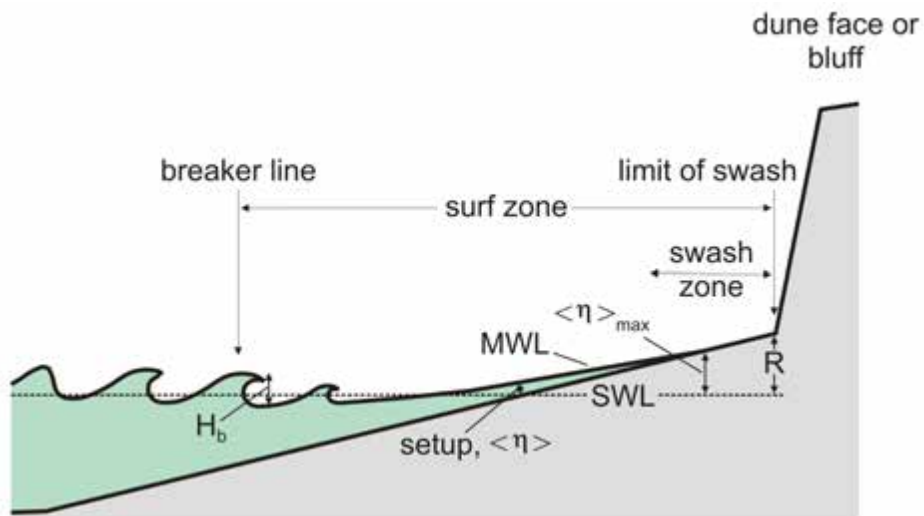


Figure 6-1. Conceptual model showing the components of wave runup associated with incident waves (modified from Hedges and Mase, 2004).

6.1 Runup models for beaches

6.1.1 Stockdon runup model

For sandy beaches, Stockdon and others (2006) developed an empirical model based on analyses of 10 experimental runup datasets obtained from a wide variety of beach and wave conditions and by separately parameterizing the individual runup processes: setup and swash. Stockdon and others proposed the following general relationship for the elevation of extreme (2%) runup, R_2 , for any data run:

$$R_2 = 1.1[\langle \eta \rangle + \frac{S}{2}] \quad (\text{eq. 6.2})$$

where

$$S = \sqrt{(R_{inc})^2 + (\hat{\eta})^2} \quad (\text{eq. 6.3})$$

and

$$\langle \eta \rangle, R_{inc}, \hat{\eta} = f(H_o, T_o, \beta_f),$$

where β_f is the slope of the beach face, and S reflects both the dynamic, $\hat{\eta}$, and incident runup, R_{inc} , components. The 1.1 coefficient value was determined because the swash level assumes a slightly non-Gaussian distribution. The final parametrized runup equation is:

$$R_{2\%} = 1.1 \left(0.35 \tan \beta (H_o L_o)^{1/2} + \frac{[H_o L_o (0.563 \tan \beta^2 + 0.004)]^{1/2}}{2} \right) \quad (\text{eq. 6.4})$$

which may be applied to natural beaches over a wide range of morphodynamic conditions. In developing Equation 6.4, Stockdon and others (2006) defined the slope of the beach as the average slope over a region $\pm 2\sigma$ around the wave setup, $\langle \eta \rangle$, where σ is the standard deviation of the continuous water level record, $\eta(t)$. Simply put, the setup reflects the height of the mean-water level (MWL) excursion above the SWL, such that the slope is determined to span the region around mid beach. For Coos County, the slope of the beach was determined by fitting a linear regression through those

data points spanning the region located between mean sea level (1.09 m) and the highest observed tide (3.26 m).

Stockdon and others (2006) further observed that for extremely dissipative²⁴ beach conditions, where $\zeta_o < 0.3$, the following equation could be used:

$$R_2 = 0.043(H_o L_o)^{0.5} \quad (\text{eq. 6.5})$$

Combining either Equation 6.4 or Equation 6.5 with the measured tide produces the total water level, T_{WL} , at the shore, important for determining the erosion or flood risk potential. Given that Equation 6.4 has been derived from quantitative runup measurements spanning a range of beach slopes (beach slopes ranged from 0.01 to 0.11 and Iribarren numbers, ζ , ranged from 0.1 [fully dissipative conditions] to ~ 2.2 [reflective conditions]; see Table 1 of Stockdon and others [2006]), the model is valid for the range of slopes and conditions observed along the Coos County coastline and elsewhere on the Oregon coast.

6.1.2 Direct integration method — beaches

The West Coast FEMA coastal flood mapping guidelines (NHC, 2005) present an alternative method for calculating runup. According to NHC (2005), the Direct Integration Method (DIM) approach allows for the wave and bathymetric characteristics to be taken into consideration; specifically, the spectral shape of the waves and the actual bathymetry can be represented. Here we review the parameterized set of runup equations that may be used to calculate runup on beaches. The equations are based on a parameterized JONSWAP spectra and uniform beach slopes.

Similar to Equation 6.1, the runup of waves using DIM can be defined according to three components: the wave setup, $\langle \eta \rangle$, a dynamic component, $\hat{\eta}$, and the incident runup, R_{inc} . Wave setup can be calculated using:

$$\langle \eta \rangle = 4.0 F_H F_T F_{Gamma} F_{slope} \quad (\text{eq. 6.6})$$

²⁴ Dissipative beaches are so termed because they are characterized by having low slopes and wide surf zones (Wright and Short, 1983). Thus, on dissipative beaches, waves tend to break well offshore from the dry beach, with the bores formed from the broken waves crossing a wide surf zone and losing most of their energy before they reach the shore and swash up the beach face. In the opposite extreme, on reflective beaches the profile slope is steep so the waves break very close to the shore (often breaking on a plunge step) and immediately develop into a strong swash up the beach face. As a result, reflective beaches lose very little wave energy during shoaling, so that the bulk of the energy is expended during the wave breaking process.

while the root mean square (rms) of the dynamic component, η_{rms} , may be estimated using:

$$\eta_{rms} = 2.7 G_H G_T G_{\text{Gamma}} G_{\text{slope}} \quad (\text{eq. 6.7})$$

where the units of $\langle \eta \rangle$ and η_{rms} are in *feet* and the factors (F) are for the wave height (F_H and G_H), wave period (F_T and G_T), JONSWAP spectrum narrowness (F_{Gamma} and G_{Gamma}), and the nearshore slope (F_{slope} and G_{slope}). These factors are summarized as a series of simple equations in Table D.4.5-1 of NHC, (2005). For the purposes of defining an average slope, NHC recommended that the nearshore slope be based on the region between the runup limit and twice the wave breaking depth, h_b , where:

$$h_b = H_b/k \quad (\text{eq. 6.8})$$

and

$$H_b = 0.39(g^{0.2} T_p H_o)^{0.4} \quad (\text{eq. 6.9})$$

where H_b is the breaker height calculated using Equation 6.9 (Komar, 1998), g is acceleration due to gravity (9.81 m/s), and for the purposes here k (breaker depth index) can be taken to be 0.78.

To derive the statistics of the oscillating wave setup and the incident wave runup components, the recommended approach is to base the calculations on the standard deviations (σ) of each component. The standard deviation of the incident wave oscillation (σ_2) on natural beaches may be calculated from:

$$\sigma_2 = 0.3 \zeta_o H_o \quad (\text{eq. 6.10})$$

Because the standard deviation of the wave setup fluctuations (σ_1) is proportional to Equation 6.7, the total oscillating component of the dynamic portion of the wave runup can be derived from:

$$\widehat{\eta}_T = 2.0 \sqrt{\sigma_1^2 + \sigma_2^2} \quad (\text{eq. 6.11})$$

Combining the results of Equations 6.11 and 6.6 yields the 2% wave runup; when combined with the tidal component the results is the total water level, T_{WL} .

6.1.3 Comparison of Stockdon and DIM runup calculations

Fundamentally, the wave runup model proposed by Stockdon and others (2006) and the DIM method described by NHC (2005) are basically the same, as both models account for the three components of runup described in Equation 6.1. Here we examine the runup results derived from both models based on two contrasting beach slope conditions characteristic of the Bandon shore. Figure 6-2 provides a comparison of the total water levels (2% wave runup + tide) calculated for the Bandon 1 profile site, where the slopes differed from 0.016 in the nearshore (DIM) to 0.079 determined for the beach face (Stockdon). From these slopes, T_{WL} s calculated using DIM are found to range from 4.5 to 7.54 m (mean = 5.74 m), while the Stockdon model produced T_{WL} s that ranged from 5.5 to 8.96 m (mean = 6.96 m). Thus, differences between the maximum and mean values are, respectively, 1.42 m and 1.22 m, with the Stockdon model producing the highest T_{WL} s. In contrast, Figure 6-3 shows the same T_{WL} comparison for the Bandon 15 site to the south, but where the beach is characterized by much lower beach slopes (0.033, Stockdon), while the nearshore slope calculated for DIM is 0.019. For the Bandon 15 site, T_{WL} s calculated using DIM are found to range from 4.3 to 7.31 m (mean = 5.64 m), while the Stockdon model produced T_{WL} s that ranged from 4.6 to 6.52 m (mean = 5.17 m). Differences between the maximum and mean values are, respectively, 0.79 m and 0.47 m, with the DIM model now producing the highest T_{WL} s.

While differences between DIM and the Stockdon runup calculations appear to be relatively similar for the lower sloping beach states, there are clear differences in the runup estimates where the beach foreshore is steep relative to the nearshore slope. Thus it is possible that the parameterization of the DIM equations may be skewed to lower beach slopes. This raises questions about the reliability of this method for determining wave runup on beaches of varying slopes. Because of these uncertainties and because the Stockdon model has been extensively validated against measured runup data, including measurements on the Oregon coast by Ruggiero and others (2001), and qualitative observations of runup during storms by DOGAMI staff at multiple sites along the coast, 1% extreme values of T_{WL} s calculated for beaches along the Coos County coast will be based primarily on the Stockdon and others (2006) model.

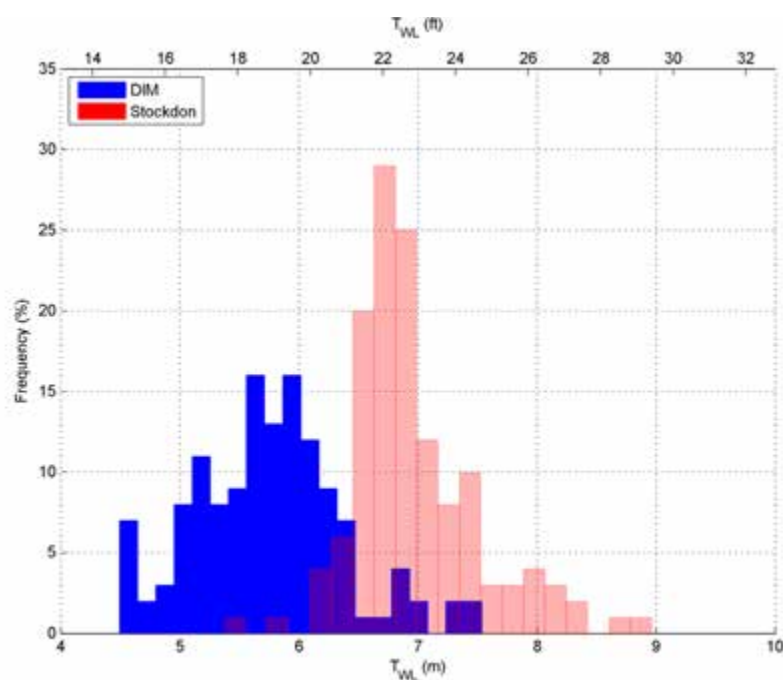


Figure 6-2. Total water level calculations using the Stockdon and DIM runup equations and the Bandon 1 site. Slope values used in the calculation were 0.016 (DIM) and 0.079 (Stockdon).

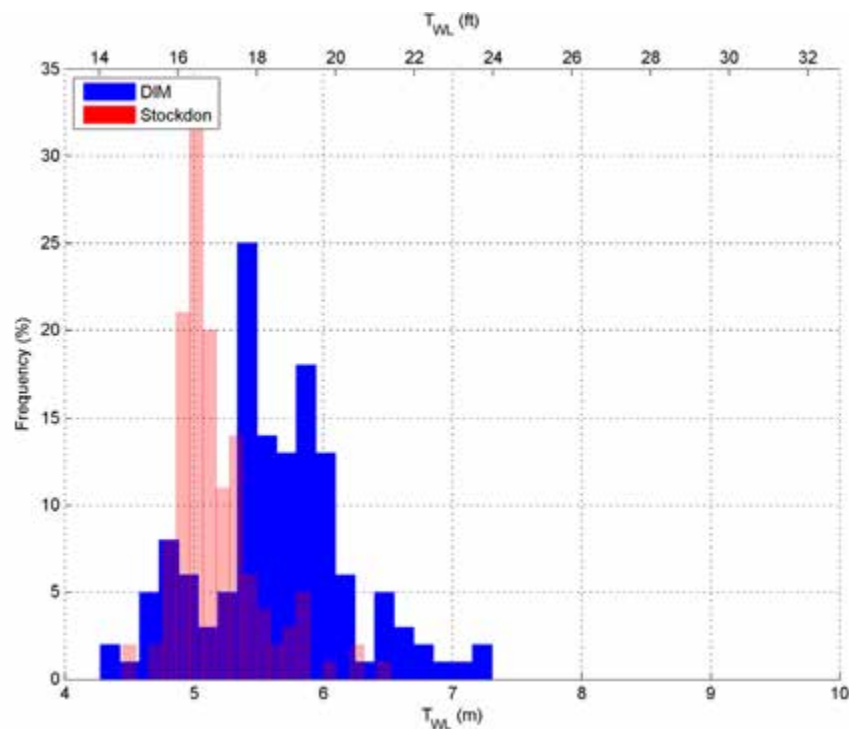


Figure 6-3. Total water level calculations using the Stockdon (2006) and DIM runup equations at the Bandon 15 site. Slope values used in the calculation were 0.019 (DIM) and 0.033 (Stockdon).

6.2 Barrier runup calculations

6.2.1 Introduction

According to NHC (2005), an alternate approach is recommended for use in calculating runup on steep barrier. By definition, barriers include “steep dune features and coastal armoring structures such as revetments” (section D.4.5.1.5.2), although little guidance is offered in terms of the range of slopes to which this alternate approach would apply. Throughout this document we will use the generic term barrier to define the range of morphological and engineering conditions where barrier runup calculations may apply. In general, runup on a barrier depends not only on the height and steepness of the incident wave defined through the Iribarren number, or breaker parameter ($\zeta_{m-1,0}$), but also on the geometry (e.g., the slope of the barrier and/or if a berm is present), design characteristics of the structure, and its permeability.

The recommended approach for calculating runup on a barrier is to use the TAW (Technical Advisory Committee for Water Retaining Structures) method, which provides a mechanism for calculating the runup, adjusted for various reduction factors that include the surface roughness, the influence of a berm (if present), and effects associated with the angle of wave approach (NHC, 2005; Pullen and others, 2007; van der Meer, 2002). According to NHC (2005), the TAW method is useful as it includes a wide range of conditions for calculating the wave runup (e.g., both smooth and rough slopes) and because it agrees well with both small- and large-scale experiments.

Figure 6-4 is a conceptual model of the various components required to determine the extent of runup on a barrier. Of importance is first determining the 2% dynamic water level ($DWL_{2\%}$) at the barrier, which includes the

combined effects of the measured still water level (SWL), the wave setup ($\langle \eta \rangle$), and the dynamic portion ($\hat{\eta}$) of the runup (Figure 6-4), which is then used to establish the spectral significant wave height (H_{mo}) at the toe of the barrier (NHC, 2005).

The general formula for calculating the 2% wave runup height on a barrier is given in a nondimensional form by equation 6.12:

$$\frac{R_{2\%}}{H_{mo}} = c_1 \cdot \gamma_b \cdot \gamma_f \cdot \gamma_\beta \cdot \zeta_{m-1,0} \quad (\text{eq. 6.12})$$

with a maximum of:

$$\frac{R_{2\%}}{H_{mo}} = \gamma_f \cdot \gamma_\beta \left(c_2 - \frac{c_3}{\sqrt{\zeta_{m-1,0}}} \right)$$

where:

$R_{2\%}$ = wave runup height exceeded by 2% of the incoming waves

H_{mo} = spectral significant wave height at the structure toe

c_1 , c_2 , and c_3 = empirical coefficients with:

γ_b = influence factor for a berm (if present),

γ_f = influence factor for roughness element of slope,

γ_β = influence factor for oblique wave attack,

$\zeta_{m-1,0}$ = breaker parameter ($\tan \beta / (H_{mo}/L_{m-1,0})^{0.5}$),

$\tan \beta$ = slope of the barrier,

$L_{m-1,0}$ = the deep-water wave length ($gT_{m-1,0}^2/2\pi$), and

$T_{m-1,0}$ can be calculated from $T_p/1.1$, where

T_p is the peak spectral wave period.

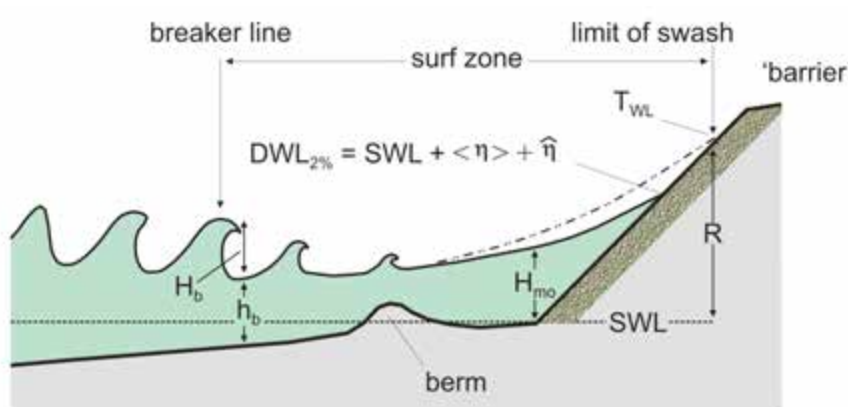


Figure 6-4. Wave runup on a beach backed by a structure or bluff (modified from NHC, 2005).

Substituting the empirical coefficients derived from wave tank experiments and incorporating a 5% upper exceedence limit into the general Equations of 6.13 (van der Meer, 2002; Pullen and others 2007), runup on a barrier may be calculating using:

$$R_{2\%} = H_{mo} \left(1.75 \cdot \gamma_b \cdot \gamma_f \cdot \gamma_\beta \cdot \zeta_{m-1,0} \right) \quad (\text{eq. 6.13})$$

where $0.5 \leq \gamma_b \cdot \zeta_{m-1,0} \leq 1.8$

with a maximum of:

$$R_{2\%} = H_{mo} \left(1.0 \cdot \gamma_f \cdot \gamma_\beta \left(4.3 - \frac{1.6}{\sqrt{\zeta_{m-1,0}}} \right) \right)$$

where $1.8 \leq \gamma_b \cdot \zeta_{m-1,0}$

There are however notable differences between Equation 6.13 originally described by van der Meer (2002) and Pullen and others (2007) from that presented as Equation D.4.5-19 in the FEMA West Coast methodology (NHC, 2005). For example, Equation D.4.5-19 in the NHC report contains a higher coefficient value (1.77), along with one additional reduction factor (porosity) for calculating runup when the breaker parameter is less than 1.8. Similarly, for conditions where the breaker parameter exceeds 1.8 and the maximum runup equation is used, Equation D.4.5-19 in the NHC report contains two extra reduction factors (berm and porosity reduction factors) that are not included in the original solution, which potentially could have a very significant effect on the calculated runup. Due to these differences and for the purposes of calculating runup on barrier along the Coos County shoreline we have used the original solution (Equation 6.13) as presented by van der Meer (2002) and Pullen and others (2007).

6.2.2 Specific procedure for calculation of "barrier" runup

For those cases where the TAW method is appropriate for determining runup on barrier (i.e., steep dunes, beaches backed by structures, or beaches backed by bluffs), the refracted deep-water wave climate conditions defined in

Section 5.4 for the relevant transect site were first imported into MATLAB. The overall approach used for determining runup on a barrier follows the general approach laid out in section D.4.5.1.5.2 in NHC (2005), with the exception that we use the TAW barrier runup equation (Equation 6.13) for calculating runup on the bluff.

The breaker height, H_b , is first calculated using Equation 6.9, while the breaker depth, h_b , was estimated using Equation 6.8. Having identified these two parameters, the nearshore slope²⁵ was determined for the transect of interest. The parametrized DIM equations for wave setup ($\langle \eta \rangle$, Equation 6.6) and for the root mean square of the dynamic component (η_{rms} , Equation 6.7) were then calculated. In the case of Equation 6.7, this was undertaken for both the gamma of interest (determined using Equation 5.3) and for a gamma value of 3.3, and the difference between these two calculations ($\sigma_{1\ diff}$) was identified. The dynamic wave setup at the toe of the barrier was then reduced using Equation 6.14:

$$\widehat{\eta_T} = 2.0 \sqrt{(\sigma_1^2 - \sigma_{1\ diff}) + \sigma_2^2} \quad (\text{eq. 6.14})$$

The 2% dynamic water level ($DWL_{2\%}$) was then determined for each storm using the storm's associated still water level (SWL) plus the wave setup ($\langle \eta \rangle$) plus $2 * \sigma_{1\ diff}$ (i.e., two times the difference between the gamma of interest and gamma = 3.3) as defined by NHC (2005)²⁶.

Because waves are depth limited at the toe of a barrier, NHC indicated that H_{mo} may be adequately estimated from knowledge of the 2% dynamic water level ($DWL_{2\%}$) at the barrier using a breaker index of 0.78 (i.e., $H_{mo} = DWL_{2\%} \times 0.78$), while the spectral wave period is calculated from $T_{m-1,0} = T_p / 1.1$. Thus, estimates of H_{mo} and $T_{m-1,0}$ derived using the adjusted DIM procedures provide the critical input parameters required for estimating barrier runup values.

Having determined H_{mo} and $T_{m-1,0}$, the next step is to calculate the runup using the TAW equations. One complicating factor is the determination of an appropriate barrier slope, used in the breaker parameter ($\zeta_{m-1,0}$). This is especially important if the morphology of the barrier exhibits a composite morphology characterized by different slopes,

²⁵ The nearshore slope defined for the DIM approach is the average slope between the runup limit and twice the break point of the significant wave height, h_b .

²⁶ Note that $2 * \sigma_{1\ diff}$ is based on example 2 provided on page D.4.5.20 of the FEMA West Coast Coastal Methodology report (NHC, 2005) and is the only way one can match their example result presented in Table D.4.5-5; as an aside, example 2 indicates the structure toe height is in their case 2 ft below NAVD88 (Table D.4.5-5) and is thus included in their example calculation of $DWL_{2\%}$ for a structure.

such that errors in estimating the slope will translate to either significant underestimation or overestimation of the runup. According to van der Meer (2002) and Pullen and others (2007), because the runup process is influenced by the change in slope from the breaking point to the maximum wave runup, the characteristic slope should be specified for this same region. Because the maximum wave runup is the desired outcome and is unknown when initially defining the slope, the process is iterative, requiring two steps. First, the breaking limit is defined as $1.5H_{mo}$ below the still water line, whereas $1.5H_{mo}$ above the still water line defines the upper limit of the first slope estimate (excluding any berms that may be present)(Figure 6-5). Therefore the first estimate is of the form:

$$\tan \alpha = \frac{3 \cdot H_{mo}}{L_{slope 1} - B} \quad (\text{eq. 6.15})$$

where $L_{slope 1}$ is the total distance between $-1.5H_{mo}$ and $+1.5H_{mo}$ above and below the still water line, and B is defined here as the beach foreshore distance located between mean lower low water (MLLW) and the barrier toe (B_T). Having determined the first slope estimate, barrier runup is calculated using Equation 6.13 and reduced based on the appropriate reduction factors.

A second slope estimate is then performed based on the runup calculated using the first slope estimate. The breaking limit is again defined as $1.5H_{mo}$ below the still water line, while $R_{2\%}$ above the still water line defines the upper limit for the second slope estimate. Therefore the second slope estimate reflects:

$$\tan \alpha = \frac{1.5 \cdot H_{mo} + R_{2\% \text{ 1st estimate}}}{L_{slope 2} - B} \quad (\text{eq. 6.16})$$

Having determined the second slope estimate, the final barrier runup estimate is calculated using Equation 6.13 and is reduced based on the appropriate reduction factors.

Finally, it is important to note that runup estimates based on barrier runup calculations are very much dependent on correctly estimating the average slope of the beach and near-shore. We have found for several sites along the Bandon and Bastendorff/Lighthouse shore where the beach is backed by a bluff (e.g., Bandon 7-11 profiles and Coos 7-11 profiles), that runup calculations derived using the TAW approach produced in some cases relatively low runup levels (maximum runup of 5.1 m). This is entirely due to there being a very wide dissipative surf zone at these transect locations that results in very low slope estimates, while profile sites to the south (e.g., Bandon 12-14, and Bandon 19-21) are characterized by a narrower surf zone and hence a higher average slope. For those sites (e.g., Bandon 7-11 profiles and Coos 7-11 profiles) where the calculated runup seems unreasonably low (relative to the morphology of the beach and observations of storm wave runup along this shore and elsewhere), we have defaulted to the 1% total water levels calculated using the Stockdon and others model; note that for the Bandon 7-11 profiles the 1% T_{WLS} calculated using the Stockdon and others model were about 1-2 m higher than the barrier runup estimates calculated using DIM and the TAW approach.

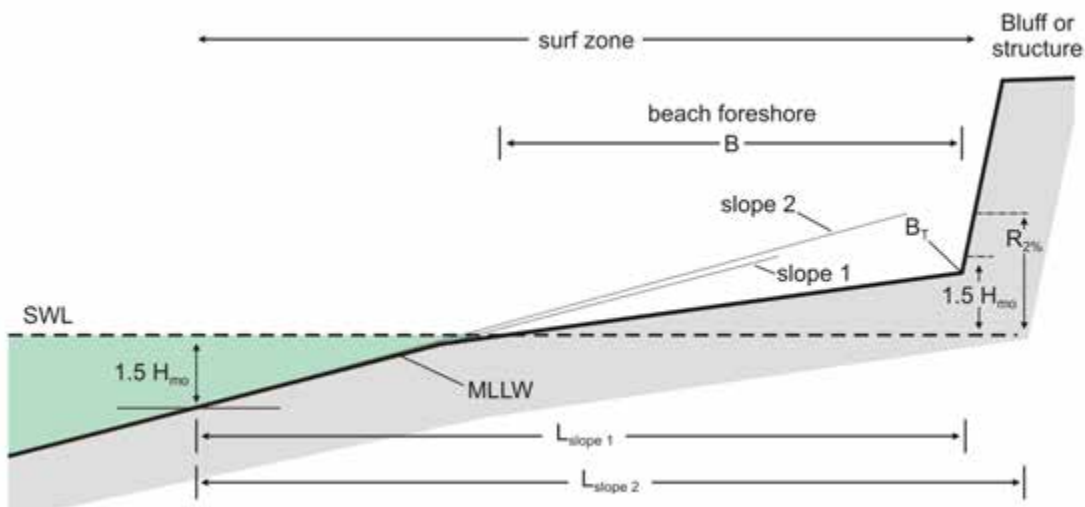


Figure 6-5. Determination of an average slope based on an iterative approach. The first estimate is initially based on $1.5H_{mo} \pm \text{SWL}$, while the second estimate is based on $1.5H_{mo}$ below the SWL and the calculated $R_{2\%}$ above the SWL that is based on the first slope estimate. SWL is still water level; MLLW is mean lower low water.

6.2.3 Barrier runup reduction factors

Table 6-1 and Table 6-2 provide the barrier runup reduction factors used for those selected profile sites along the Bandon and Bastendorff/Lighthouse beach shorelines. In the case of bluff roughness along the Bandon shore, we used a value of 0.6 due to the highly vegetated nature of the Bandon bluffs. These bluffs are located at their stable angle of repose and are covered with salal plants (*Gaultheria shallon*), where the plants form a deep, nearly impenetrable thicket. The decision to use 0.6 was based on discus-

sions with W. G. McDougal (Coastal Engineer, Oregon State University and Technical Coordinator of the North Pacific FEMA West Coast Guidelines, pers. commun., April 2010). Wave direction (γ_β) reduction factors presented in Table 6-1 and Table 6-2 are the mean values determined for all storms for each transect site. However, when calculating barrier runup, the actual values estimated using Equation D.4.5-22 (NHC, 2005, p. D.4.5-13) were used.

Table 6-1. “Barrier” runup reduction factors used for calculating runup on beaches backed by bluffs along the Bandon shore.

Bandon Profile	Surface Roughness,		Wave Direction,		Description
	γ_f	γ_b	γ_β		
1	N/A	N/A	N/A		dune backed
2	N/A	N/A	N/A		dune backed
3	N/A	N/A	N/A		dune backed
4	N/A	N/A	N/A		dune backed
5	N/A	N/A	N/A		dune backed
6	N/A	N/A	N/A		dune/bluff backed
7	0.6	1.0	0.81		dune/bluff backed
8	0.6	1.0	0.89		bluff backed
9	0.6	1.0	0.90		bluff backed
10	0.6	1.0	0.99		bluff backed
11	0.6	1.0	0.98		bluff backed
12	0.6	1.0	0.99		bluff backed
13	0.6	1.0	1.0		bluff backed
14	0.6	1.0	1.0		bluff backed
15	N/A	N/A	N/A		dune/bluff backed
16	N/A	N/A	N/A		dune/bluff backed
17	N/A	N/A	N/A		dune/bluff backed
18	N/A	N/A	N/A		dune/bluff backed
19	0.6	1.0	0.96		dune/bluff backed
20	0.6	1.0	1.0		dune/bluff backed
21	0.6	1.0	1.0		dune/bluff backed

Note: values reported for the wave direction (γ_β) reduction factor reflect the mean value determined for all storms. However, the actual value calculated using Equation D.4.5-22 of NHC (2005) was used in the individual runup calculations.

Table 6-2. “Barrier” runup reduction factors used for calculating runup on beaches backed by bluffs along the Lighthouse Beach shore.

Coos Profile	Surface Roughness,		Wave Direction,		Description
	γ_f	γ_b	γ_β		
1	N/A	N/A	N/A		dune backed
2	N/A	N/A	N/A		dune backed
3	N/A	N/A	N/A		dune backed
4	N/A	N/A	N/A		dune backed
5	N/A	N/A	N/A		dune backed
6	N/A	N/A	N/A		dune backed
7	1.0	1.0	0.73		bluff backed
8	1.0	1.0	0.74		bluff backed
9	1.0	1.0	0.72		bluff backed
10	1.0	1.0	0.68		bluff backed
11	1.0	1.0	0.64		bluff backed
11	N/A	N/A	N/A		dune-/bluff backed

Note: values reported for the wave direction (γ_β) reduction factor reflects the mean value determined for all storms. However, the actual value calculated using Equation D.4.5-22 of NHC (2005) was used in the individual runup calculations.

6.3 Coos County wave runup and total water level calculations

Using the transformed wave conditions and the measured alongshore varying beach slopes, wave runup is computed for each of the input conditions at each of the beach profiles shown in Figure 6-6 by using a combination of the Stockdon and others (2006) runup equation for dune-backed beaches (Equation 6.4) and the DIM method for calculating wave runup on a barrier. In terms of the latter, this is the only approach described in the revised Coastal Flood Hazard and Analysis and Mapping guidelines developed for U.S. West Coast beaches (NHC, 2005) that can be adopted for calculating wave runup along bluff-backed beaches, as is the case along the Bandon shore and at Lighthouse Beach near Coos Bay.

For both models, the calculated runup is combined with the appropriate measured tides to develop the T_{WL} conditions used to generate both the 100-year (1%) return level event and the 500-year (2%) return event. We computed these extreme flood hazard statistics using the Stockdon and others (2006) runup model (Equation 6.4) at all 21 profiles at the Bandon focus site and 12 profiles along Bandon/Lighthouse Beach adjacent to Coos Bay. “Barrier” runup calculations were undertaken using the methods described above for the Bandon 7–14 and 19–21 profile sites and for the Coos 7–11 profiles. The locations of these profiles are given in Figure 3-1, and the beach slopes and backshore features are provided in Table 6-3 and 6-4. Due to the variability of the shoreline orientation at each of the focus areas, the shore perpendicular transects were extended from the backshore to where they intersected the 20-m contour (Figure 6-6 and 6.7). These intersections are where wave statistics from the SWAN output were extracted.

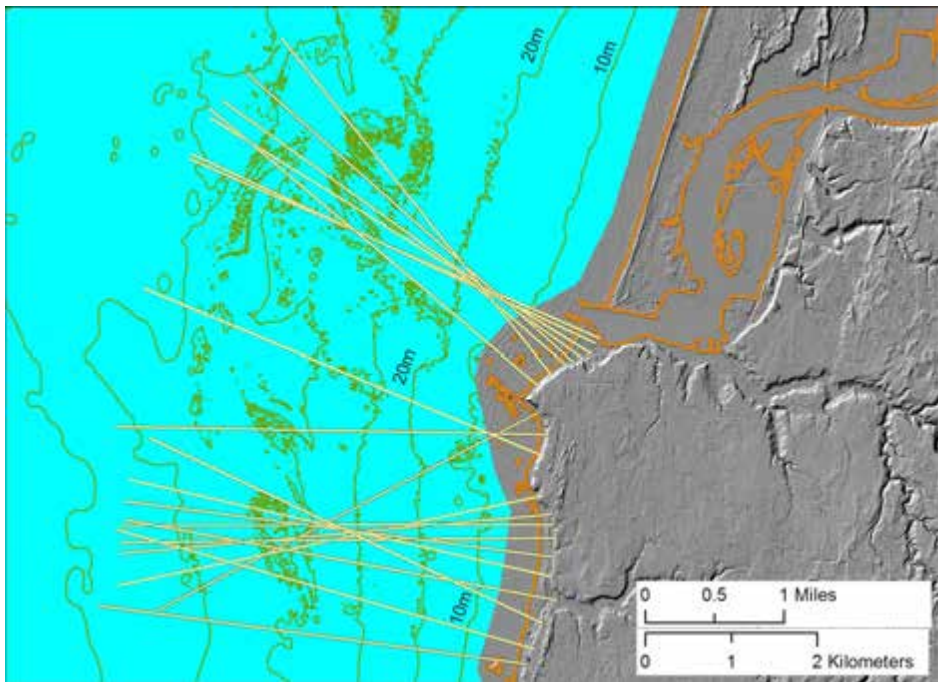


Figure 6-6. Locations of the Bandon, Oregon, beach profiles and intersection points with the 20-m contour.

Table 6-3. 100-year (1%) and 500-year (0.2%) total water levels calculated for Bandon profile sites.

Bandon Profile	Beach Slope	100-year ¹ (m)	100-year ² (m)	500-year ¹ (m)	500-year ² (m)	E_j (m)	D_c (m)	Description
1	0.079	9.17	N/A	9.62	N/A	5.30	6.24	dune backed
2	0.092	9.93	N/A	10.43	N/A	6.07	6.97	dune backed
3	0.078	9.11	N/A	9.51	N/A	4.89	6.60	dune backed
4	0.075	8.96	N/A	9.36	N/A	5.14	6.61	dune backed
5	0.050	7.71	N/A	8.06	N/A	4.99	5.91	dune backed
6	0.042	7.22	N/A	7.48	N/A	3.66	5.34 / 24.0	dune/bluff backed
7	0.032	6.87	5.16	7.16	5.24	4.58	6.35 / 25.3	dune/bluff backed
8	0.024	6.55	5.19	6.89	5.35	4.15	24.8	bluff backed
9	0.034	6.98	5.60	7.50	5.80	3.89	24.6	bluff backed
10	0.034	7.00	5.66	7.49	5.89	3.74	25.7	bluff backed
11	0.032	7.04	5.70	7.66	5.94	4.17	20.3	bluff backed
12	0.026	6.48	10.01	6.89	10.38	3.30	22.8	bluff backed
13	0.032	6.70	11.02	7.13	12.32	4.81	20.1	bluff backed
14	0.028	6.54	9.6	6.95	10.03	3.88	6.31 / 18.8	dune/bluff backed
15	0.033	6.76	N/A	7.21	N/A	4.79	8.80 / 19.0	dune/bluff backed
16	0.024	6.35	N/A	6.73	N/A	4.40	7.71 / 15.4	dune/bluff backed
17	0.024	6.35	N/A	6.71	N/A	4.82	10.2 / 15.5	dune/bluff backed
18	0.021	6.28	N/A	6.67	N/A	4.27	7.28	dune/bluff backed
19	0.013	5.96	9.33	6.28	9.53	3.84	9.61 / 16.1	dune/bluff backed
20	0.030	6.45	8.14	6.86	8.93	5.93	10.57 / 15.6	dune/bluff backed
21	0.026	6.42	9.62	6.88	9.78	4.53	14.0	bluff backed

Note:

100-year¹ is based on the Stockdon and others (2006) runup model, while 100-year² is based on the barrier DIM/TAW runup model (same for 500-year estimates).

100-year and 500-year total water level (T_{WL}) values relative to NAVD88 vertical datum.

D_c is the dune crest elevation determined for the eroded profile.

Red text denotes that the dune crest is overtopped.

Table 6-4. 100-year (1%) and 500-year (0.2%) total water levels calculated for Coos profile sites.

Coos Profile	Beach Slope	100-year ¹ (m)	100-year ² (m)	500-year ¹ (m)	500-year ² (m)	E_j (m)	D_c (m)	Description
1	0.038	7.25	N/A	7.65	N/A	5.56	6.75	dune backed
2	0.036	7.30	N/A	7.77	N/A	5.28	7.27	dune backed
3	0.026	6.90	N/A	7.49	N/A	5.10	6.63	dune backed
4	0.023	6.58	N/A	7.10	N/A	4.13	5.38	dune backed
5	0.039	7.22	N/A	7.76	N/A	4.83	5.80	dune backed
6	0.037	7.12	N/A	7.68	N/A	4.73	7.30	dune backed
7	0.101	11.01	10.04	11.90	10.36	5.80	18.3	bluff backed
8	0.078	9.63	9.52	10.35	9.91	5.02	18.5	bluff backed
9	0.087	10.13	8.03	10.88	8.28	5.10	18.1	bluff backed
10	0.072	9.53	6.15	10.16	6.28	6.66	16.5	bluff backed
11	0.060	8.07	5.06	8.51	5.17	3.83	19.1	bluff backed
12	0.068	8.85	N/A	9.43	N/A	4.91	5.43	dune backed

Note:

100-year¹ is based on the Stockdon and others (2006) runup model, while 100-year² is based on the barrier DIM/TAW runup model (same for 500-year estimates).

100-year and 500-year total water level (T_{WL}) values relative to NAVD88 vertical datum.

D_c is the dune crest elevation determined for the eroded profile.

Red text denotes that the dune crest is overtopped.

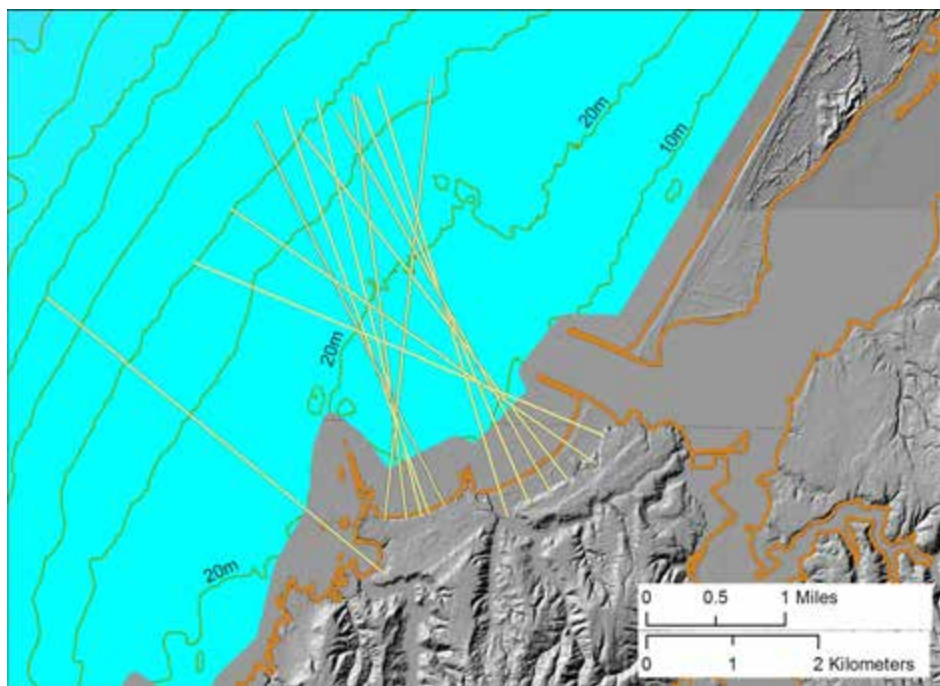


Figure 6-7. Locations of the Coos beach profiles and intersection points with the 20-m contour.

Having calculated runup, we used the generalized extreme value (GEV) family of distributions (specifically the peak-over-threshold [POT] approach) to estimate the 100-year and 500-year total water levels for each of the beach profile sites. Specific information about the extreme value techniques used to estimate these total water levels is

described in Section 4.1. Figure 6-8 gives an example of the extreme value (GPD-Poisson) model for the Coos Profile 4 site in which the 100-year event is 6.58 m and the 500-year event is estimated to be 7.1 m. The results for all of the profiles can be found in Table 6-3 and 6-4.

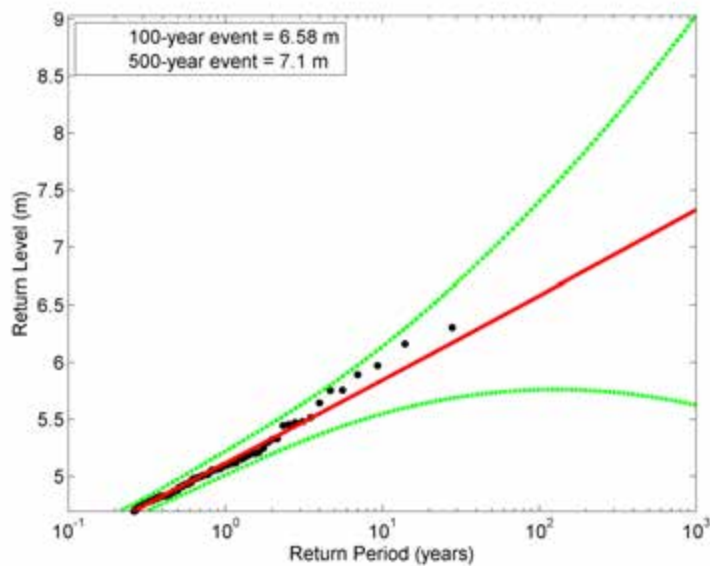


Figure 6-8. Example peak-over-threshold (POT) extreme value results for the 1% and 0.2% total water levels at Coos Profile 4, located at Bastendorff Beach (dune-backed beach). Note the y-axis vertical datum is relative to NAVD88.

6.4 Overtopping calculations

Overtopping of natural features such as foredunes and spits and of coastal engineering structures and barriers occurs when the wave runup superimposed on the tide exceeds the crest of the foredune or structure (Figure 6.9). Hazards associated with wave overtopping can be linked to a number of simple direct flow parameters including (Pullen and others, 2007):

- mean overtopping discharge, q
- overtopping velocities over the crest and farther landward, V
- overtopping flow depth, h , at a distance, y , landward of the foredune crest or barrier
- landward extent of green water and splash overtopping $y_{G\ outer}$

NHC (2005) noted that there are three physical types of wave overtopping:

1. Green water or bore overtopping occurs when waves break onto or over the foredune or barrier and the overtopping volume is relatively continuous.
2. Splash overtopping occurs when the waves break seaward of the foredune or barrier, or where the foredune or barrier is high relative to the wave height and

overtopping consists of a stream of droplets. Splash overtopping can be a function of its momentum due to the runup swashing up the barrier and/or may be enhanced due to onshore direct winds.

3. Spray overtopping is generated by the effects of wind blowing droplets and spray that are derived from the wave crests.

Mapping these respective flood inundation zones requires an estimate of the velocity, V , or discharge, q , of the water that is carried over the crest, the envelope of the water surface that is defined by the water depth, h , landward of the barrier crest, and the inland extent of green water and splash overtopping. According to NHC (2005), these hazard zones are ultimately defined on the basis of the following two derivations:

- Base flood elevations (BFEs) are determined based on the water surface envelope landward of the barrier crest; and
- Hazard zones are determined based on the landward extent of green water and splash overtopping, and on the depth and flow velocity in any sheet flow areas beyond that, defined as $hV^2 = 5.7 \text{ m}^3/\text{s}^2$ or $200 \text{ ft}^3/\text{s}^2$.

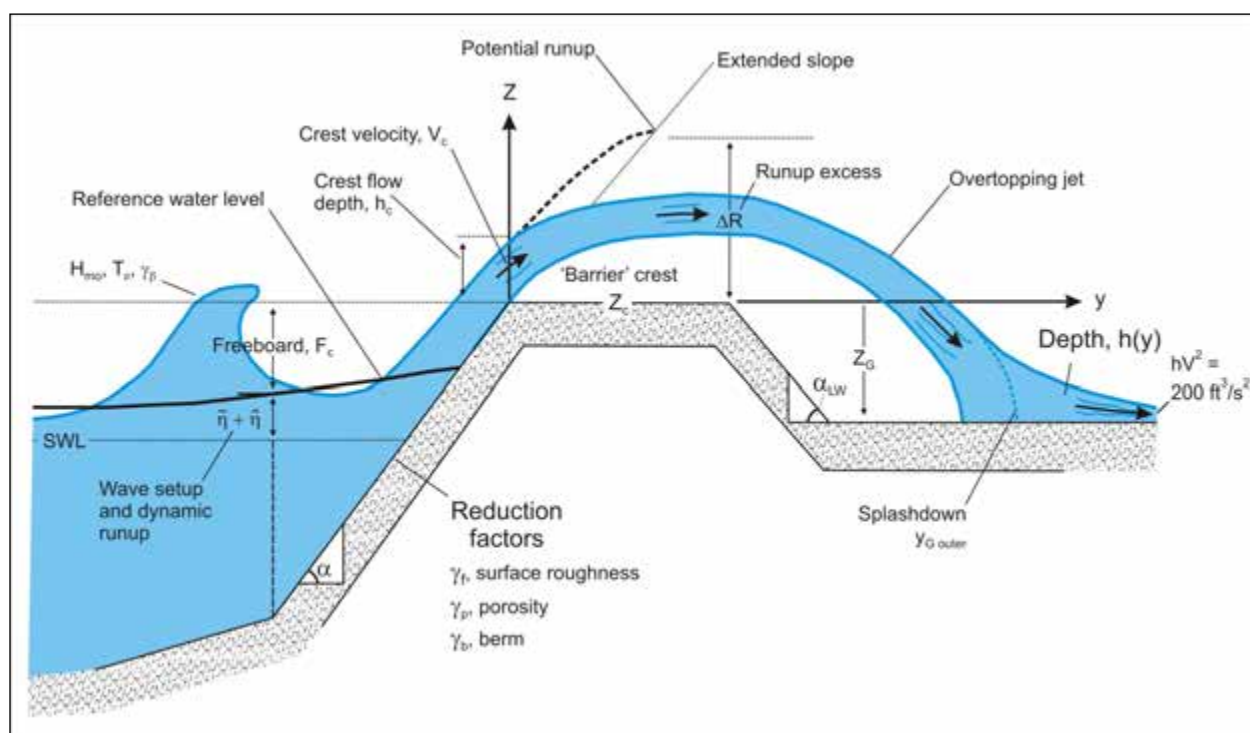


Figure 6-9. Nomenclature of overtopping parameters available for mapping base flood elevations (BFEs) and flood hazard zones (after NHC, 2005).

A distinction can be made between whether green water (or bore) or splash overtopping predominates at a particular location that is dependent on the ratio of the calculated wave runup height relative to the barrier crest elevation, R/Z_c . When $1 < R/Z_c < 2$, splash overtopping dominates and for $R/Z_c > 2$, bore propagation occurs. In both cases, R and Z_c are relative to the 2% Dynamic Water Level ($DWL_{2\%}$) at the barrier (Figure D.4.5-12 of NHC [2005, p. D.4.5-22]).

6.4.1 Mean overtopping rate at the "barrier" crest

Wave overtopping of dunes and barrier is a function of both hydraulic and barrier structure parameters whereby:

$$q = f(H_{mo}, T_p, \beta, F_c, DWL_{2\%}, \text{geometry}) \quad (\text{eq. 6.17})$$

where q is the overtopping discharge (expressed as cubic meters per second per meter, $\text{m}^3/\text{s}/\text{m}$ [$\text{ft}^3/\text{s}/\text{ft}$]), H_{mo} is the significant wave height at the toe of the structure, T_p is the peak period, β is the angle of wave attack, F_c is the freeboard, and $DWL_{2\%}$ is 2% depth of water at the toe of the structure (Figure 6.9).

Prior to calculating the mean overtopping rate at the barrier crest it is necessary to first distinguish between four contrasting types of wave-breaking situations that may impact a particular barrier or dune overtopping situation. There four conditions include *non-breaking* or *breaking* on normally sloped barrier, and *reflecting* or *impacting* on steeper barrier. Of these, the only one that applies to the Coos County detailed coastal study sites is the breaking-wave situation, where the waves have already broken across the surf zone and are reforming as bores prior to swashing up the beach face or barrier.

For beaches and normally sloping barrier (where $0.05 < \tan \alpha < 0.67$), a distinction can be made between situations where waves break directly on the barrier versus those situations where the waves have not yet broken. These conditions can be determined using the surf similarity parameter (Iribarren number) defined here in terms of the beach or structure slope ($\tan \alpha$), and the wave steepness ($S_{op} = H_{mo}/L_o$):

$$\xi_{op} = \frac{\tan \alpha}{\sqrt{\frac{H_{mo}}{L_o}}} = \frac{\tan \alpha}{\sqrt{S_{op}}} \quad (\text{eq. 6.18})$$

Breaking on normally sloping surfaces generally occurs where the surf similarity number, $\xi_{op} \leq 1.8$, while non-

breaking conditions occur when $\xi_{op} > 1.8$. As noted above, for the Coos County coastline the identified Iribarren numbers always fell below the 1.8 criteria, indicating that the incident waves are always broken prior to reaching the beach or the barrier face.

At the beach or barrier crest, the relative freeboard (F_c/H_{mo}), Figure 6.9, is a particularly important parameter because changing these two parameters controls the volume of water that flows over the barrier crest. For example, increasing the wave height or period increases the overtopping discharge, as does reducing the 'beach or barrier crest height or raising the water level.

A variety of prediction methods are available for calculating the overtopping discharge and are almost entirely based on laboratory experiments based on a range of structure slopes (slopes between 1:1 and 1:8, with occasional tests at slopes around 1:15 or lower). Factors that will serve to reduce the potential overtopping discharge include the barrier surface roughness (γ_f), the presence of a berm (γ_b), wave approach directions (γ_β), and the porosity of the barrier (γ_p) (Figure 6.9). In terms of porosity, increasing this variable effectively reduces the wave runup and overtopping discharge as more of the water is able to be taken up by the voids between the clasts and particles. As noted by NHC (2005), the effect of the porosity factor makes it convenient to distinguish between impermeable and permeable structures. Methods for determining the reduction factors are described by NHC (2005, Table D.4.5-3, p. D.4.5-13), with one difference whereby the approach recommended for determining the wave approach (γ_β) reduction factor for wave overtopping calculations is based on the following equation:

$$\gamma_\beta = \begin{cases} 1 - 0.0033|\beta|, (0 \leq |\beta| \leq 80^\circ) \\ 1 - 0.0033|80|, (|\beta| \geq 80^\circ) \end{cases} \quad (\text{eq. 6.19})$$

Of the four reduction²⁷ parameters, only the angle of wave attack (γ_β) was used to reduce the overtopping discharge along the Coos County detailed study sites.

For normally sloping barrier (where $0.05 < \tan \alpha < 0.67$) and where the Iribarren number (ξ_{op}) < 1.8 , the following

²⁷ The presence of a berm (γ_b) can be ignored as berms are nonexistent in a most eroded winter profile. The surface roughness (γ_f) was ignored because the beach face and backshore are composed of sand and hence have only a nominal effect on reducing overtopping. Porosity (γ_p) was also ignored as the beach is characterized by medium to coarse sand and during major storms the beach is typically in a "saturated" state due to the combination of high runup and the storm duration, such that the beach is less capable of taking up additional water.

formulation can be used to determine the mean overtopping discharge (both dimensional [q] and nondimensional [Q] forms) at the barrier crest:

$$q = Q \sqrt{\frac{gH_{mo} \tan \alpha}{S_{op}}}, \text{ where:} \quad (\text{eq. 6.20})$$

$$Q = 0.06e^{-4.7F'} \text{ and,}$$

$$F' = \frac{F_c}{H_{mo}} \frac{\sqrt{S_{op}}}{\tan \alpha} \frac{1}{Y_f Y_b Y_\beta Y_p}$$

6.4.2 Overtopping limits and flood hazard zones landward of the “barrier” crest

Estimates of the landward limit of the splashdown distance associated with wave overtopping and the landward limit of the hazard zone require several calculation steps. These steps include:

1. The excess potential runup, $\Delta R = R - Z_c$, crest flow rate, $V_c \cos \alpha$ (where $V_c = 1.1 \sqrt{g \Delta R}$), and initial flow depth, h_c (where $h_c = 0.38\Delta R$) are first calculated.
2. The associated onshore wind component, W_y is determined from available wind data. For the purposes of this study, we used $W_y = 19.6 \text{ m/s}$ (64.3 ft/s), which was determined from an analysis of winds (mean from a select number of storms) measured at the Cape Arago C-MAN station operated by the NDBC. In the absence of wind data, NHC (2005) recommended a wind speed of 13.4 m/s (44 ft/s).
3. The enhanced onshore water velocity component ($V_c \cos \alpha'$) is then calculated using Equation 6.21:

$$(V_c \cos \alpha)' = V_c \cos \alpha + 0.3(W_y - V_c \cos \alpha) \quad (\text{eq. 6.21})$$

4. The effective angle, α_{eff} , is calculated from:

$$\tan \alpha_{eff} = \frac{V_c \sin \alpha}{(V_c \cos \alpha)'}$$

5. Having determined the above parameters, the outer limit of the splash region, $y_{G,outer}$ is calculated using Equation 6.22. Here we have used an algorithm developed by W. G. McDougal (Coastal Engineer, Oregon State University, and Technical Coordinator of the

North Pacific FEMA West Coast guidelines) of the form:

$$y_{G,outer} = \frac{(V_c \cos \alpha)'}{g} * \quad (\text{eq. 6.22})$$

$$V_c \sin \alpha - mBackshore * (V_c \cos \alpha)' *$$

$$1 + \sqrt{\frac{1 - 2g * bBackshore}{(V_c \sin \alpha - mBackshore * (V_c \cos \alpha)')^2}}$$

and

$$Z_G = bBackshore + (mBackshore * y_{G,outer}) \quad (\text{eq. 6.23})$$

where $bBackshore$ is the intercept for the backshore slope adjacent to the barrier crest and $mBackshore$ is the slope of the backshore. Equation 6.22 is ultimately based on Figure D.4.5-15 of NHC (2005, p D.4.5-30).

6. The total energy, E , of the splashdown is calculated from $E = \Delta R - Z_G$.
7. Finally, the initial splashdown velocity, V_o (where $V_o = 1.1 \sqrt{g E}$), and depth, h_o (where $h_o = 0.19E$) are calculated. In the case of green water or bore overtopping, the splashdown velocity, V_o , can be calculated from $V_o = 1.1 \sqrt{g \Delta R}$, while the flow depth is determined as $h_o = 0.38E$.

Having determined the initial splashdown velocity, V_o , and flow depth, h_o , the landward extent of the overland flow is calculated using an approach modified from that originally proposed by Cox and Machelel (1986). The version presented by NHC (2005) effectively calculates the flow depth, h , with distance, y , from the barrier crest, such that the flow depth decays asymptotically as y increases away from the barrier crest, eventually approaching zero. The NHC (2005) equation is shown as Equation 6.24:

$$h(y) = \left[\sqrt{h_o} - \frac{5(y - y_o)}{A \sqrt{g T^2}} \right]^2 \quad (\text{eq. 6.24})$$

where h_o is determined from step 7 above and, for an initial approximation, the nondimensional A parameter may be taken as unity. For sloping backshores, the A parameter

in Equation 6.24 can be modified such that $A_m = A (1 - 2 \times \tan \alpha_{LW})$, and the value in parentheses is limited to the range 0.5 to 2. According to NHC (2005), if the maximum distance of splash or bore propagation calculated using Equation 6.24 does not appear reasonable or match field observations, the A parameter can be adjusted in order to increase or decrease the landward wave propagation distance. In addition, for green water or bore propagation the A parameter value is taken initially to be 1.8.

For the purposes of this study we have adopted a modified version of Equation 6.24 developed by W. G. McDougal of the form:

$$h(y) = \left[h_o^{1/2} - \frac{y - y_o}{2\alpha(\alpha + 1)^{1/2} (1 - 2m) g^{0.5} T} \right]^2 \quad (\text{eq. 6.25})$$

where m is the slope of the backshore and α is a constant that can be varied in order to increase or decrease the landward wave propagation distance.

Finally, the landward limit of the hazard zone defined as $hV^2 = 5.7 \text{ m}^3/\text{s}^2$ (or $200 \text{ ft}^3/\text{s}^2$) is determined, whereby h is the water depth given by the modified Cox and Machemehl (1986) method (Equation 6.25) and $V = V_o$ is calculated from step 7 above.

6.4.3 Initial testing of the landward limit of wave overtopping

Our initial computations of the landward extent of wave overtopping using the steps outlined above yielded narrow hazard zones for Coos County. To calibrate Equation 6.25, we performed wave overtopping calculations and inundation for a site on the northern Oregon coast where there are field observations of wave overtopping. The site is Cape Lookout State Park, located on the northern Oregon coast in Tillamook County (Allan and others, 2006; Allan and Komar, 2002a; Komar and others, 2003). The southern portion of Cape Lookout State Park is characterized by a wide, gently sloping, dissipative sand beach backed by a moderately steep gravel berm and, ultimately, by a low fore-dune that has undergone significant erosion since the early 1980s (Komar and others, 2000).

On March 2-3, 1999, the crest of the cobble berm/dune at Cape Lookout State Park was overtopped during a major storm; significant wave heights reached 14.1 m (46.3 ft), while peak periods were 14.3 seconds as measured by a deep-water NDBC wave buoy (Allan and Komar, 2002b). Wave overtopping of the dune and flooding extended 70 m (230 ft) into the park (P. Komar, Emeritus Professor, College of Oceanic and Atmospheric Sciences, Oregon State University, pers. commun., 2010), evidence for which included photos and field evidence including pockmarks at the base of the tree trunks located in the park. These pockmarks were caused by cobbles having been carried into the park from the beach by the overtopping waves, where the cobbles eventually slammed into the bases of the trees as ballistics. Because the average beach slopes at Cape Lookout State park are analogous to those observed along the shore near the Bandon south jetty and because large wave events associated with extratropical storms affect significant stretches

(hundreds to thousands of kilometers) of the coast at any single point in time, we believe these data provide a reasonable means in which to investigate a range of alpha (α) values that may be used to determine the landward extent of wave inundation in the park.

Using beach morphology data (slope ($\tan \beta$) = 0.089, barrier crest = 5.5 m [18 ft]) from Cape Lookout State Park and deep-water wave statistics from a nearby NDBC wave buoy (46050), we experimented with a range of alpha values

(Figure 6-10) in order to replicate the landward extent of the inundation. As can be seen in Figure 6-10, in order to emulate the landward extent of flooding observed at Cape Lookout our analyses yielded an alpha of 0.58. Using alpha = 0.58, we in turn calculated the extent of the hazard zone where $h(y) = 200 \text{ ft}^3/\text{s}^2$, which was found to be $\sim 34 \text{ m}$ from the crest of the cobble berm/dune, consistent with damage to facilities in the park.

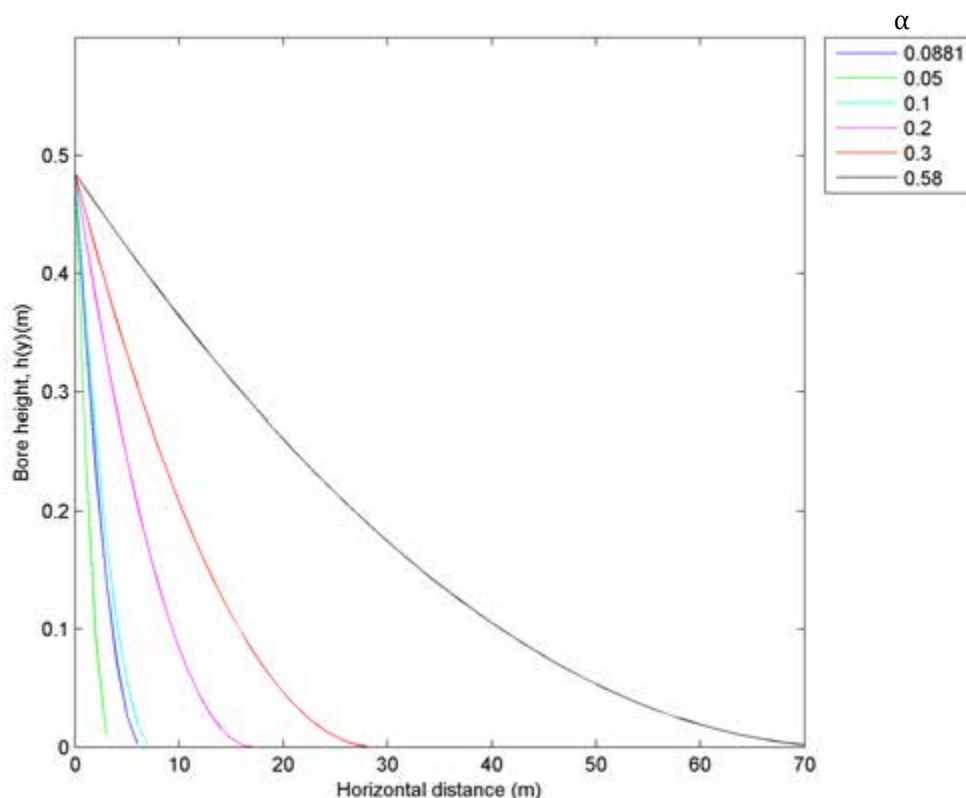


Figure 6-10. Calculations of bore height decay from wave overtopping at Cape Lookout State Park at the peak of the March 2-3, 1999, storm based on a range of alpha (α) values.

6.4.4 Wave overtopping and hazard zone limits calculated for Coos County

Table 6-5 presents the results of the calculated splashdown distances ($y_{G\ outer}$) and the landward extent of the flow (hV^2) where the flows approach $5.7 \text{ m}^3/\text{s}^2$ (or $200 \text{ ft}^3/\text{s}^2$). As can be seen from the table, the calculated splashdown distances ($y_{G\ outer}^1$) based on a default wind speed of 13.4 m/s (44 ft/s) (NHC, 2005) ranged from 0 to 3.5 m (0 to 11.5 ft); 1.0 to 3.2 m (3.3 to 10.5 ft) along the Bandon shore and 0 to 3.5 m (0 to 11.5 ft) along Bastendorff Beach. The Coos profile 2 site presents an interesting situation where the calculated 1% total water level (7.3 m [24 ft]) approximately equals the beach/dune crest elevation (7.29 m [23.9 ft]), suggesting that overtopping would probably not occur; in this situation the landward location of the primary frontal dune would determine the width of the hazard zone. Overall, the calculated splashdown distances produced narrow zones.

Table 6-5 includes a second, slightly more conservative splashdown distance, based on an enhanced wind velocity of 19.6 m/s (64.3 ft/s). This enhanced wind velocity was determined from an analysis of wind speeds measured by the Cape Arago C-MAN²⁸ station located adjacent to the mouth of Coos Bay. We examined the range of wind speeds identified at Cape Arago for each storm event defined for this study and identified a wide range of values, with the maximum being 19.6 m/s (64.3 ft/s). Because the measured wind speeds reflect a 2-minute average such that higher wind speeds have been measured throughout the entire record (e.g., the maximum 2-minute average wind speed was 29.3 m/s [96 ft/s], while the maximum 5-second wind gust reached 38.1 m/s [125.0 ft/s]), we believe it is justified to use the more conservative enhanced wind velocity of 19.6 m/s (64.3 ft/s).

²⁸ http://www.ndbc.noaa.gov/station_page.php?station=CAR03

Table 6-5. Splashdown and hazard zone limits calculated for Coos County detailed coastal sites.

Profile	Number of Wave Overtopping Events, and Events Where $hV^2 > 5.7 \text{ m}^3/\text{s}^2$ ($200 \text{ ft}^3/\text{s}^2$)	Maximum Splashdown $y_{G\ outer}^1$ (m)	Maximum Splashdown $y_{G\ outer}^2$ (m)	Maximum $hV^2(y) = 5.7$ (m)	Maximum Width of Hazard Zone (m)	Distance from Profile Benchmark (m)
Bandon						
1	127 / 11	1.0	1.3	45.5	46.7	161.3
2	115 / 15	2.6	3.4	59.0	62.4	131.8
3	103 / 12	2.6	3.4	50.3	53.7	160.0
4	83 / 15	3.2	4.1	56.0	60.1	112.0
5	55 / 1	0.9	1.5	8.9	10.2	83.8
6	101 / 3	1.2	1.9	21.1	22.9	46.4
Coos						
1	6 / 0	0.4	0.6	—	0.6	304.4
2	0 / 0	—	—	—	—	—
3	3 / 0	2.3	3.1	—	3.1	192.4
4	105 / 25	3.5	4.5	45.7	50.2	183.5
5	14 / 0	2.0	2.6	—	2.6	256.0
12	132 / 132	1.3	1.7	113.9	115.6	-15.5

Note: $y_{G\ outer}^1$ is based on the default wind speed of 13.4 m/s , while $y_{G\ outer}^2$ uses a higher wind speed of 19.6 m/s . Values reported in the table reflect the maximum values derived from all calculations.

The calculated splashdown distances based on the enhanced wind velocity component ($y_{G_outer}^2$) ranged from 0 to 4.5 m (0 to 14.8 ft); 1.3 to 4.1 m (4.3 to 13.5 ft) along the Bandon shore and 0 to 4.5 m (0 to 14.8 ft) along Bastendorff Beach. The difference between the two enhanced velocity components is ~30%. Because gale force winds are common on the Oregon coast during the winter, we believe it is justified to base the overtopping and hazard zone calculations on the slightly more conservative enhanced wind velocity component.

Hazard zone calculations shown in Table 6-5 indicate a similarly broad range of values that vary from ~0 m to 116 m (0 ft to 381 ft), with the widest zones observed along the Bandon shore, where overtopping significantly exceeds the eroded beach crest elevations, and at Sunset Bay State Park near Cape Arago. As described previously in Section 2.4.1, field observations of past storm wave overtopping events at Bandon indicate that logs and debris (Figure 2-9, Figure 2-10, and Figure 2-12) have been carried onto the parking lot adjacent to the Coquille south jetty, with flotsam having been observed as much as 200 ft landward of the beach. At Bandon, the width of the calculated flow hazard zone varies from 9 to 59 m (29.5 to 193.6 ft) relative to the barrier crest. Hence, the field observations appear to be consistent with the calibrated results identified in Table 6-5. For the Bandon shore, the widest hazard zone occurs between the Bandon 2 and 4 profile sites, with the hazard zone decreasing to the south due to a combination of increasing beach crest elevations and reduced wave heights (identified from

the wave shoaling modeling) due to the sheltering effects of the offshore sea stacks and reefs.

Along Bastendorff Beach, the prescribed $5.7 \text{ m}^3/\text{s}^2$ (200 ft^3/s^2) cutoff is reached at only two beach profile sites: Coos 4 and Coos 12. This response is entirely due to the generally lower wave heights observed on the north side of Cape Arago (and hence lower calculated total water levels) and the higher dune crest elevations identified along this section of shore, effectively limiting the number of overtopping events (Table 6-5), despite overtopping having been identified at a few of the sites. The one exception is the Coos 12 profile site at Sunset State Park, which shows an anomalously high inundation zone; the anomaly is largely due to the high calculated total water levels identified for this particular site. These latter estimates appear to be much higher than anticipated given that the bay head is protected by a narrow bay mouth, while the area offshore the bay is characterized by extensive reefs and exposed rocks that would almost certainly reduce the waves arriving in the bay. Discussions with Oregon State Parks and Recreation Department (OPRD) officials who manage and know the area confirmed that wave overtopping of the barrier occurs approximately every couple of years. Furthermore, a number of the events have resulted in damage to park facilities, including flooding of the restroom, damage to the road and pathways (e.g., chunks of asphalt having been ripped up), and ponding in the parking lot. However, while overtopping has occurred, the degree of the modeled overtopping response appears to be significantly higher than in reality.

7.0 COASTAL EROSION

In order to estimate beach (or bluff) erosion and the resulting profile changes that occur during a particular storm, it is important to first establish the initial profile conditions that existed prior to that storm. As outlined in Section 3.2, this initial profile morphology represents the most likely winter profile (MLWP) and forms the basis for determining profile changes that could occur as a result of a particularly severe storm or storms. After the MLWP for a site has been established, the profile is modified according to the amount of erosion estimated to occur during a specified storm as a result of the increased water levels (tide + surge + El Niño Southern Oscillation [ENSO]) as well as from wave processes, specifically wave runup. This section describes the approaches used to establish the eroded profiles along the Bandon shore and at Bastendorff Beach in Coos County.

7.1 Geometric model of foredune erosion

The erosion potential of sandy beaches and foredunes along the Pacific Northwest coast of Oregon and Washington is a function of the total water level produced by the combined effect of the wave runup, R , plus the tidal elevation (E_T), exceeding some critical elevation of the fronting beach, typically the elevation of the beach-dune junction (E_J). This basic concept is depicted conceptually in Figure 7-1A based on the model developed by Ruggiero and others (2001), and in the case of the erosion of a foredune backing the beach the application of a geometric model formulated by Komar and others (1999), Figure 7-1B. Clearly, the more extreme the total water level elevation, the greater the resulting erosion that occurs along both dunes and bluffs.

As can be seen from Figure 7-1B, estimating the maximum potential dune erosion (DE_{max}) is dependent on first determining the total water level elevation, T_{WL} , diagrammed in Figure 7-1A, which includes the combined effects of extreme high tides plus storm surge plus wave runup, relative to the elevation of the beach-dune junction (E_J). Therefore, when $T_{WL} > E_J$, the foredune retreats landward by some distance, until a new beach-dune junction is established, the elevation of which approximately equals the extreme water level. Because beaches along the high-energy Oregon coast are typically wide and have a nearly uniform slope ($\tan \beta$), the model assumes that this slope is maintained, and the dunes are eroded landward until the dune face reaches point B in Figure 7-1B. As a result, the model is geometric in that it assumes an upward and landward shift of a triangle, one

side of which corresponds to the elevated water levels, and then the upward and landward translation of that triangle and beach profile to account for the total possible retreat of the dune (Komar and others, 1999). An additional feature of the geometric model is its ability to accommodate further lowering of the beach face due to the presence of a rip current. This feature of the model is represented by the beach-level change ΔBL shown in Figure 7-1B, which causes the dune to retreat some additional distance landward until it reaches point C. As can be seen from Figure 7-1B, the distance from point A to point C depicts the total retreat, DE_{max} , expected during a particularly severe storm event that includes the localized effect of a rip current. Critical, then, in applying the model to evaluate the susceptibility of coastal properties to erosion is an evaluation of the occurrence of extreme tides (E_T), the runup of waves R , and the joint probabilities of these processes along the coast (Ruggiero and others, 2001). See Section 6, "Wave Runup and Overtopping" for discussion.

The geometric model gives the maximum potential equilibrium cross-shore change in the shoreline position landward of the MLWP resulting from a storm. However, in reality, it is unlikely that this extreme degree of response is ever fully realized, because of the assumptions made in deriving the geometric model with the intent of evaluating the maximum potential dune erosion. As noted by Komar and others (1999), in the first instance the geometric model projects a mean linear beach slope. As a result, if the beach is more concave, it is probable that the amount of erosion would be less, though not by much. Perhaps of greater significance is that the geometric model assumes an instantaneous erosional response, with the dunes retreating landward as a result of direct wave attack. However, the reality of coastal change is that it is far more complex, there in fact being a lag in the erosional response behind the forcing processes. As noted by Komar and others, extremely high runups typically occur for only a short period of time (e.g., the period of time in which the high wave runup elevations coincide with high tides). Because the elevation of the tide varies with time (e.g., hourly), the amount of erosion can be expected to be much less when water levels are lower. Thus, it is probable that several storms during a winter may be required to fully realize the degree of erosion estimated by the geometric model; this did, for example, occur during the winter of 1998-1999, when the last five storms were the most extreme and erosive (Allan and Komar, 2002b). In

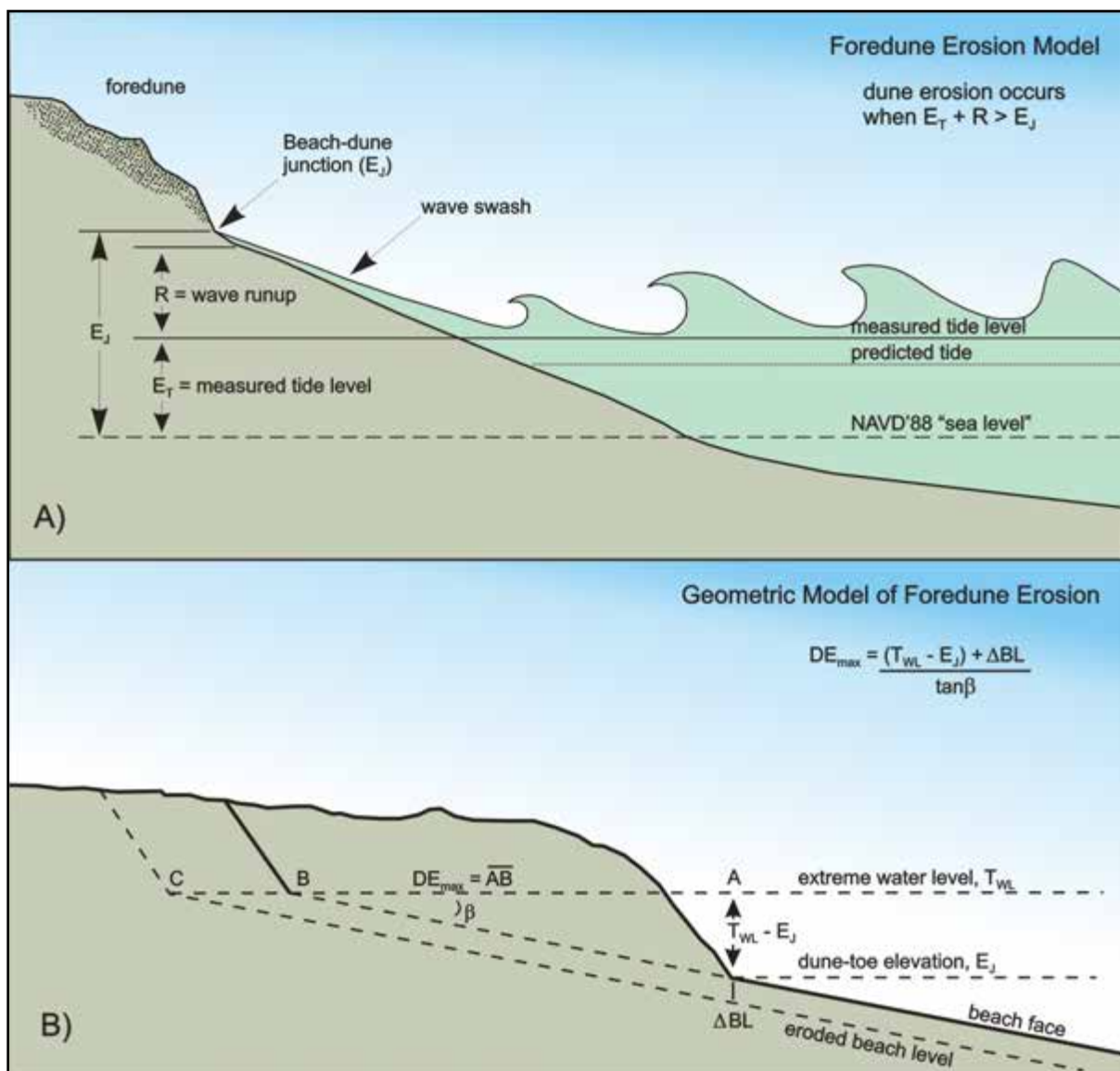


Figure 7-1. (A) Foredune erosion model. (B) Geometric model used to assess the maximum potential beach erosion in response to an extreme storm (Komar and others, 1999).

addition, as beaches erode, sediment is removed offshore (or farther along the shore) into the surf zone, where the sediment accumulates as nearshore sand bars. This process helps mitigate incoming wave energy by causing the waves to break farther offshore—dissipating much of the wave energy and forming the wide surf zones that are character-

istic of the Oregon coast. In turn, this process helps reduce the rate of beach erosion. In summary, the actual amounts of beach erosion and dune recession are dependent on many factors, the most important of which include the incident wave conditions, the T_{WL} , and the duration of the storm event(s).

Tables 7-1 and 7-2 provide a summary of the input parameters used to calculate the maximum potential dune erosion (DE_{max}) along the Bandon shore and at Bastendorff Beach. However, because significant portions of the Bandon and Bastendorff shorelines are backed by resistant bluffs, the geometric model calculations and the storm duration recession reduction factors will be applied only to those bluffs that are fronted by a dune, and the remaining bluff sections will not be eroded. For these latter sites (denoted by red in Tables 7.1 and 7.2), the most eroded winter profile will reflect the initial condition on which to perform the barrier runup calculations. The resulting calculated estimates for the maximum potential erosion based on this model are listed in Table 7-1 and Table 7-2, respectively, for Bandon and Bastendorff Beach. The estimated erosion distances range from 17 to 160 m (56 to 525 ft); again, it needs to be recognized that these estimates reflect the maximum potential extent of dune erosion for that site.

Because the duration of a storm is a major factor controlling beach and dune erosion, Kriebel and Dean (1993) developed an approach to account for the duration effects of storms with respect to the response time scale of a beach profile. The time scale for the erosion of a dune can be estimated using Equation 7.1:

$$T_s = C_1 \frac{H_b^{3/2}}{g^{1/2} A^3} \left(1 + \frac{h_b}{B} + \frac{mW_b}{h_b} \right)^{-1} \quad (\text{eq. 7.1})$$

where T_s is the time scale of response, C_1 is an empirical constant (= 320), H_b is the breaker height, h_b is the breaker depth, g is acceleration due to gravity, B is the berm elevation, m is the slope of the foreshore, W_b is the surf zone width, and A is the beach profile parameter that defines an equilibrium profile. The beach profile parameter can be estimated by

$$h = Ay^{2/3} \text{ or, equivalently, } x = \left(\frac{h}{A}\right)^{3/2} \quad (\text{eq. 7.2})$$

where h is the water depth at a distance x offshore from the still-water level and A is a parameter that governs the overall steepness of the profile and is a function of the beach grain size. Using Equation 7.1 yields typical response times for complete profile erosion that are on the order of 10 to 100 hours (NHC, 2005). In general, as the surf zone width increases due to larger wave heights, smaller grain sizes, or gentler slopes, the response time increases. In addition, the response time will also increase as the height of the berm increases.

Table 7-1. Maximum potential dune erosion (DE_{max}) values determined for Bandon using the geometric model.

Profile	1% T_{WL} (m)	E_{jMLWP} (m)	Beach Slope ($\tan \beta$)	1% Storm MPED (m)	Description
1	9.17	5.30	0.079	49.0	dune backed
2	9.93	6.07	0.092	42.0	dune backed
3	9.11	4.89	0.078	54.1	dune backed
4	8.96	5.14	0.075	50.9	dune backed
5	7.71	4.99	0.050	54.4	dune backed
6	7.22	3.66	0.042	84.8	dune/bluff backed
7	6.87	4.58	0.032	71.6	dune/bluff backed
8	—	4.15	0.024	—	bluff backed
9	—	3.89	0.034	—	bluff backed
10	—	3.74	0.034	—	bluff backed
11	—	4.17	0.032	—	bluff backed
12	—	3.30	0.026	—	bluff backed
13	—	4.81	0.032	—	bluff backed
14	6.54	3.88	0.028	95.0	dune/bluff backed
15	6.76	4.79	0.033	59.7	dune/bluff backed
16	6.35	4.40	0.024	81.3	dune/bluff backed
17	6.35	4.82	0.024	63.8	dune/bluff backed
18	6.28	4.27	0.021	95.7	dune/bluff backed
19	5.96	3.84	0.013	163.1	dune/bluff backed
20	6.45	5.93	0.030	17.3	dune/bluff backed
21	6.42	4.53	0.026	72.7	dune/bluff backed

Table 7-2. Maximum potential dune erosion (DE_{max}) values determined for Bastendorff and Lighthouse Beach using the geometric model.

Profile	1% T_{WL} (m)	E_{jMLWP} (m)	Beach Slope ($\tan \beta$)	1% Storm MPED (m)	Description
1	7.25	5.56	0.038	44.6	dune backed
2	7.30	5.28	0.036	56.1	dune backed
3	6.90	5.10	0.026	69.3	dune backed
4	6.58	4.13	0.023	106.5	dune backed
5	7.22	4.83	0.039	61.3	dune backed
6	7.12	4.73	0.037	64.6	dune backed
7	—	5.80	0.101	—	bluff backed
8	—	5.02	0.078	—	bluff backed
9	—	5.10	0.087	—	bluff backed
10	—	6.66	0.072	—	bluff backed
11	—	3.83	0.060	—	bluff backed
12	8.85	4.91	0.068	57.9	dune/bluff backed

Results of the time scale of profile response (T_s) calculated for every storm at each profile site is summarized graphically in Figure 7-2 and Table 7-1 for the two detailed study sites. For the purposes of this study, the breaker height, H_b , was calculated using the equation of (Komar and Gaughan, 1972) where:

$$H_b = 0.39 g^{1/5} (TH_o^2)^{2/5} \quad (\text{eq. 7.3})$$

The breaker depth, h_b , was calculated using a breaker index of 0.78, the berm elevation was established at 3 m (typical for PNW beaches), while the surf zone width, W_b , was determined for each h_b value by interpolating along a profile line of interest (Figure 7-3). Although we do have grain size information available that can be used to define the A parameter for Coos County, the approach we took was to iteratively determine an equilibrium A value based on the actual beach profile data. Here we used the profile data seaward to the 8 m (26.3 ft) water depth, and a range of A values were fit to the data until a value was found that best matched the profile morphology. This approach was adopted for all profile sites. However, at a few sites, the calculated A value was erroneous, and the regional mean value was used in its place. The mean A value determined from

the profile data was 0.133 for Bandon and 0.141 along Bastendorff/Lighthouse Beach.

As can be seen in Table 7-3 and Figure 7-2, values for T_s identified for Coos County are estimated to range from a minimum of 8.8 to a maximum of 142 hours, consistent with the analyses of NHC (2005). The highest T_s value was observed at the Bandon 19 profile site and is due to the low beach slopes that characterize this area as well as the orientation of the shore relative to the bathymetry, effectively extending the width of the surf zone and producing an anomalously large time scale of profile response when compared to adjacent profile site. Furthermore, the Bandon

Table 7-3. Simple statistics determined from an analysis of the time scale of profile response (T_s) values along the Coos County shore.

Region/ Beach Slope	Mean T_s (hrs)	STD T_s (hrs)	Minimum T_s (hrs)	Maximum T_s (hrs)
Bandon/low slope	51.4	18.3	18.7	141.8
Bandon/high slope	29.6	9.6	14.8	73.6
Coos/low slope	48.6	11.9	26.8	88.9
Coos/high slope	21.9	10.8	8.8	46.3

Values reported here are based on the two predominant beach conditions of low ($\tan \beta = 0.03$) and high ($\tan \beta = 0.08$) slopes. STD is standard deviation.

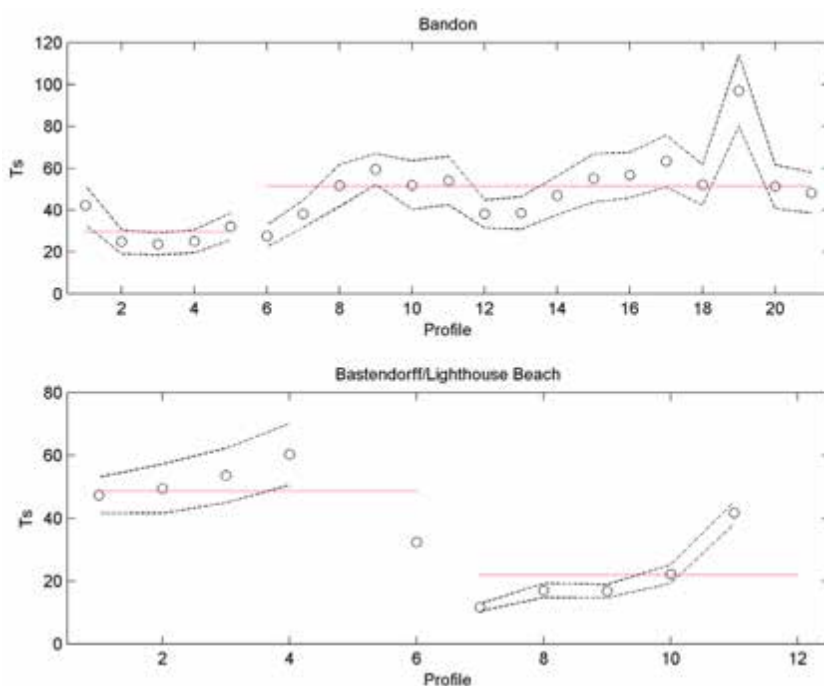


Figure 7-2. Plot of time scale of profile response, T_s , for the Bandon and Bastendorff Beach shorelines. Note: mean values are indicated by circles and standard deviation by dashed black lines; dashed red lines denote the values adopted for Coos County.

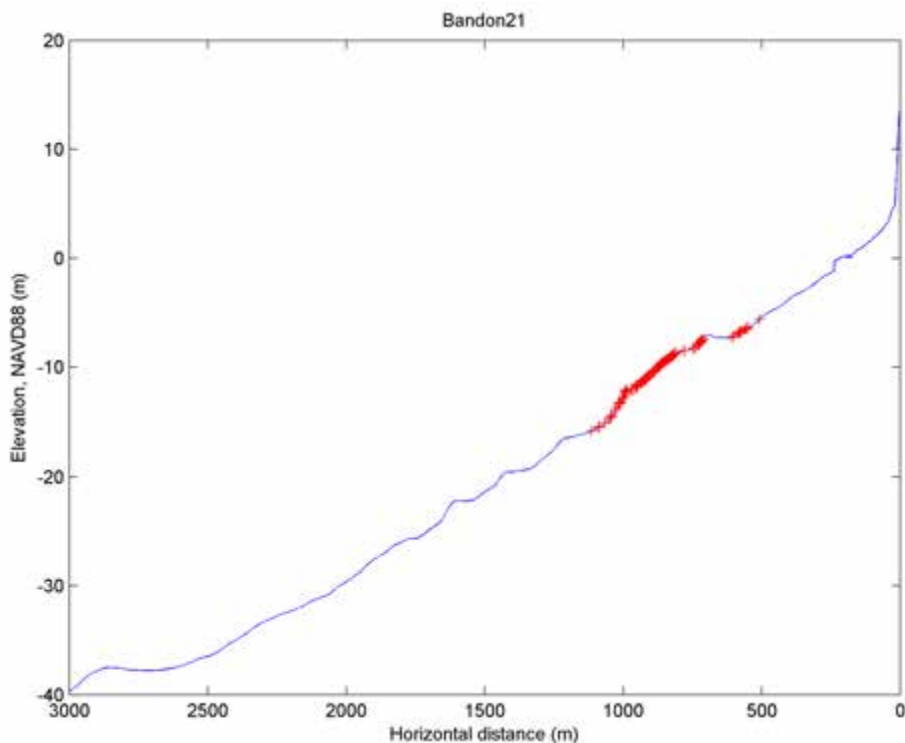


Figure 7-3. The Bandon 21 profile site showing the locations of breaker depth, h_b , (red crosses) used to define the cross-shore width (W_b) of the surf zone.

19 site is further complicated by the fact that Johnson Creek flows to the south along this stretch of shore, which helps to maintain the low beach elevations (due to saturation of the beach face) and hence slopes at Bandon 19. Mean values for T_s are shown as open circles in Figure 7-2, along with the ± 1 standard deviation demarcation lines (black dashed lines). Rather than calculating individual T_s values for every profile site, for the purposes of this study we used an average T_s value determined for our low (high) sloping beach conditions that effectively characterize the two detailed study shores. These values are shown as the red dashed lines in Figure 7-2. Thus for steeper beaches, the mean time scale of profile response is found to range from about 22 to 30 hours, while less steep beaches require time frames on the order of 50 hours (Table 7-3). This approach is probably reasonable, as the inclusion of any additional conservatism would effectively extend the time scale of profile response and hence would potentially reduce the degree of erosion once the reduction factor is resolved.

The beach profile response is determined by a convolution integral. According to NHC (2005), the time dependency of the storm hydrograph may be approximated by:

$$f(t) = \sin^2\left(\frac{\pi t}{T_D}\right) \text{ for } 0 < t < T_D \quad (\text{eq. 7.4})$$

where t is time from the start of the storm and T_D is the storm duration. The convolution integral is:

$$R(t) = \frac{R_\infty}{T_s} \int_0^t f(\tau) e^{-(t-\tau)/T_s} d\tau, \quad (\text{eq. 7.5})$$

which integrates to:

$$\begin{aligned} \frac{R(t)}{R_\infty} = & \left\{ 1 - \frac{\beta^2}{1 + \beta^2} \exp\left(-\frac{t}{T_s}\right) \right. \\ & \left. - \frac{1}{1 + \beta^2} \left[\cos\left(\frac{2\pi t}{T_D}\right) + \beta \sin\left(\frac{2\pi t}{T_D}\right) \right] \right\} \end{aligned} \quad (\text{eq. 7.6})$$

where $\beta = 2\pi T_s / T_D$ and R_∞ is the maximum potential recession that would occur if the storm duration were infinite. Thus, if the storm duration, T_D , is long relative to the time scale of profile response, T_s , then a significant portion of the estimated erosion determined by the geometric model will occur. As the ratio of these two values decreases, the amount of erosion will also decrease. The time required for maximum beach and dune recession is determined by set-

ting the derivative of Equation 7.6 to zero and solving for time. This yields:

$$\exp\left(-\frac{t_m}{T_s}\right) = \cos\left(\frac{2\pi t_m}{T_D}\right) - \frac{T_D}{2\pi T_s} \sin\left(\frac{2\pi t_m}{T_D}\right) \quad (\text{eq. 7.7})$$

in which t_m is the time that the maximum erosion occurs with respect to the beginning of the storm. Unfortunately, this equation can only be solved by approximation or numerically. Thus the maximum recession associated with a duration-limited storm can be calculated by:

$$\alpha = \frac{R_m}{R_\infty} = 0.5 \left[1 - \cos\left(2\pi \frac{t_m}{T_D}\right) \right] \quad (\text{eq. 7.8})$$

where α is the duration reduction factor and R_m is the maximum recession that occurs for a given storm duration that occurs at time t_m . As a result, the duration-limited recession is:

$$R_m = \alpha R_\infty \quad (\text{eq. 7.9})$$

In order to determine the duration reduction factor, α , the duration of each storm event has first to be identified. The approach used here involves an analysis of the number of hours a specific total water level (T_{WL}) event was found to exceed a particular beach profile's beach-dune junction elevation. Figure 7-4 is an example of the approach we used, which is based on a script developed in MATLAB. In essence, the blue line is the T_{WL} time series for a particular profile ± 3 days from the event that was first identified using the single high/low beach slopes (black circles in Figure 5-9). The script moves backward and forward in time from the identified event until the T_{WL} falls below the critical threshold shown as the dune toe elevation line depicted in Figure 7-4, which reflects the beach-dune junction elevation. The duration of the storm is then determined as the period where the T_{WL} exceeds the threshold and includes the shoulders of the event (i.e., when the T_{WL} first falls below the critical threshold). This process was repeated for every storm and for each profile site. One limitation of this approach that was encountered is that it is possible for the duration to be underestimated if the T_{WL} dips below the threshold for an hour or more and then rises again above the threshold, as depicted in Figure 7-4.

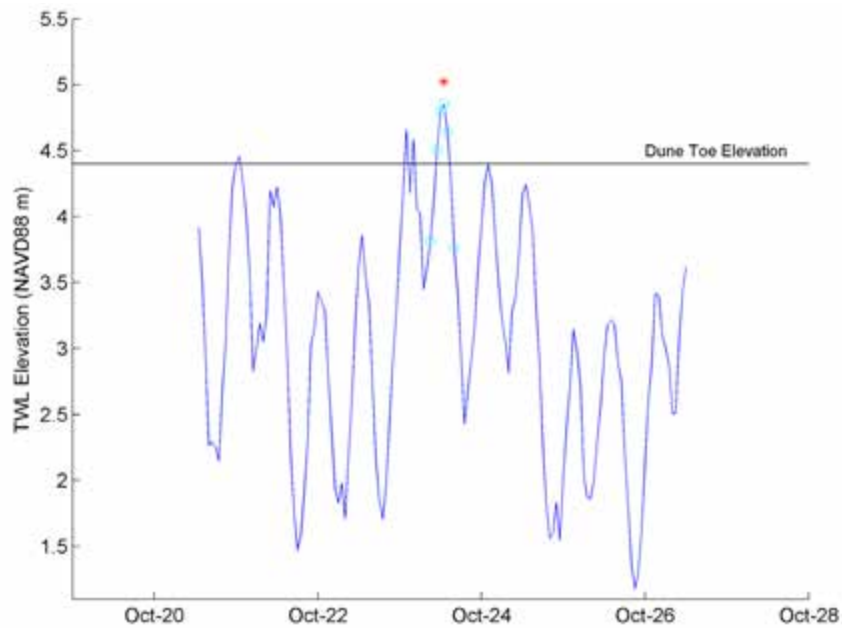


Figure 7-4. Example plot of the approach used to define storm duration along the Coos County shoreline. Note: The red asterisk denotes the original storm event identified using the low sloping beach condition ($\tan \beta = 0.03$), and the total water level, T_{WL} , curve is determined for a representative profile located in Bandon. The cyan blue circles denote the hours when the event exceeded the critical beach-dune junction toe elevation (including the shoulders) that are used to define the “duration” of the event.

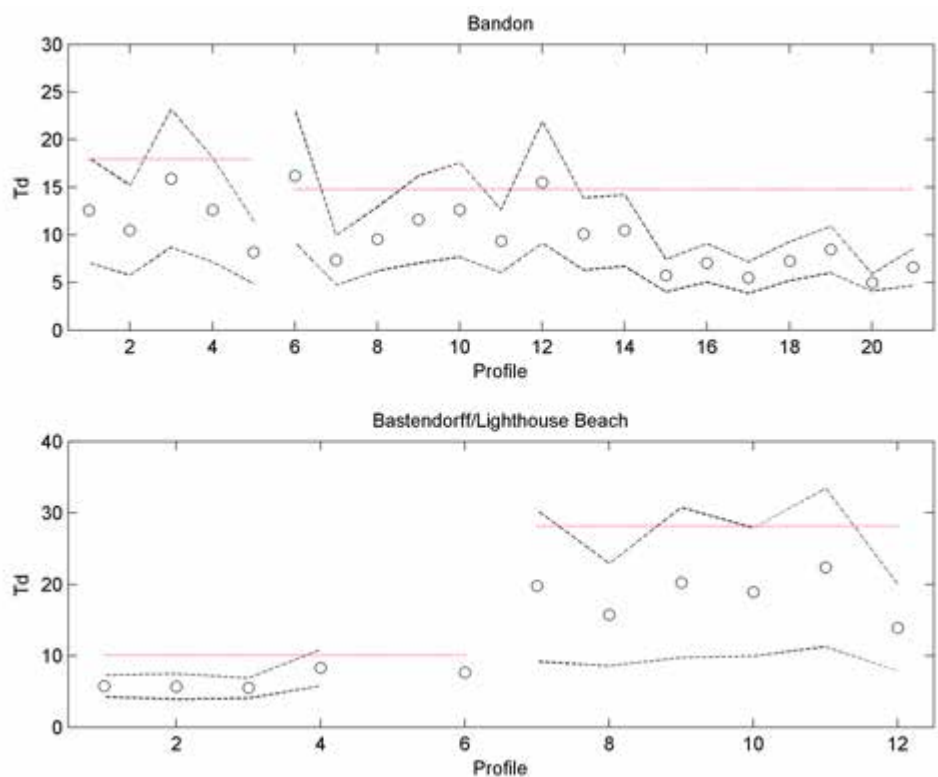


Figure 7-5. Plot of storm duration, T_d , for the Bandon and Bastendorff/Lighthouse beach shorelines. Note: mean values are indicated by circles and standard deviation by dashed black lines, The dashed red line denotes the values adopted for Coos County. Tables 7-5 and 7-6 contain summary values.

Table 7-4. Simple statistics determined from an analysis of storm duration values determined for the Coos County shore.

Region / Beach Slope	Mean Duration (hrs)	Standard Duration (hrs)	Design Duration (hrs)
Bandon / low slope	9.78	4.98	14.76
Bandon / high slope	11.99	5.97	17.96
Coos / low slope	7.43	2.67	10.09
Coos / high slope	18.5	9.64	28.14

Values reported here are based on the two predominant beach slope conditions of low ($\tan \beta = 0.03$) and high ($\tan \beta = 0.08$) slopes.

Figure 7-5 and Table 7-4 provide a summary of the duration values determined using the storm duration analysis technique. As can be seen in Figure 7-5, estimates of storm duration were found to range from several hours to as much as 35 hours. Mean duration values are plotted in Figure 7-5 (open circles) along with estimates of the mean ± 1 standard deviation (black dashed line). Because of the uncertainty of this technique and the potential to underestimate the actual duration of the storm, we decided to use the mean duration value determined for the two predominant beach slope conditions plus one standard deviation (Table 7-4). This latter value is shown as the red dashed line in Figure 7-5. Using this approach, we have effectively increased the potential for the dune to be eroded by having added some level of conservatism. From this approach, storm duration values identified for Coos County can be seen to range from 10 hours for the low sloping beaches at Bastendorff Beach to as much as 28 hours for the steeper shore that characterizes Lighthouse Beach. At Bandon the values ranged from 15 to 18 hours.

Having calculated T_s and T_d , the final parameter, t_m , was solved numerically using Equation 7.8. Table 7-5 provides a summary of all the parameters used to identify the storm recession reduction factor, α . As can be seen from Table 7-5 this yielded a recession reduction factor that ranges from 0.13 to 0.24 along the Bandon shore and 0.17 at Bastendorff Beach. Applying these recession reduction factors to the maximum potential erosion distances estimated using the geometric model (Table 7-1) effectively reduces the extent of dune erosion by about 13% to 24% along the Bandon shore and 17% at Bastendorff Beach. Table 7-6 provides a summary of the maximum potential erosion distances and the reduced erosion distances calculated by Equation 7.9, which is based on the recession reduction factors presented in Table 7-5. As can be seen from Table 7-6, estimated storm recession values range from 10 to 13 m (32.8 to 42.7 ft) for the steeper beaches adjacent to the Bandon jetties, to between 8 to 20 m (26.3 to 65.6 ft) for the dissipative beaches that make up the bulk of this shore. Comparable dune erosion estimates are provided for Bastendorff Beach.

Table 7-5. Summary parameters used to determine the storm recession reduction factor, α .

Region / Beach slope	Design T_s (hrs)	Design Duration (hrs)	Design t_m (hrs)	Design Recession Reduction Factor, α
Bandon / low slope	51.4	14.76	13.04	0.127
Bandon / high slope	29.6	17.96	15.03	0.240
Coos / low slope	48.6	10.09	18.8	0.173
Coos / high slope	21.9	28.14	21.86	0.416

Table 7-6. Calculated duration limited recession (R_m) for the Bandon shore and along Bastendorff Beach.

Profile	Bandon			Bastendorff		
	Description	1% Storm MPED (m)	R_m (m)	Description	1% Storm MPED (m)	R_m (m)
1	dune backed	47.1	11.8	dune backed	44.6	7.7
2	dune backed	40.3	10.1	dune backed	56.1	9.7
3	dune backed	52.2	13.0	dune backed	69.3	12.0
4	dune backed	48.9	12.2	dune backed	106.5	18.4
5	dune backed	51.4	13.1	dune backed	61.3	10.6
6	dune/bluff backed	81.2	20.4	dune backed	64.6	11.2
7	dune/bluff backed	66.9	9.1	bluff backed	—	—
8	bluff backed	—	—	bluff backed	—	—
9	bluff backed	—	—	bluff backed	—	—
10	bluff backed	—	—	bluff backed	—	—
11	bluff backed	—	—	bluff backed	—	—
12	bluff backed	—	—	dune/bluff backed	57.9	24.1
13	bluff backed	—	—			
14	dune/bluff backed	89.6	12.19			
15	dune/bluff backed	55.2	7.6			
16	dune/bluff backed	75.0	10.3			
17	dune/bluff backed	57.5	8.1			
18	dune/bluff backed	88.6	12.2			
19	dune/bluff backed	151.5	20.8			
20	dune/bluff backed	12.3	2.2			
21	dune/bluff backed	66.9	9.3			

MPED is maximum potential erosion distance.

The degree of dune erosion presented in Table 7-6, which is based on monitoring of more than 150 beach profile sites along the Oregon coast over a period of several years²⁹, provides a reasonable estimate when compared with actual observed storm recession values.

Figure 7-6 and Figure 7-7 provide two examples where the most eroded winter profile has undergone additional erosion using the calculated duration limited recession (R_m) value for those particular sites. The first example is the Bandon 16 profile site, where the beach is backed by a dune and, farther landward, by a bluff. In this example, the calculated maximum potential dune erosion (DE_{max}) is ~64 m (210 ft), while the duration reduced recession is ~8 m (26 ft). The location of the beach-dune junction is depicted in Figure 7-6 by the solid black circle, while the most eroded winter profile is shown as the black line; note that in this example the beach has accreted since the late 1990s (green line) such that the duration-reduced erosion is occurring on the most eroded winter profile as recommended by NHC

²⁹ <http://www.oregongeology.org/sub/Nanoos1/index.htm>

(2005). Because the underlying principle of the geometric model is for the slope to remain constant, the dune is eroded landward by shifting the location of the beach-dune junction upward and landward by 8 m to its new location, where it forms an erosion scarp (Figure 7-6). In this example, overtopping occurs on a small portion of the profile but not the full profile, as the elevation of the remaining back-shore is higher than the calculated 1% T_{WL} .

Figure 7-7 provides an example where overtopping occurs in response to the calculated 1% T_{WL} for the Bandon 4 profile site. The calculated maximum potential dune erosion (DE_{max}) for Bandon 4 is ~51 m (167 ft), while the duration-reduced recession is ~12 m (40 ft). The location of the beach-dune junction is depicted in Figure 7-7 by the solid black circle, while the most eroded winter profile is shown as the black line. As noted by NHC (2005), when dunes are subject to major overtopping events, breaching of the dune typically results in significant lowering of the dune morphology and the development of an overwash fan on the lee side of the dune. Because present methodologies are unable to account for such responses, NHC recommended that

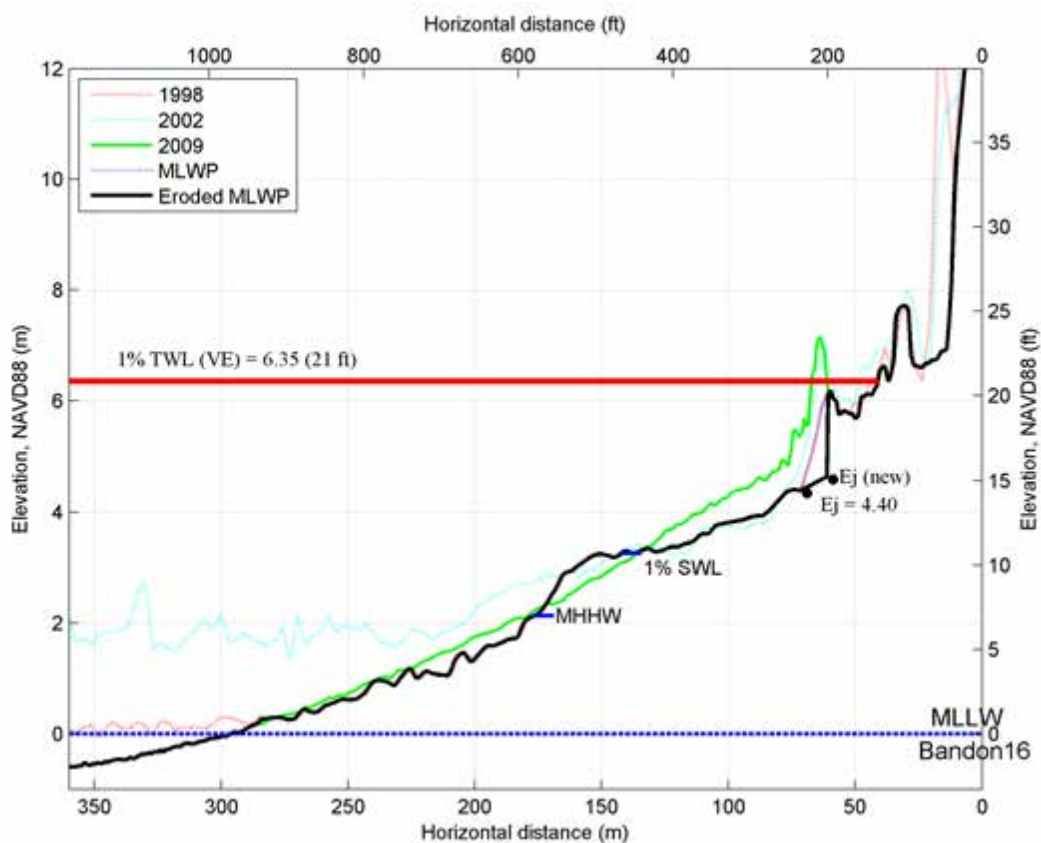


Figure 7-6. Application of the duration-reduced erosion estimate to the most eroded winter profile at Bandon 16.

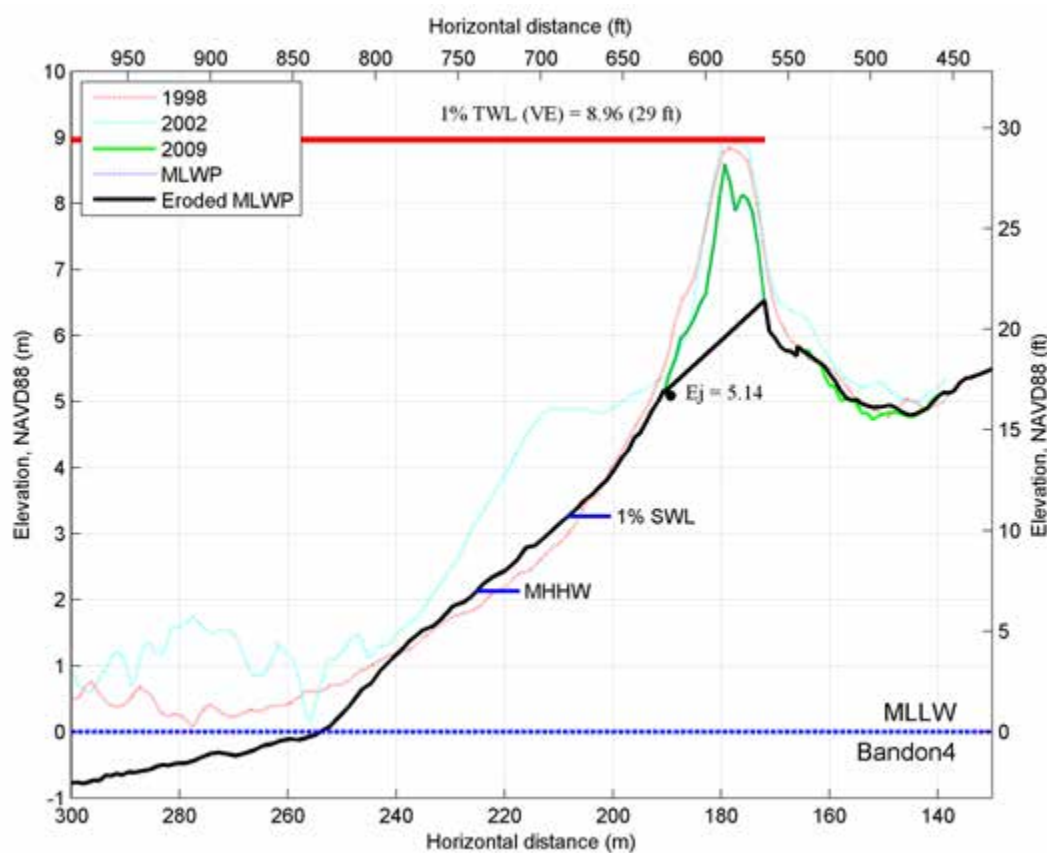


Figure 7-7. Application of the duration-reduced erosion estimate to the most eroded winter profile at Bandon 4 where overtopping occurs.

the dune profile be adjusted by extending the most likely winter profile slope to the backside of the dune. This type of adjustment is demonstrated in Figure 7-7, where the entire foredune is assumed to be eroded and removed as a result of a major storm.

Unfortunately, there are no measured examples of the type of response depicted in Figure 7-7 for the Coos County area that can be used for comparison. However, monitoring of beaches by DOGAMI on the Oregon coast provides some suggestion that this approach is probably reasonable. Figure 7-8 is an example of beach profile changes measured along a barrier beach adjacent to Garrison Lake, Port Orford, located south of Bandon. In this example, the barrier beach, which has a crest elevation of 8-9 m NAVD88

(26–29 ft), is known to have been overtopped during several major storms in February/March 1999 (Figure 7-9) (Allan and others, 2003). Analyses of the mean shoreline position at this site indicate that changes in the morphology of the beach are primarily controlled by the occurrence of these major storms as well as by El Niño climate events that result in hotspot erosion. Examination of the beach profile changes along the Garrison Lake shore indicates that during major events characterized by overtopping, the crest of the barrier beach is lowered, with some of the eroded sand carried landward where it forms washover fans, while the bulk is removed seaward to form sand bars. Ultimately though, the top of the beach and any dune is entirely removed, consistent with the response depicted in Figure 7-7.

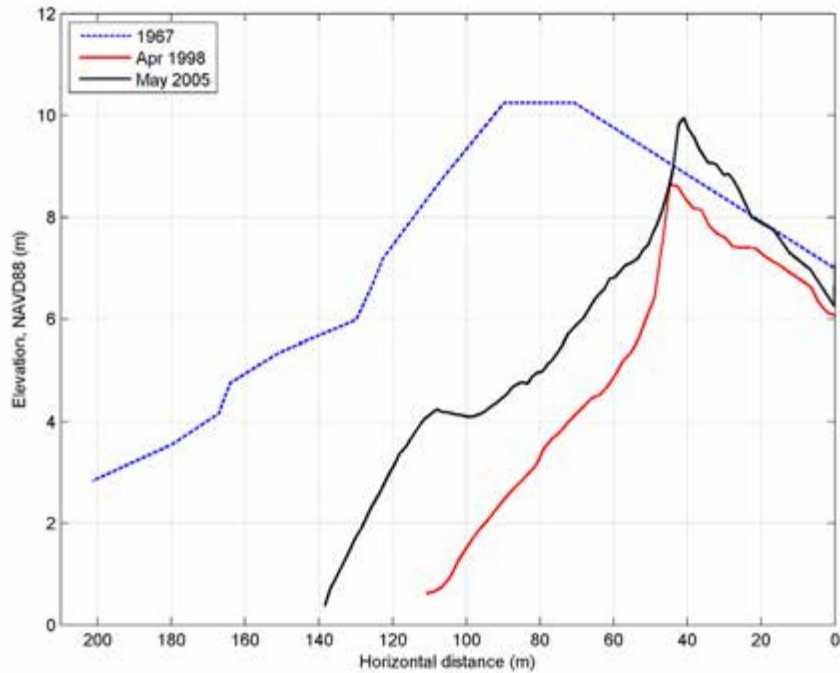


Figure 7-8. Example profile where a barrier beach is overtapped and eroded. This example is based on measured beach profile changes at Garrison Lake, Port Orford, on the southern Oregon coast.



Figure 7-9. Overtopping of the barrier beach adjacent to Garrison Lake, Oregon, during a major storm on February 16, 1999. (Photo courtesy of a Port Orford resident.)

8.0 FLOOD MAPPING

8.1 Detailed coastal VE flood zone mapping

Detailed mapping of the 1% chance flood event within selected areas of Coos County was performed using two contrasting approaches, controlled ultimately by the geomorphology of the beach and backshore. In all cases we followed the methods described in the final draft guidelines of the Coastal Flood Hazard Analysis and Mapping for the Pacific Coast of the United States (NHC, 2005, section D.4.9).

8.1.1 Bluff-backed beaches

For bluff-backed beaches, total water level (T_{WL}) values calculated in Section 6.3, "Coos County wave runup and total water level calculations" were extended into the bluff. The first step involved identifying specific contours of interest, which were extracted from the 1-m resolution bare-earth lidar grid (surveyed in 2008). In all cases, the calculated total water level (T_{WL}) values were rounded to the nearest whole foot. For bluff-backed beaches the landward extent of the coastal flood (VE) zone is defined by the contour repre-

resenting the total water level (T_{WL}) elevation calculated for each of the represented detailed surveyed transects (e.g., Figure 8-1; Table 6-3 and 6-4).

To define the velocity zones between transects, we used professional judgment to establish appropriate zone breaks between the various transects. For example, along-shore geomorphic barriers were identified within which the transect total water level (T_{WL}) value is valid (Figure 8-2). Slope and hillshade derivatives of the lidar surface and 1-m orthophotos (acquired in 2009) provided base reference. An effort was made to orient zone breaks perpendicular to the beach at the location of the geomorphic barrier. In all cases, the seaward extent of the flood zones was inherited from the 2009 effective DFIRM.

8.1.2 Dune-backed beaches

For dune-backed beaches, the flood zone was determined by calculating the degree of wave overtopping at each transect location, which included the calculated splashdown distances (Y_G outer), bore height associated with wave overtopping

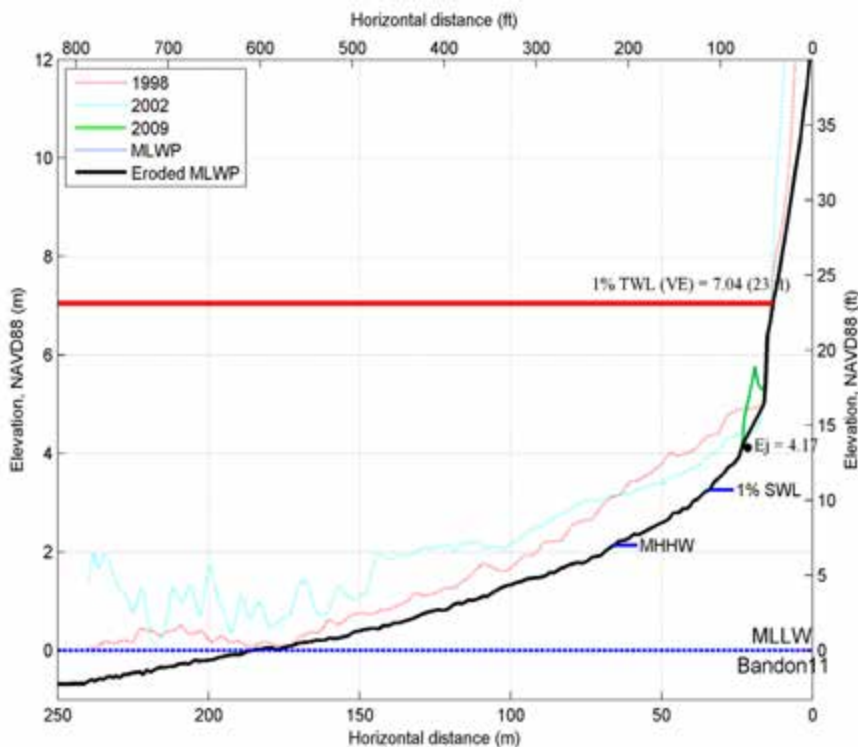


Figure 8-1. Example of a bluff-backed beach (Bandon 11) where the calculated total water level and defined velocity (VE) zone extend into the bluff. MLWP is most likely winter profile, MHHW is mean higher high water, and MLLW is mean lower low water.

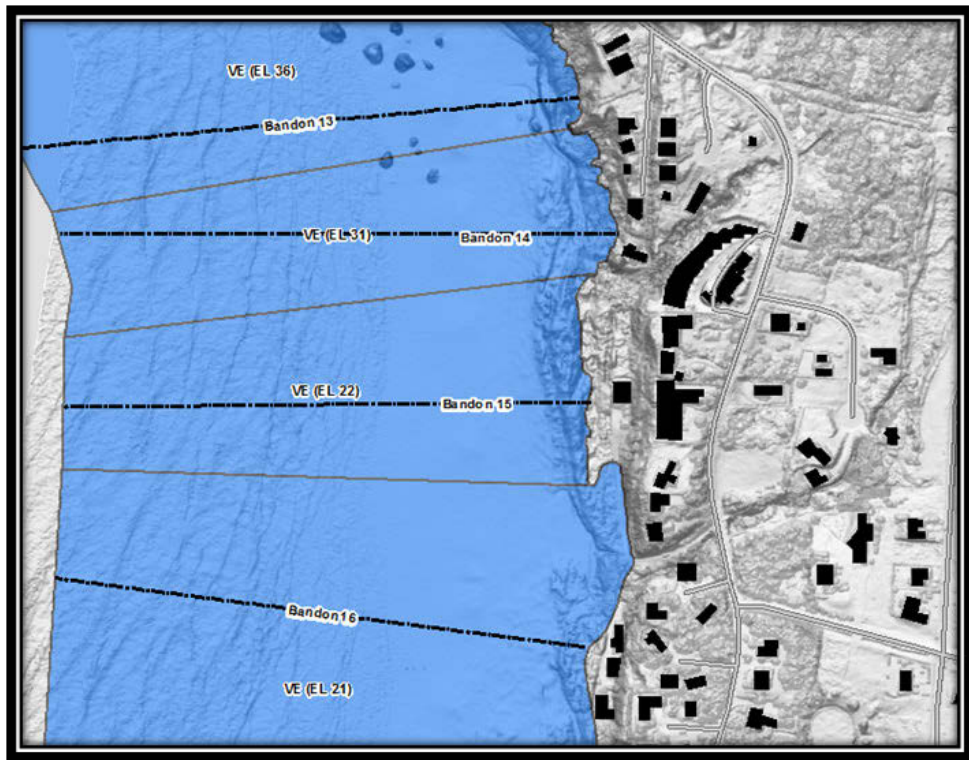


Figure 8-2. Example of along-shore zone breaks and their relationship to geomorphic barriers and surveyed transects. Surveyed transects are symbolized as black dashed lines; zone breaks are solid gray lines.

(h_o), and the landward extent of the flow (hV^2), where the flows approach $5.7 \text{ m}^3/\text{s}^2$ (or $200 \text{ ft}^3/\text{s}^2$). Table 8.1 lists the overtopping calculations for each transect characterized by a dune-backed beach. “Distance” reflects the farthest point landward of the dune crest that experiences coastal flooding due to overtopping and is ultimately controlled by the extent of the landward flow where it approaches $5.7 \text{ m}^3/\text{s}^2$ (or $200 \text{ ft}^3/\text{s}^2$); values greater than $5.7 \text{ m}^3/\text{s}^2$ (or $200 \text{ ft}^3/\text{s}^2$) are located within the velocity (VE) zone, while lower values are outside the velocity zone.

“Distance from x where $\text{Bore} > 2 < 3 \text{ ft}$ ” marks the landward extent of flood zones where the bore height (h_o) was determined to be between 0.61 and 0.91 m (2 and 3 ft high) and were ultimately rounded up to the nearest whole foot (i.e., having an elevation of 0.91 m [3 ft] above the land surface). “Distance from x where $\text{Bore} < 1$ ” marks the seaward extent of flood zones where the bore height falls below 0.3 m (1 ft) (i.e., having an elevation of 0.3 m [1 ft]) above the land surface; all values less than 0.3 m (1 ft) were rounded up to the nearest whole foot. Areas where flood zones exhibited bore height elevations of 0.61 m (2 ft) above the land surface were inferred as existing in the area between the two previously described regions (i.e., between “Distance from x where $\text{Bore} > 2 < 3 \text{ ft}$ ” and “Distance from x where $\text{Bore} < 1$ ”). The final column, “ hV^2 Transition” repre-

sents the landward extent of the VE zones. As noted previously, any landward flow greater than $5.7 \text{ m}^3/\text{s}^2$ (or $200 \text{ ft}^3/\text{s}^2$) was determined to be located within the velocity (VE) zone, while values less than this threshold were designated as AE zone.

Similarly to the process for bluff-backed beaches, professional judgment was used to establish appropriate zone breaks between the detailed transects. This was achieved through a combination of having detailed topographic information of the backshore and from knowledge of the local geomorphology. Some interpretation was required to produce flood zones appropriate for the printed map scale. Elevations were identified from the 1-m resolution bare-earth lidar grid to aid in establishing zone breaks due to changes in flood depth landward of the dune crest (Figure 8-3). Slope and hillshade derivatives of the lidar surface and 1-m orthophotos provided base reference.

For flood zones seaward of the dune crest, the calculated total water level (T_{WL}) values were used. As with the bluff-backed beaches, along-shore geomorphic barriers were identified within which the transect total water level (T_{WL}) value is valid. In all cases, an effort was made to orient zone breaks perpendicular to the beach at the location of the geomorphic barrier. The seaward extent of the flood zones was inherited from the 2009 effective DFIRM.

Table 8.1. Overtopping calculations for surveyed transects located on dune-backed beaches.

Transect ID	Distance, x (m)	Maximum Splashdown Distance, $y_{G_{Outer}}$ (m)	Maximum Bore Height at Splashdown, h_o (ft)	Distance from x where Bore $> 2 < 3$ ft (m)	Distance from x where Bore < 1 ft (m)	hV^2 Transition (m)
Bandon						
1	208	1.3	1.71	NA	26.03	46.7
2	194.13	3.4	1.93	NA	36.4	62.4
3	213.65	3.4	1.75	NA	29.1	53.7
4	172.03	4.1	1.83	NA	33.5	60.1
5	94	1.5	1.09	NA	4	10.2
6	69.31	1.9	1.24	NA	10.6	22.9
Bastendorff						
1	305	0.6	0.64	NA	NA	0.6
2	324.9	NA	NA	NA	NA	NA
3	195.5	3.1	0.77	NA	NA	3.1
4	233.72	4.5	1.73	NA	28.7	50.2
5	258.56	2.6	0.97	NA	NA	2.6
12	100.07	1.7	2.05	1.6	40.9	115.6

Note: Location of x (m) is based on the crest of the eroded profile. All landward boundaries are relative to the location of x (m).



Figure 8-3. Example of zone breaks for dune-backed beaches. Surveyed transects are symbolized as black dashed lines; zone breaks are solid gray lines. Blue flood zones are VE zones; orange zones are AE zones.

8.2 Coastal V-zone mapping along Coos County shoreline

8.2.1 Dune-backed beaches

The FEMA guidelines provide little direct guidance for mapping velocity (V) zones in areas where no detailed studies have occurred, other than by defining the location of the primary frontal dune (PFD). The PFD is defined as a

continuous or nearly continuous mound or ridge of sand with relatively steep seaward and landward slopes immediately landward and adjacent to the beach and subject to erosion and overtopping from high tides and waves during major coastal storms. The landward limit of the primary frontal dune, also known as the toe or heel of the dune, occurs at a point where there is a distinct change from a relatively steep slope to a relatively mild slope. The primary frontal dune toe represents the landward extension of the Zone VE coastal high hazard velocity zone. (Part 44 of the U.S. Code of Federal Regulations, Section 59.1; FEMA Coastal Hazard Bulletin, No. 15³⁰)

The approach developed by DOGAMI to define the morphology of the beach and dune system, including the location of the PFD, was based on detailed analyses of light detection and ranging (lidar) data measured by USGS/NASA/NOAA in 1998 and 2002 and by DOGAMI in 2008. However, because the lidar data flown by USGS/NASA/NOAA is of relatively poor resolution (~ 1 point/m 2) and is unclassified (i.e., single return such that it includes vegetation where present), while the lidar data flown by DOGAMI has a higher resolution (8 points/m 2) and was classified (i.e., multiple returns) to allow the development of a bare-earth digital elevation model (DEM), determination of the PFD was based entirely on analysis of the 2008 DOGAMI lidar data. In addition to identifying the PFD, we processed all available lidar data in order to assess a suite of other important morphological parameters, including beach-dune juncture elevations, beach/bluff slopes, dune crest/bluff top, and contour changes (e.g., dune erosion).

To perform these morphological assessments, lidar data flown in 1998 and 2002 were downloaded from NOAA's Coastal Service Center³¹ and gridded in ArcGIS using a nearest neighbor algorithm, while the 2008 lidar data were independently quality controlled and were gridded by the lidar contractor, Watershed Sciences, Inc. Transects spaced 50 m apart were cast for the full length of the county coast-

line using the Digital Shoreline Analysis System (DSAS) developed by the USGS (Thieler and others, 2009). For each transect, xyz values for the 1998, 2002, and 2008 lidar data were extracted at 1-m intervals along each transect line and were saved as a text file using a customized ArcGIS script.

Processing of the lidar data was undertaken in MATLAB using a custom beach profile analysis script developed by DOGAMI. This script requires the user to interactively define various morphological features including the dune/bluff crest/top, bluff slope (where applicable), landward edge of the PFD, beach-dune juncture elevations for each year, and the slope of the beach foreshore. Figure 8-4 provides two examples from profiles 1380 and 1386 on the north Coos spit. In these two examples, the dune crest ranges in elevation from 10 to 11 m high. Also evident is that the seaward face of the dune eroded landward by 17.2 m (56.4 ft, profile 1380) and 18.2 m (59.7 ft, profile 1386) between 1998 and 2008; shoreline change (erosion/accretion) was determined based on the change in position of the 6 m (19.7 ft) contour elevation, which is an excellent proxy for determining the effects of storm erosion (Allan and others, 2003). In the case of profile 1386, if erosion continues unabated, it can be expected that this section of shore will lose the bulk of the existing primary dune. Figure 8-5 is a graph showing the change in position of the 6 m (19.6 ft) contour for all dune-backed beaches in Coos County. As can be seen from Figure 8-5, erosion predominates along both the north Coos Spit and along much of the New River Spit, while much of the shore along Hubbards Beach located north of Bandon appears to be accreting.

Figure 8-6 shows the locations of the PFD (yellow dots) determined from the 2008 lidar data, overlaid on a 2009 orthophoto, while the shaded polygon reflects the original A zone established for this area in the 1970s. As can be seen in Figure 8-6, for these locations the original A zone clearly excludes a significant portion of the active beach face and, importantly, the PFD. This difference probably highlights the extent of erosion that has taken place over the past 40 years (i.e., since the A zone was originally drawn). Alternatively, some or all of these differences may also reflect inherent errors associated with the original base maps.

The approach we developed to establish new V zones for the dune-backed beaches involved several steps. First, the actual locations of the PFD were plotted in ArcGIS and overlaid on both current and historical aerial photos of the county. In a number of locations the PFD was found to be located either farther landward or seaward relative to adjacent PFD locations. This response is entirely a function of

³⁰ https://www.floodmaps.fema.gov/listserv/ch_jul02.shtml

³¹ <http://www.csc.noaa.gov/digitalcoast/data/coastallidar/index.html>

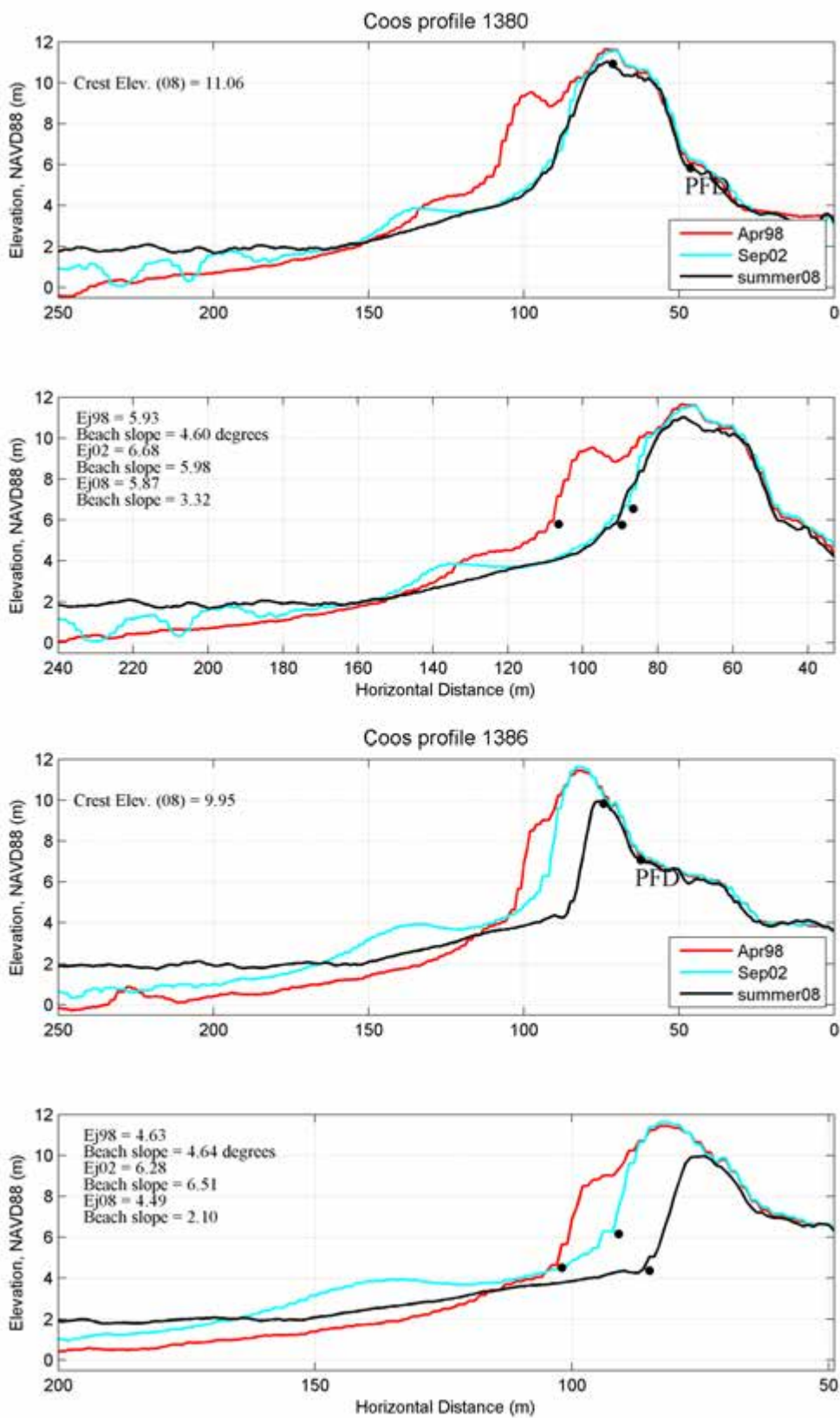


Figure 8-4. Example beach profiles for the north Coos Spit derived from 1998, 2002, and 2008 lidar data. Solid black dots denote locations of the dune crest and primary frontal dune (upper plots for each profile) and the beach dune juncture elevations (lower plots for each profile).

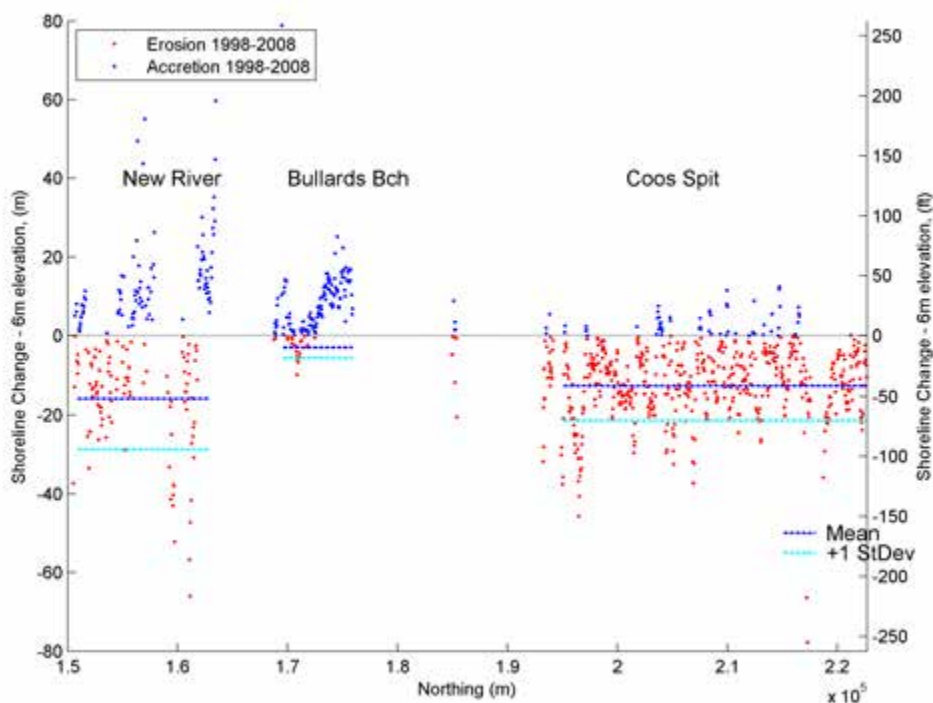


Figure 8-5. Storm-induced dune response determined for dune-backed beaches in Coos County for the period 1998–2008. Change estimates are based on the maximum erosion/accretion response determined over the 10-year period (typically 1998–2008).

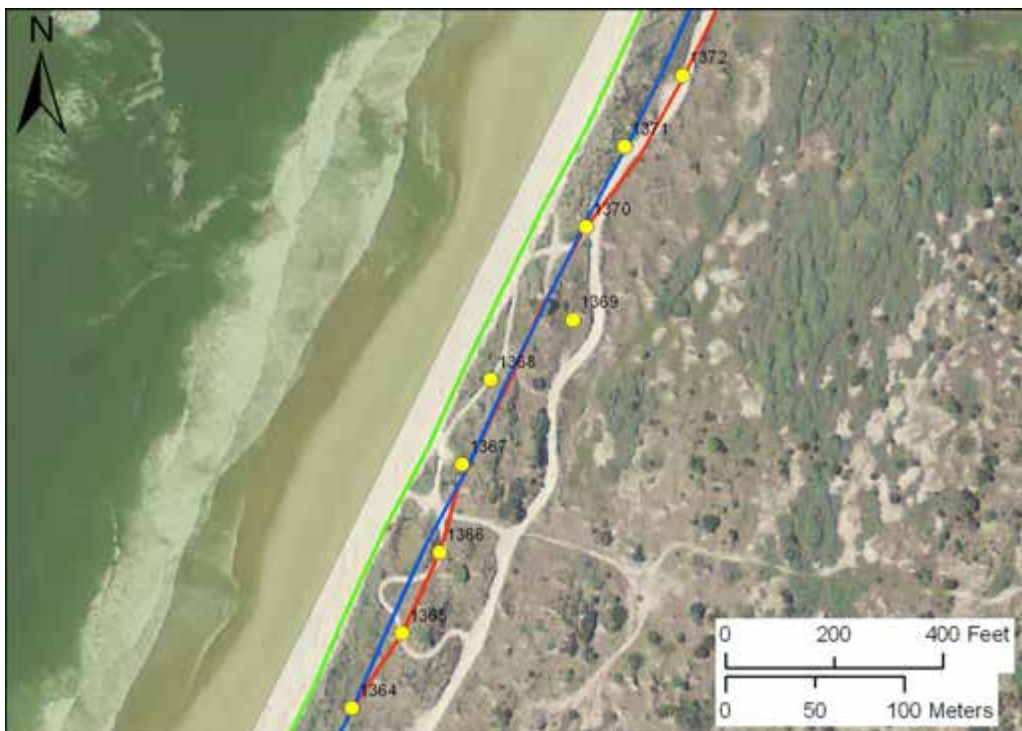


Figure 8-6. Plot showing the locations of the primary frontal dune (PFD; yellow dots), 6-m contour (green line), projected storm-induced erosion (blue line), and final V zone (red line). Green shading denotes the original A zone established in the 1970s. This example shows three profile sites (1368, 1369, and 1371) where the location of the V zone have been shifted east, initially to match the estimated storm erosion line, and then farther east to better conform with the adjacent PFDs (e.g., profiles 1367 and 1370).

the ambiguity of defining the PFD as defined above in the FEMA definition. Our observations of the PFD approach highlighted a number of uncertainties, including:

1. There were numerous examples of smaller dune features that have begun to develop in front of a main dune (or are the product of erosion of the dune) but have not yet attained dimensions and volumes where they would be considered an established dune or may continue to erode and could disappear entirely (Figure 8-7). However, the PFD approach does not account for such features. In this example, the smaller dunes are almost certainly subject to erosion and periodic overtopping and have morphologies that resemble the FEMA PFD definition. However, because they are subject to erosion responses they are more ephemeral in nature and it is debatable whether they should be defined as PFDs. Furthermore, over the life of a typical map (~10 years) these dunes could be eroded and removed entirely, leaving a "gap" between the original polygon boundary and the eroding dune. For example, from repeated observations of beach profile transects on the northern Oregon coast, single storm events
- have been documented to remove as much as 9–25 m (30–80 ft) of the dune (Allan and Hart, 2007; Allan and Hart, 2008);
2. The PFD does not adequately account for broad (i.e., several hundred meter wide) barrier spits with no dune development or for parts of the spit characterized by low elevations that are subject to frequent wave overtopping. The landward edge of the barrier may be bounded by a river (e.g., the New River Spit) or in some cases an estuary.
3. The PFD does not adequately account for a large established foredune, where the dune may have attained heights of 10–15 m (33–50 ft), with cross-shore dimensions on the order of 50–100 m (165–330 ft) wide. In this example, there may be a clear landward heel located well inland away from the beach (e.g., profile 1369 in Figure 8-6), but the PFD is clearly not subject to "frequent" wave overtopping due to its height and erosion (because of its large volume of sand). Defining the PFD at the location of the heel may be reasonable but would almost certainly generate a very conservative V zone. Furthermore, because the

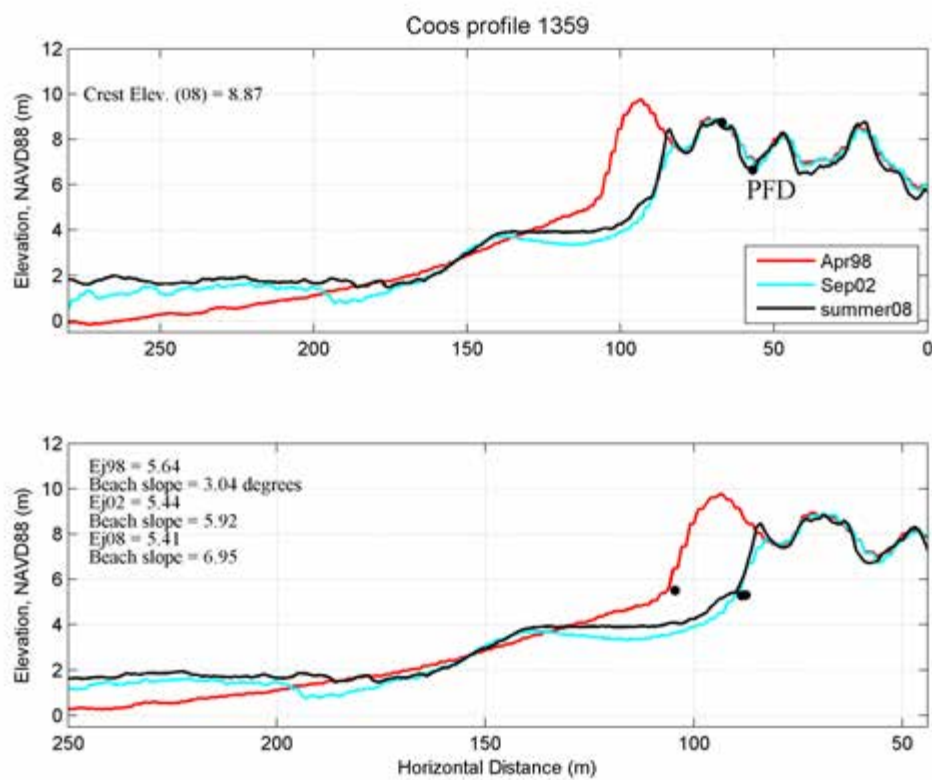


Figure 8-7. Example profile from Coos Spit with multiple dune features. In this example the primary frontal dune (PFD) could conceivably be drawn seaward of its existing location and meet the FEMA definition of PFD.

morphology of dunes along Coos County is not uniform (e.g., as observed along linear type dunes), adjacent PFDs were found to fluctuate significantly from one transect to another.

To account for these variations and uncertainties, the PFDs shown on the profile plots (e.g., Figure 8-4) were re-examined and adjustments were made where necessary. These adjustments included the following steps:

1. At some locations, the V-zone line running through a particular PFD was physically moved so that it was more in keeping with the adjacent PFD locations to its immediate north and south.
2. At a number of locations, the identified PFD was found to be located very close to the active beach (i.e., the PFDs in those locations were relatively narrow and hence had generally low sand volumes contained in the dune). Because of their close proximity to the beach and hence susceptibility to erosion from a storm event(s), and because of the degree of erosion that has occurred during the last 10 years along the north Coos Spit and New River Spit, additional adjustments in the location of the V-zone line were undertaken; note that we did not adopt this approach everywhere along the Coos County shore — only along those sections of shore that exhibited strong evidence of existing erosion activity. Included in Figure 8-6 is the location of the 6-m contour (green line), which provides a good proxy for the transition from dune face to active beach foreshore. The blue line in Figure 8-6 corresponds to a projected storm erosion line that is based on the expectation that the dune will probably continue to erode landward over the next several years. The blue “erosion” line was defined as the mean erosion value determined for a particular reach of shore (e.g., north Coos Spit) plus one standard deviation. The purpose of including one standard deviation to the mean erosion value is to account for the alongshore variation in the existing dune erosion response. This last assumption is reasonable given the following:

- The current phase of ocean wave heights contains the highest observed waves of the past 30–40 years, such that the 100-year storm wave of a decade ago now occurs in almost every winter, increasing the risk of beach and dune erosion;
- GPS beach monitoring on the northern Oregon coast by DOGAMI indicates that the majority of sites presently being monitored are continuing to erode and, more importantly, to have less

sand volume today compared with a decade ago — indicating little to no post-storm recovery.

- Sea level is gradually rising along the Coos County coast and will likely accelerate due to climate change effects (Komar and others, 2011). The current estimate of the rate of sea level rise determined for the Charleston tide gauge is $1.12 \pm 0.95 \text{ mm} \cdot \text{yr}^{-1}$. Furthermore, the PNW coast experiences El Niños approximately every 3–7 years, with major events occurring on the order of 10–15 years. These latter events increase ocean water levels along the PNW coast by 50–60 cm (20–24 in), relative to the summer minima and coincide with the seasonal peak of the winter waves, enabling waves to reach to much higher elevations on the beach.
- Although the PNW coast FEMA flood methodology does not explicitly define an approach for dealing with erosion when mapping V zones, it is required when mapping VE zones (i.e., VE-zone mapping is based on the most eroded winter profile, plus a geometric erosion response of the dune associated with a major storm[s], in order to map wave runup elevations and overtopping).
- Using historical beach profile data to adjust the location of the PFD results in an updated map that reflects conditions expected over the typical useful life of the map, which is approximately 10–15 years. This process is not intended to account for long-term erosion expected at the study site.

Having identified the PFD, beach/dune line, and projected erosion in GIS, the V zone was adjusted to account for these various evaluations. As can be seen in Figure 8-6, two of the PFDs fall seaward of the storm erosion line. In this example, the two PFDs are analogous to the PFD adjustment 1 category described above. Furthermore, because of the high probability that the shore will continue to erode from storms over the next decade, the V zone has been shifted slightly farther landward so that it lands either on the blue erosion line or slightly landward of it (depending on the configuration of adjacent PFDs to the north and south). Figure 8-6 also provides an example where the V-zone line is shifted seaward at profile 1369, due to the presence of a very high, broad dune, which places the heel of the dune well landward relative to adjacent dune morphologies. With this approach, similar adjustments were made elsewhere along the length of the Coos County shore (Figure 8-8).

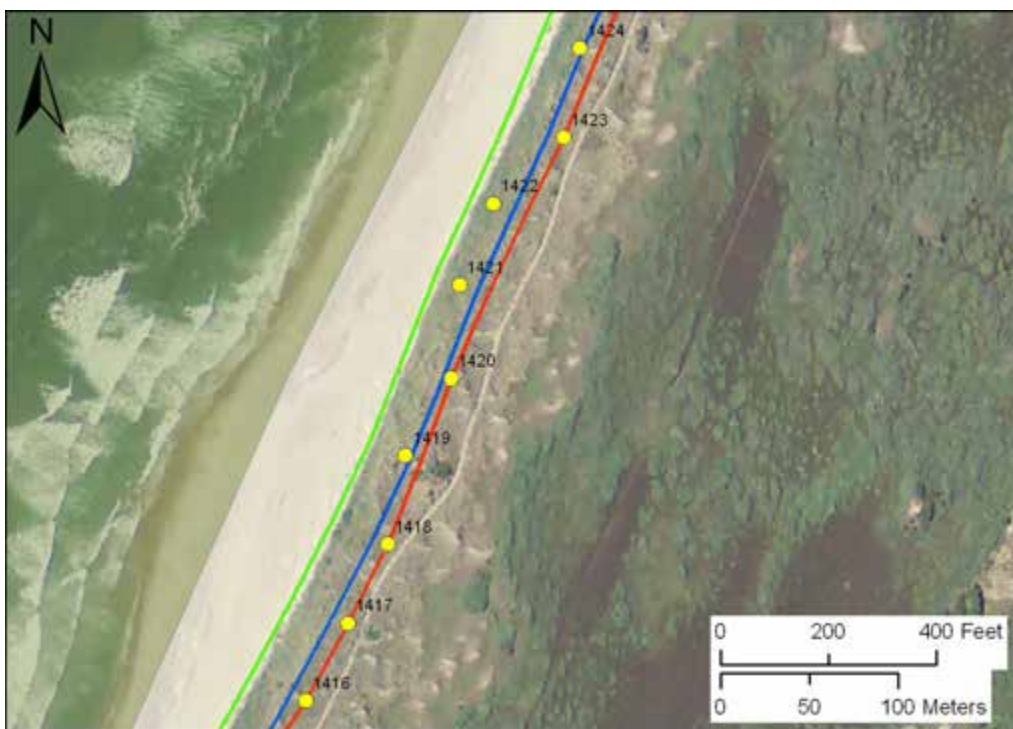


Figure 8-8. Plot showing the locations of the primary frontal dune (PFD; yellow dots), 6-m contour (green line), projected storm-induced erosion (blue line), and final V zone (red line). Green shading denotes the original A zone established in the 1970s. This example shows several profile sites (1419, 1421, 1422, and 1423) where the location of the V zone has been shifted east, initially to match the estimated storm erosion line, and then farther east to better conform with the adjacent PFDs (e.g., profiles 1420 and 1423).

8.2.2 V-zone mapping at creek mouths

At Ten Mile Creek in northern Coos County the creek eventually reaches the beach on the north Coos Spit. Figure 8-9 is a map of the alongshore morphology of the creek and beach. In this example, it can be seen that the PFDs are in fact located well seaward of the identified V zone. The reason for this discrepancy is that examination of 1967 historical aerial photographs of the area indicates that the mouth of the creek has varied its position significantly over the past 40 years. As can be seen in Figure 8-9 (top), the mouth of Ten Mile creek is presently (2009) located slightly north of the central part of the beach. In contrast, the mouth of the creek in 1967 was located much farther to the south. This type of morphological response is not unusual along the Oregon coast; many creeks are characterized by similar temporal variability. Furthermore, from observations else-

where on the Oregon coast (e.g., along Rockaway Beach and Gold Beach), it is not uncommon for creek mouths to change position in response to high ocean waves. Changes in sediment transport patterns may also push the creek mouth in one direction or the other. Periodically, during high river discharge, creeks may even breach sections of the beach. The variability of the location of the creek mouth increases the risk and uncertainty of flooding in these areas. Because of these issues, mapping of the V-zone line was adjusted on the basis of a combination of assessments of recent historical information (i.e., aerial photos) and contemporary information. We used a combination of approaches to help define the landward limit of the V zone, including information derived from the aerial photographs such as the presence of flotsam and debris, geomorphic indicators such as depressions where water may be ponding (e.g., wetlands), and lidar data to better constrain the terrain.

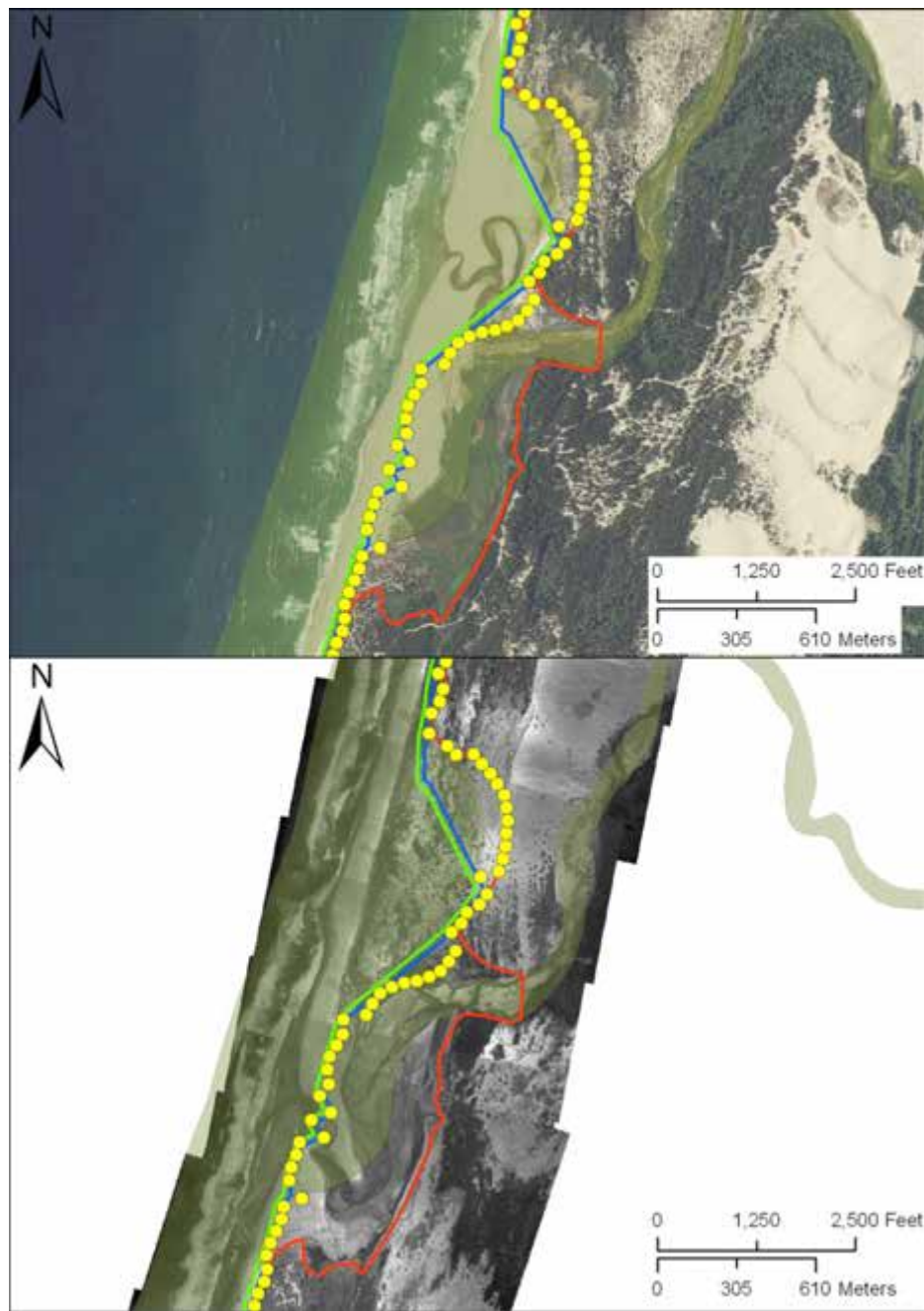


Figure 8-9. Example of V-zone mapping undertaken where a creek arrives at the coast and is subject to varying outlet locations. This example is for Ten Mile Creek in northern Coos County, Oregon.



Figure 8-10. V-zone mapping along coastal bluffs located on the south side of Cape Arago, Coos County, Oregon. Yellow dots denote the locations of the bluff/cliff top, while the red line reflects the 17-m (56-ft) runup contour elevation estimated using an adjusted DIM approach that is based on a pre-defined (deterministic) extreme storm scenario. The latter was used as a simple example to contrast two potential approaches for mapping V zones along coastal bluffs.

8.2.3 V-zone mapping along coastal bluffs

Finally, a significant section of coastline midway along Coos County is characterized by coastal bluffs of varying heights. We explored a variety of approaches that could be used to define V zones along this section of the coast. These options included:

1. Mapping the top of the bluff (Figure 8-10, yellow dots), which is a readily identifiable feature that can be used to constrain the landward extent of the V zone;
2. Defining a worst-case storm and based on a few representative bluff slopes, perform total water level calculations using the adjusted DIM approach. Figure 8-10 includes one such example, which yielded a 1% total water level of ~17 m (56 ft); and,
3. 1% total water level calculations could be undertaken based on the morphological parameters derived from the lidar profile analyses, and from the wave modeling results determined for the 20-m (65 -ft) bathymetry contour.

Each of these approaches has limitations. For example, the deterministic approach is problematic since it reflects a range of pre-defined storm parameters, including some form of average bluff slope and average adjustment factors. Alternatively, the complete total water level analysis would require significantly more time to complete at a far greater cost than is probably warranted for a section of coast that is largely unpopulated. As a result and after careful consideration and discussion with FEMA coastal staff, the approach adopted by DOGAMI was to map the top of the bluff using a combination of the lidar profile analyses (i.e., mapping the bluff top), assessments of lidar contour data, and examination of aerial photographs.

Acknowledgment. Funding provided by Federal Emergency Management Agency as part of the Flood Map Modernization program under Cooperating Technical Partner award EMS-2008-GR-0013.

9.0 REFERENCES

- Aguilar-Tunon, N. A., and Komar, P. D., 1978, The annual cycle of profile changes of two oregon beaches: Ore Bin, v. 40, no. 2, 25–39.
- Allan, J. C., and Hart, R., 2007, Assessing the temporal and spatial variability of coastal change in the neskowin littoral cell: Developing a comprehensive monitoring program for oregon beaches: Oregon Department of Geology and Mineral Industries Open-File Report O-07-01.
- Allan, J. C., and Hart, R., 2008, Oregon beach and shoreline mapping and analysis program: 2007-2008 beach monitoring report: Oregon Department of Geology and Mineral Industries Open-File Report O-08-15.
- Allan, J. C., and Komar, P. D., 2002a, A dynamic revetment and artificial dune for shore protection: American Society of Civil Engineers, Proceedings of the 28th International Conference on Coastal Engineering, Cardiff, Wales, July 7–12, 2002, v. 2, p. 2044-2056.
- Allan, J. C., and Komar, P. D., 2002b, Extreme storms on the pacific northwest coast during the 1997–98 El Niño and 1998–99 La Niña: *Journal of Coastal Research*, v. 18, no. 1, 175–193.
- Allan, J. C., and Komar, P. D., 2006, Climate controls on U.S. West Coast erosion processes: *Journal of Coastal Research*, v. 22, no. 3, 511–529.
- Allan, J. C., Komar, P. D., and Priest, G. R., 2003, Shoreline variability on the high-energy Oregon coast and its usefulness in erosion-hazard assessments, in Byrnes M. R., Crowell, M., and Fowler, C. (eds.), *Shoreline mapping and change analysis: technical considerations and management implications*: *Journal of Coastal Research*, Special Issue 38, p. 83–105.
- Allan, J. C., Hart, R., and Tranquilli, V., 2006, The use of passive integrated transponder tags (pit-tags) to trace cobble transport in a mixed sand-and-gravel beach on the high-energy Oregon coast, USA: *Marine Geology*, v. 232, no. 1-2, 63–86.
- Allan, J. C., Komar, P. D., Ruggiero, P., and Witter, R. C., 2012, The March 2011 Tōhoku tsunami and its impacts along the U.S. West Coast: *Journal of Coastal Research*, v. 28, no. 5, p. 1142–1153.
- Atwater, B. F., and others, 2005, The orphan tsunami of 1700—Japanese clues to a parent earthquake in North America: U.S. Geological Survey Professional Paper 1707, 133 p. Web: <http://pubs.usgs.gov/pp/pp1707/>.
- Baird, W. F., 2005, Pacific ocean wave information study validation of wave model results against satellite altimeter data: Madison, Wisc., Baird and Associates Ltd.
- Baldwin, E. M., and others, 1973, Geology and mineral resources of Coos County, Oregon: Oregon Department of Geology and Mineral Industries Bulletin 80.
- Bernstein, D. J., and others, 2003, Survey design analysis for three-dimensional mapping of beach and nearshore morphology: American Society of Civil Engineers, *Coastal Sediments '03*, St. Petersburg, Fla., p. 12.
- Booij, N., Ris, R. C., and Holthuijsen, L. H., 1999, A third-generation wave model for coastal regions, part I: model description and validation: *Journal of Geophysical Research*, v. 104, no. C4, 7649–7666.
- Carignan, K. S., and others, 2009, Digital elevation model of Port Orford, Oregon: procedures, data sources and analysis: U.S. Dept. of Commerce, Boulder, Colo., NOAA Technical Memorandum NESDIS NGDC-21, 32 p.
- CH2M HILL, 1995, Intermediate draft engineering report coastal flood insurance study for Bandon (Incorporated area) Coos County, Oregon (Community No. 410043): Bellevue, Wash., 130 p.
- Coles, S., 2001, An introduction to statistical modeling of extreme values. Springer-Verlag, London, 208 p.
- Cox, J. C., and Machemehl, J., 1986, Overload bore propagation due to an overtopping wave: *Journal of Waterway, Port, Coastal and Ocean Engineering*, v. 112, no. 1, 161–163.
- Dean, R. G., and Walton, T. L., 2009, Wave setup. In: K.C. Young (Editor), *Handbook of coastal and ocean engineering*. World Scientific Publishing, 1–23.
- Goldfinger, C., 2009, Paleoseismically derived probabilities for Cascadia great earthquakes: Geological Society of America 2009 Meeting, Oct. 18–21, 2009, Portland, Oreg., Program Abstracts, p. 520.
- Goldfinger, C., Nelson, C. H., and Johnson, J. G., 2003, Holocene earthquake records from the Cascadia Subduction Zone and northern San Andreas Fault based on precise dating of offshore turbidites: *Annual Review of Earth and Planetary Sciences*, v. 31, 555–577.
- Goldfinger, C., and others, 2009, Turbidite event history: methods and implications for holocene paleoseismicity of the Cascadia Subduction Zone: U.S. Geological Survey Professional Paper 1661-F.
- Hedges, T. S., and Mase, H., 2004, Modified Hunt's equation incorporating wave setup: *Journal of Waterway, Port, Coastal and Ocean Engineering*, v. 130, no. 3, 109–113.
- Holman, R. A., 1986, Extreme value statistics for wave runup on a natural beach: *Coastal Engineering*, v. 9, 527–544.

- Kelsey, H. M., Nelson, A. R., Hemphill-Haley, E., and Witter, R. C., 2005, Tsunami history of an Oregon coastal lake reveals a 4600 yr record of great earthquakes on the Cascadia subduction zone: Geological Society of America Bulletin, v. 117, no. 7/8, 1009–1032.
- Komar, P. D., 1997, The Pacific Northwest coast: living with the shores of Oregon and Washington: Duke University Press, Durham and London, 195 p.
- Komar, P. D., 1998, Beach processes and sedimentation: Englewood Cliffs, N. J.: Prentice Hall, Inc., 544 p.
- Komar, P. D., and Gaughan, M. K., 1972, Airy wave theory and breaker height prediction: Proceedings Thirteenth Coastal Engineering Conference, Vancouver, B.C., p. 405–418.
- Komar, P. D., Lizarraga-Arciniega, J. R., and Terich, T. A., 1976, Oregon coast shoreline changes due to jetties: Journal of the Waterways, Harbors and Coastal Engineering Division, American Society of Civil Engineers, v. 102(WW1), 13–30.
- Komar, P. D., Torstenson, R.W., and Shih, S.-M., 1991, Bandon, Oregon: Coastal development and the potential for extreme ocean hazards: Shore & Beach, v. 59, no. 4, 14–22.
- Komar, P. D., McDougal, W. G., Marra, J. J., and Ruggiero, P., 1999, The rational analysis of setback distances: applications to the oregon coast: Shore & Beach, v. 67, 41–49.
- Komar, P. D., Allan, J. C., Diaz-Mendez, G. M., Marra, J. J., and Ruggiero, P., 2000, El Niño and La Niña—erosion processes and impacts: American Society of Civil Engineers, Proceedings of the 27th International Conference on Coastal Engineering, Sydney, Australia, July 16–21, 2000, p. 2414–2427.
- Komar, P. D., Allan, J. C., and Winz, R., 2003, Cobble beaches—the “design with nature” approach for shore protection: Coastal Sediments’ 03, 5th International Symposium on Coastal Engineering and Science of Coastal Sediment Processes, Clearwater Beach, Fla., May 18–23, 2003.
- Komar, P. D., Allan, J. C., and Ruggiero, P., 2011, Sea level variations along the U.S. Pacific Northwest coast: tectonic and climate controls: Journal of Coastal Research, v. 27, no. 5, 808–823.
- Komar, P. D., Diaz-Mendez, G. M., and Marra, J. J., 2001, Stability of the new river spit, and the position of oregon’s beach-zone line: Journal of Coastal Research, v. 17, no. 3, 625–635.
- Kriebel, D. L., and Dean, R. G., 1993, Convolution method for time-dependent beach-profile response: Journal of Waterway, Port, Coastal and Ocean Engineering, v. 119, no. 2, 206–226.
- Marra, J., 2002, Background report, chronic coastal natural hazards: 2002 update.
- Mori, N., Takahashi, T., Yasuda, T., and Yanagisawa, H., 2011, Survey of 2011 Tōhoku earthquake tsunami inundation and run-up: Geophysical Research Letters, v. 38(L00G14), 6.
- Morton, R. A., Leach, M.P., Paine, J. G., and Cardoza, M. A., 1993, Monitoring beach changes using GPS surveying techniques: Journal of Coastal Research, v. , no. 3, 702–720.
- NHC (Northwest Hydraulics Consultants), 2005, Final draft guidelines for coastal flood hazard analysis and mapping for the Pacific coast of the United States: West Sacramento, Calif., Northwest Hydraulics Consultants, report prepared for FEMA, final draft prepared November 2004, Section D.4.5 revised January 2005.
- Ozkan-Haller, H. T., and others, 2009, Sediment transport study; baseline observations and modeling for the Reed-sport wave energy site, Oregon State University and the Oregon Department of Geology and Mineral Industries, Corvallis, Oreg., 35 p.
- Peterson, C. D., Darienzo, M. E., Hamilton, D., Pettit, D. J., Yeager, R. K., Jackson, P. L., Rosenfeld, C. L., and Terich, T. A., 1994, Beach-shoreline database, Pacific Northwest Region, USA: Portland, Oreg., Oregon Department of Geology and Mineral Industries Open-File Report 0-94-2, 29 p.
- Peterson, C. D., and others, 2007, Ages, distributions, and origins of upland coastal dune sheets in Oregon, USA: Geomorphology, v. 91, 80–102.
- Priest, G. R., Goldfinger, C., Wang, K., Witter, R. C., Zhang, Y., and Baptista, A., 2009, Confidence levels for tsunami-inundation limits in northern Oregon inferred from a 10,000-year history of great earthquakes at the Cascadia subduction zone: Natural Hazards, v. 54, no. 1, p. 27–73.
- Pullen, T., and others, 2007, EurOtop — wave overtopping of sea defences and related structures: assessment manual. Web: <http://www.overtoppingmanual.com>
- Ris, R. C., Booij, N., and Holthuijsen, L. H., 1999, A third-generation wave model for coastal regions, part II: Verification: Journal of Geophysical Research, v. 104(C4), 7667–7681.
- Ruggiero, P., and Voigt, B., 2000, Beach monitoring in the Columbia River littoral cell, 1997–2000: Olympia, Wash., Washington Department of Ecology, Coastal Monitoring and Analysis Program, Publication No. 00-06-026., 113 p.
- Ruggiero, P., Komar, P. D., McDougal, W. G., Marra, J. J., and Beach, R. A., 2001, Wave runup, extreme water levels and the erosion of properties backing beaches: Journal of Coastal Research, v. 17, no. 2, 407–419.

- Ruggiero, P., Kaminsky, G. M., Gelfenbaum, G., and Voight, B., 2005, Seasonal to interannual morphodynamics along a high-energy dissipative littoral cell: *Journal of Coastal Research*, v. 21, no. 3, 553–578.
- Ruggiero, P., Buijsman, M. C., Kaminsky, G. M., and Gelfenbaum, G., 2010a, Modeling the effects of wave climate and sediment supply variability on large-scale shoreline change: *Marine Geology*, v. 273, 127–140.
- Ruggiero, P., Komar, P. D., and Allan, J. C., 2010b, Increasing wave heights and extreme value projections: the wave climate of the U.S. Pacific Northwest: *Coastal Engineering*, v. 57, no. 5, 539–552.
- Satake, K., Shemazaki, K., Yoshinobu, T., and Ueda, K., 1996, Time and size of a giant earthquake in Cascadia inferred from Japanese tsunami records of January 1700: *Nature*, v. 379, no. 6562, 246–249.
- Smith, J. M., Sherlock, A. R., and Resio, D. T., 2001, STWAVE: Steady-state spectral wave model user's manual for stwave, version 3.0: Vicksburg, Miss., U.S. Army Engineer Research and Development Center, Coastal and Hydraulics Laboratory, Technical Report ERDC/CHL SR-01-1, 80 p.
- Stockdon, H. F., Holman, R. A., Howd, P. A., and Sallenger, A. H., 2006, Empirical parameterization of setup, swash, and runup: *Coastal Engineering*, v. 53, no. 7, 573–588.
- Thieler, E. R., Himmelstoss, E.A., Zichichi, J.L., and Ayhan, E., 2009, Digital shoreline analysis system (DSAS) version 4.0—an ArcGIS extension for calculating shoreline change: U.S. Geological Survey Open-File Report 2008-1278. Web: <http://woodhole.er.usgs.gov/project-pages/dsas/version4/>
- Tillotson, K., and Komar, P. D., 1997, The wave climate of the Pacific Northwest (Oregon and Washington): A comparison of data sources: *Journal of Coastal Research*, v. 13, no. 2, 440–452.
- Trimble, 2005, Trimble 5700 GPS system datasheet: Dayton, Ohio, Trimble Navigation Limited, 2 p. Web: http://www.trimble.com/5700_ds.asp
- van der Meer, J. W., 2002, Technical report wave run-up and wave overtopping at dikes: Delft, Netherlands, Technical Advisory Committee on Flood Defence, 42 p.
- Witter, R. C., 2008, Prehistoric Cascadia tsunami inundation and runup at Cannon Beach, Clatsop County, Oregon: Oregon Department of Geology and Mineral Industries Open-File Report 0-08-12.
- Witter, R. C., Kelsey, H. M., and Hemphill-Haley, E., 2003, Great Cascadia earthquakes and tsunamis of the past 6700 years, Coquille River estuary, southern coastal Oregon: *Geological Society of America Bulletin*, v. 115, 1289–1306.
- Witter, R. C., Zhang, Y., Goldfinger, C., Priest, G. R., and Wang, K., 2010, Validating numerical tsunami simulations in southern Oregon using late Holocene records of great Cascadia earthquakes and tsunamis: *Seismological Society of America 2010 Annual Meeting*, Portland, Oreg. p. 290.
- Wright, L. D., and Short, A. D., 1983, Morphodynamics of beaches and surf zones in Australia, in Komar, P. D. (Ed.), *Handbook of coastal processes and erosion*: CRC Press, Boca Raton, Fla., p. 35–64.
- Yamamoto, M., 2011, IOC/UNESCO Bulletin No. 17 (April 5, 2011) - Tōhoku Tsunami March 11, 2011 p.

APPENDIX A. GROUND SURVEY ACCURACY ASSESSMENT PROTOCOLS DETERMINED BY WATERSHED SCIENCES, INC.

A.1 Base station protocols

Whenever possible, existing and established survey benchmarks shall serve as control points during lidar acquisition. The National Geodetic Survey (NGS) provides an online searchable database of survey benchmarks. In addition, county surveyor's offices often establish their own benchmarks. NGS benchmarks are preferred for control. In the absence of NGS benchmarks, county survey offices may be able to provide additional control points. While some county surveyor's offices will make benchmark data available online, a phone call to the office will likely be needed to determine whether benchmark data exist and whether they can be accessed. All GPS measurements should be taken on public property or public easements when possible. For GPS measurements on private property, the property owner must grant access.

The project control point will be occupied by a GPS base station for an initial period of at least six hours. This occupation occurs during the lidar acquisition. When NGS benchmarks are available as project control points, the occupation time can be reduced to match the data acquisition period if acquisition requires less than six hours, but the occupation period should be no less than four hours on a NGS benchmark.

All GPS measurements must be made with dual frequency L1-L2 receivers with carrier-phase correction. All GPS measurements must be made during periods with PDOP (position dilution of precision) less than or equal to 3.0 and with at least six satellites in view of both a stationary reference receiver and the roving receiver.

To provide redundancy in project control measurements, a second GPS base station occupation occurs during the same period as the initial project control point occupation. The second base station is placed in close enough proximity to cover the acquisition area should something go wrong and the initial base station fails.

The NGS online positioning user service (OPUS) is used to generate a corrected position for all base station observations. OPUS provides a measurement solution based on three surrounding continuously operating reference stations (CORS). OPUS output includes a solution report with positional accuracy confidence intervals for adjusted coordinates and elevations. The solution report is one component in assessing the quality of the adjusted static GPS measurements.

Further occupations for project control points are required when a NGS or other established benchmark is not used. Subsequent observations during the acquisition period will require an occupation of at least three hours, unless the nearest CORS station is greater than 80 km (50 mi) away from the project control point. A minimum occupation period of four hours is required when the distance exceeds 80 km (50 mi).

Statistical checks of GPS base station positions and repeat control point observations include the OPUS extended output report that results when an OPUS solution is created. These checks also include the standard deviation, kurtosis, and skew of the measurement distribution for each base station occupation. Longitude, latitude, and elevation distributions are separated, and graphic distributions of the positions are plotted. Mission detail for each occupation should also include length of observation time and dilution of precision (DOP) ranges (average, minimum, and maximum) that occurred during the observation. The combination of this statistical output is used to assess whether measurement distributions are normally distributed and within acceptable tolerances.

A.2 RTK protocols

Real-time kinematic (RTK) GPS positions are collected throughout the project area to provide individual checkpoints for lidar positions. RTK positions include coordinates and elevations. All RTK measurements should be taken on public property or public easements when possible. For RTK measurements on private property, the property owner must grant access.

RTK positions must be collected on 20% of the flight lines and on bare-earth locations such as roads, mowed fields, and other locations where the ground is clearly visible (and is likely to remain visible) from the sky during the data acquisition and RTK measurement period(s). In order to facilitate comparisons with lidar measurements, RTK measurements should not be taken on highly reflective surfaces such as center line stripes or lane markings on roads. In addition, it is desirable to include locations that can be readily identified and occupied during subsequent field visits in support of other quality control procedures described later. Examples of identifiable locations include manhole and other flat utility structures that have clearly indicated center points or other measurement locations. In

the absence of utility structures, a PK nail can be driven into asphalt or concrete and marked with paint or an aluminum tag.

RTK measurements should be collected no closer than 3 m (10 ft) (about four steps for most people) from one another to support measurement independence. An RTK point acquisition period shall be 5 seconds long and include three individual 1-second measurements that will be averaged together. This is the default Trimble Specification for RTK. The 5-second observation period allows the GPS rover to check and ensure an accurate point is taken. RTK points will not be taken during periods with PDOP greater than 3, horizontal and vertical RMS values are greater than 0.030, or with fewer than than six visible satellites. An RTK checkpoint shall also be taken at the beginning and end of each base station session as close to the base station location as possible to provide an on-the-spot vertical accuracy check.

The position of flight lines to be tested is also important. Flight lines should be selected on the basis of transportation access and location on publicly owned lands and right-of-ways unless permission has been secured from the property owner ahead-of-time. In addition to these considerations, potential testable flight lines are evaluated by calculating the number of flight lines needed to meet the 20% criteria. In the case of 34 flight lines, 0.20 is multiplied by 34, with the result (6.4) being rounded up to the next highest integer: 7 flight lines. When possible the flight lines should also be systematically spread throughout the project area and not consistently located adjacent to each other. A goal in this example would be to have RTK measurements taken generally every fourth or fifth flight line such that at least seven flight lines are visited. A minimum of 60 RTK positions should be recorded along each flight line wherever possible.

A comparison of RTK elevations and the lidar-derived modeled ground surface provides a means of assessing overall vertical accuracy for the entire lidar dataset. The distribution of elevation differences between RTK data and the ground surface model are plotted and characterized with descriptive statistics to provide a means for evaluating internal consistency of the RTK point dataset. Root mean squared error (RMSE) and standard deviation for the differences between RTK points and ground surface model are calculated to evaluate bias in the lidar data. Systematic bias identified by the RMSE statistic is modeled out of the lidar dataset. The value for 1-sigma of the differences between RTK and modeled ground surface is defined as the 67th percentile of the absolute value of the differences. To meet vertical accuracy specifications, the 1-sigma value for a delivered lidar dataset must not exceed 15 cm (5.9 in).

A.3 Monument and RTK results

A.3.1 Monuments

Whenever possible, multiple sessions were observed at base station locations. All sessions were statistically compared to each other in order to ensure accurate base station coordinates and elimination of systematic errors that might otherwise be incorporated into the data. At least three observations and a standard deviation of 1 cm or less among observations in the Northing, Easting, and Ellipsoidal fields was required for a base station location to be used for lidar flight processing purposes, with NGS sites being the exception to this rule. In some cases of monuments used for RTK purpose a three-session minimum was not possible. This occurred in locations where flight acquisition locations changed in the span of a day or two and the ground crew had to move base locations in order to collect RTK in new acquisition flightline locations. For these locations an initial minimum 6-hour first session was observed and was followed by a half-hour session to verify measurements from initial occupation. Table A.1 lists the base stations and measurement statistics from the Oregon Lidar Consortium (OLC) South Coast Project.

A.3.2 RTK

All RTK points were collected in reference to base station locations that followed base station protocols. RTK checkpoints were preformed both before and after RTK survey points were collected in order to provide on-the-spot quality control checks and to ensure accurate data. As of March 23, 2009, the RTK count for the OLC South Coast Project was 24,277 points and the flightline count was 2012. These numbers are subject to small changes as the project is completed. Of the 2012 total project flightlines, 533 include RTK. The percentage of flightlines covered is 26%, 6% above the 20% threshold target.

Table A.1. Base stations and measurement statistics from the Oregon Lidar Consortium South Coast Project.

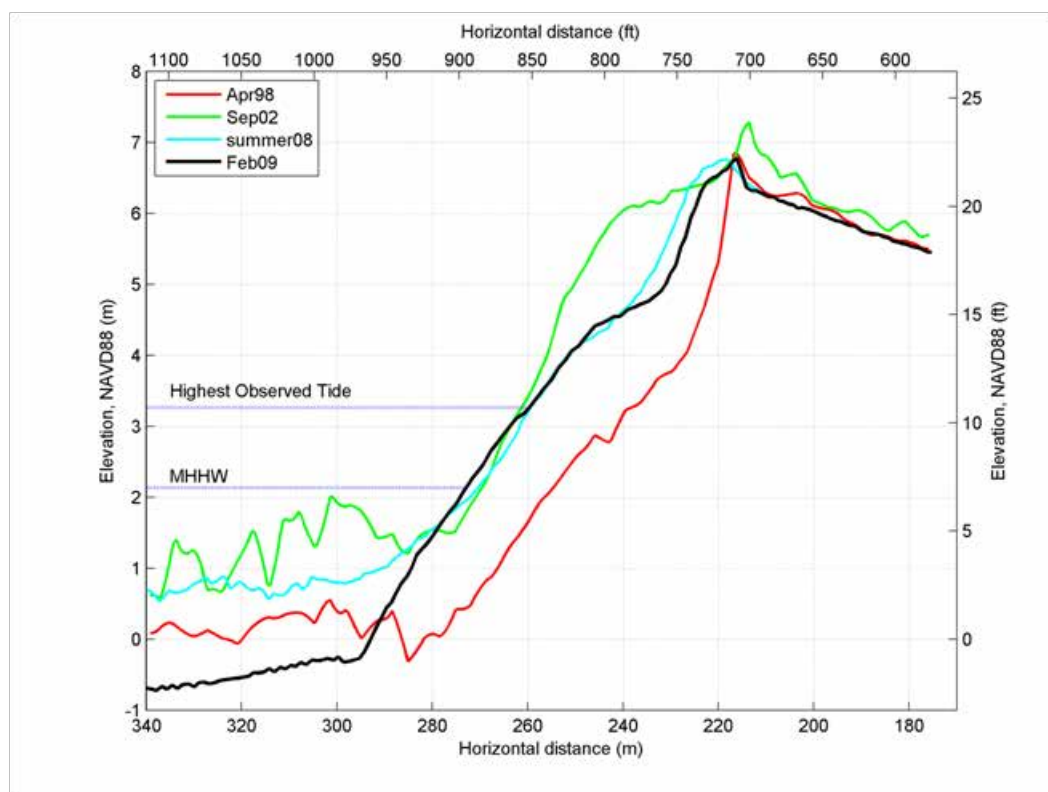
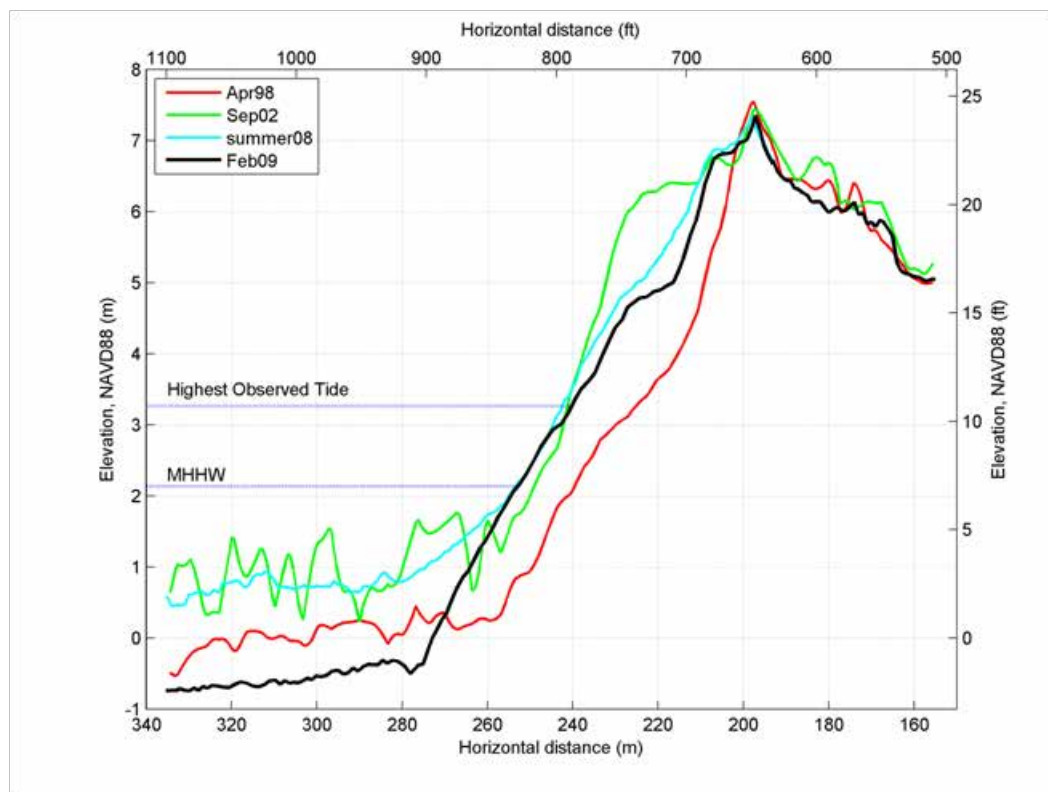


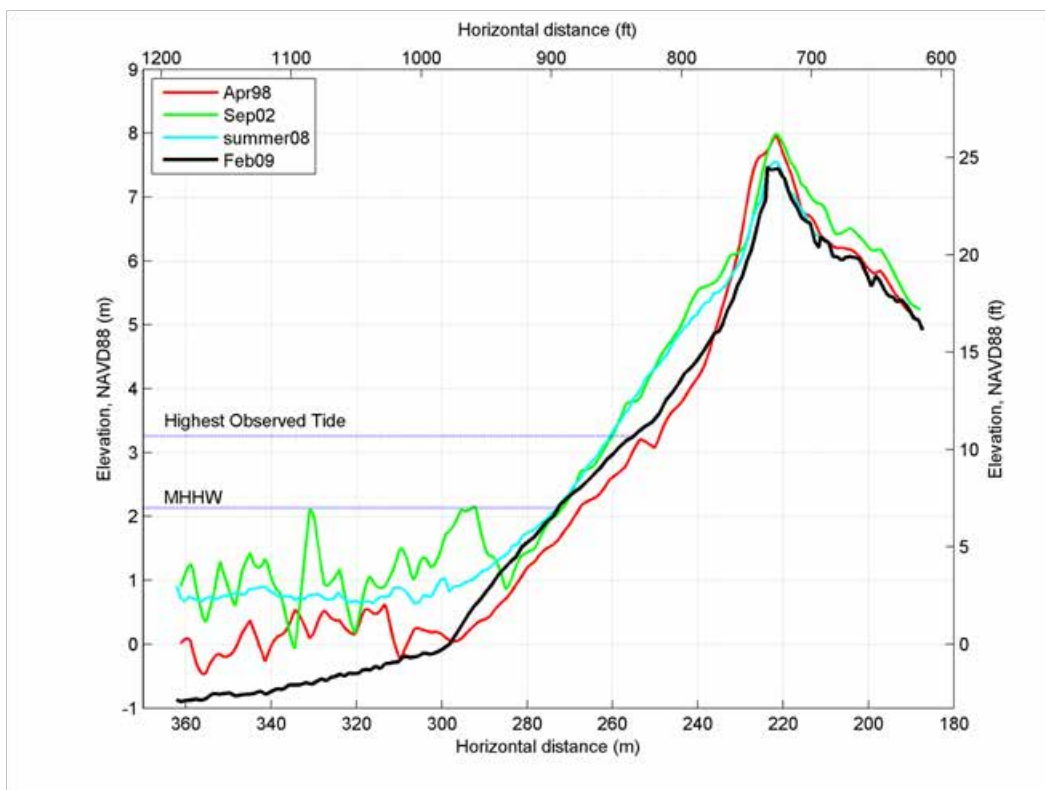
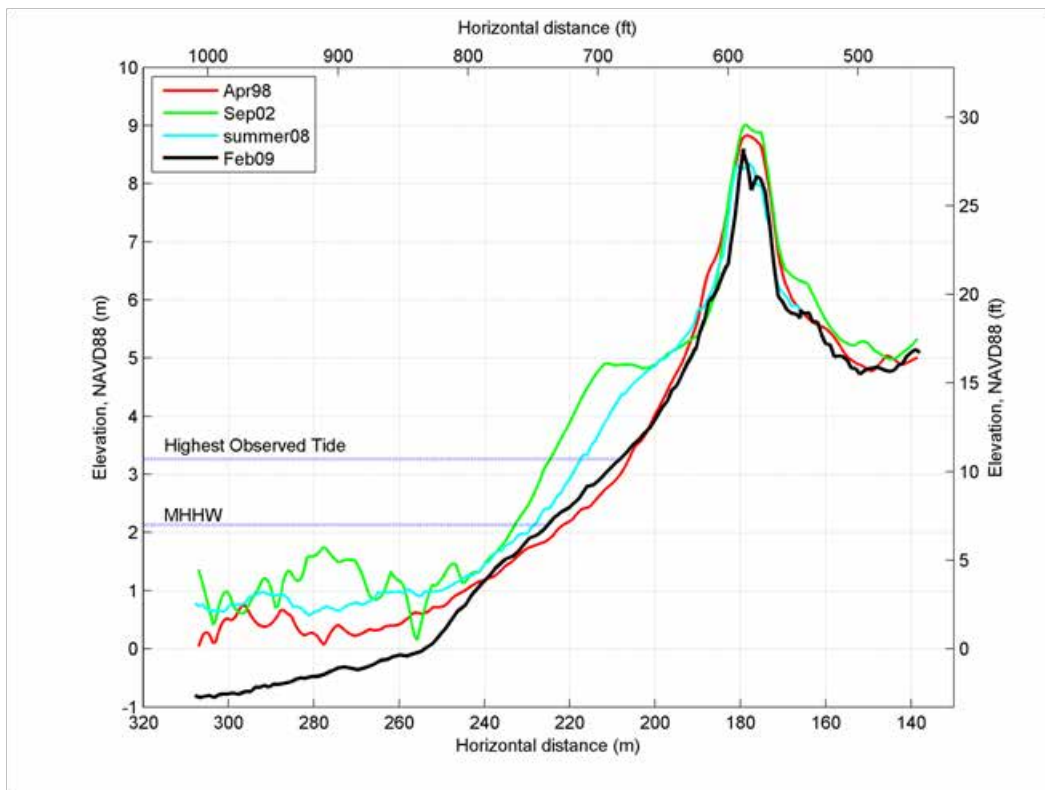
: Used for flight processing
: RTK only

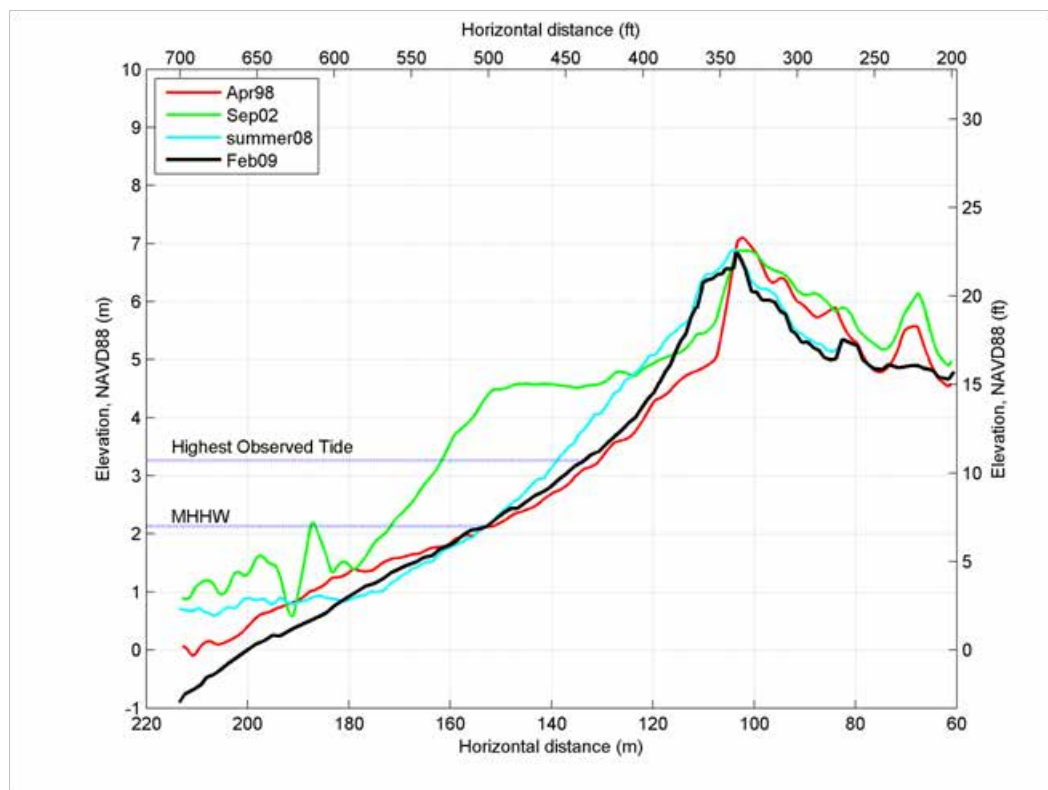
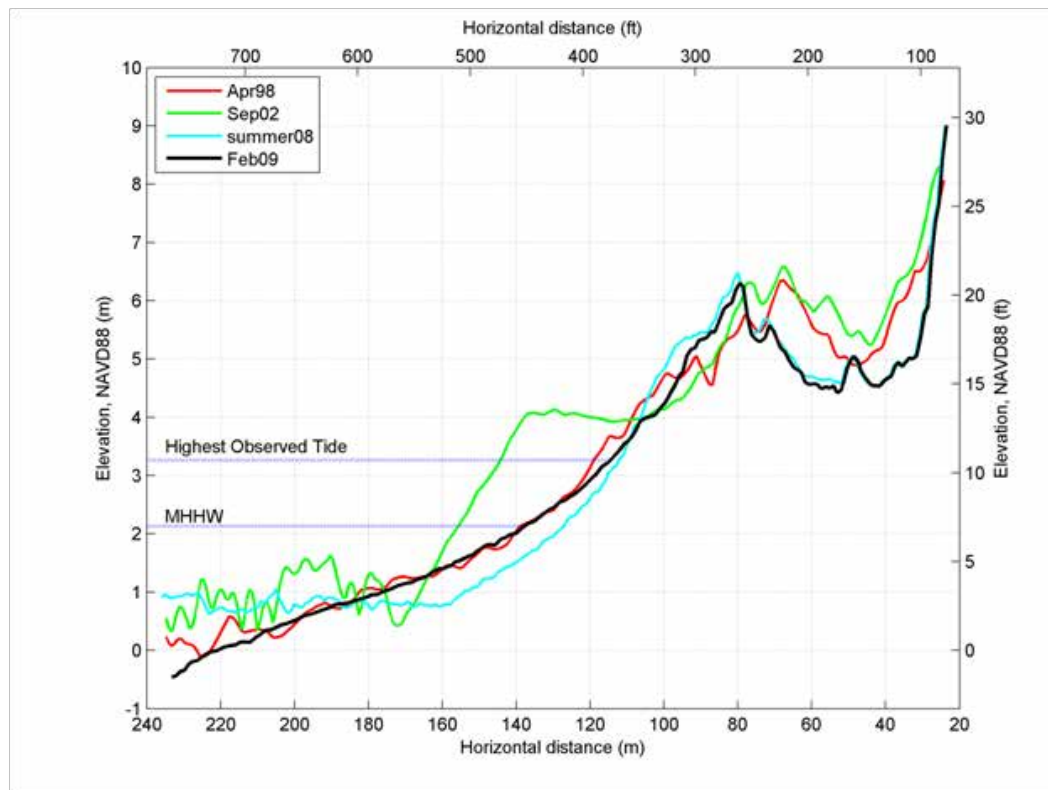
PID	Northing (m)	Std Dev	Easting (m)	Std Dev	Ellip (m)	Std Dev	# Obs
OLCJN1	4666220.858	<0.01	399711.396	<0.01	428.475	<0.01	12
OLCJN2	4666155.322	<0.01	399706.338	<0.01	427.870	<0.01	8
OLCJN3	4656275.052	n/a	393108.055	n/a	1.811	n/a	1
OLCJN4	4657589.207	<0.01	399651.388	<0.01	31.933	<0.02	2
OLCJN5	4702637.625	<0.01	389332.665	<0.01	-21.890	<0.01	2
OLCJN6	4698044.799	<0.01	382642.986	<0.01	-19.346	<0.01	2
OLCJN7	4740657.581	<0.01	378229.471	<0.01	33.225	<0.01	2
OLCJN8	4779201.413	<0.01	387890.854	<0.01	-19.734	<0.01	2
OLCJN9	4738140.397	n/a	378849.089	n/a	-13.568	n/a	1
OLCJN10	4762425.185	<0.01	443449.247	<0.01	307.728	<0.01	9
OLCJN11	4756051.474	n/a	436586.997	n/a	543.201	n/a	1
OLCPWH1	4687270.124	<0.01	382506.977	<0.01	177.778	<0.01	19
OLCPWH2	4710287.912	<0.01	385042.422	<0.01	-13.175	<0.01	19
OLCPWH3	4702124.511	<0.01	387970.167	<0.01	-15.340	<0.01	2
OLCPWH4	4681309.086	<0.01	384202.897	<0.01	-21.678	<0.01	2
OLCPWH5	4740298.491	<0.01	390768.356	<0.01	68.264	<0.01	14
OLCPWH6	4776402.725	<0.01	389970.028	<0.01	-22.854	<0.01	12
OLCPWH7	4743708.796	<0.01	372662.857	<0.01	32.003	<0.01	2
OLCPWH8	4780741.819	<0.01	402442.921	<0.01	-19.743	<0.01	11
OLCPWH9	4759314.063	<0.01	434620.842	<0.01	733.518	<0.01	9
OLCPWH10	4790269.129	<0.01	433439.918	<0.01	285.251	<0.01	5
OLCPWH11	4779682.074	<0.01	414713.410	<0.01	62.611	<0.01	11
OLCPWH12	4790270.270	<0.01	4790270.270	<0.01	285.248	<0.01	2
OLCPWH13	4761862.735	<0.01	427539.620	<0.01	50.495	0.01	7
OLCPWH14	4760221.999	n/a	431534.642	n/a	328.574	n/a	1
OLCPWH15	4755161.790	<0.01	410445.287	<0.01	43.503	0.01	5
OLCPWH16	4750402.292	<0.01	408211.552	<0.01	117.941	<0.01	3
OLCPWH17	4801727.123	<0.01	412411.585	<0.01	-19.865	<0.01	5
OLCBTK1	4664562.643	n/a	391698.742	n/a	295.173	n/a	1
OLCBTK2	4658270.548	<0.01	391242.844	<0.01	-16.064	<0.01	2
OLCBTK3	4666680.742	n/a	387928.675	n/a	-6.578	n/a	1
OLCBTK4	4655631.143	n/a	395065.180	n/a	-21.946	n/a	1
OLCCF1	4757729.860	n/a	409032.158	n/a	28.559	n/a	1
OLCCF2	4757586.134	<0.01	408789.877	<0.01	102.674	<0.01	3
OLCCF3	4764953.485	<0.01	409391.804	<0.01	-7.289	<0.01	2
6NCM1	4864905.915	<0.01	416192.929	<0.01	41.926	<0.01	10
6NCM2	4839596.009	<0.01	410973.605	<0.01	-19.441	<0.01	10
7SLM1	4822112.593	<0.01	433279.632	<0.01	162.416	<0.01	5
7NCM1	4842411.205	n/a	442191.044	n/a	467.113	n/a	1
7NCA1	4842411.196	<0.01	442191.046	<0.01	467.110	<0.01	3
7NCA2	4842403.553	<0.01	442186.080	<0.01	467.500	<0.01	4
OLC5CD1	4789602.399	<0.01	427784.309	<0.01	217.600	<0.01	4
OLC5CD2	4799242.703	<0.01	402825.444	<0.01	-20.988	<0.01	7
OLC5CD3	4799963.451	n/a	426243.777	n/a	241.631	n/a	1
OLC5PGW1	4800631.429	<0.01	391634.520	<0.01	-2.435	<0.02	3
OLC6MSD1	4834028.062	<0.01	426389.093	<0.01	-18.560	<0.01	2
OLC6MSD2	4834030.383	<0.01	426376.813	<0.01	-18.419	<0.01	10
OLC6MSD3	4816762.790	<0.01	401446.106	<0.01	-12.939	<0.01	12
OLC7SAR1	4822812.778	<0.01	433574.635	<0.01	107.432	<0.01	5
OLC7SAR2	4823831.775	0.01	431686.482	<0.01	273.317	<0.01	8
OLC7SAR3	4822804.862	n/a	433577.377	n/a	107.470	n/a	1
CPOLC8_1	4870228.327	<0.01	413213.139	<0.01	-16.692	<0.01	5
JCALR1	4822669.266	<0.01	455210.461	<0.01	46.642	<0.01	3
JCMSD1	4822667.079	<0.01	455208.743	<0.01	46.580	<0.01	2
JCMSD2	4804407.327	n/a	471039.121	n/a	103.132	n/a	1
JCMSD3	4813754.699	<0.03	460961.284	<0.01	51.759	<0.01	2
OLC6AR1	4838594.441	n/a	416264.271	n/a	-20.149	n/a	1
DH7020	4771371.788	n/a	385455.552	n/a	7.977	n/a	1
OA0754	4772733.838	n/a	384826.047	n/a	-0.860	n/a	1
AA5136	4747265.302	n/a	387928.675	n/a	-6.578	n/a	1

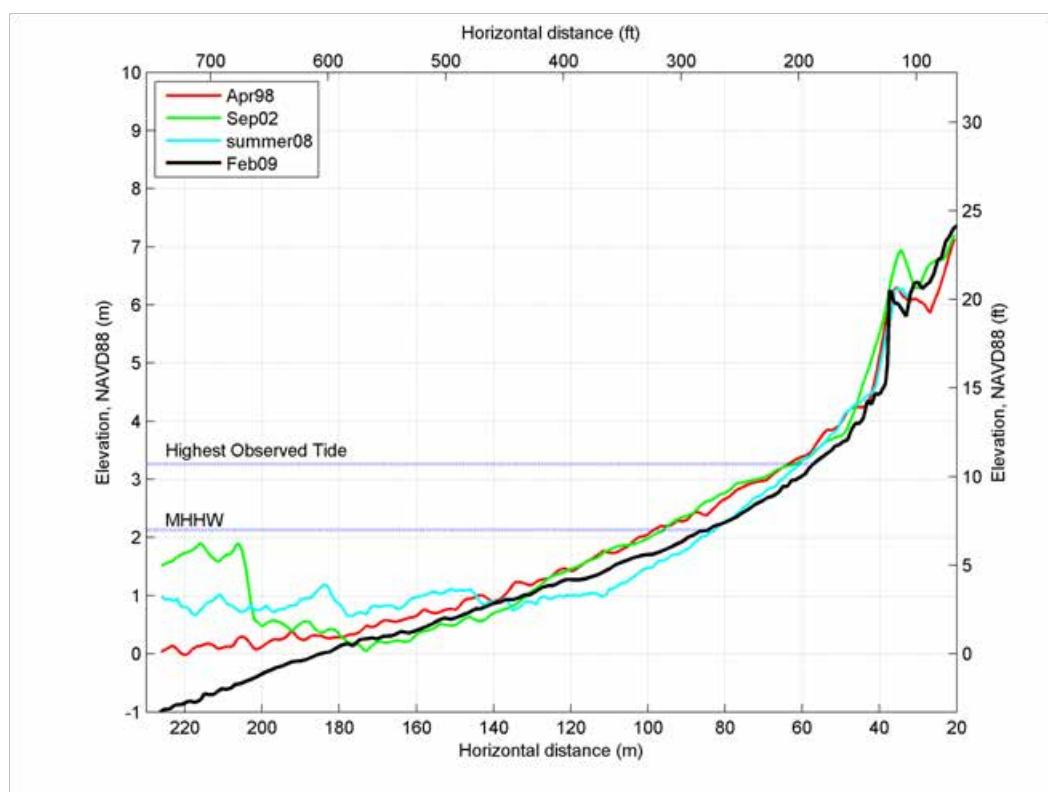
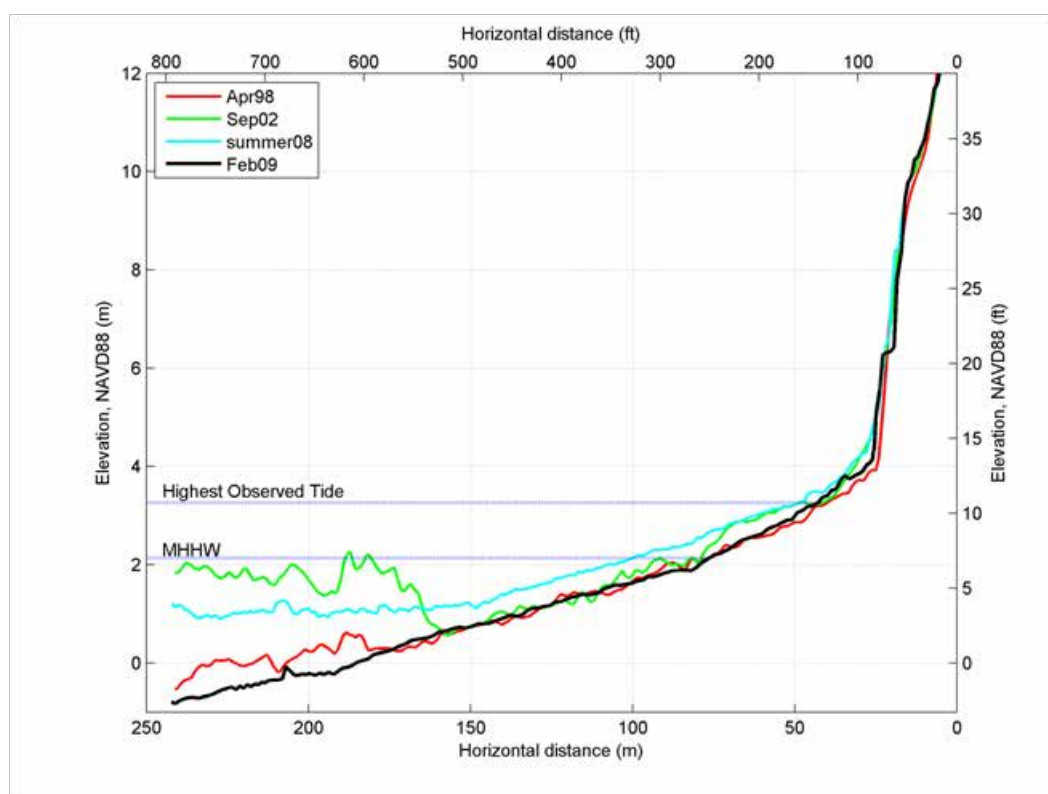
PID is the NGS Permanent Identifier, Std Dev is standard deviation, Ellip is ellipsoidal, and #Obs is number of observations.

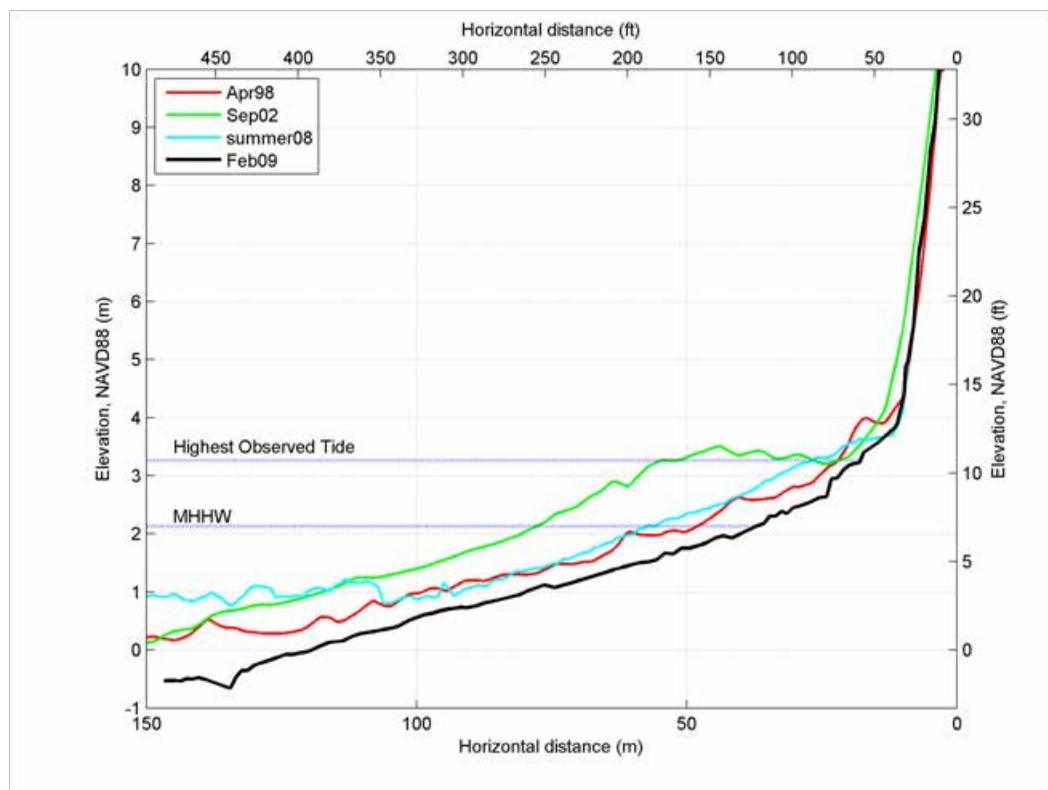
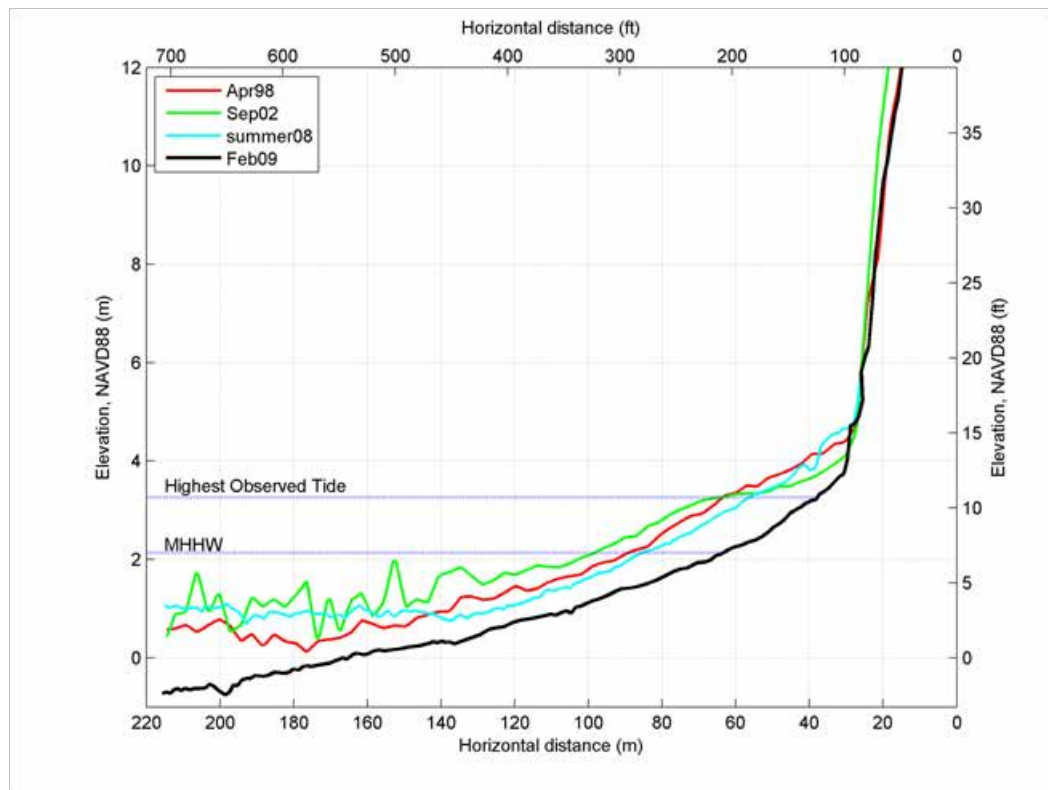
BANDON BEACH PROFILES

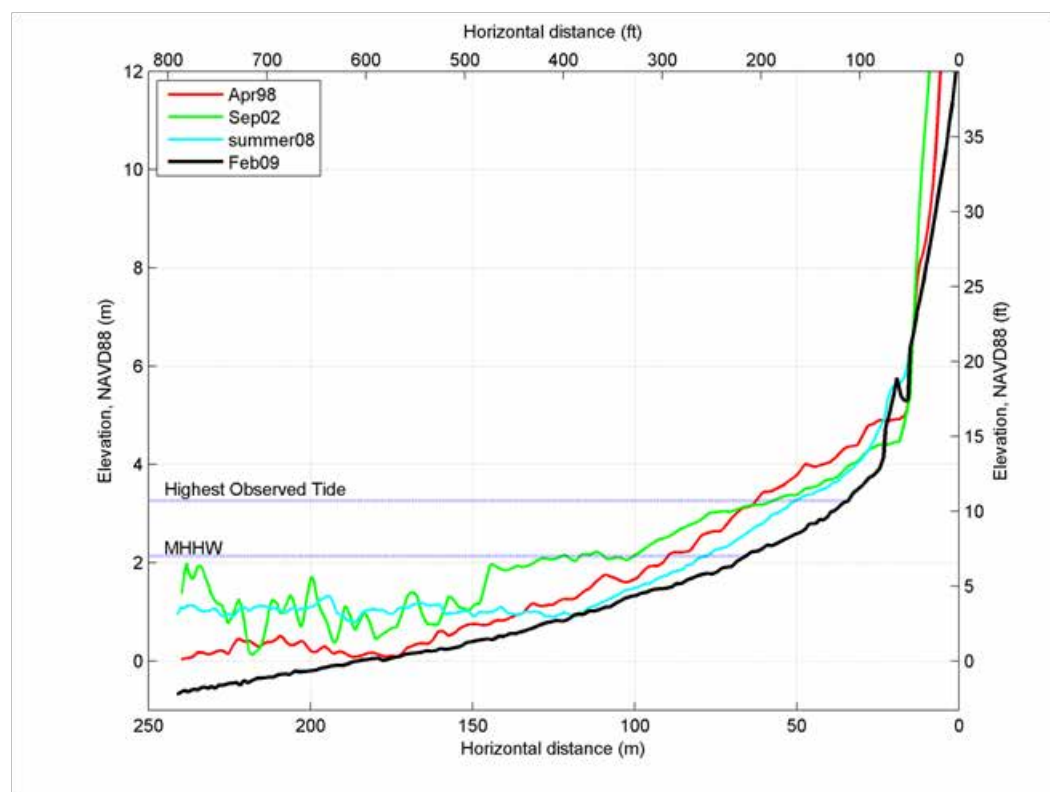
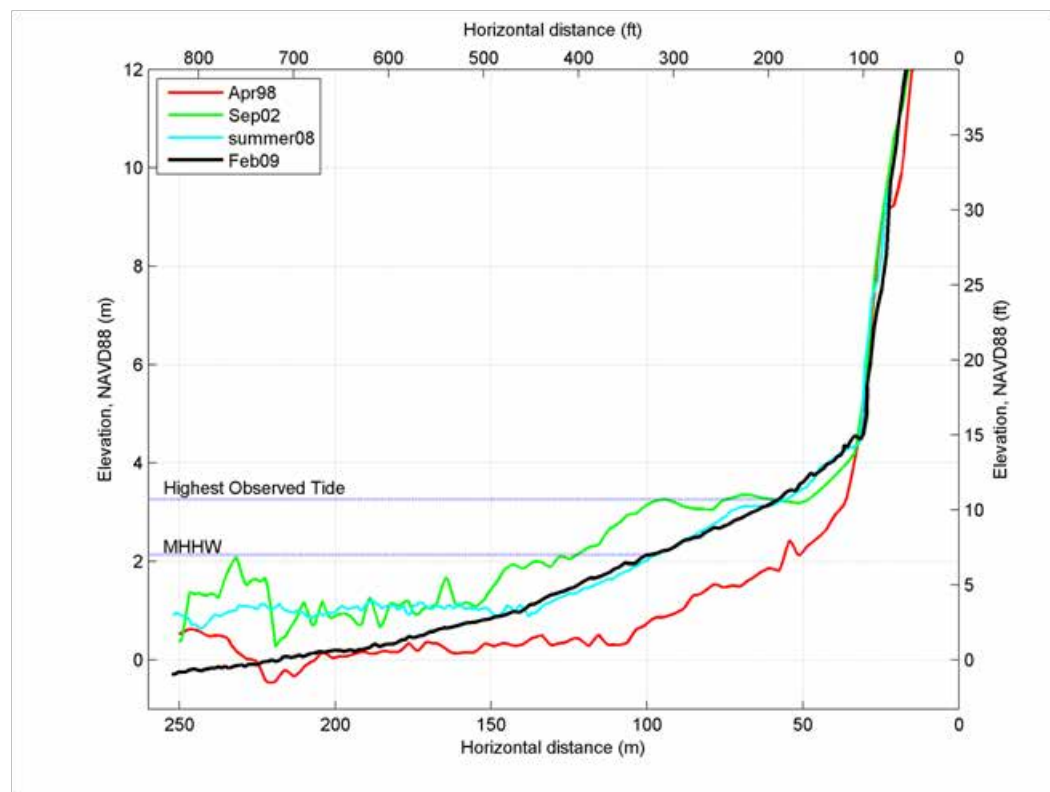
Bandon 1**Bandon 2**

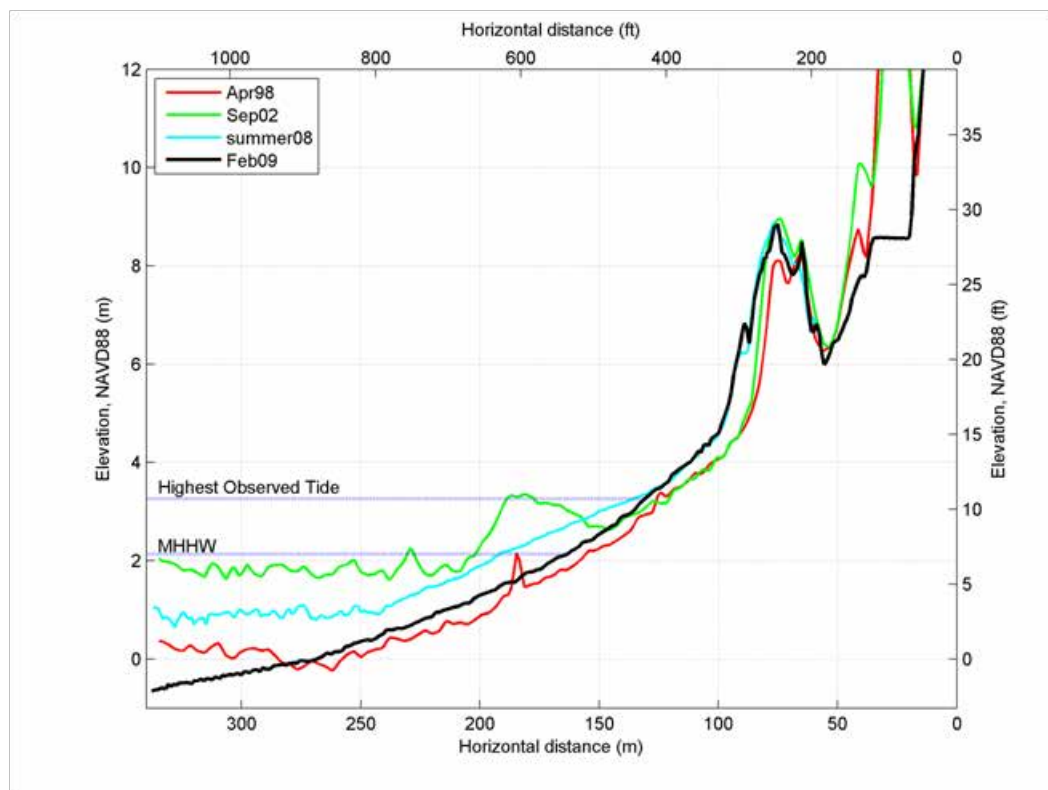
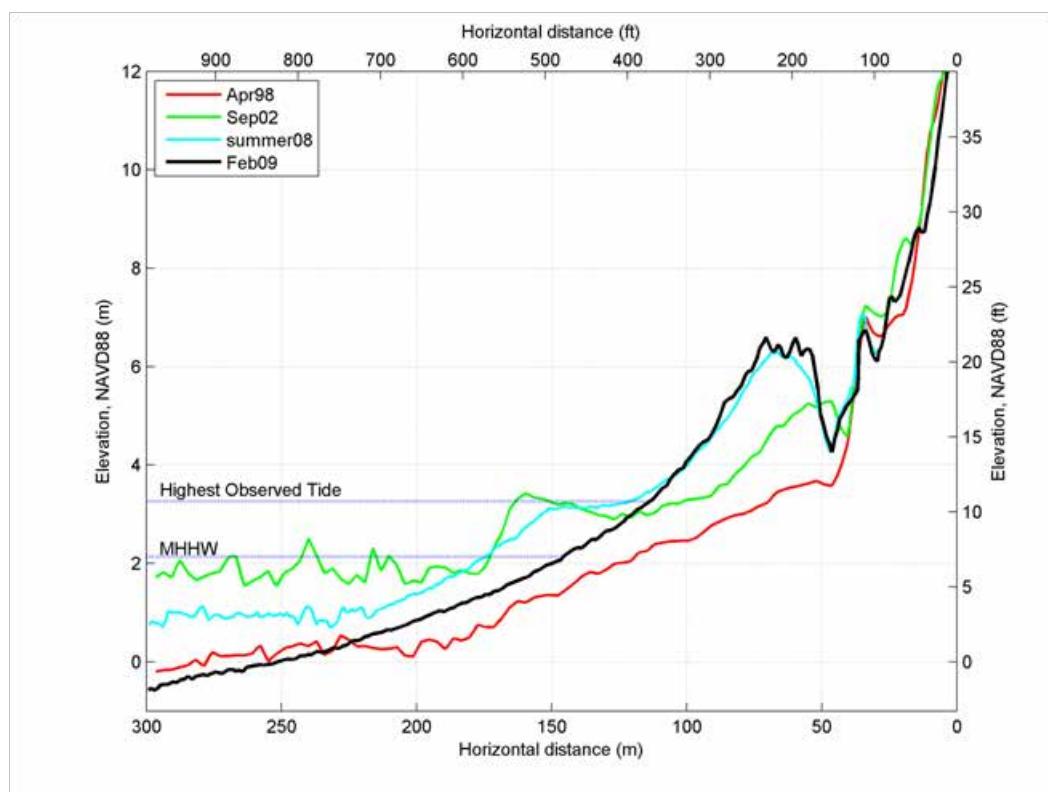
Bandon 3**Bandon 4**

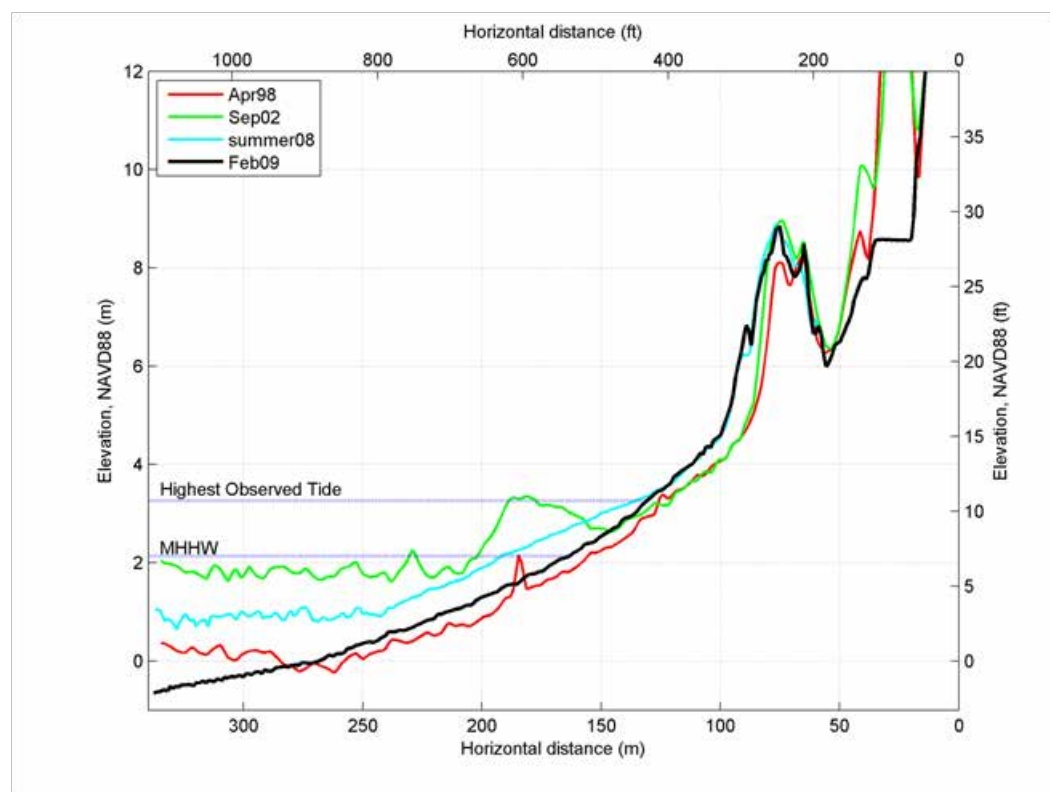
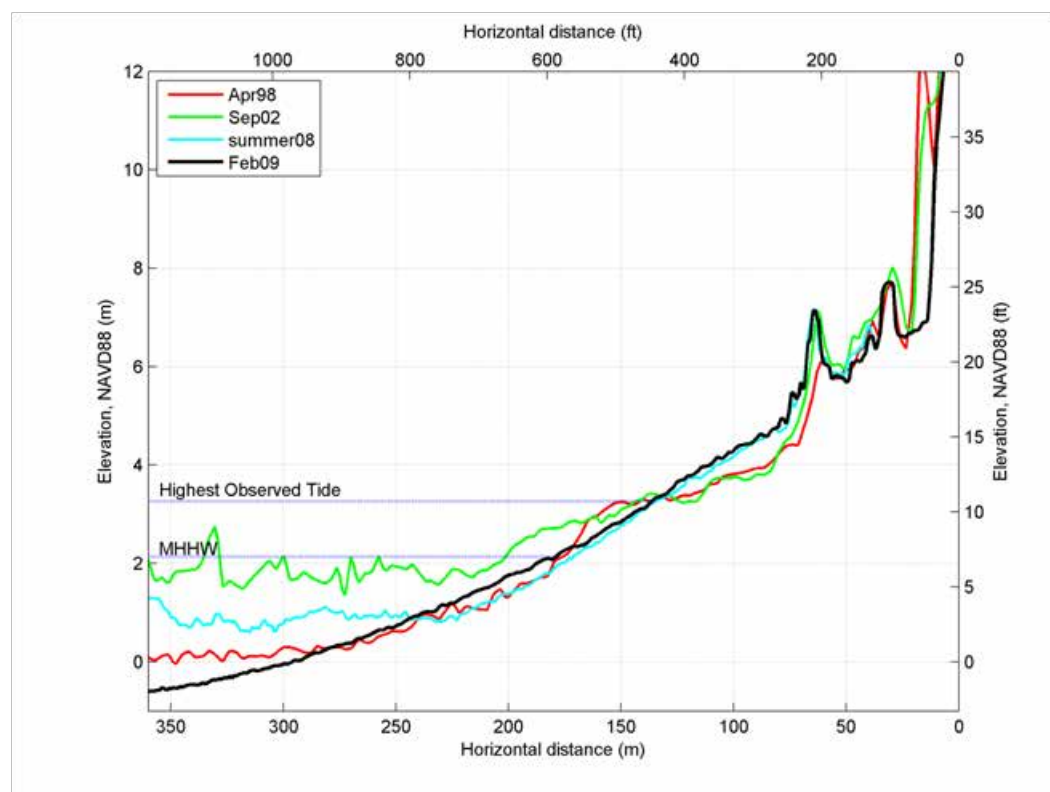
Bandon 5**Bandon 6**

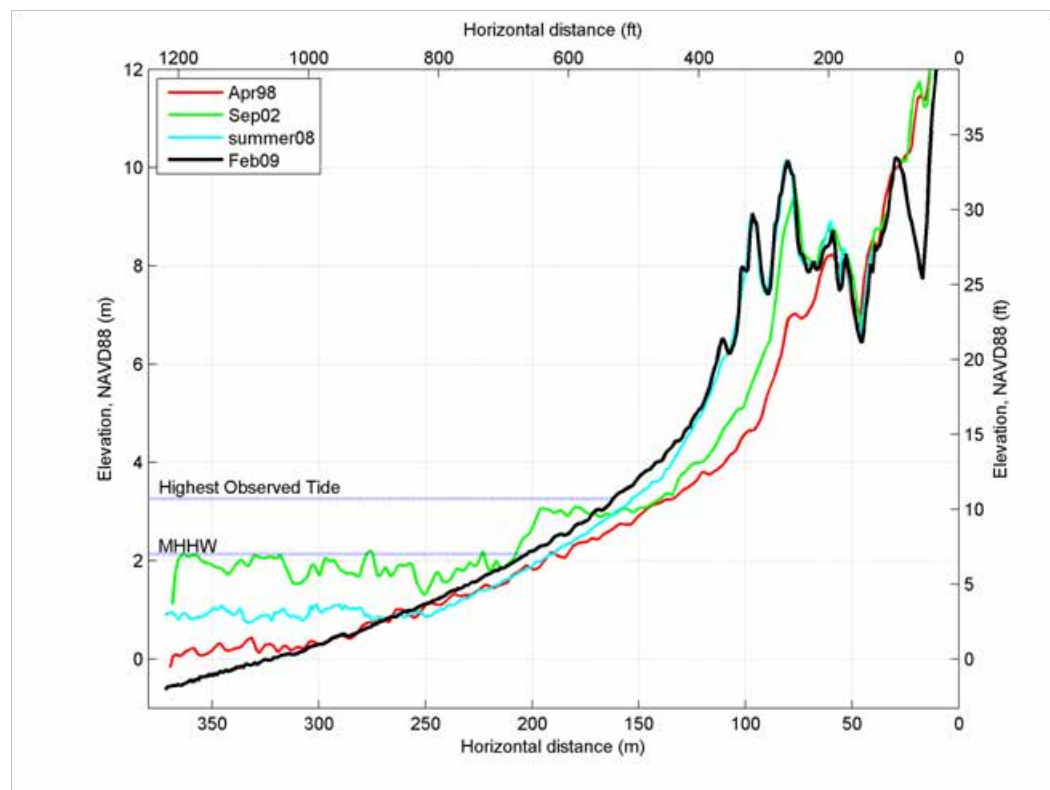
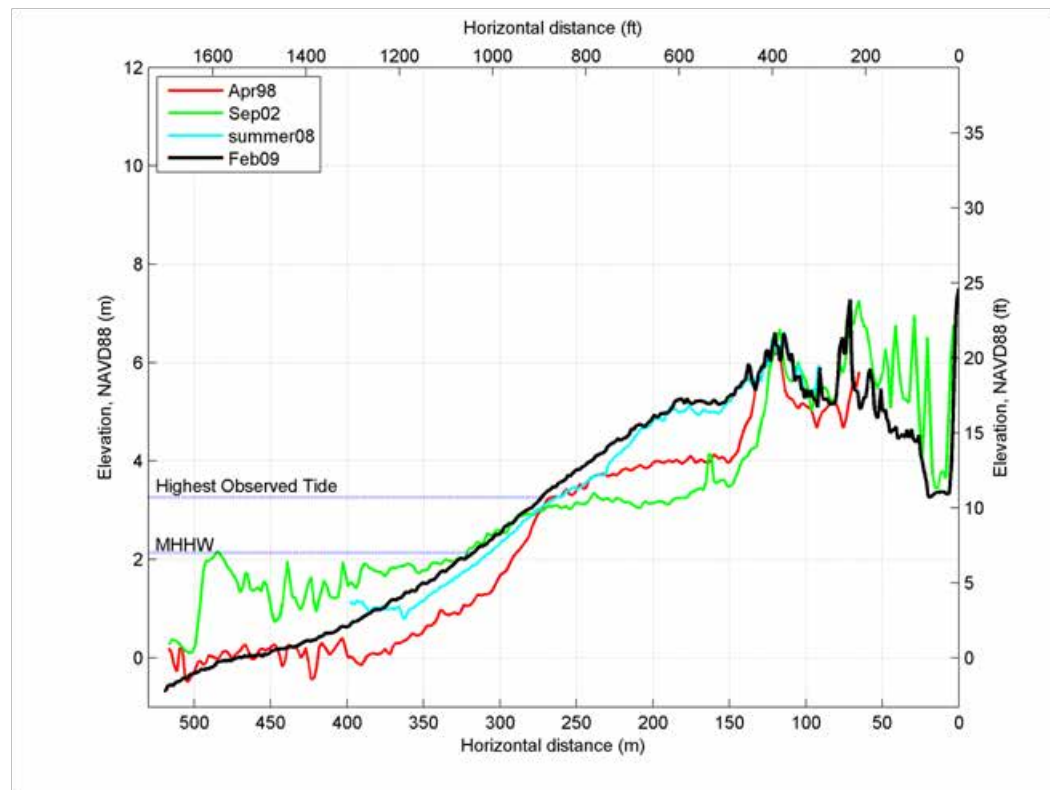
Bandon 7**Bandon 8**

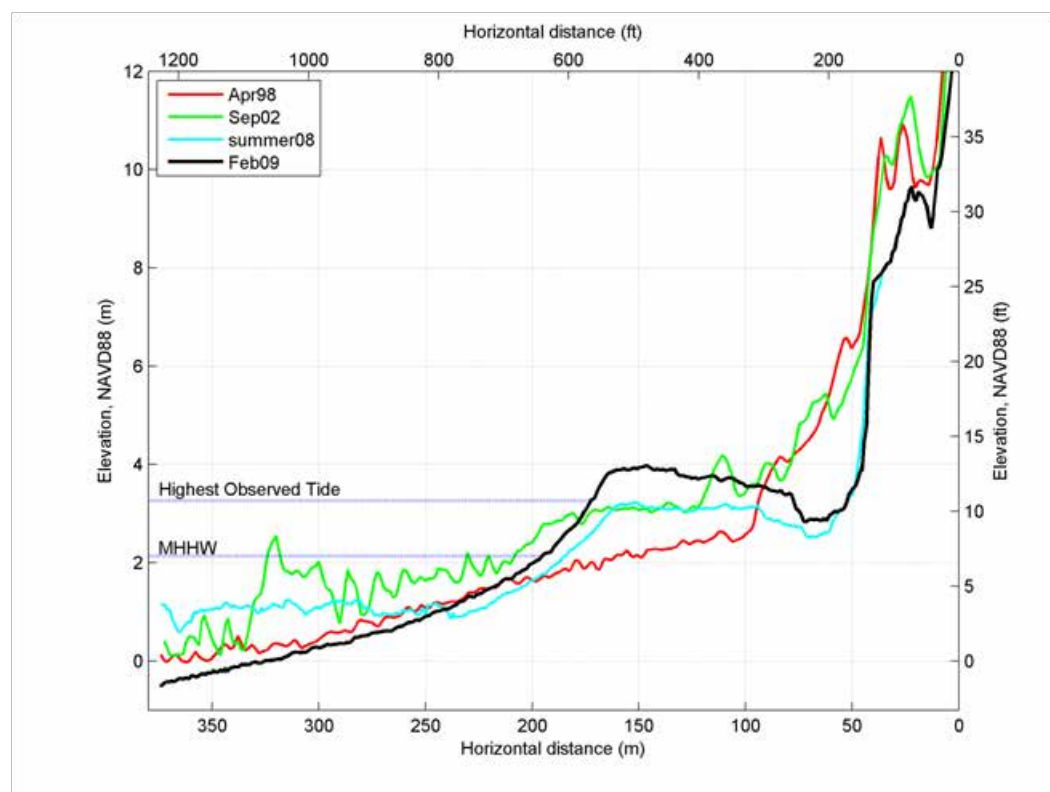
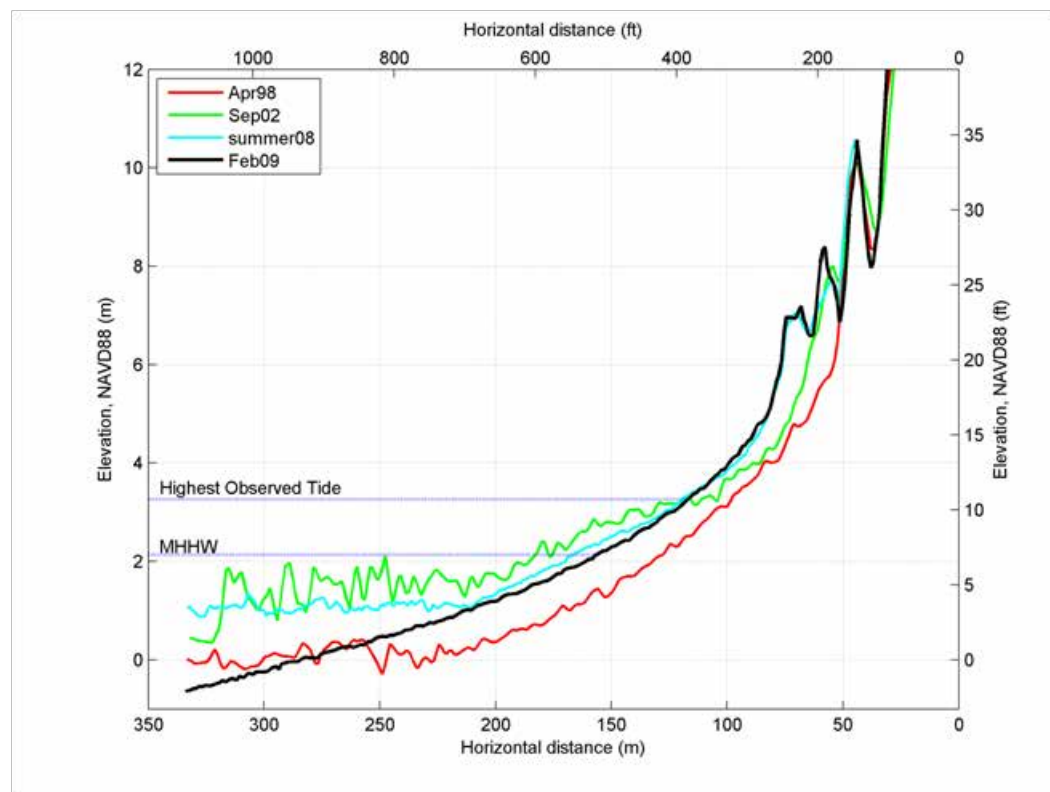
Bandon 9**Bandon 10**

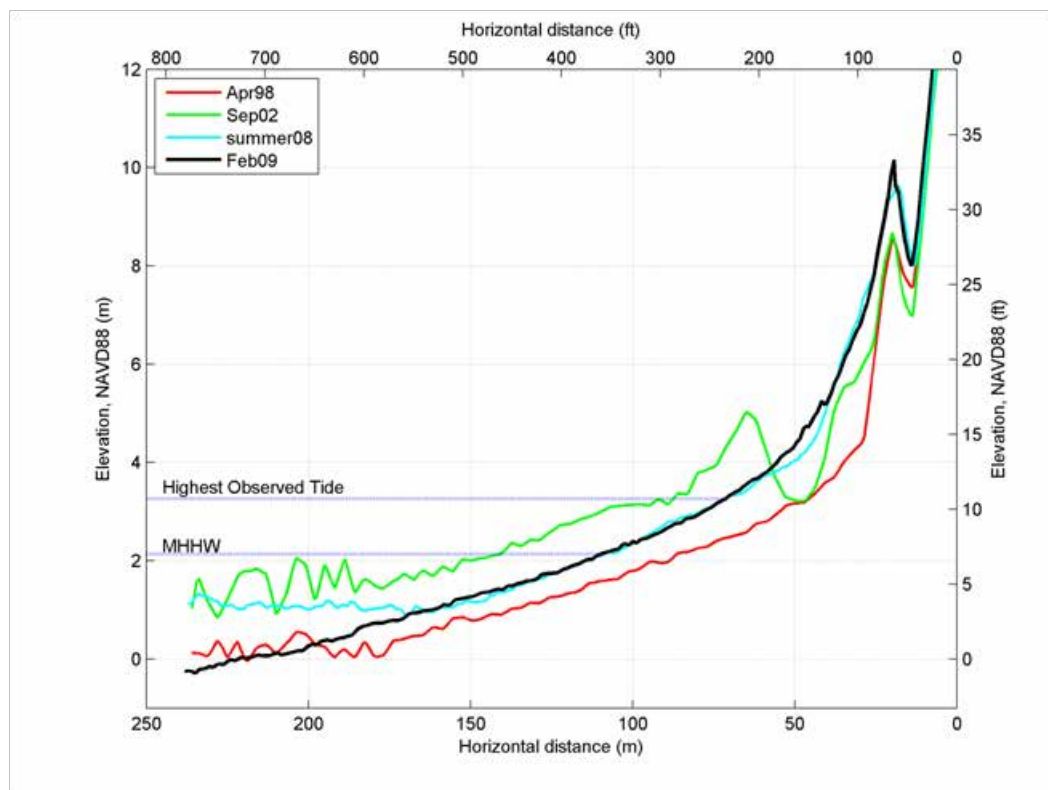
Bandon 11**Bandon 12**

Bandon 13**Bandon 14**

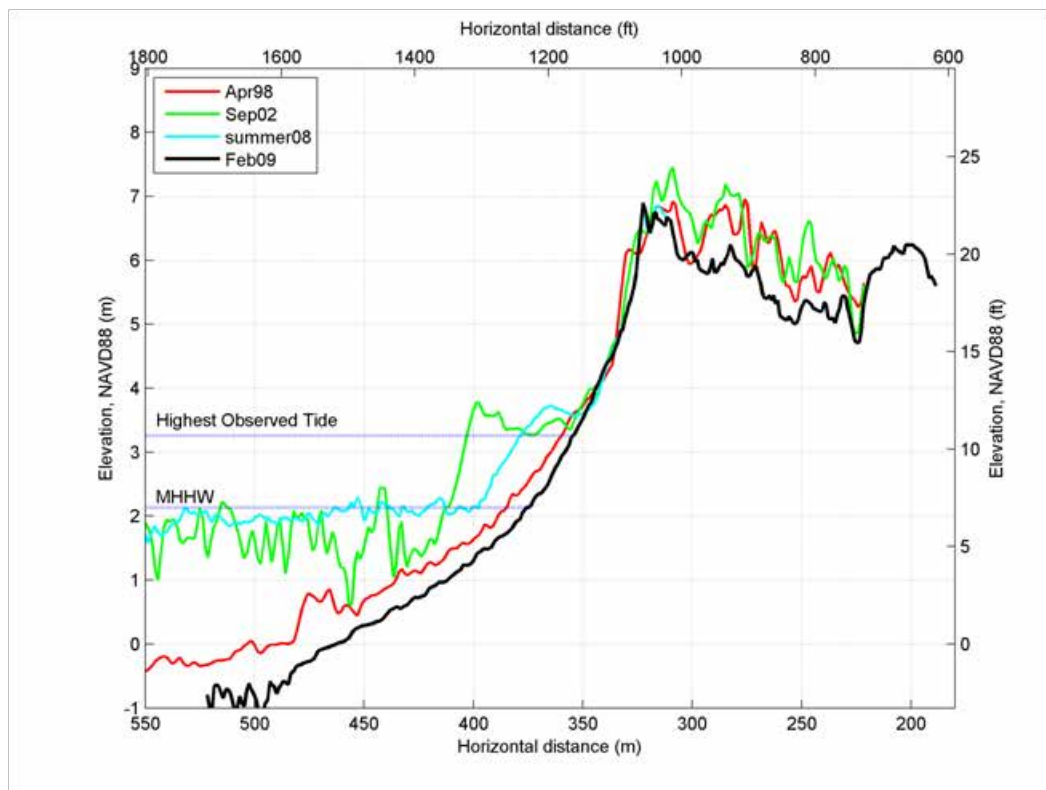
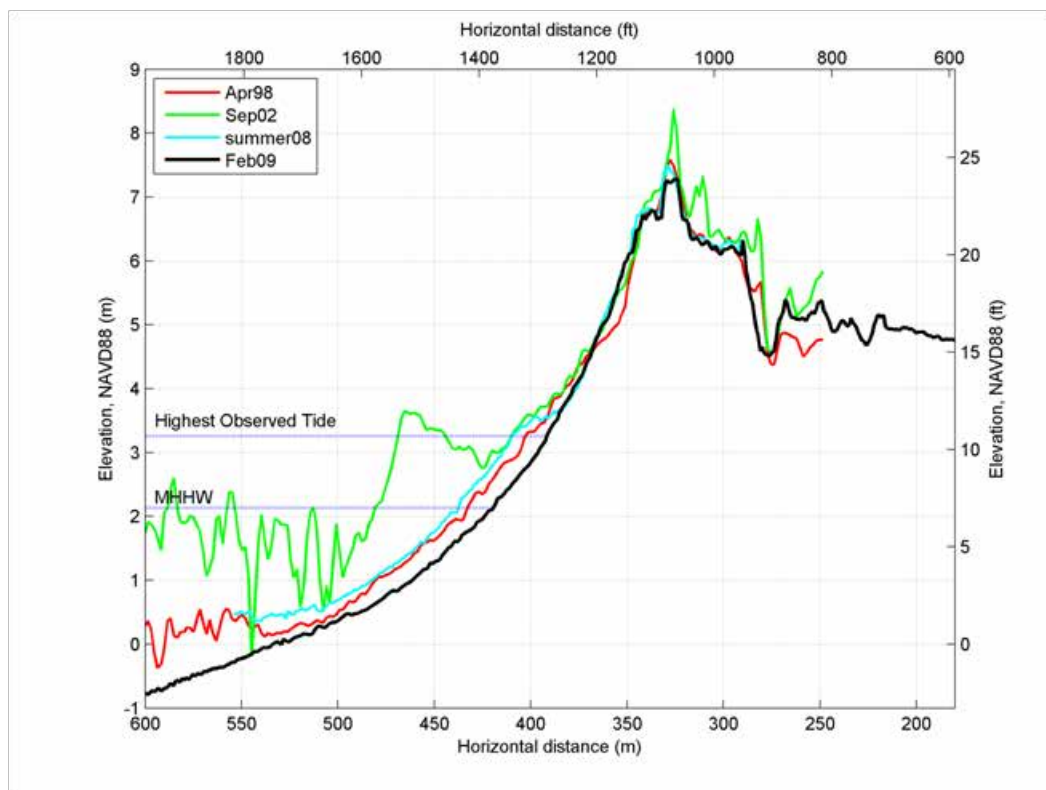
Bandon 15**Bandon 16**

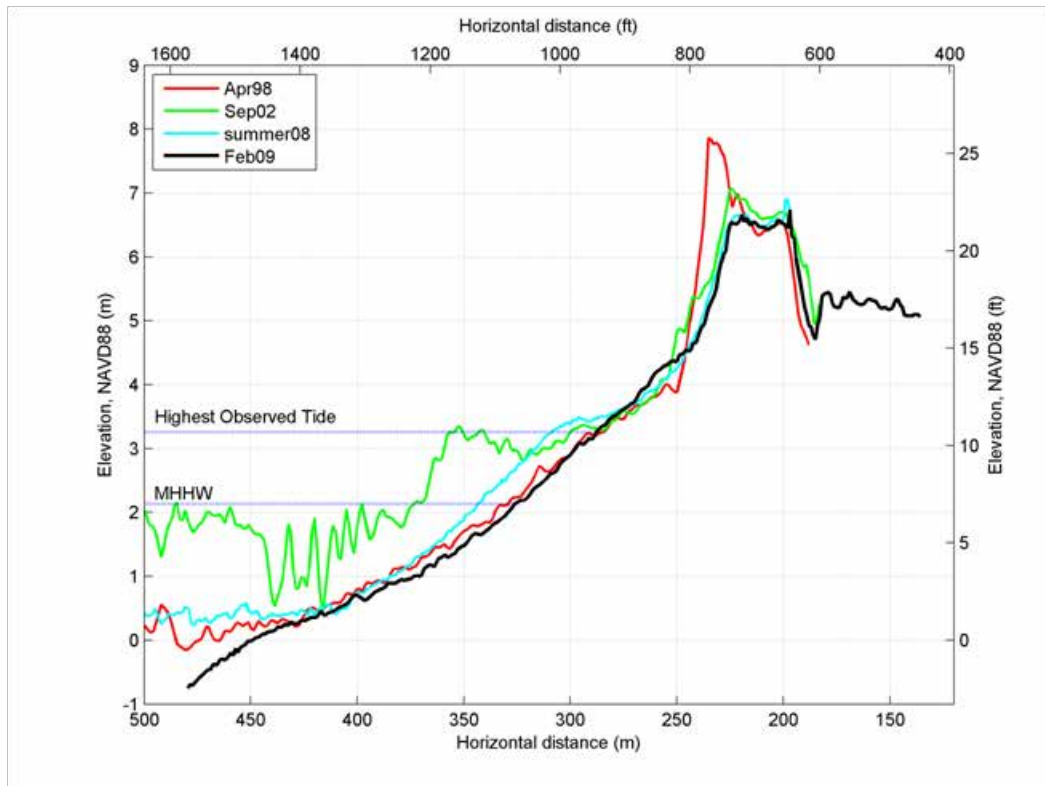
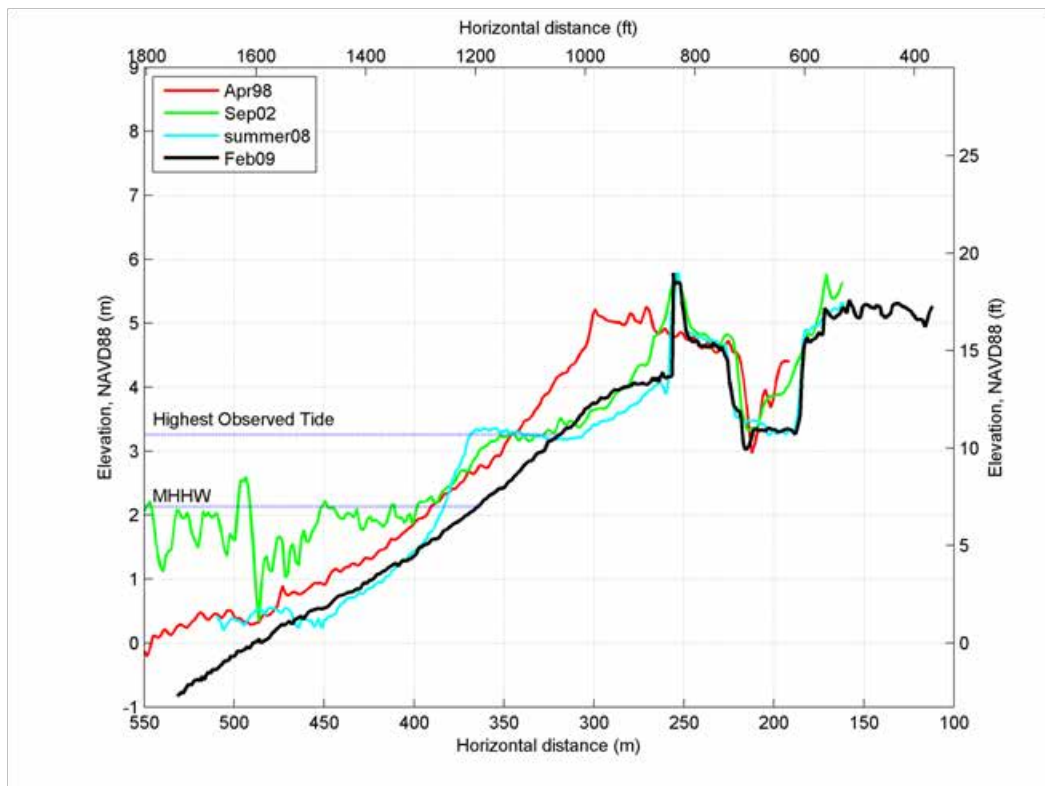
Bandon 17**Bandon 18**

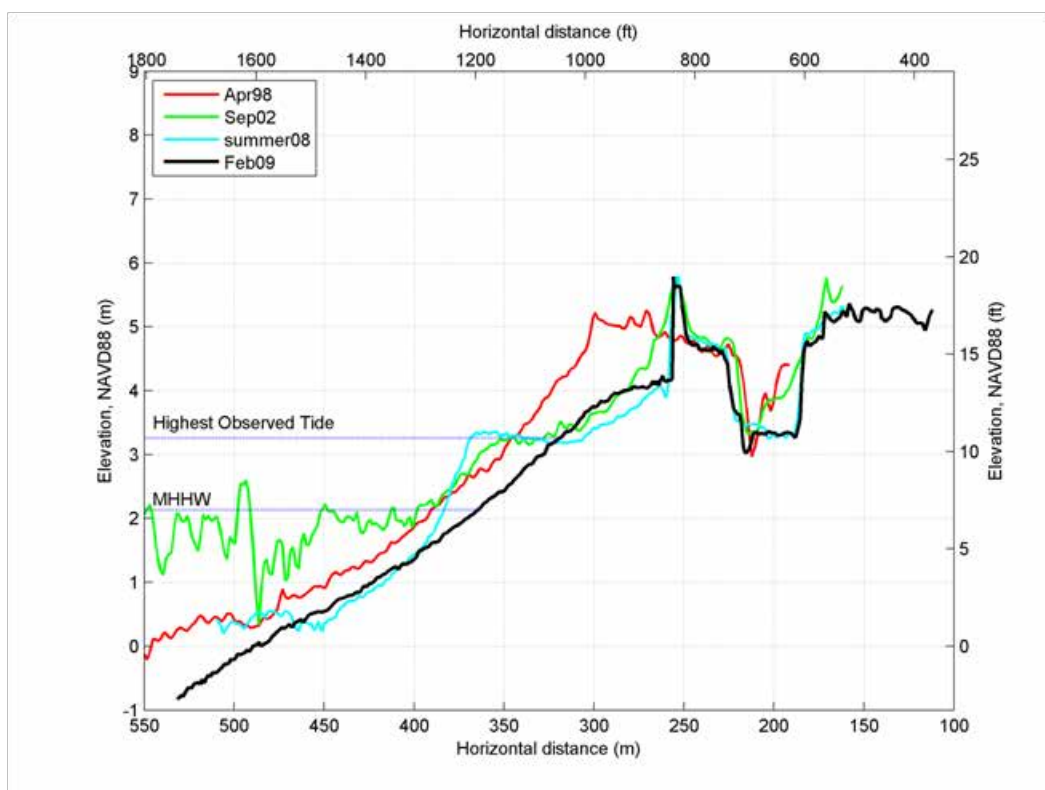
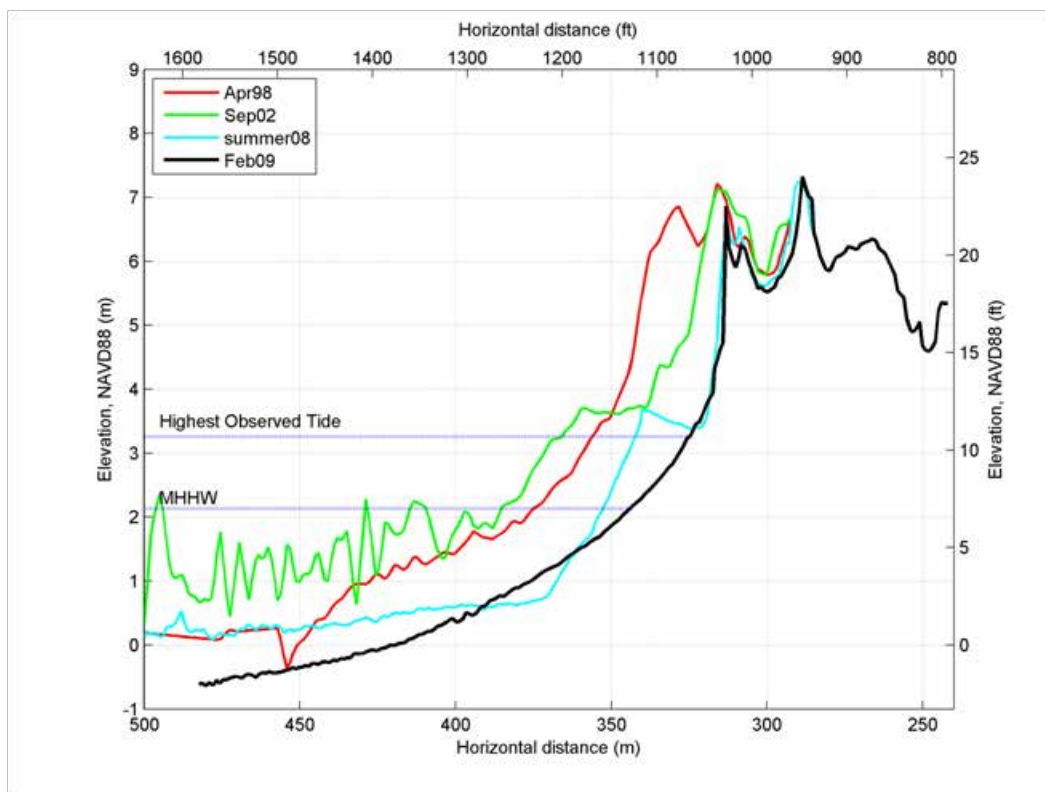
Bandon 19**Bandon 20**

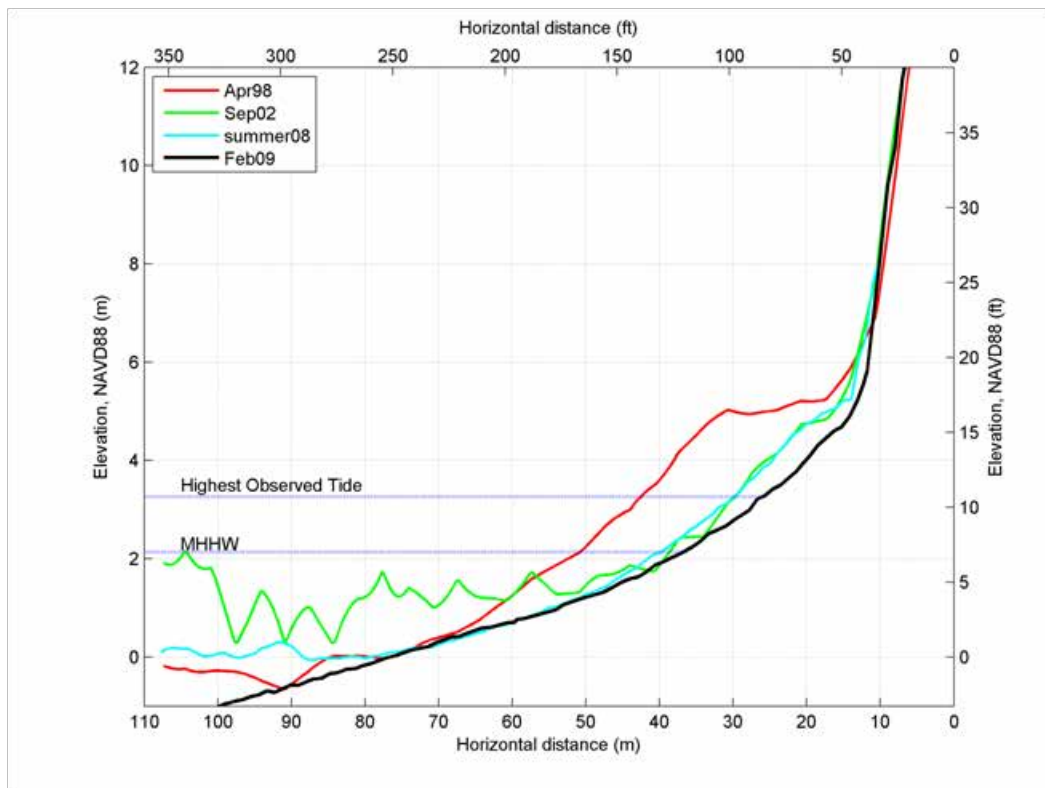
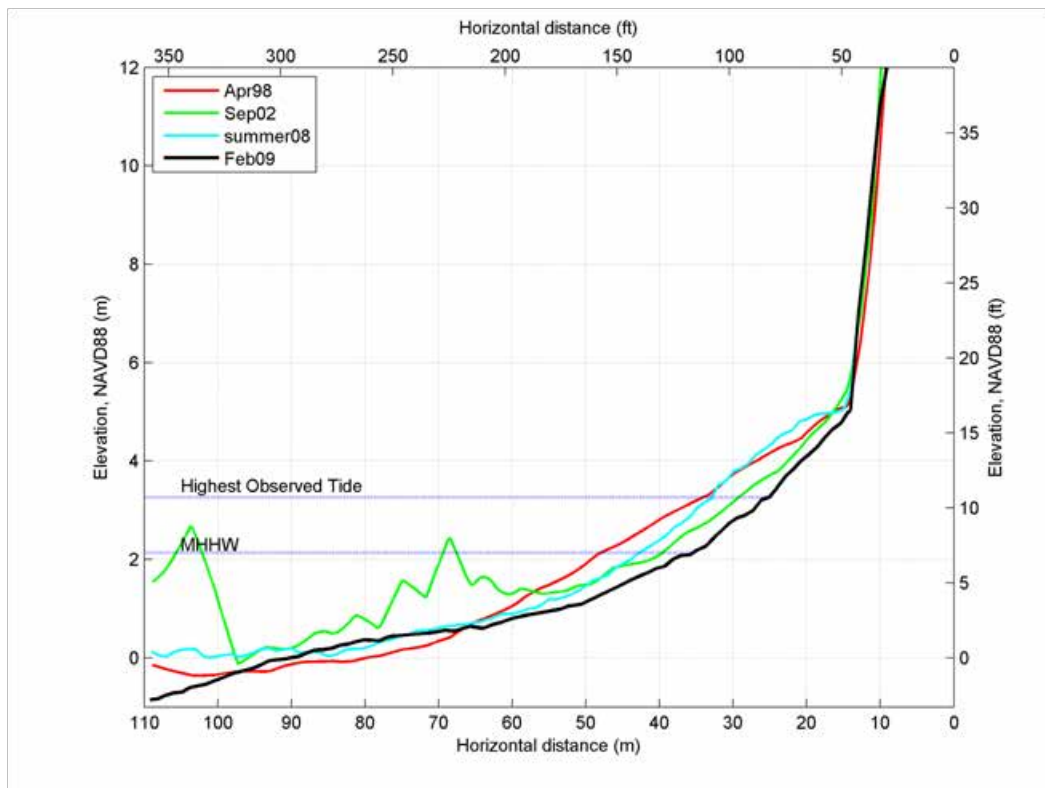
Bandon 21

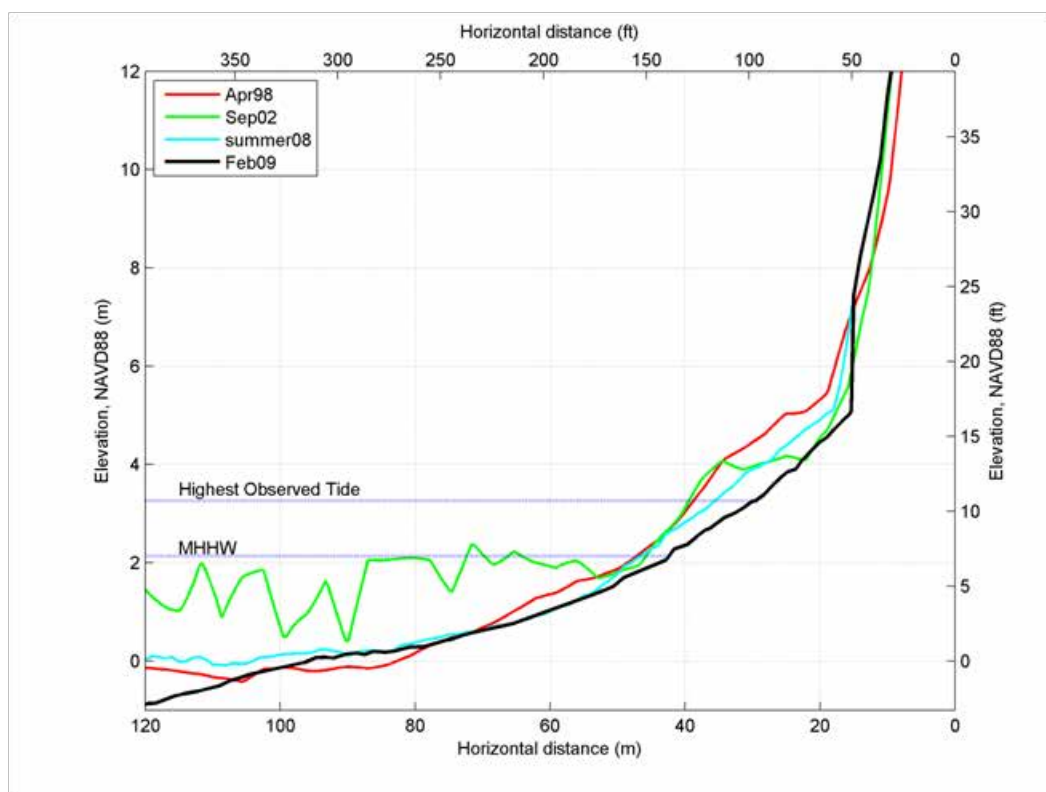
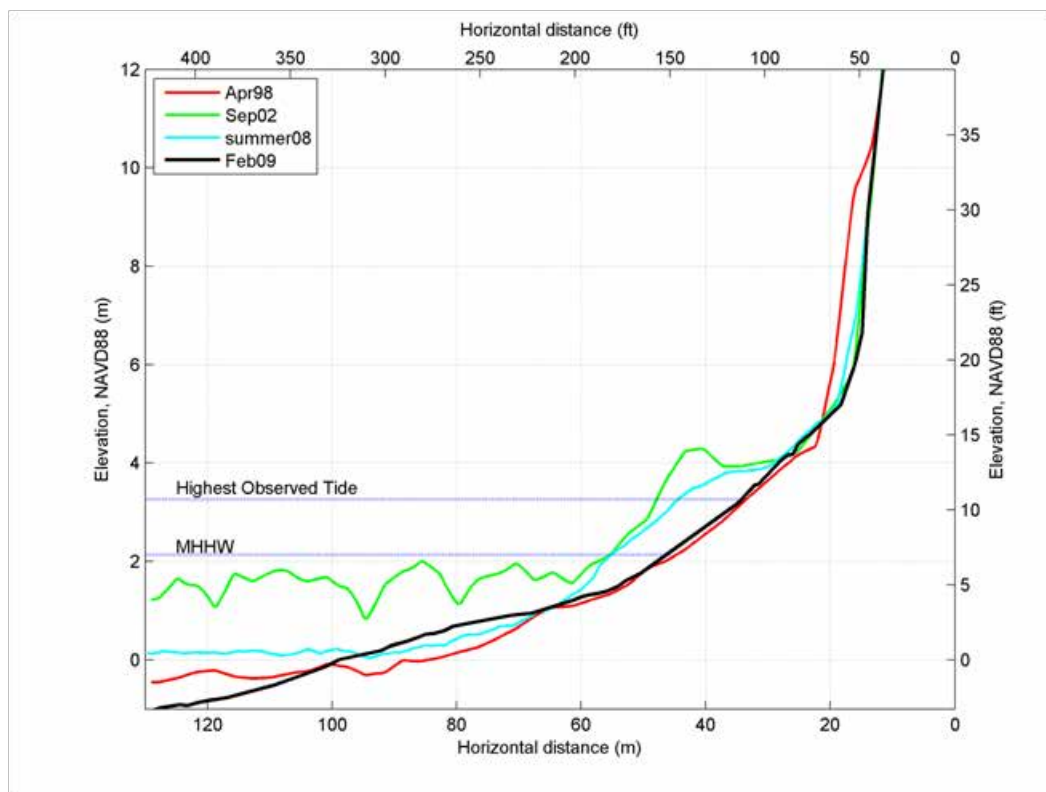
APPENDIX C. COOS-BASTENDORFF/LIGHTHOUSE BEACH PROFILES

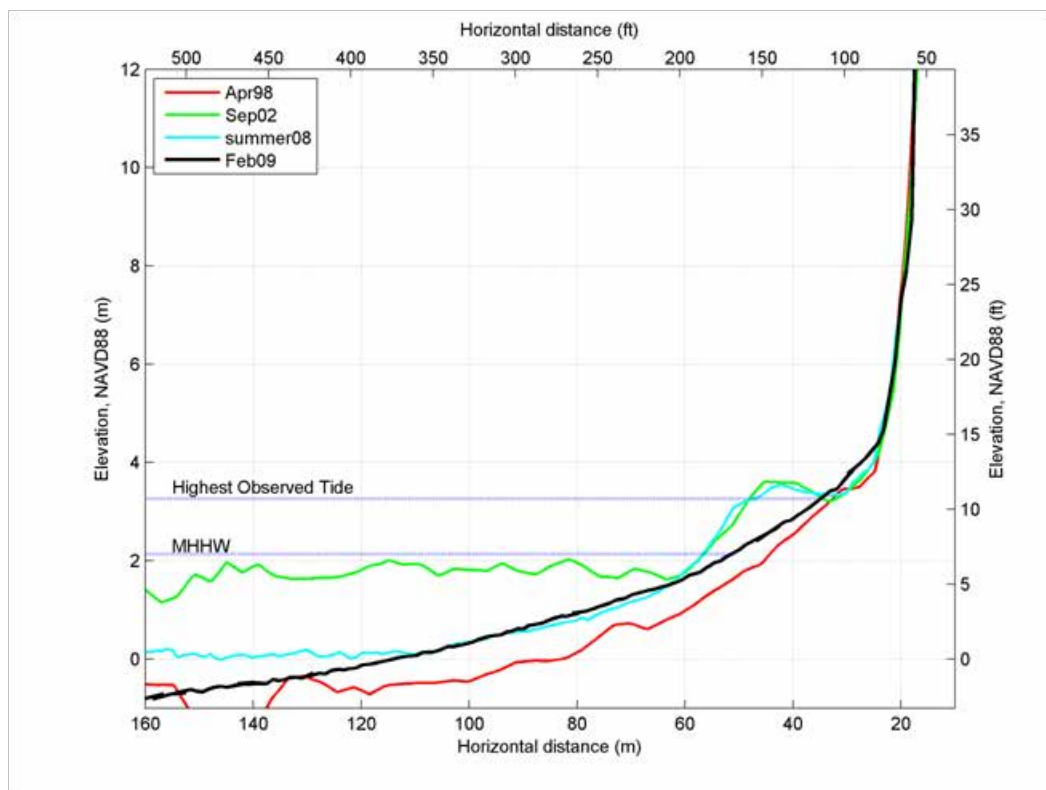
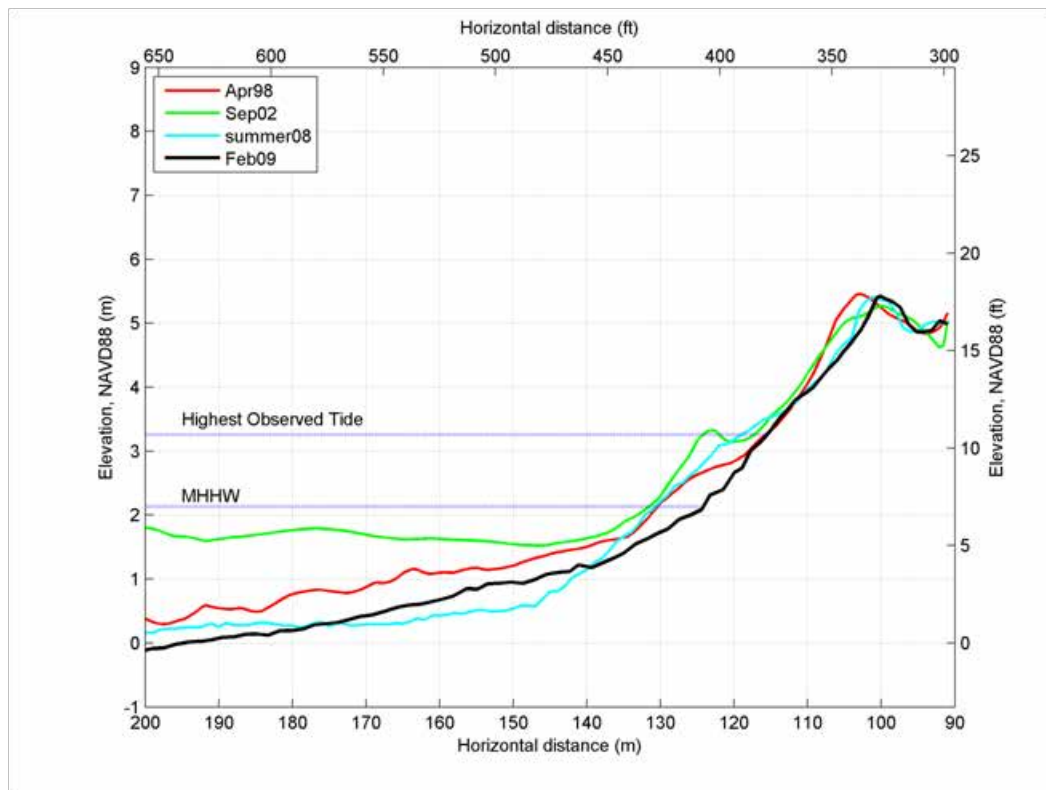
Coos 1**Coos 2**

Coos 3**Coos 4**

Coos 5**Coos 6**

Coos 7**Coos 8**

Coos 9**Coos 10**

Coos 11**Coos 12**

APPENDIX D. SPLASH OVERTOPPING NOTES DERIVED BY W. G. McDougall

(Coastal Engineer, Oregon State University, and Technical Coordinator of the North Pacific FEMA West Coast Guidelines)

WG McDougall
PO Box 699, Philomath, OR 97370
T: 541-929-6467, F: 541-929-6457
E: mcdougal@wgmc dougal.com

PROJECT FEMA Splash Overtopping
BY W DATE 14 May 2010 PAGE 1 OF 3

1) Velocity Components

$$A + \textcircled{1}$$

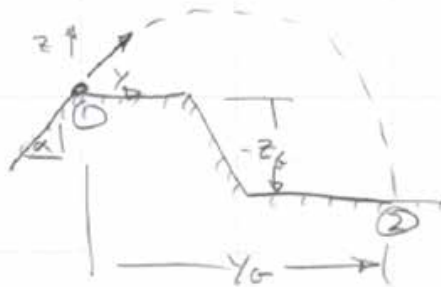
$$v_{cx} = v_c \sin \alpha$$

But the wind modifies

v_{cy} . In the FEMA
GFS, this is written

$$v'_{cy} = (v_c \cos \alpha)' = v_c \cos \alpha + 0.3(w_y - v_c \cos \alpha)$$

The change in the horizontal velocity
results in a different α' for the angle
of the ramp. The GFS calls this α_{eff} ,
but a more crescent wave would have been
 α' . Doesn't matter, because not needed.



2) trajectory eqns

Assume the horizontal velocity is no longer
influenced by the wind once it goes into
the air. (Can check this later.) Then the
traj. eqn is

$$y_g = (v_c \cos \alpha)' \Delta t \Rightarrow \Delta t = \frac{y_g}{(v_c \cos \alpha)'} \quad \text{---}$$

The vertical eqn can be written as (generic)

PO Box 889, Philomath, OR 97370
 T: 541-929-6467, F: 541-929-6457
 E: mcdougal@wgmc dougal.com

PROJECT _____
 BY ① DATE _____ PAGE 2 OF 3

$$s = s_0 + v_0 t + \frac{1}{2} a t^2$$

which for our case is

$$\pm z_g = 0 + (v_c \sin \alpha) \Delta t - \frac{1}{2} g \Delta t^2$$

(initial value can be negative)
 Using the horizontal leg

$$\pm z_g = v_c \sin \alpha \frac{y_g}{(v_c \cos \alpha)} - \frac{1}{2} g \left[\frac{y_g}{(v_c \cos \alpha)} \right]^2$$

This is allowed motion. Using v_c' is better
 so collecting terms, this is

$$y_g^2 - \left(\frac{2}{g} v_{cy}' v_{cz} \right) y_g + \frac{2}{g} (v_{cy}')^2 z_g = 0$$

3) Quadratic Eqn

$$y_g = \frac{v_{cy}' v_{cz}}{g} \left[1 + \left(1 - 2z_g \frac{z_g}{v_{cz}^2} \right)^{1/2} \right]$$

u) Yikes!

I have $\frac{z_g}{v_{cz}^2}$ in the code rather than

$\frac{z_g}{v_{cy}'^2}$. Please check this math to see if OK.

The Fortran code has never been used on
 a project or fully debugged/tested. Please

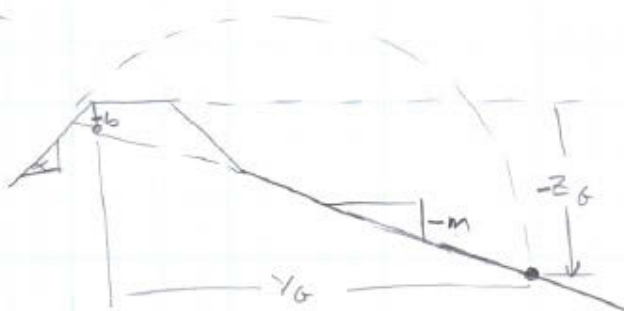
WG McDougal
 PO Box 899, Philomath, OR 97370
 T: 541-929-6467, F: 541-929-6457
 E: mcdougal@wgmc dougal.com

PROJECT _____
 BY 6 DATE _____ PAGE 3 OF 3

5) Sloping Backshore

$$z_g = b + my_g$$

$$y_g = v_{cy}' \Delta t$$



$$z_g = v_c \sin \alpha \frac{y_g}{v_{cy}'} - \frac{1}{2} S \left(\frac{y_g}{v_{cy}'} \right)^2$$

so

$$b + my_g = v_c \sin \alpha \frac{y_g}{v_{cy}'} - \frac{1}{2} S \left(\frac{y_g}{v_{cy}'} \right)^2$$

Collecting terms

$$y_g^2 - \left[\frac{2}{g} v_{cy}' v_{cz} - \frac{2m}{g} (v_{cy}')^2 \right] y_g + \frac{2b}{g} (v_{cy}')^2 = 0$$

Quadratic equation gives

$$y_g = \frac{v_{cy}'}{g} (v_{cz} - m v_{cy}') \left\{ 1 + \left[1 - \frac{2gb}{(v_{cz} - m v_{cy}')^2} \right]^{1/2} \right\}$$